Laser Interaction with Minerals Common on Asteroids

Niklas Anthony

Onboard Space Systems

LULEÅ
UNIVERSITY
OF TECHNOLOGY

Laser Interaction with Minerals Common on Asteroids

Niklas Anthony

Division of Space Technology
Dept. of Computer Science, Electrical and Space Engineering
Luleå University of Technology
Kiruna, Sweden

To the giants upon whose shoulders I stood.

Abstract

Asteroids are worth studying for three reasons: planetary defense, industrial applications, and scientific knowledge. It is critical we develop technologies capable of diverting objects on collision courses with our planet. We can use the same technology to move or process asteroids and comets for materials to build structures or refuel in Low-Earth Orbit. Asteroids are also windows into the past; they were formed in the early Solar System, and could potentially have been the source of water and/or life on Earth. There are unique challenges to manipulating an asteroid or asteroid materials, which means that much of what we know about material processing needs to be revamped to fit the situation. One of the motivating drives of this research was that a laser would be an excellent tool to perform many tasks at an asteroid.

One process of interest is laser drilling. The surface composition of asteroids is altered by aeons of space weathering; by studying the subsurface composition we can ascertain just how much it is altered and possibly by which processes. It is possible that hydrated minerals or ices exist below the surface as well, which are of great economic interest in asteroid mining. One of the greatest challenges to get under the surface of an asteroid is the low gravity: any forces or torques generated by a sampling mechanism may tip the spacecraft or launch it into deep space. A laser does not generate any significant forces, and can even be used without having to land; lasers do use a lot of electric power so the laser parameters need to be optimized to minimize the size and power requirements of the spacecraft. We found that nearly 1-cm deep holes can be made with as little as 18 J of energy using a 300-W laser.

Laser ablation has been studied as a mechanism to redirect asteroids, but it is not particularly energy efficient at material removal. If the idea is to create a momentum exchange by removing surface material beyond an object's gravitational pull, then there could perhaps be more energy efficient mechanisms. One mechanism we investigated was spallation, where the shock wave of a laser pulse breaks off a relatively large chunk of material without having to melt and vaporize it. We found that spallation may be many times more energy efficient than ablation.

Laser welding of metals has been of industrial interest for decades, though the welding of two different materials is still a challenge. We sought to develop a laser-based wire-attachment mechanism that can be used to anchor spacecraft to the surface of a small body or to maneuver boulders or small asteroids. When attempting to follow a traditional welding process, it was found that the two melt pools would not mix, and if it did, it was very weak. Instead, we used the laser to drill a hole and melt a wire while inserting it into the hole. This produced a solid anchor with a hold strength over 115 N.

Asteroider är värdefulla att studera av tre skäl: planetförsvar, industriella applikationer och vetenskaplig kunskap. Det är viktigt att vi utvecklar tekniker som kan ändra asteroiders kollisionskurser med vår planet. Vi kan använda samma teknik för att flytta eller bearbeta asteroider och kometer för material för att bygga strukturer eller tankstationer i jordbana. Asteroider är också fönster in i det förflutna; de bildades i det tidiga solsystemet och kunde potentiellt ha varit källan till vatten och/eller liv på jorden. Det finns unika utmaningar att manipulera en asteroid eller asteroidmaterial, vilket innebär att mycket av det vi vet om materialbearbetning måste moderniseras för att passa situationen. En av de motiverande drivkrafterna för denna forskning var att en laser skulle vara ett utmärkt verktyg för att utföra många uppgifter vid en asteroid.

En process av intresse är laserborrning. Ytans sammansättning av asteroider förändras av aeoner av rymdförvitring; genom att studera underytans sammansättning kan vi fastställa hur mycket den förändras och eventuellt genom vilka processer. Det är möjligt att hydratiserade mineraler eller is finns också under ytan, vilket är av stort ekonomiskt intresse för asteroidbrytning. En av de största utmaningarna att komma under ytan på en asteroid är låg tyngdkraft: alla krafter eller vridmoment som genereras av en provtagningsmekanism kan tippa rymdfarkosten eller skjuta ut den i djupt utrymme. En laser genererar inga signifikanta krafter och kan användas utan att behöva landa; lasrar använder mycket elektrisk kraft så laserparametrarna måste optimeras för att minimera rymdskeppets storlek och effekt. Vi fann att nästan 1 cm djupa hål kan göras med så lite som 18 J energi med en 300-W laser.

Laserablation har studerats som en mekanism för att omdirigera asteroider, men det är inte särskilt energieffektivt vid materialborttagning. Om tanken är att skapa ett momentumutbyte genom att ta bort ytmaterial bortom ett objekts gravitation, kan det kanske finnas mer energieffektiva mekanismer. En mekanism som vi undersökte var spallation, där chockvågen hos en laserpuls bryter av en relativt stor bit material utan att behöva smälta och förånga den. Vi fann att spallation kan vara många gånger mer energieffektivt än ablation.

Lasersvetsning av metaller har varit av industriellt intresse i årtionden, även om svetsning av två olika material fortfarande är en utmaning. Vi försökte utveckla en laserbaserad trådfästningsmekanism som kan användas för att förankra rymdfarkoster på ytan av en liten kropp eller för att manövrera stenblock eller små asteroider. När man försökte följa en traditionell svetsprocess, fann man att de två smältbassängerna inte skulle blandas, och om det gjorde det var det mycket svagt. Istället använde vi lasern för att borra ett hål och smälta en tråd medan vi satte in den i hålet. Detta gav ett fast ankare med en hållfasthet över 115 N.

Contents

ACKNOWLEDGMENTS

x

CHAPTER 1

Introduction

1.1 Motivation

Asteroids are worthy of studying for three primary reasons: planetary defense, industrial applications, and scientific knowledge. It is widely accepted that a massive asteroid caused the mass-extinction event ∼65 million years ago. Estimates of size range between 10 km and 80 km in diameter, and the impact velocity was estimated to be 20 km/s [1]. Another famous impact event was the one that occurred over Tunguska, Russia in 1908. In this case, an object roughly 60 m in diameter entered the atmosphere at 15.2 km/s exploded roughly 6-10 km in the air above a forest with the force of a large nuclear bomb [2]. Arguably the most documented impact event was the Chelyabinsk meteorite in 2013. Here, an object only 20 m in size exploded at an altitude of roughly 27 km. Its 19 km/s atmospheric entry velocity produced an explosion that injured over one thousand people and damaged over 3,000 buildings in 50 villages [3]. If life on Earth is to continue as we know it, it is vital that we develop the capabilities to deflect potentially hazardous Near-Earth Asteroids (NEAs).

In developing the technologies required to divert or disrupt Potentially Hazardous Asteroids (PHAs), we open up the possibility to utilize asteroid material to manufacture things in space, as opposed to launching them from Earth's surface. For example, the same ion engine used to push a PHA off of a collision course with Stockholm could also be used to transfer asteroid (16) Psyche's roughly 10 quadrillion tons of metal [4] to Low-Earth Orbit (LEO) to build a refueling platform for spacecraft.

In addition to their material aspect, asteroids contain a wealth of scientific mysteries. Asteroids could have contributed to the creation of life on Earth over 3 billion years ago. Scientists have documented the existence of organic matter in meteorites since before the 1900s [5]. Thermal evolution models of carbonaceous asteroids (accounting for variable such as porosity and permeability) suggest they could host liquid water or enable biotic processes for millions of years while cooling down after formation [6]. If, in the end, there is no life on asteroids themselves, they certainly could have enabled life

on Earth. Experiments showed that the energy released from an asteroid impact could ionize organic matter, creating the building blocks of life [7]. Asteroid impacts have also been suggested as the primary source of water delivery to early Earth [8].

1.2   Research Questions and Motivation

The primary research questions that underlined this PhD thesis were:

RQ1: What is the state of the art in asteroid-related technologies, and are there knowledge gaps to be filled?

RQ2: How energy efficient is laser drilling of minerals?

RQ3: How does laser drilling and laser-induced spallation compare to laser ablation in terms of asteroid redirection?

RQ4: How can a laser be used to anchor a spacecraft to a small body?

The first research question set the stage for the entire PhD project. It is based on both my own personal interest in asteroid mining, but also the need for planetary defense. From an academic perspective, it was not clear what the state of the art in asteroid engineering was, that is, asteroid detection, redirection methods, and mining technologies. What kind of research was being done in what aspects and by who? And what research questions remain open? By answering this question, I could apply my skills and research to best suit the field.

A laser has a multitude of uses in the aerospace industry and research, and could potentially be used in a number of ways at an asteroid. It is vital to determine the processing efficiency in any case, as a laser is known to use a relatively large amount of power and produce a considerable amount of heat. For any spacecraft, especially one going to an asteroid, overall mass, power requirements, and thermal noise must be kept to a minimum. So what laser parameters (i.e. power level, pulse length, repetition rate, and power density) can be used to minimize the size, power requirements, and waste heat of a laser? What processes occur or can be induced to maximize the energy efficiency of laser drilling?

Landing and staying anchored to a small body is challenging. Can a laser be used to make this process less risky and more successful? In what situations would it be applicable?

1.3   Author Contributions to Appended Papers

There are four appended papers that make up this compilation thesis. I will briefly describe the work I personally contributed to each one:

Paper A: Asteroid engineering: The state-of-the-art of Near-Earth Asteroids science and technology, Niklas Anthony, M. Reza Emami *Progress in Aerospace Sciences*, Volume 100, 2018, 1–17

I wrote this paper, which is an extensive literature review of asteroid-related science and technology. It involved reading hundreds of journal and conference papers on asteroid detection, redirection methods, and mining technology. I then compiled the information into a coherent report, and produced several figures.

Paper B: Laser processing of minerals common on asteroids, Niklas Anthony, Jan Frostevarg, Heikki Suhonen, Christina Wanhainen, Antti Penttilä, Mikael Granvik *Optics & Laser Technology*, Volume 135, 2021, 106724

This paper reports the results of experiments with laser drilling on rocky materials. I originated the idea to use a laser on an asteroid and performed a majority of the experiments on all three samples. I wrote the paper and produced all of the figures except the thin-slice petrography, spectral response, and X-ray MicroTomography (XMT) visualizations. I performed data analysis and visualization using both High-Speed Imaging (HSI) and the hole measurements.

Paper C: Laser-induced spallation of minerals common on asteroids, Niklas Anthony, Jan Frostevarg, Heikki Suhonen, Christina Wanhainen, Mikael Granvik *Acta Astronautica*, Volume 185, 2021, 325–331

This paper presents the results of further experiments with laser drilling, this time using a process called spallation. I performed a majority of the experiments, wrote the paper, and produced all of the figures except for the XMT visualizations.

Paper D: Laboratory experiments with a laser-based attachment mechanism for small bodies, Niklas Anthony, Jan Frostevarg, Heikki Suhonen, Mikael Granvik *Acta Astronautica*, Submitted, 2021

The fourth and final appended paper reports the results of initial experiments developing a laser-based anchoring mechanism for spacecraft intending to land on the surface of small celestial bodies. I lead the ideation of the two sets of experiments and performed most of them. I created a 3-D model of a holder to attach the samples to a universal test machine, which was then printed and used successfully. I wrote the paper and produced all of the figures except the XMT visualizations.

Asteroids

2.1 Populations

Asteroids and comets are bodies that survived the formation of the Solar System without being consumed by the Sun or planets. It is theorized that the Solar System formed in the same way we observe other systems throughout their formation processes: we started out as a nebula of gas and dust, and gravity slowly did the rest. The nebula collapsed, forming a proto-sun and accompanying accretion disk. Most of the material in the disc was captured by the proto-planets, and eventually, the Solar System as we know it took shape: four rocky inner planets and four gas giants in the outer system, separated by a belt of asteroids, known as the Main Belt (see Fig. 2.1).
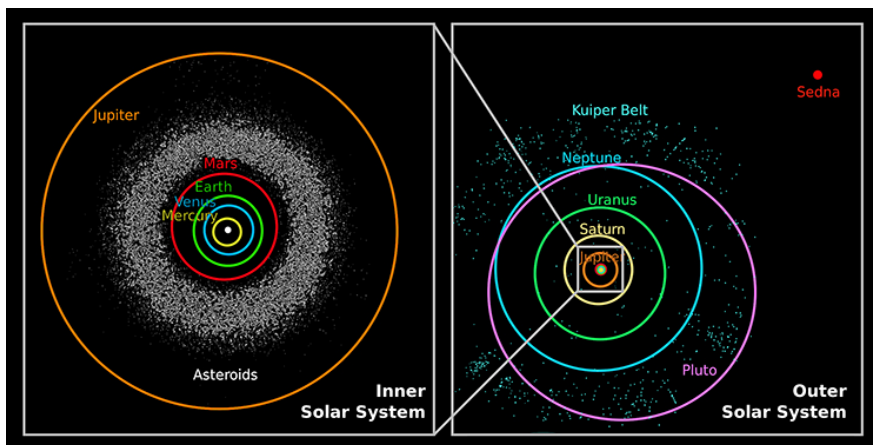

Figure 2.1: Solar System. Credit: Whittet 2017 [9]

5

There is a significant population of objects that lie beyond the orbit of Neptune, known as the Kuiper Belt. This is where we find objects like Pluto and Arrokoth. Occasionally, we observe objects on highly eccentric orbits whose aphelia extend well beyond the Kuiper Belt. It is theorized these objects come from a population of objects known as the Oort cloud, which exist outside the heliosphere some 2,000 AU to 200,000 AU (Astronomical Units) away.

Asteroids can and do become dislodged from their orbits in a number of ways. The obvious way this happens is via collision: two asteroids collide with each other, and lose orbital energy, causing them to "fall" closer to the Sun. The collision rate for MBAs is relatively low, for instance, the average collisional lifetime for a 1-km asteroid is about 1 Gyr [10]. Another mechanism by which asteroids have their orbits altered is by gravitational perturbations. We can see, for instance, that there are gaps in the orbital distribution of MBAs corresponding to the resonances of Jupiter's orbit (Fig. 2.2), first noticed by Daniel Kirkwood in 1866.
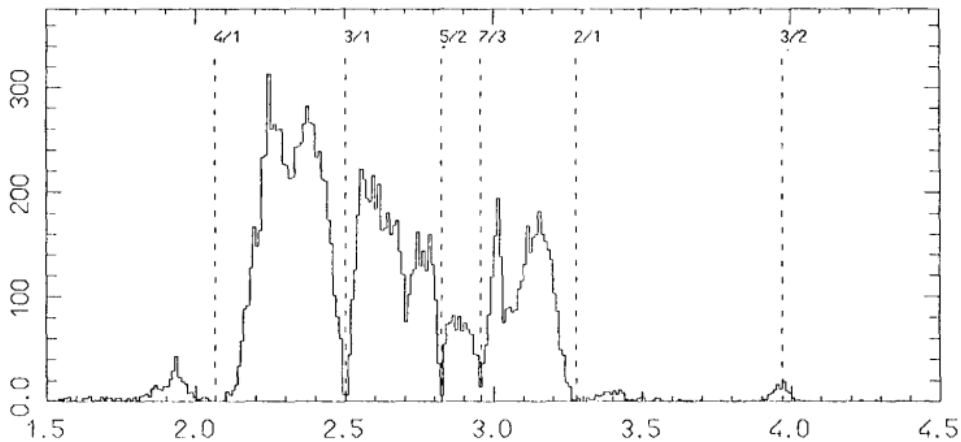
Figure 2.2: Population histogram of MBAs from Moons 1996 [11]. The X-axis is the semi-major axis in AU, and the Y-axis is the number of MBAs.

Objects that were in, or eventually enter, these resonances can end up in a number of places. They can be just shifted outside the resonance, they could be launched into the Sun, some are sent flying out into the outer Solar System, and still others are sent to the inner Solar System. One Ivan Osipovich Yarkovsky theorized some time near the year 1900 that small rotating bodies can slowly have their orbits altered by an-isotropic thermal radiation. Known as the Yarkovsky effect, it was first directly observed on asteroid (6489) Golevka [12]. Asteroids can be pushed or pulled into orbits in resonance with those of Jupiter and Saturn, thus sourcing asteroids to the inner Solar System.

The International Astronomical Union (IAU) operates the Minor Planet Center (MPC), which is the global database for all minor planets, comets and outer irregular natural satellites of the major planets. There are roughly 1 million objects registered, with over 268 million unique observation points. Of those objects, only 24,000 are considered "Near-Earth Asteroids" (NEAs), which are defined as asteroids with perihelia less than 1.3 AU. These objects range in size from 37.6-km-wide (1036) Ganymed (not to be confused with Jupiter's moon Ganymede) to the smaller-than-one-meter 2008 TS_{26}.

Since 1994, there have been two mandates from the US Congress to NASA to first "discover, characterize and catalog potentially hazardous NEOs larger than 1 kilometer in size" and in 2005, to "find at least 90 percent of potentially hazardous NEOs sized 140 meters or larger by the end of 2020". I prepared a plot of a handful of NEA population estimates (i.e. size-frequency distributions) and the discovery statistics as of October 2017 , shown in Fig. 2.3 [13]. Absolute magnitude (H) is a measure of how bright an object would be if it was 1 AU away from the Sun and Earth, and smaller numbers signify brighter objects. It can be used as an estimate of an asteroid's size, assuming a perfectly spherical shape and assumed albedo.
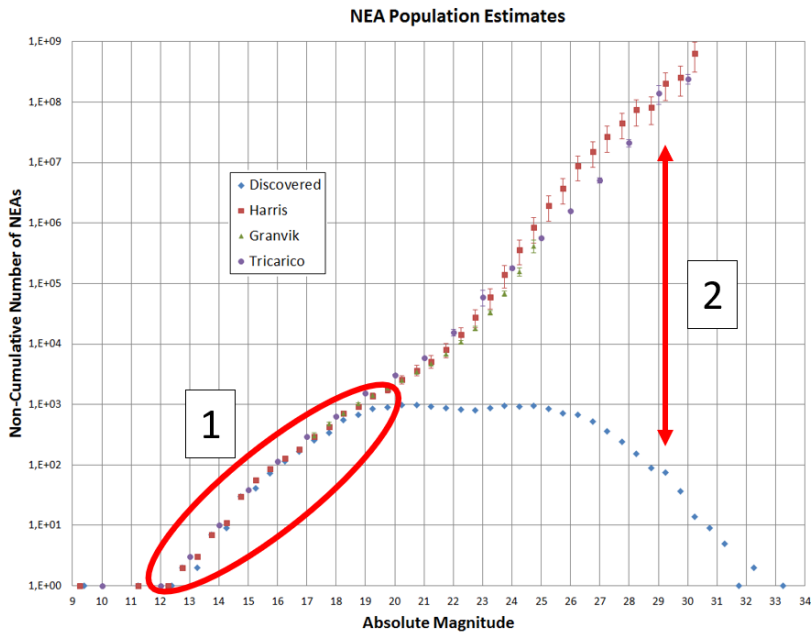

Figure 2.3: Comparison of size-frequency distributions of predicted and measured NEAs as of October, 2017 [13]. The circle #1 shows the matching region, and the arrow #2 shows the gap in discoveries of smaller objects.

Albedo can vary depending on a number of factors; NASA uses a flat value of 0.14 for estimation purposes, and so shall we. A 1-km asteroid would thus have H = 17.75 and a 140-m-sized asteroid would have H = 22. We can see from the plot that the first congressional mandate has been fulfilled, but the second had not yet been fulfilled. The discovery statistics are limited by telescope availability and technological limitations; there is a lot of sky to cover, and too few sufficiently-large telescopes to find small/faint objects. It is also possible to use space-based telescopes for this purpose, such as the NEO-WISE program.

One of the primary drivers for a mission to an asteroid is how close of an orbit to Earth the target has. Closer, slower moving objects require less fuel to get to, and missions to them are thus cheaper. There is a subset of NEAs called Temporarily-Captured Asteroids (TCAs), or "minimoons"; they enter the Earth-Moon System (EMS) at a velocity that allows them to orbit the Earth at least once before exiting the system again. They represent the closest and slowest-moving asteroids of the entire NEA population, making them ideal targets for any sort of asteroid engineering mission. A simulation of the TCA population shows that at any given time, there is at least one TCA $\sim$1.0 m in size in temporary orbit around Earth at any given time [14]. A full graph is shown in Fig. 2.4, which suggests there is a greater population of smaller objects, and larger objects can become temporarily captured, just less frequently (i.e. a kilometer-sized object is expected to be captured once every million years). Minimoons usually orbit in the retrograde motion, and stay for only nine months. It has been suggested that if their velocities can be altered by less than 10 m/s before entering the EMS, the duration of their capture can be increased by several years [15].

To date, there have only been two minimoons catalogued: 2006 RH_{120} and 2020 CD_3. The object 2006 RH_{120} entered the EMS on a retrograde orbit in June 2006, revolved around the Earth three times, and exited the system in July 2007. It is estimated to be 4 m in diameter and has a very fast rotation period of $\sim$2.3 min, suggesting it is a monolithic body and not a rubble pile [16]. The object 2020 CD_3 is thought to have entered the EMS in September 2017, and exited in March 2020, an unusually long capture duration, most likely due to its encounter with the Moon [17]. It is estimated to be 1.5 m in diameter, and rotates once per 3.2 min. In both cases, they were only discovered after they entered the EMS, and herein lies the challenges when considering a mission to a minimoon: the short warning time and dearth of clear targets.

Most missions take years to prepare, build, test, and launch; even CubeSat missions, with their relatively rapid development times, would be too slow. It seems the only feasible solution is to have a satellite that is already in space, which would be ready to rendezvous moments after the confirmation of a suitable target. The Comet Interceptor mission (selected by ESA for development) is operating under the same concept: comets have relatively short times between detection and their perihelion (where the comet can completely break up), so they will send a spacecraft to wait in the Sun-Earth Lagrange Point L2 until a suitable target can be identified. In the case of a mission to a minimoon, rendezvous simulations from Earth's geostationary orbit suggest it would take as little as 10 days using low thrust [18].
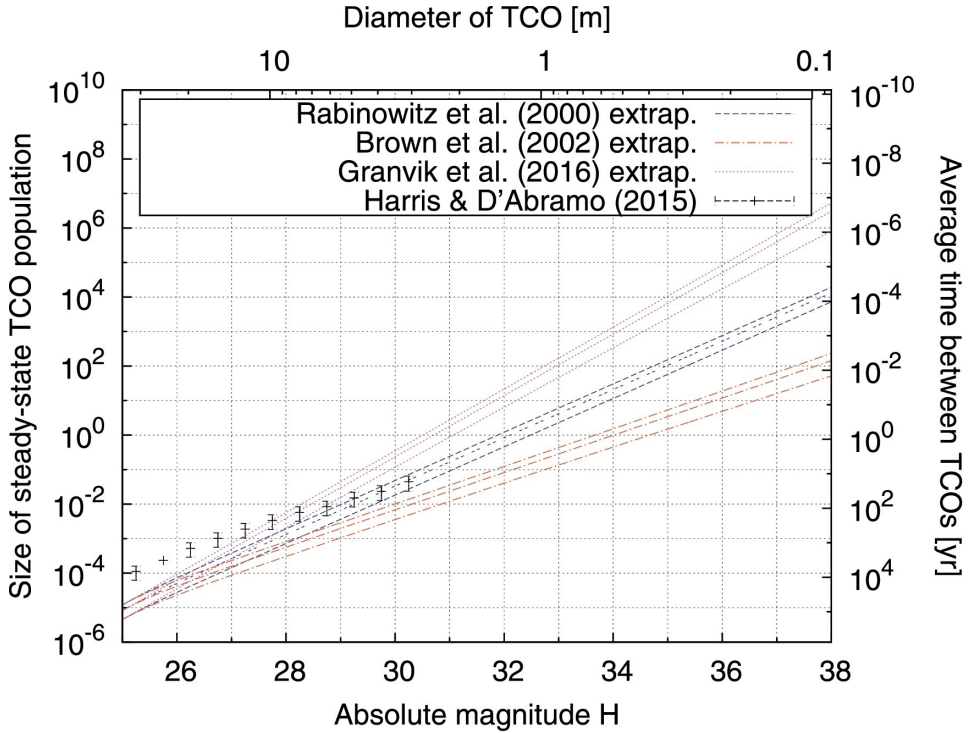
Figure 2.4: Simulation estimates of the steady-state TCA population [14]

2.2 General Properties

Asteroids were formed in the early Solar System as the hot gas and dust began to cool down and gravitate towards each other. They formed small clumps or "chondrules", which would clump together to form asteroids and planetesimals. If the temperature were high enough these chondrules could melt and merge into a new shape. The early planetesimals were hot enough and massive enough to cause differentiation, a process where denser materials would sink to the center of the planetesimal, and lighter elements would float to the surface. If a planetesimal were disrupted, the composition and structure of the fragments would remain differentiated. These fragments could also clump together to form "rubble-pile" asteroids, like asteroid (101955) Bennu (see Fig. 2.5).
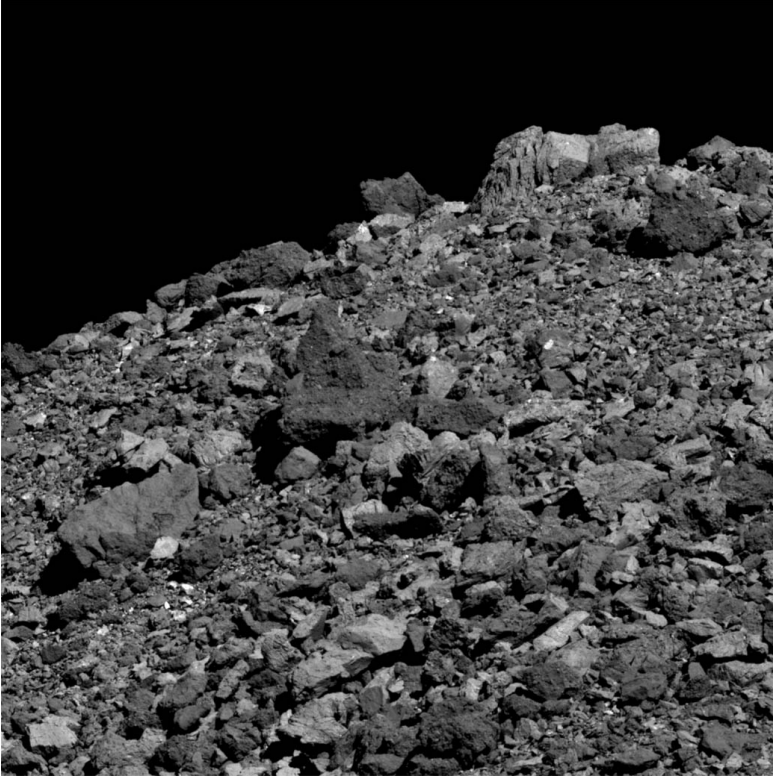
Figure 2.5: Image taken by the OSIRIS-REx spacecraft of the surface of (101955) Bennu. Credit: NASA, Goddard Space Flight Center, University of Arizona.

Elements and minerals in the early Solar System as a whole were also differentiated: the lighter elements and minerals would be more common in the outer Solar System, while the denser metals and silicates would be clustered in the inner Solar System. This would explain the abundance of stoney and metallic asteroids in the near-Earth environment, and the presence of gas giants in the outer Solar System. Temperature decreases the further away from the center of the system, and beyond a certain distance, gases would cool down enough to deposit into solid ices. Known as the "frost line", the distance for our Solar System was around 2.7 AU (right in the middle of the current Main Belt) [19]. We can observe these ices melting and vaporizing or sublimating as they come close to the Sun.

Asteroids' physical and chemical properties can be determined using telescopes from Earth's surface. Physical properties, i.e. mass, size, shape, and spin, can be determined remotely, but it is difficult. Mass can be determined if two asteroids (or a spacecraft) pass by each other [20]. It can be challenging to isolate the effects an asteroid's size plays on its

overall albedo (other factors include thermal, geometric, and composition). An asteroids exact size can be determined during a stellar occultation [21]. Occultations used to be difficult to predict, but with release of Gaia data, has become relatively easier to find an occultation in reasonable time. Size can also be estimated by studying an asteroid in thermal IR [22]. Shape and spin can reliably be estimated by studying an asteroid's light curve, its brightness over a relatively short time (minutes to hours) [23]. A simple peak-to-peak measurement can determine an asteroids rotation rate, but a complex inversion needs to be performed using multiple sets of observations from different viewing angles to derive a shape.

Asteroids both spin and tumble, mostly about their primary axes. If the momentum vector is not colinear with the spin vector, the object "tumbles" or experiences sharp and sudden changes in surface velocity. The spin for most objects was most likely generated during the formation of the object, as each addition of mass followed an elliptical trajectory (not straight down the center of mass) on its way to the parent body. Spin can be generated by collisions as well. The Yarkovsky effect can also influence an object's spin state, known as the Yarkovsky–O'Keefe–Radzievskii– Paddack (YORP) effect, usually affecting smaller bodies moreso than larger ones. A spinning asteroid can cause material to slide down to the equator, causing a build-up of material. If the asteroid begins to spin too quickly (i.e. faster than the escape velocity), loose material may be ejected from the system entirely. Alternatively, asteroids can acquire moons, such as the (65803) Didymos system.

The YORP effect can be so strong over time that the centripetal force of an object will rip the object apart, especially in objects with relatively weak cohesive strength (e.g. rubble piles). We can observe that there is a limit to the rotation rate of large objects, driven by the cohesive strength; any large objects that spun faster than the limit broke up and are thus unobservable (see Fig. 2.6). We can see a horizontal line at a rotation period of roughly 2 hours that seems to be the limit of large body rotations. The population above that line mostly have H> 20, which corresponds to a diameter of 300 m or less. These "fast rotators" must have a cohesive strength stronger than gravity alone.

One of our best tools for studying asteroids composition and structure are meteorites: asteroids and comets that make it to Earth's surface without burning up in the atmosphere. The Meteoritical Society has a database that lists over 65,000 known meteorites that range in size from less than a millimeter to several meters. In general, they are classified based on their composition and structure. To the layman, that is: stony, iron, or stony-iron; a more accurate classification, based on [24], would be chondrite, achondrite, and primitive-chondrite. Chondrites are unaffected by melting or differentiation. Achondrites show evidence of those processes from a parent body (differentiated asteroid, planet, or moon) before being ejected into space. Primitive chondrites are similar to achondrites, but their parent bodies must have been very chondritic, and thus form some kind of hybrid.
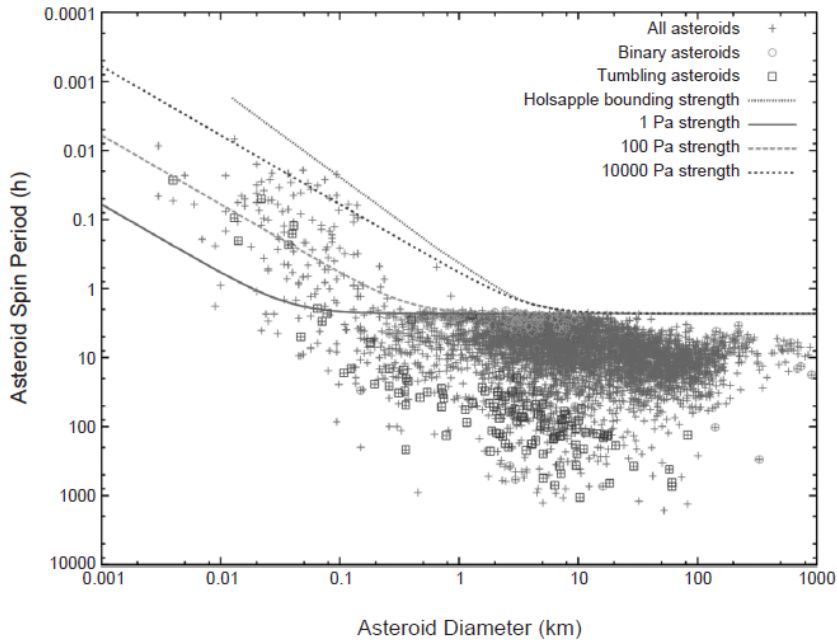
Figure 2.6: Distribution of spin rates of asteroids by size [25].

2.3   Surface Properties

For most asteroids, the only information we have on what the object looks like is a single point (how bright the object is). It is rare that an asteroid gets close enough to Earth to discern shapes and surface features, so most of the detailed data we have comes from spacecraft flybys and rendezvouses. The first asteroid to be studied with a flyby spacecraft was main-belt asteroid (951) Gaspra, by the Galileo spacecraft in 1991. From a 5300-km distance, the ∼12-km asteroid looks like it has a smooth surface, with some craters visible (see Fig. 2.7). Composition data confirmed remote observations and studies of the craters confirmed the theory that Gaspra has a lot of regolith, though its strength could not be determined (hard packed or fluffy).

Figure 2.7: Mosaic image of (951) Gaspra taken by the Gallileo spacecraft at a distance of 5300 km. Each pixel is roughly 54 m^2. Credit: NASA/JPL.

The next step forward in surface analysis was the encounter with NEA (433) Eros by the Near-Earth Asteroid Rendezvous (NEAR)-Shoemaker spacecraft in 1998. NEAR entered into an orbit around Eros, which allowed for unprecedented closeups and high resolution imaging of an asteroid's surface. The surface contains a variety of features, ranging in size from an 18-km trough/ridge to fine grooves and boulders on the order of one meter [26]. The only way these cracks and ridges could form is if the parent body were solid and strong enough to transfer the stress of an impact throughout the body. Evidence of regolith drainage in craters suggests there are tens of meters of regolith on the surface. NEAR-Shoemaker eventually landed on the surface of Eros (see Section 3.4 for more details) and sent back images showing the surface is littered with boulders at varying stages of burial (Fig. 2.8). Boulders and rocks become buried by regolith that is tossed up during an impact event. Boulders that do not appear too buried must thus not have been on the surface very long.
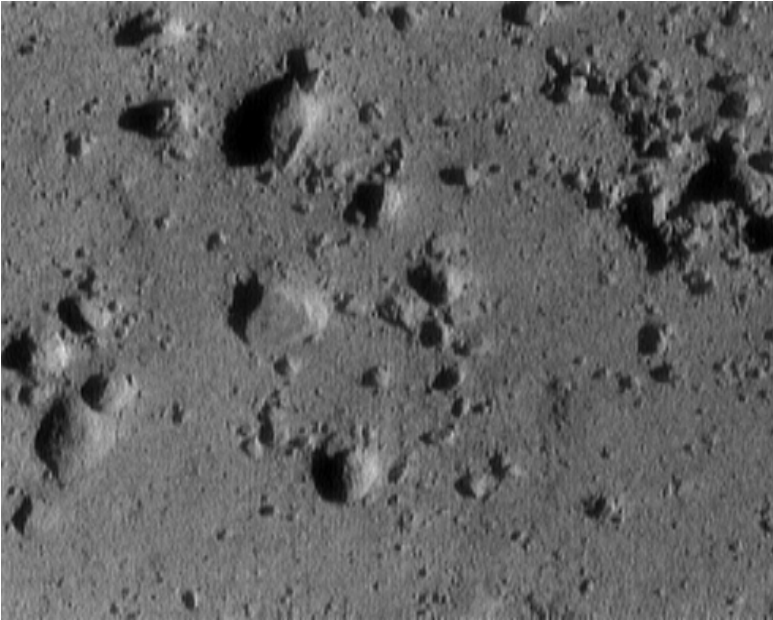
Figure 2.8: Image taken by the NEAR-Shoemaker spacecraft during its descent onto the surface of (433) Eros. The distance from the surface is 250 m, and the picture width is 12 m.

A huge advance in asteroid exploration was the return of a sample of one back to Earth. The Hayabusa mission achieved this by visiting NEA (25143) Itokawa in 2005, taking a sample of roughly 1,500 dust particles, and returning it to Earth in 2010. Itokawa is relatively small, compared to Gaspara and Eros, only 500 m end-to-end. The surface

was covered in boulders and cobble, which was a surprise, due it its small size (see Fig. 2.9) [27]; the surface also, surprisingly, contained regions of fine (sub-centimeter) regolith. The lack of any ridges or grooves, or of any significant crater formations suggest that the asteroid is a rubble pile. The regolith and boulders appeared to have a mass gradient (large boulders at the tips to regolith near the middle), most likely due to the fact that smaller regolith has less friction, and found its way to the center of the object from seismic forces from the initial formation impact. Analysis of the returned samples show no signs of melting, some round edges, and overall are different in size and shape than that of lunar regolith [28]. The regolith is thought to have formed from impact events, and over time, seismic forces erode some edges.
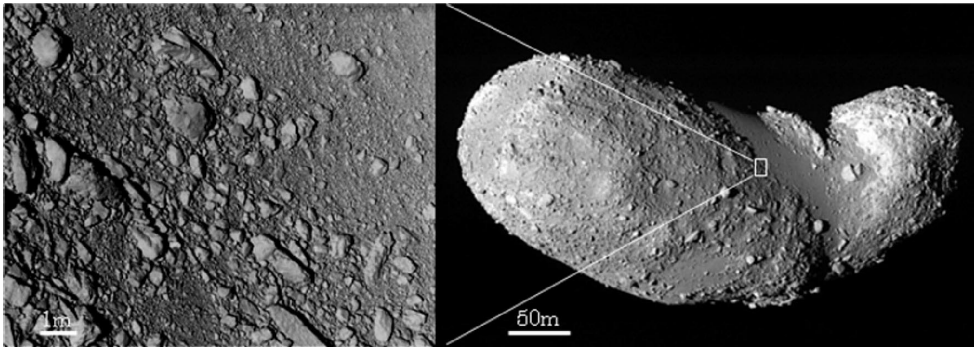
Figure 2.9: Close-up of the surface of (25143) Itokawa taken by the Hayabusa spacecraft as it was approaching for a sample. Credit: [29].

The Hayabusa2 mission recently returned collected samples from (162173) Ryugu, an 800-m C-type NEA, in December 2020. Previous observations suggested the surface consisted of mostly regolith, but Hayabusa2 revealed a jagged surface, completely covered with cobble and boulders (see Fig. [30]. This object is most likely a rubble pile. An analysis of one boulder, assumed to be representative of a majority of the whole asteroid, showed that it had a very low thermal albedo, much lower than that predicted from remote observations, and that the boulder was highly porous with weak cohesive strength. This confirms the idea that most carbonaceous meteors burn up in the atmosphere, leaving a biased collection of meteorites.

The OSIRIS-REx mission visited NEA (101955) Bennu, a 500-m B-type asteroid (that is, a carbonaceous chondrite that has a slightly blue reflectance spectrum) in 2018, took a sample in 2020, and is currently on its way back to Earth. Similarly to the Hayabusa2 team, the scientists behind OSIRIS-REx expected large swaths of regolith for their sampler, but were surprised to find it mostly covered in cobble and boulders [31]. It has been observed to be an "active asteroid", which is an asteroid that ejects gas, dust, or rocks like that of a comet, but on a much smaller scale (see Fig. 2.11).
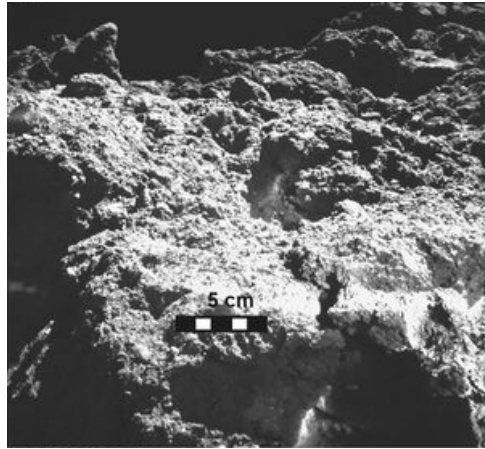
Figure 2.10: Image of the surface of NEA (162173) Ryugu taken from the MASCOT lander, part of the Hayabusa2 mission [32].
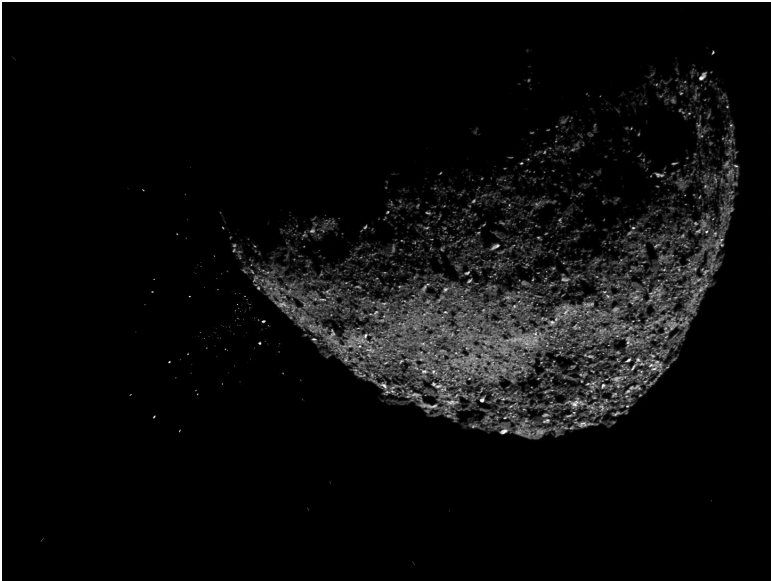
Figure 2.11: Evidence of activity on NEA (101955) Bennu. Credit: NASA/Goddard/University of Arizona/Lockheed Martin.

2.4   Minerals

The chemical properties of an asteroid (what materials it is made of) can be determined remotely. It is primarily done by studying reflected sunlight at different wavelengths, and then comparing the relative intensities to calibrated samples we find on Earth (including meteorites). We find that over 60% of NEAs are "S-type", containing mostly siliceous materials and roughly 20% of NEAs are "C-type", or carbonaceous [33]. Two of the most common minerals we assume are present on these types of asteroids are olivine and pyroxene [34]. Serpentine-group minerals are the most common hydrated minerals in meteorites [35]. In my research, I decided to focus on these three minerals.

Olivine is a mineral that is thought to be the most abundant mineral in the inner Solar System. It makes up a majority of Earth's mantle, and dominates the reflectance spectrum of a majority of S-type and C-type NEAs. Its chemical formula is M_2SiO_4 and it crystallizes in the orthorhombic system (M stands for metal). In general, olivine has a hexagonal array of oxygen ions with metal ions occupying the octahedral sites; it also contains occasional SiO_4 tetrahedra. The two most common metals are iron and magnesium; when it contains mostly iron, it is called "Fayelite", and when it contains mostly magnesium, it is called "Forsterite". A spectral response in the NIR-range is shown in Fig. 2.12; olivine has a characteristic absorption band at 1 µm.

Pyroxene is a more complex silicate mineral, but is also very abundant in the inner Solar System (including NEAs). Its general formula is $M_1M_2Si_2O_6$ and forms chains of SiO_4 tetrahedra, with metals (M_1 and M_2) in between. The three most common metals in pyroxenes are calcium, iron, and magnesium (the nomenclature of which forms the "pyroxene quadrilateral". Due to the fact that the mineral forms chains, it has intersecting cleavages (planes where the mineral usually breaks) at roughly 87°and 93°. Pyroxene has characteristic absorption bands at 1 µm and 2 µm (see also Fig. 2.12).
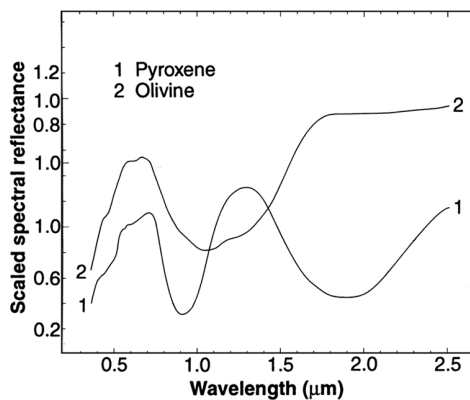

Figure 2.12: Reflectance spectra of lunar olivine and pyroxene. Adapted from Foing et al., 2004 [36]

Serpentine is the name given to a group of minerals that have undergone the process of hydrothermal metamorphism to include water or hydroxyl groups. This could have taken place in asteroids in the early Solar System, when the protoplanetary disc was still warm. The general formula is $M_3Si_2O_5(OH)_4$, with the two most common metals being iron and magnesium. The crystal structure can vary greatly, but ultimately consists of sheets of tetrahedra and octahedra.

The three minerals can be compared under cross-polarized light to show their characteristics (Fig. 2.13. The colored tiles in olivine are in fact the olivine crystals; their colors vary depending on the angle relative to the camera. The dark spots are solid pieces of iron. The pyroxene image shows cracks on the right half of the sample, which are, as mentioned, the characteristic cleavages. The serpentine sample appears more diverse and smooth, compared to the other two minerals.
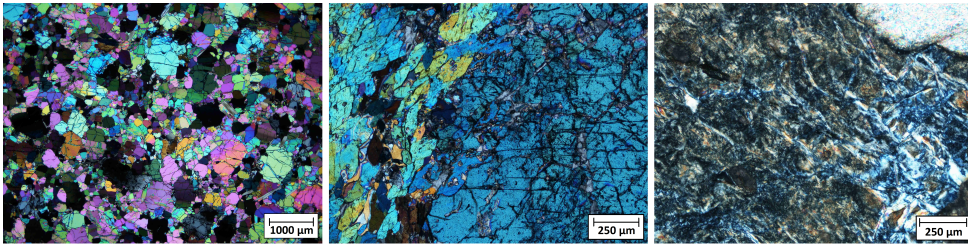
Figure 2.13: Thin-slice segments viewed with cross-polarized light of olivine (left), pyroxene (middle), and serpentine (right).

Space weathering alters the surface composition via a number of ways such as interaction with solar wind and UV radiation. In the context of resource extraction, it is vital that the bulk (or at least sub-surface) composition be determined before an asteroid can be selected as a mining target. For instance, it was recently confirmed that (1) Ceres has a considerable amount of water ice in the pores of its regolith [37]. That was made possible with the DAWN mission's GRaND instrument, which measured the hydrogen content of the upper-most few decimeters of the surface over the course of five months.

2.5   Deflection and Redirection

Moving an asteroid is no easy task, and there are numerous suggestions on how to accomplish this. The methods can be grouped into two categories: deflection of Potentially Hazardous Asteroids (PHAs) and redirection of profitable ones. While the words are often used interchangeably, they do not mean the same thing; when we consider deflecting an object, the only thing that matters is changing the orbit as fast as possible and as much as possible. Redirecting implies the slow and controlled movement of an asteroid to a desired location or orbit (this can include the movement of a PHA that is expected

to collide with Earth far in the future). The selection of a method depends on a number of factors, such as size/mass, composition/structure, and time of detection. The time of detection determines how much delta-V is necessary to change an asteroid's delta-V, regardless of the other factors.

The result of the application of delta-V to an orbit is heavily dependent on two factors: the first being at what point in the orbit the delta-V is applied, and the second being the direction that delta-V is applied. The simplest model of an asteroid redirection analysis would be an optimization of the two-body problem. Even in this model, the optimization (i.e. minimization of delta-V required to divert an asteroid by a specific distance at a certain point) is quite involved and non-intuitive [38]. What is apparent is that for Earth-crossing asteroids detected more than one orbital period (of the asteroid) in advance, the optimal point in the orbit for delta-V application is at the earliest possible perihelion; the ideal direction of application of delta-V is near-parallel with the velocity vector. Using a similar model, an estimate for the required delta-V to deflect a PHA by one Earth radius by year is given as 7 cm/s divided by the number of years in advance the asteroid is deflected (e.g. an asteroid deflected 3 years in advance would require only about 2.33 cm/s of delta-V to avoid collision) [39].

A tested deflection method is kinetic impactor, operating on the principle of a collision and momentum exchange, thus a change of trajectory. The strengths of this method are its simplicity and ability to impart momentum instantaneously at a desired point. Though not its primary purpose, the Deep Impact mission demonstrated that a spacecraft can be used to alter the trajectory of a comet. The 370-kg impactor was travelling at 10.3 km/s relative to comet Tempel 1 when it made contact, which had an equivalent delta-V of 56 µm/s. The Double Asteroid Redirect Test (DART) mission, scheduled for launch in July this year, will also demonstrate the kinetic impact method of (65803) 1 Dimorphous, the smaller moon of (65803 Didymos) (see Fig. 2.14). If the direct momentum exchange from a spacecraft alone is not sufficient, a spacecraft can be used to alter the trajectory of a smaller NEA, which would then collide with the primary body, resulting in a larger momentum exchange than could be provided by the spacecraft alone [40].

Another deflection method would be using explosives, most likely nuclear. There are numerous ways that this can be implemented: a high-velocity collision, a remote detonation, or landing the payload on the surface. The first is difficult to implement due to the relative velocity (up to 60 km/s); as of 2013, the maximum velocity of state-of-the-art nuclear detonation is 300 m/s; anything faster prematurely destroys the fusing mechanisms [41]. There is also not a stark difference in resultant delta-V change between remote detonation and landing the payload [39]; the decision is dependent on how confident mission operators are on landing technology and/or if there is a weak point that can be exploited. An explosion has the potential to fragment the parent body, whether intended or unintended, depending on the size and structural strength of the asteroid.

There are a number of redirection methods, each with their own strengths and weaknesses. An up-to-date analysis of gravity tractor, ion beam shepherd, laser ablation, tugboat, and mass driver is presented in [42]. I will briefly describe each method.
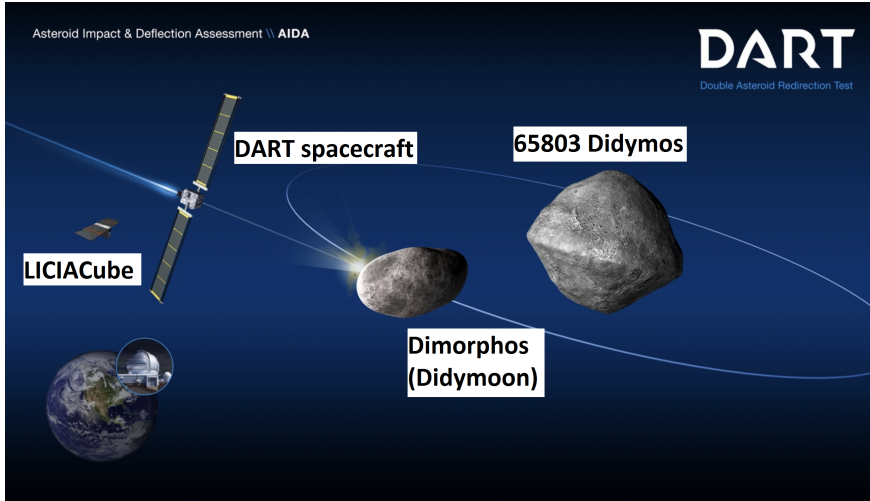
Figure 2.14: An overview of the DART kinetic impactor test.
Credit: NASA/Johns Hopkins Applied Physics Lab

Gravity tractor is the concept of keeping a spacecraft in a specific position near an asteroid. The attractive force due to gravity will "pull" on the asteroid towards the spacecraft. The spacecraft will feel the same force, and must thus use thrusters to maintain its position. It does not require any technology development, but does require a relatively large amount of fuel and the force decreases over time as the spacecraft uses the fuel. The more massive the spacecraft, the more force it can exert on an asteroid, which has the trade-off of launch costs.

Ion beam shepherd involves using the exhaust of an ion thruster to exert a "pushing" force on an asteroid [43]. The spacecraft must have a diametrically opposed thruster to prevent it from flying away from the object, and thus consumes a considerable amount of fuel. It has been estimated that the spacecraft could be an order of magnitude less massive than an equivalent gravity tractor. A preliminary design procedure framework has been developed which specifies a feasible mission based on a number of parameters such as target mass, separation distance, power requirements, etc [44].

The tugboat method involves landing a spacecraft on an asteroid and using thrusters to push the asteroid in a desired direction [45]. It would nearly half the fuel required by the ion beam shepherd, but does require complex landing (and anchoring) equipment as well as precise placement and thrust vector alignment. Another challenge is the rotation of the asteroid; unless the force vector is in line with the asteroid spin vector, energy that would be used to push on the object is instead used to spin or tumble the asteroid. Getting power to the thruster would also be a challenge depending on the spin and location of the tugboat relative to the Sun.

The remaining two methods involve removing asteroid material beyond escape velocity to impart momentum. A mass driver is a spacecraft that lands on the surface, digs up and processes materials that are then launched from the surface in a desired direction. This method would require little to no fuel, but very complex landing and processing/launching equipment, which, as of 2020, is at a very low technology readiness level.

And finally we come to the ablation method. The first mention of using ablation to redirect an asteroid was in 1993 [46]; a spacecraft with enormous solar collectors (a variation of solar sail technology) would be used to focus sunlight on a small meter-sized spot on the surface of an asteroid. The material would rapidly sublimate causing the escaping gas to create a momentum exchange (see Fig. 2.15). The solar collector can be replaced by solar panels and a laser [47]. This method is discussed in detail in Section 3.3.
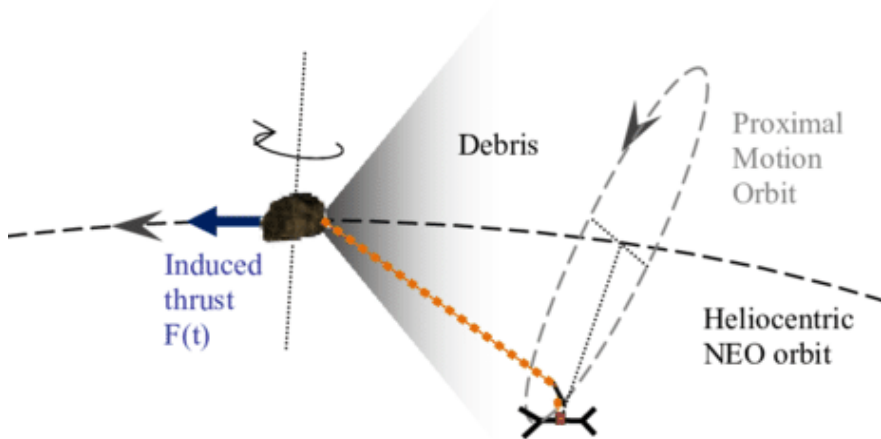
Figure 2.15: A model of a laser-ablation redirection method. Credit: Gibbings et al., 2011 [48].

2.6   Mining

To-date the only way humanity has been able to build things in space has been to bring the raw materials with them from Earth's surface. This gets prohibitively expensive as the total payloads increase in mass: the well known Tsiolkovsky rocket equation shows us that the fuel requirements increase logarithmically. There have been numerous theorized solutions to this like using an electromagnetic rail launcher or building a space elevator, each with their own unique advantages and challenges. Another popular solution is to

source the materials required in space *from* space itself, whether that be from the lunar surface or asteroids.

One of the most valuable things that is desired in LEO is rocket fuel. The United Launch Alliance (ULA) has publicly stated they are willing to pay $3,000 USD per kilogram of fuel available in LEO, part of their roadmap to the cislunar economy (Fig. 2.16). The most likely fuel will be derived from pure water. It can be electrolyzed into hydrogen and oxygen, which can be burned together in an engine to produce thrust. Water has several other uses as well, regarding human habitation of space. Potable drinking water, breathable oxygen, and radiation shielding.
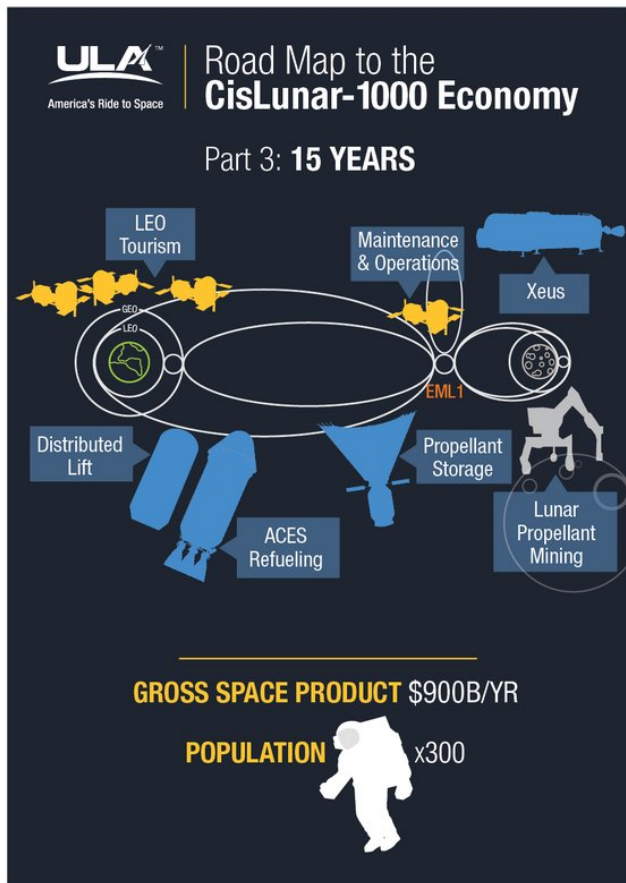
Figure 2.16: Part 3 of ULA's roadmap to space, showing a space architecture where propellant is mined from the Moon. Credit: ULA.

Metals are also desirable in LEO. Iron, aluminum, and titanium can be used to construct large structures that cannot fit inside a rocket's payload fairing. Gold and platinum can be used in creating complex circuitry or catalysts. Silicates can be used to make semiconductors and carbonaceous asteroids can source carbon for fuel or food. If rare earth metals can be found in asteroids in considerable volumes, it could alleviate the need for dangerous jobs involved in mining and processing it here on Earth. So the desire for asteroid mining is present, the question is: how do we do it?

Asteroid mining can be broken up into five phases: prospecting, excavating, processing, refining, storing. Prospecting is the process of locating valuable materials on and inside an asteroid, as well as how much there is, and in what form (for instance, water can be in the form of ice or hydrated minerals). Excavation is the removal of the raw materials from the asteroid, terrestrially this involves using digging machines or explosives. Processing is a sort of middle-step which takes the raw excavated materials and turns them into something that can be refined, i.e. turning large rocks into smaller ones. Refining is the process of turning the processed materials into useful materials, like producing an iron ingot from iron ore pieces. Finally, the refined material needs to be stored and transported to a useful location.

Prospecting has a relatively higher technology readiness level. As mentioned, we are currently categorizing asteroids based on their reflectance spectra from Earth, which is a good start. But again, in order to determine if a particular asteroid is worth mining, a spacecraft needs to be sent to it to determine its physical and chemical properties in detail. For instance, the Gamma Ray and Neutron Detector (GRaND) instrument on the DAWN spacecraft is capable of remotely measuring the hydrogen content of the uppermost meter of a celestial body [49]. This, combined with other data such as infrared spectroscopy can be used to estimate the amount of water or hydroxide in the surface.

Excavation has a relatively lower technology readiness level; it is challenging for a spacecraft to land, operate moving parts, and remain attached to the surface while processing in a micro-gravity environment. A majority of non-terrestrial excavation technologies are focused on planetary uses, such as the Moon or Mars. These can include typical shovels and scoops, drills and cutters. The Colorado School of Mines is exploring a method of asteroid material excavation which uses concentrated sunlight [50]. This process has also been replicated with lasers [51].

Refining in zero gravity is again a challenge. For instance, in terrestrial iron processing, iron ore is melted in a giant pot; gravity pulls the heavier iron to the bottom, while the slag floats to the top. In a micro-gravity environment, there is no force to separate the molten slag from the pure iron. It has been shown that ices can be produced from volatile gases extracted from heating asteroid stimulants using cryogenic condensation [52].

Processing and storage/transportation are almost forgotten when considering the state of the art in asteroid mining. Typical grinders (turning large rocks into smaller ones) use gravity to funnel and separate rocks by their sizes. In zero gravity, it is likely that any destructive force would send a rock flying away, so containment is a challenge. There is also little developments in collecting processed materials and moving them into a storage container on board a delivery system.

Laser Processing

3.1 Fundamentals

A laser is a device that produces coherent light, which can be focused to small areas, allowing for very high irradiance. Lasers have three primary components: an energy source, a resonating chamber, and the lasing medium. There are numerous types of energy sources, such as a lamp or an electric field, but their purpose remains the same: induce the the lasing medium to emit photons at a specific wavelength. The photons then bounce around inside the resonating chamber, which has a hole or lens on one side to allow the beam to form (Fig. 3.1).
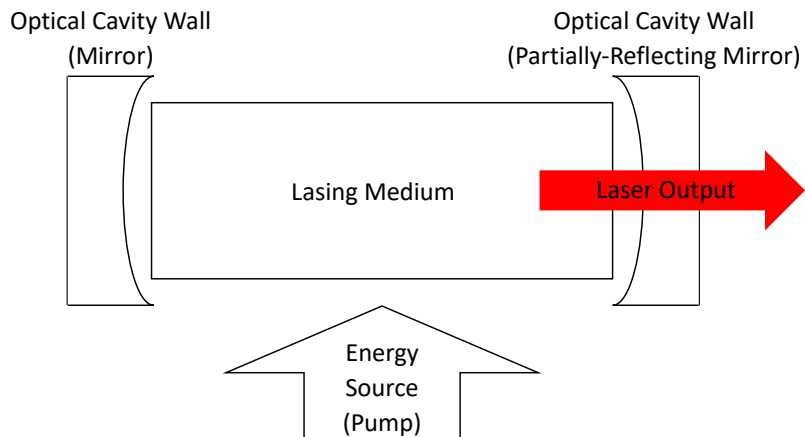
Figure 3.1: A simple model of a laser.

The resulting laser beam has the form of a "gaussian beam", meaning the transverse beam profile resembles a Gaussian function, though in reality it is not perfect. The beam is quantified by two components: the beam width (ω_0 in Fig. 3.2 below) and the divergence angle (Θ in Fig. 3.2). The beam parameter product (the product of the beam radius at the smallest point and the divergence angle) will always be maintained, which means a smaller beam width will thus have a larger divergence angle and vice versa. A system of mirrors, lenses, or optical fibers can be used to direct the beam from the source to the target with the desired power density (irradiance).
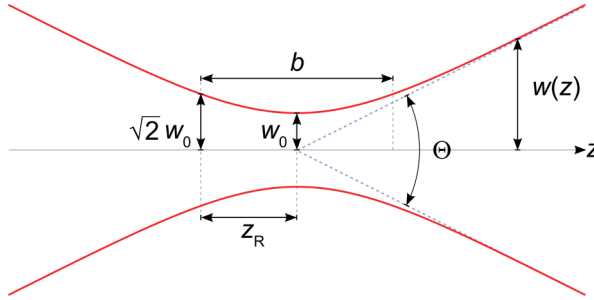
Figure 3.2: A simple model of a laser beam.

The lasing medium determines the laser's wavelength and how energy efficient it is (i.e. input power to output laser beam power). The first laser was fired in 1960, using a ruby crystal as a medium [53]. It was limited, though, by its energy efficiency, pulse width control, and complicated cooling system. In 1964, the first CO_2 gas laser was demonstrated [54]; it had better power efficiency, higher power levels, and was cheaper than using rubies. It produces infrared light at 10.6 µm, though the linewidth is relatively wide, since it is based on vibration/rotation energies, as opposed to direct electron recombination or de-excitation. They are still in use today, and remain the highest power continuous-wave lasers on the market. Another popular lasing medium in use today is Nd:YAG (Neodymium-Yttrium-Aluminum-Garnet) which produces light at 1070 nm. It was also first demonstrated in 1964, though remained prohibitively expensive until modern manufacturing techniques were developed [55]. Since the 1960s, laser technologies (pumps, media, optics, and cavities) have exploded in number, and the selection of a specific laser is highly dependent on the application. A plot of the reflectance spectra of some common metals with the wavelengths of a CO_2 and Nd:YAG laser is given in Fig. 3.3.

There are numerous space-related applications for lasers. Already in 1962, scientists studied reflected laser light from the lunar surface to determine the distance between the Earth and Moon [57]. Later, the astronauts on the Apollo 11 mission deployed retroreflectors on the lunar surface, which allowed for a stronger and more accurate return signal. Another use is for spacecraft attitude determination via instruments like the ring
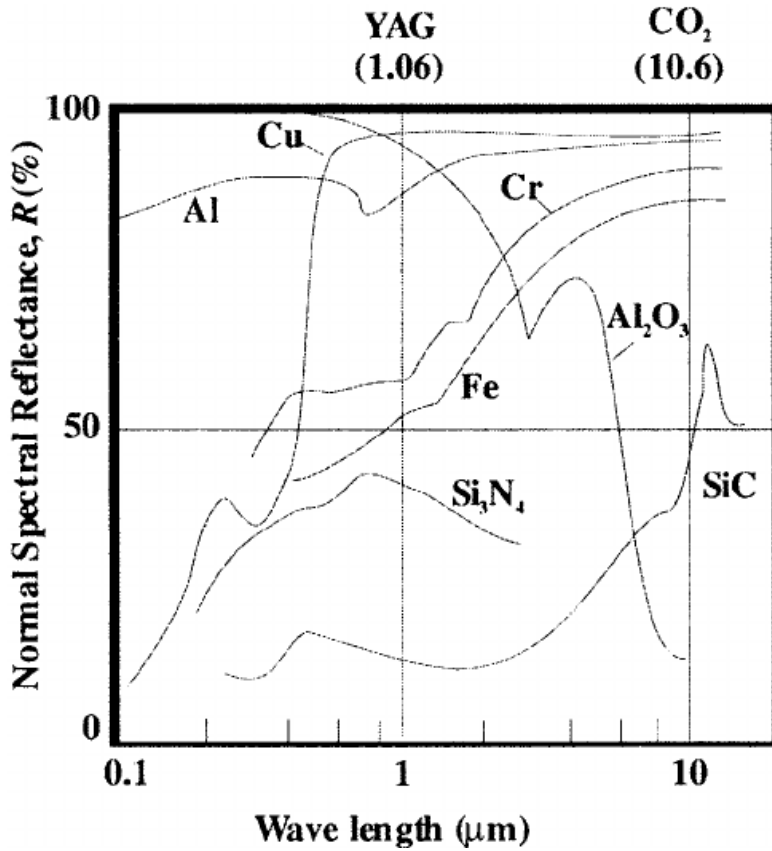
Figure 3.3: Normalized reflectance of several materials from 0.1 µm to 10 µm [56]. The characteristic wavelength of a Nd:YAG and CO_2 laser are shown as vertical lines.

laser gyroscope (gyro) and fiber-optic gyro. The first mention of a ring laser gyro was in 1963 [58], but the first mention of its use on a spacecraft was the 1996 Midcourse Space Experiment [59]. A third use is in communications: a laser has a relatively small beam divergence compared to typical radio antennae. This can reduce the power requirements for a spacecraft, and since laser beams are coherent, there is less noise compared to a typical radio system. JAXA first demonstrated a laser communication link in 1996 with their ETS-VI GEO satellite [60]. Another use is for composition analysis, which can come in two forms: laser-induced mass spectroscopy, like the LIMA-D instrument on board the Phobos 1/2 spacecraft [61], or Laser-Induced Breakdown Spectroscopy (LIBS) on board the Curiosity rover currently on Mars [62]. A similar process is also being suggested to determine asteroid composition using small satellites [63].

For the first case, Light Detection And Ranging (LIDAR) uses relatively low powers (not enough to alter the target surface) and millisecond pulses to perform time-of-flight calculations, which gives the distance between the laser and a target. Laser gyros use very low power, but continuous-mode lasers; they measure the phase change or frequency shift caused by rotation to estimate angular position and velocity. Laser communications also use relatively low powers (enough to be detected by a "camera") but pulse frequencies as high as 100 GHz. For composition analysis, a nanosecond-pulsed laser can be used to produce power densities high enough to vaporize a small portion of the surface material of a target. The vapor is then ionized by the laser beam, which can be measured by a number of instruments. For laser-induced mass spectroscopy, the ions are collected and subjected to an electric field; this causes the ions' trajectory to "bend" and collide with a detector. The intensity of the electric field, combined with the charge of the ion will only allow a particle of certain mass to pass through, thus determining the composition. In LIBS, the ions are not collected, but the plasma is allowed to cool. As the plasma cools, electrons recombine with ions and emit characteristic photons depending on what quantum state the atom is occupying (Fig. 3.4). The novel method mentioned in Moura, et al. 2018 [63] measures composition by creating a plasma, and measuring the dips/gaps in the spectrum. These gaps are caused by the chemicals present in between the plasma and the detector, which absorb the light from the plasma.
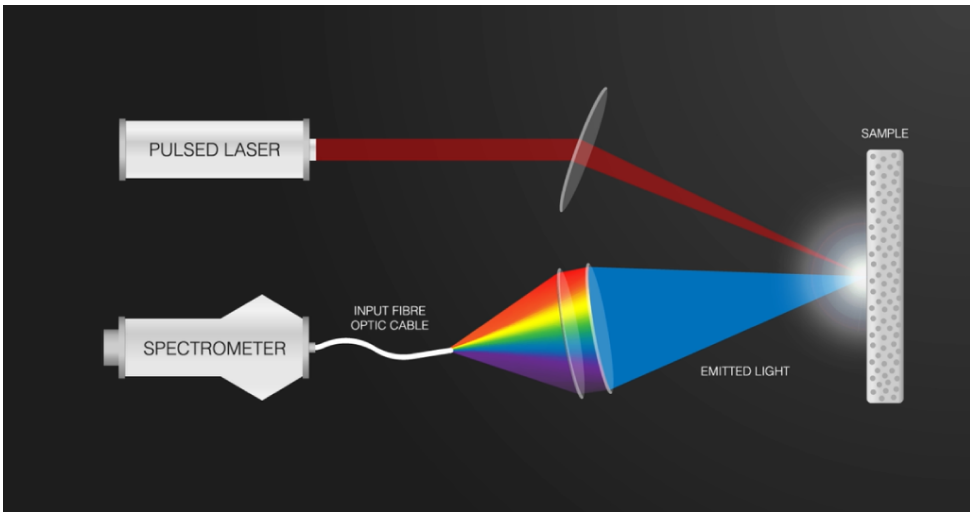
Figure 3.4: Simple model of the LIBS process. Credit: Mikko Jarvikivi.

It thus seems there is a gap in laser parameters in the range commonly used for domestic laser cutting/welding/drilling (i.e. high powers in the millisecond pulse to continuous range).

3.2 Drilling

The first patent for using a laser to drill holes was filed in 1964 [64] and the fundamental model of laser drilling was presented in 1965 [65]. The system can be modeled as a balance between the incoming laser energy and the sum of heat conduction into the target, phase changes, and plasma absorption (Fig. 3.5). For any material, a certain ratio of light will be reflected or absorbed. Things that can affect this number are the smoothness of the surface, the composition of the material, the light incidence angle, and the wavelength(s) of the light. The absorbed energy begins to increase the local temperature, and diffuse through the target. Once the temperature is high enough, the material will begin to melt, which will sputter away. As the temperature climbs even higher, the melt will begin to vaporize, creating a cloud of gas above the spot. This vapor will begin to absorb the incoming laser energy, preventing some of it from interacting with the target below. As material is removed, the laser beam begins to de-focus; eventually, the system enters a state of equilibrium, where the laser beam intensity is so low, that it can only keep a melt pool warm at the bottom of the hole. If the laser penetrates the target, it is known as "piercing", a process first studied in 1973 [66].
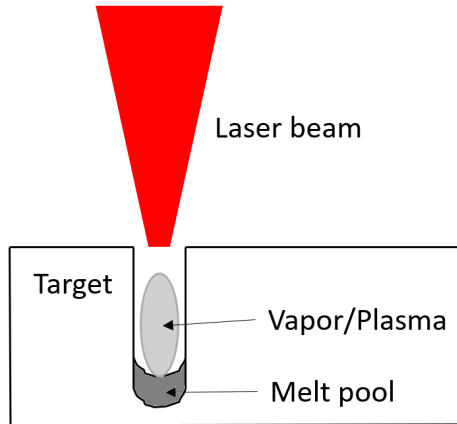
Figure 3.5: A simple model of laser drilling.

The laser can be operated in a number of ways. Assuming the laser and target remain fixed (not moving relative to each other), there are two modes of operation: continuous or pulsed. The continuous mode can be thought of as one long pulse, where the laser is turned on and left on until the laser penetrates the target. The pulsed mode (known as percussion mode when considering laser drilling) uses pulses in rapid succession, attempting to avoid power losses via vapor absorption. Proper selection of

pulse parameters (length of pulse, and repetition rate) can increase the drilling efficiency by a factor of 27 [67]. Assuming the target is allowed to move (or the laser beam steered with special optics), more modes of operation become available. For instance, trepanning, where the laser is operated in a pulsed mode, but each successive pulse is re-positioned in a circular motion to create a hole larger than the spot size with smoother edges and less burr [68]. Here we begin to move from a drilling process to a cutting process, however.

A well-known model of laser drilling was developed in 1976 [69]. The model included the expulsion of molten material, and was capable of calculating the depth penetration rate and energy efficiency. Their experiments were focused on finding the effects of intensity of drilling rate in copper, in the range of 1 MW/cm^2 to 100 MW/cm^2. They used a Nd:YAG laser capable of producing pulses from 0.1 µs to 100 µs. They found that in terms of efficiency, there is a range of intensities that produce consistent results: between 5 MW/cm^2 and 50 MW/cm^2. Below $\sim$ 5 MW/cm^2, the drilling efficiency is low due to heat conduction and reflection losses, and above $\sim$ 50 MW/cm^2, vapor absorption and air breakdown begin to hamper results. They found a peak drilling efficiency of roughly 50×10^{-6} cm^3/kJ.

High speed imaging (HSI) has been a powerful tool in stuyding the processes that occur during laser irradiation. The research in *Pocorni et al. 2017* [70] studied the piercing process in detail with HSI using a unique emissivity filtered observation setup. They were able to observe the behavior of the melt pool produced in the piercing process and the effects that changing the pulse parameters had on its behavior. Researchers in *Schneider et al., 2007* [71] could study the effects of assist gas in laser drilling.

We studied the drilling process on samples of olivine, pyroxene, and serpentine. We used a 300-W Ytterbium fiber laser with a spot size of 0.1 mm, and operated the laser in both continuous and pulsed modes. We studied the process with high-speed imaging (HSI) and measured the resulting holes using X-ray MicroTomography (XMT). We explored 3 laser parameters and their effects on hole size and depth: power, pulse width, and repetition rate. The power settings varied from 100 W to 300 W, pulse widths between 1 ms and 16 ms, and repetition rates between 53 Hz and 500 Hz. Continuous mode experiments were run for over 350 ms.

We found a number of interesting phenomena. First, is that the drilling process changes over time. For olivine and pryoxene, the first few milliseconds of laser irradiation produced a rapid (over 200 m/s) outburst of small (sub-millimeter) pieces of material (see Fig. 3.6). The stream of ejecta had a relatively low divergence angle, and stopped after about 1.5 ms.
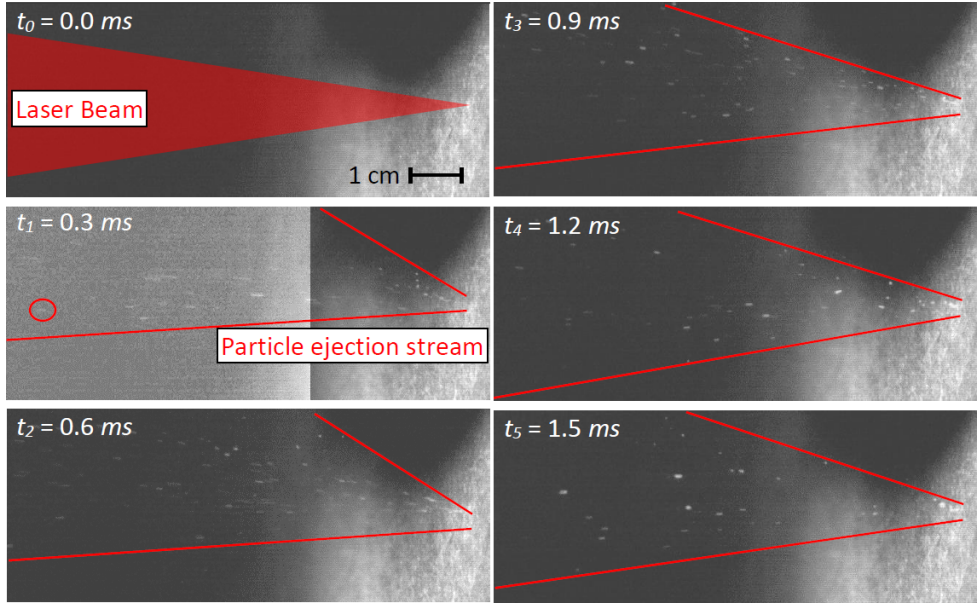
Figure 3.6: Frames from HSI of pyroxene experiment showing initial rapid outburst. The series shows the first 1.5 ms of a 4-ms pulse at 300 W.

After the first phase, all three materials began to show clear signs of melting and began ejecting molten material. At the point where the laser beam contacted the surface, a melt pool would form. The pool would undulate chaotically, depending on whether the laser was firing or between pulses. The surface tension of the melt pool would hold on to escaping material, making the angle of divergence greater than 90°(i.e. some molten spheres would re-deposit on the surface near the experiment site, even though the experiment was performed laterally. The progression of laser radiation on pyroxene, olivine and serpentine can be seen in Figs. 3.7 and 3.8, respectively.

Early   Middle   Late

t_0 = 9.9 ms t_0 = 43.9 ms t_0 = 94.6 ms

5 mm

t_1 = 10.6 t_1 = 43.2 t_1 = 95.0

t_2 = 11.3 t_2 = 43.5 t_2 = 95.4

t_3 = 12.0 t_3 = 43.8 t_3 = 95.8

t_4 = 12.7 t_4 = 44.1 t_4 = 96.2

t_5 = 13.4 t_5 = 44.4 t_5 = 96.6
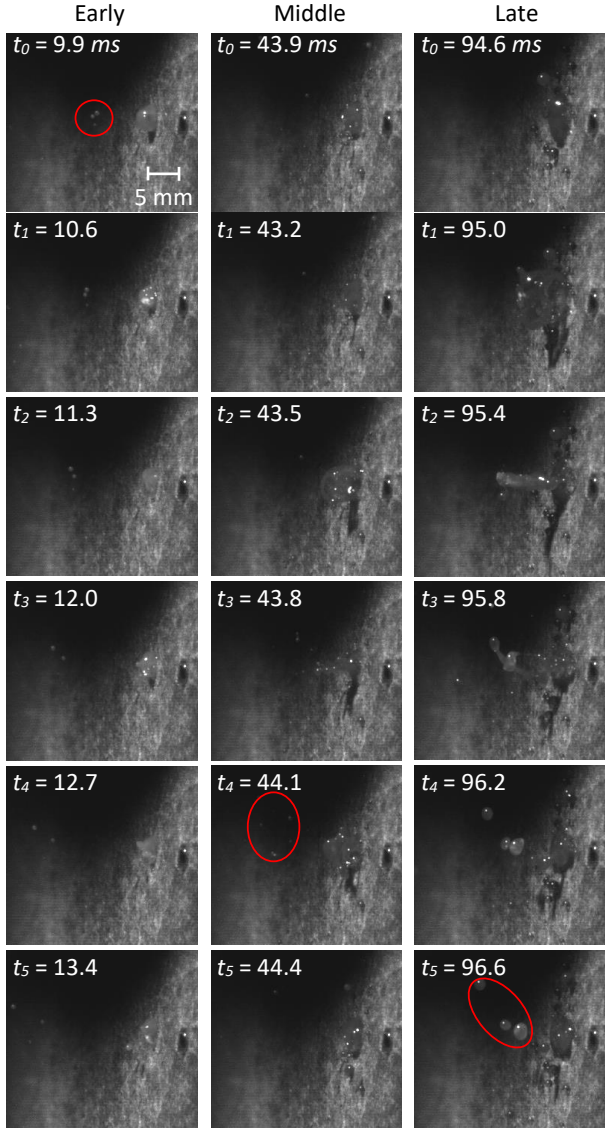
Figure 3.7: High-speed footage of pyroxene under laser irradiation over time. The pulse settings are 4 ms on and 1 ms off at 300 W. The red circles highlight the spatter for each series.
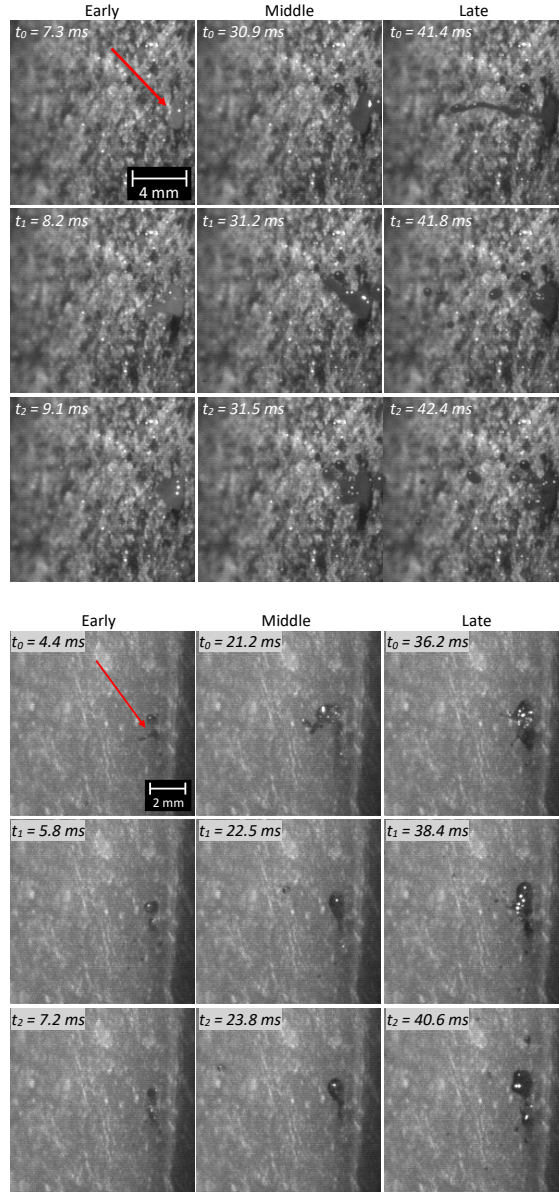
Figure 3.8: *High-speed footage of olivine (top) and serpentine (bottom) experiments over time. The power setting in both cases was 300 W, pulse length 8 ms, and pulse gap 3 ms.*

The resulting holes in all three samples were long and thin (see Fig. 3.9). We noticed a decreasing logarithmic relationship between total energy (i.e. laser power multiplied by total on time of laser) and hole depth. With as little as 16 J of energy, we were able to make a 9-mm-deep hole. Experiments using 100 J of total energy could not make holes deeper than 12 mm. This was most likely due to the defocusing of the laser beam over time. We also found a linear relationship between total energy and volume removed.
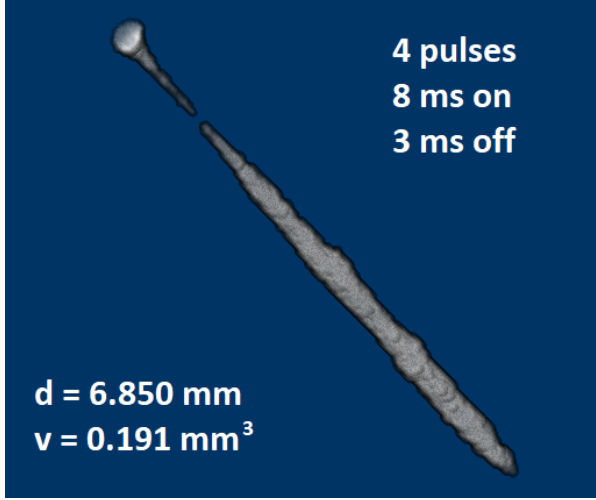
Figure 3.9: XMT rendering of hole produced in olivine. The laser power was 300 W, pulse settings given in the top right of the figure. Depth, d, and volume, v, are given in the bottom left.

3.3   Spallation

Laser ablation is a process of removing surface material using a laser to heat the substrate beyond its sublimation temperature. A model of the laser ablation process is presented in *Vasile et al., 2014* [72], which is augmented by experimental data [73]. The mass flow rate $\dot{\mu}$ is based on the equation developed in *Phipps et al., 2011* [74]:

$$\dot{\mu}[E_v + \frac{1}{2}(\bar{\nu}^2) + C_p(T_{sub} - T_0) + C_v(T_{sub} - T_0)] = P_l - Q_r - Q_c, \tag{3.1}$$

where P_l is the power absorbed by the laser (dependent on albedo) per unit area, Q_r is the power given off by radiation, Q_c is the power dissipated by conduction within the bulk material. The factor $[E_v + \frac{1}{2}(\bar{\nu}^2) + C_p(T_{sub} - T_0) + C_v(T_{sub} - T_0)]$ can be considered an "augmented enthalpy" where E_v is the latent heat of sublimation, $C_v(T_{sub} - T_0)$

is the energy required to increase the temperature of the target to the temperature of sublimation, and $\frac{1}{2}(\overline{\nu}^2) + C_p(T_{sub} - T_0)$ is the energy absorbed by the vapor/plasma produced by the process. The term T_{sub} is the sublimation temperature, T_0 is the original temperature, C_v is the specific heat at constant volume, C_p is the specific heat as constant pressure, and $\overline{\nu}$ is the speed of the ejected gas.

For the experiments performed in *Gibbings et al., 2013* [73], a 90-W, 808-nm laser was used in continuous mode. The power density at the surface was estimated to be between 1.69 kW/cm² and 2.44 kW/cm², and the experiment was run for 10 minutes. The authors noted that there was a brief period in the beginning of the experiment where some form of spallation or spattering occurred before entering their ablation phase (see Fig. 3.10). They ran experiments at power levels as low as 43 W, which would correspond to a total energy of 25.2 kJ; the other power level used was 62 W, which would correspond to a total energy of 37.2 kJ. They reported mass flow rates of 2.1×10^{-7} kg/s at the beginning of the experiment and 2.5×10^{-8} kg/s at the end. This corresponds to a total mass removed between 1.26×10^{-4} kg and 1.50×10^{-5} kg. Using a density for olivine of 3,500 kg/m³, we get volumes removed of 4.3 mm³ and 36.0 mm³, corresponding to volume processing efficiencies between 1.7×10^{-4} mm³/kJ and 14.3×10^{-4} mm³/kJ.
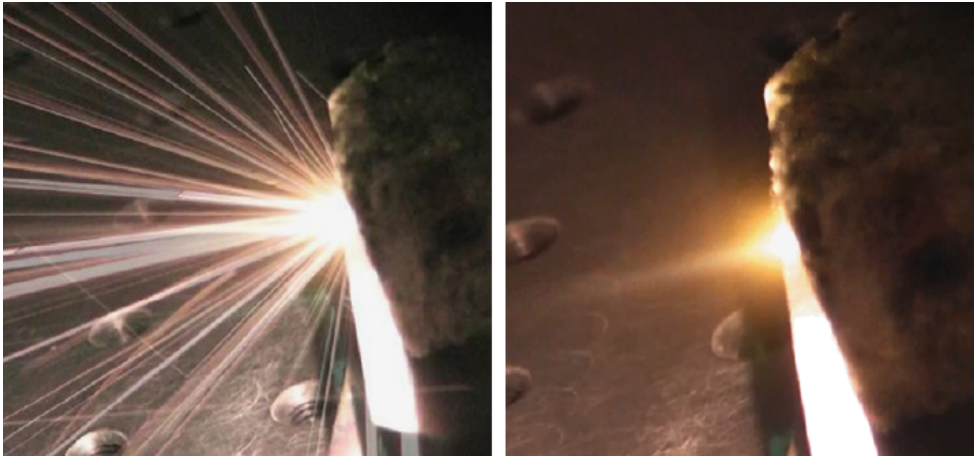
Figure 3.10: Images taken from beginning and end of experiments performed in Gibbings et al., 2013 [73]. The left image shows the ejection of small molten and solid pieces, and the right a steady-state plume of vapor/plasma.

For contrast, experiments performed in *Xu et al., 2003* [75] reported efficiencies up to 1.969×10^3 mm³/kJ. The authors of that paper were interested in finding the most energy efficient material removal power density, as opposed to modelling ablation. Their target materials were shale and sandstone, relatively brittle rocks, compared to olivine. They used a 1.6-kW Nd:YAG laser (1070 nm) at power densities less than 1 kW/cm².

They found that the power densities and pulse parameters that did not melt the material, but rather thermally fracture it (a process called spallation) are more energy efficient at material removal. This can be shown in their initial test (a linear track of varying power densities) in Fig. 3.11.
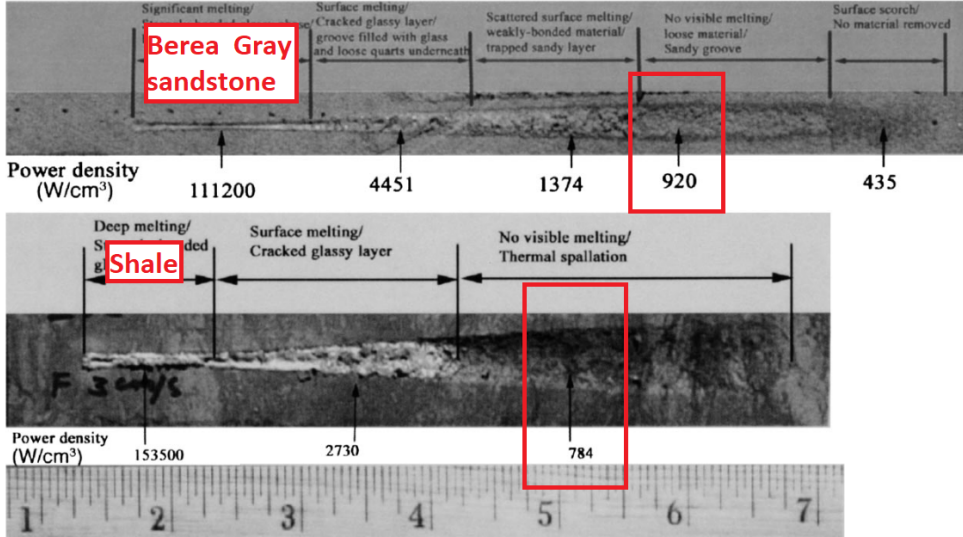
Figure 3.11: Linear track tests from [75]. Note the shown power densities are in units of W/cm^3, which is not correct. The true units are W/cm^2.

Experiments performed in *Sloane 2020* [76] used a 33-W average power laser in pulsed mode using 0.7-ns pulses at a repetition rate of 40 kHz for 500 ms. They had several different targets including aluminum, pyroxene, and several asteroid simulants (powders that are similar in composition to estimated asteroid compositions) that were compressed into bricks. They report average mass removal rates of 4.69 µg/s for aluminum, 0.41 mg/s for pyroxene, and between 5.87 mg/s and 13.53 mg/s for the simulants. Densities are not provided, but we know with certainty the density of aluminum, and can assume a density of 3.4 g/cm^3 for pyroxene. This gives us material removal efficiencies of 0.053 mm^3/kJ for aluminum and 3.65 mm^3/kJ for pyroxene.

I decided to apply the logic used by *Xu et al., 2003* [75] to minerals we expect to find on asteroids. The samples were again olivine, pyroxene, and serpentine, cut from the same source rocks. We assume they have the same reflectance spectra and general composition. In order to increase the accuracy of XMT measurements of the expected holes, some samples were sent to be scanned via XMT to have a reference shape. The other samples were used to find the laser parameters that produced spallation.

Since the rocks were relatively small, there was no room to do linear tracks. Instead, the laser was set to the lowest power, and a relatively short pulse (starting with 10 ms) was programmed, the process was viewed in HSI, and the laser settings were iteratively updated until spallation became clear. Olivine was the first test piece, as it had the most surface area. We found that, even at the lowest power settings, olivine was resistant to spallation, and tended to melt and sputter material directly. This could be due to the relatively uniform crystal structure and lack of cleavages.

We were able to induce very clear spallation in the pyroxene sample (see Fig. 3.12). This is most likely due to the fact our pyroxene sample had characteristic cleavages, and had much larger and differentiated clusters of minerals, as opposed to a homogeneous, tightly-packed structure like olivine.
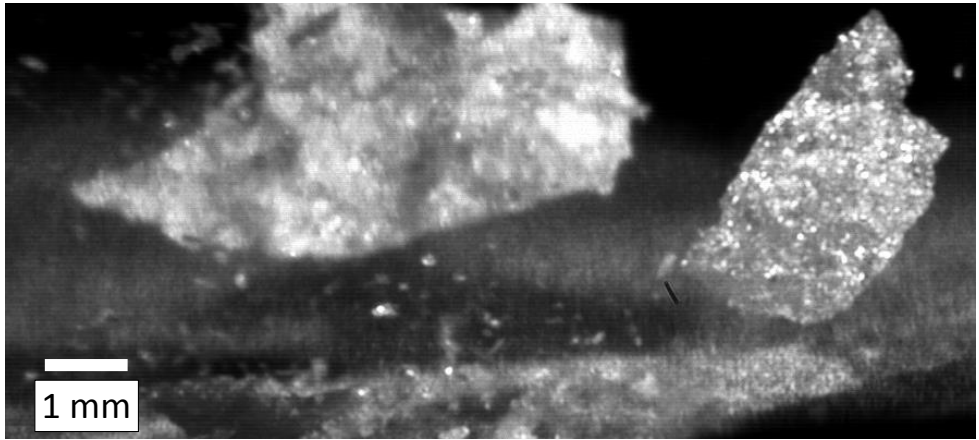
Figure 3.12: Frame from HSI of spallation experiment on a pyroxene sample. The laser parameters were 1500 W with a 1 cm^2 spot for 35 ms.

Serpentine showed behavior somewhere in between olivine and pryoxene. What I noticed was that it required significantly more power to induce any kind of behavior at all. I believe this is due to the fact that, in addition to having cleavages and relatively large and differentiated clusters of minerals similar to pyroxene, serpentine is a hydrated mineral. The water or hydroxyl groups can potentially divert heat away from the illuminated area much more efficiently than a drier mineral. Nonetheless, I was able to induce spallation for a short period, before the mineral melted and spattered (see Fig.3.13).
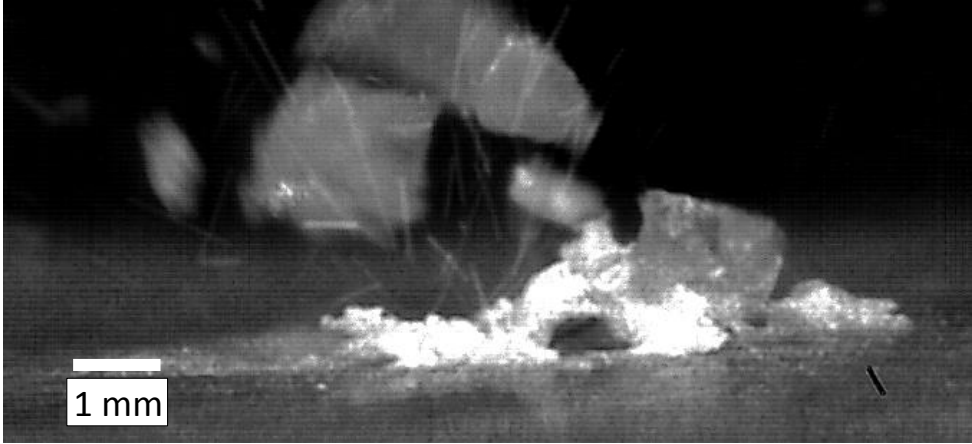
Figure 3.13: Frame from HSI of spallation experiment on a serpentine sample. The laser parameters were 13659 W with a 1 cm² spot for 30 ms.

XMT was used to measure the volumes of the holes/craters created by the laser, by subtracting the pre-experiment scans from the post-experiment scans. The olivine sample had relatively poor material removal, and was difficult to measure; two of the five experiments had measurement error bars larger than the estimated volume removed itself. For the three experiments that did have values, their volume removal efficiencies ranged from 0.6 mm^3/kJ to 14.8 mm^3/kJ. For the three spallation-driven experiments in pyroxene, the volume removal efficiencies ranged from 40.8 mm^3/kJ to 63.3 mm^3/kJ; the other two experiments had lower efficiencies: 23.5 mm^3/kJ and 33.3 mm^3/kJ. Serpentine had the largest hole of the three samples, but it was unsure which removal process dominated. Volume removal efficiencies ranged from 1.3 mm^3/kJ to 63.9 mm^3/kJ. In every case, the larger the hole, the more accurate the measurement. These results sit roughly in the middle between *Gibbings et al., 2013* [73] and *Xu et al., 2003* [75]. it is on par with *Sloane 2020* [76] and previous experiments [77].

In an ablation-dominant model such as the one in *Gibbings et al., 2013* [73], the speed of the ejected gas can be converted into a momentum change, and thus equivalent thrust, with a single equation. Ablation produces relatively high (km/s) gas velocities, which is greater than the escape velocity of any asteroid. In a sputtering/spallating-dominant model, the larger pieces are ejected at much lower velocities (m/s) which limits the size of the target asteroid to under 10 km in diameter. If the particles do not escape the asteroid's gravity well, they will fall back to the surface, negating any momentum gained from the laser in the first place.

Alternatively, one could directly measure force produced by laser irradiation, like the experiments performed in [76] and [78]. Both sets of experiments use ablation (i.e. vapor plume) exclusively in their models. In the first case, the authors report thrust coupling efficiencies between 6.0 and 26.6 μN/W. In the second case, a 20-W laser is operated in

continuous mode for two minutes. Their target is a piece of basalt, placed in a vacuum chamber, similar to the experiments in [73]. After accounting for losses, they report an overall thrust coupling of 45 μN/W (absorbed power).

Another practical application of laser ablation/spallation is to de-spin or de-tumble an asteroid [78]. One could foresee several advantages for having a relatively motionless body, such as being able to land spacecraft safely, keep solar panels in the sun, or utilizing the Yarkovsky effect to redirect an asteroid.

3.4   Anchoring

Landing and staying planted on an asteroid's or comet's surface poses several challenges, the primary one being the low gravity field. If the lander wants to have any moving parts after landing (e.g. a robotic arm,) each movement has the potential to tip or launch the spacecraft off of the surface, potentially damaging it. An effective anchoring mechanism would have to counteract any forces/torques generated by the lander's equipment. Another challenge is that asteroids rotate and/or tumble. An asteroid rotates when its angular momentum is co-linear with its principal axis. An asteroid tumbles when these two vectors are not in alignment, perhaps after a collision or merging of two bodies. A tumbling asteroid can experience rapid changes in surface velocity, making landing a spacecraft doubly difficult. This was the case for the Philae lander (described shortly), shown in Fig. 3.14.

Figure 3.14: Artist's rendition of the Philae lander anchoring itself to Comet 67p/Churyumov-Gerasimenko. Credit: ESA/ATG medialab.

The first attempt at landing on an asteroid was a surprising success. The NEAR-Shoemaker spacecraft completed its primary mission at (433) Eros, and mission controllers then attempted to soft land on the asteroid's surface. The spacecraft did not have any landing gear, but did manage to land on the surface at a velocity of roughly 1.78 m/s without damaging any components. They continued to use the gamma ray spectrometer until the spacecraft eventually stopped sending signals.

The second attempt at landing on a small body was the Philae lander, part of the Rosetta mission to comet 67P/Churyumov–Gerasimenko. This one was not as successful, and resulted in a "multiple-contact-landing". The 100-kg lander had a number of different landing mechanisms, many of which failed. The spacecraft was equipped with a thruster to give it a boost from the Rosetta mothership to land; it was also supposed to press the spacecraft against the surface while other anchoring mechanisms engaged. After the boost though, the thruster failed to respond, and could not provide an anchoring force for the other two mechanisms. The landing legs were equipped with fixed screws, which were supposed to dig a bit into the surface with the velocity provided by the boost. One or more of these failed to penetrate the surface, and the last remaining anchoring mechanism, a harpoon, failed to fire when the spacecraft was in contact with the surface for the first time. The harpoon was meant to penetrate almost a meter into the surface, and subsequently be winched up to 30 N [79].

The latest attempt to land on an asteroid was part of the Hayabusa2 mission. The spacecraft carried four landers which were deployed roughly 60 m from the surface, and gently fell to land. The MINERVA-II-2 lander failed to deploy in time, but the other three were successful. The MINERVA-II landers were 1.1 kg each, and the MASCOT lander was 9.6 kg. All three of them were designed to "crash" and bounce along the surface, as a form of locomotion as opposed to having wheels; all three of them had successful missions.

There are many more types of anchoring mechanisms, each with their own advantages and disadvantages. These include, but are not limited to: thrusters, momentum-driven, harpoons, reaction wheels, drills, fluids, envelopment, grippers, and magnetic. I will give a short summary of the different methods described in detail in *Zacny et al., 2013* [80]. I have already described thrusters and harpoons with the Philae lander; the fixed-screw would fit into the "momentum" category, as they were to be driven into the surface using the spacecraft's velocity. Reaction wheels can be used to offset angular momentum generated by payloads, though it cannot counter linear momentum changes. Drills or augers can be driven by motors to spin anchors into the surface (as opposed to fixed screws, driven by momentum), though it does require some force to keep them pressed against the surface during the anchoring. Fluid anchoring involves secreting or deploying a glue or binding agent to combine with the surface material to form a strong bond. Envelopment involves completely surrounding an object with cables or a bag, without directly attaching anything to the object itself. Magnetic anchoring can be achieved on ferrous bodies like attaching a magnet to a fridge. Grippers can be any number of instruments, such as microspines like those developed at NASA JPL (see Fig. 3.15) to cling onto the surface without digging into it.

Figure 3.15: Microspine gripper developed by NASA JPL. Small hooks on each cable use self-opposed bracing forces to maintain an anchor.

We explored a novel anchoring mechanism using a laser to attach metal to a stoney material. We began by attempting to simply "solder" a metallic wire to a sample of olivine. The concept of operations would go something like this: first, the spacecraft uses its thrusters to hover above a spot on the surface. Next, the spacecraft lowers an anchoring package containing a wire feeder and laser optical head connected via fiber optic cable down to the surface. The laser is used to melt the end of the cable, forming an anchor. The spacecraft can then winch itself down to the surface, and tension the anchor to a specific load.

This method can be used alone or in combination with other anchoring mechanisms for redundancy. It is initiated remotely, and takes less than a second to form an anchor. It can be used on a wide range of materials, from rocks to metals. It is reusable, as the laser can be used to cut the cable, allowing a lander to move to multiple landing sites and use the same anchoring mechanism (unlike a harpoon, which is single-use). Alternatively, it can be used to lift boulders or redirect small objects using the spacecraft's main thrusters.

We found, however, that surface welding or soldering between a metal and olivine was challenging to realize. To simulate the previously stated concept of operations, we taped a metallic wire on the surface of a sample of olivine. We then swept a laser beam along the wire (and sometimes both the wire and olivine) in an attempt to either create

a surface bond (i.e. soldering) or to try to create a weld (i.e. mixing of melt pools). The wire, however, would not "stick" to the surface; the surface tension of the molten metal would maintain a "bead" which would be "dragged" across the surface of the olivine (see Fig. 3.16).
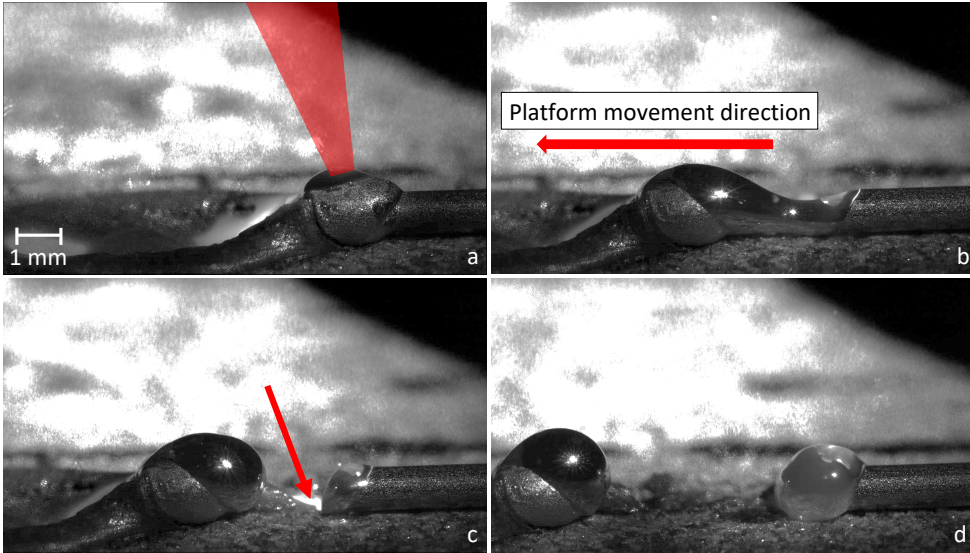
Figure 3.16: High-speed footage of an attempt to weld a stainless steel wire to olivine [81]. Frame a shows the laser beginning to melt the wire. Frame b is 288 ms later; the laser passed over the bulb, and has begun heating the wire. Frame c (at 308 ms) shows the wire breaking. The arrow shows that the laser spot covers both the wire and the olivine. Frame d (at 528 ms) shows the molten bead following the laser spot as it melts more wire.

The welding process was implemented by placing a metal plate down on the olivine sample instead of a wire, and running the same laser sweep. This would prevent the molten metal from beading up and moving. It would change the concept of operations, however, to a situation where the lander has already arrived on the surface, and the laser would be used to weld a landing leg or deployed pad to the surface. We found that two phenomena prevented a strong bond from forming. The first was that the melt pools behaved very differently, and for the most part, would not mix. The molten olivine was chaotic, bubbling and spattering material in all directions; the molten metal was more calm, with little to no spattering or bubbling. Some molten olivine did manage to escape the melt pool, but quickly rose to the top of the molten metal due to the difference in density, as shown in Fig. 3.17.
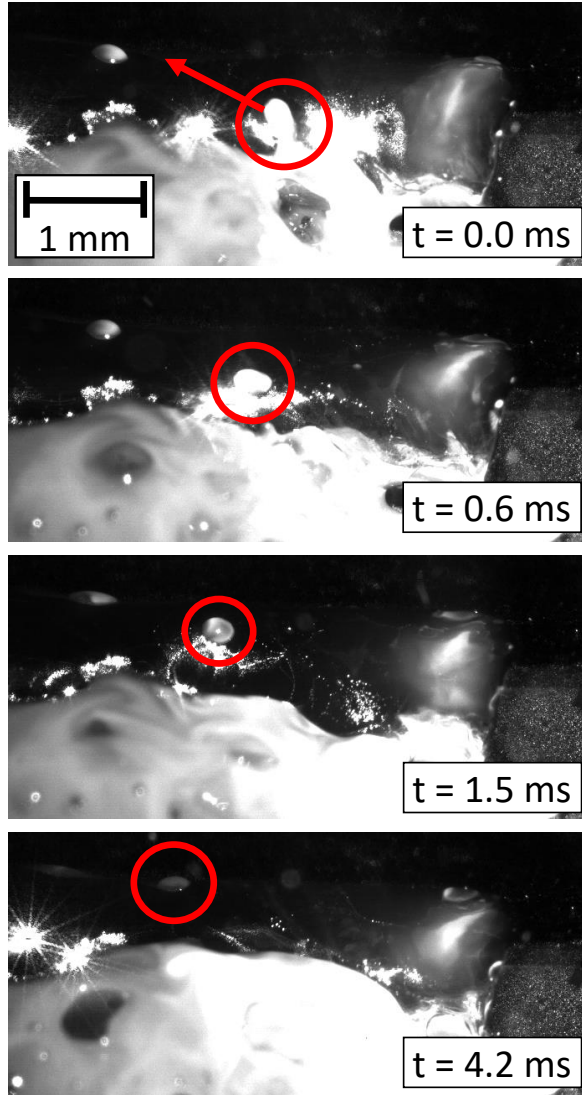
Figure 3.17: High speed footage from the experiments with welding a sheet to olivine [81]. The circles show molten olivine floating to the top of the molten metal.

One can clearly see the two different melt pools, the metal one on top and the molten olivine below it. The platform is, as it is in Fig. 3.16, moving to the left between frames with the camera focused on the point of contact with the laser beam. On the left side of the frames, one can see the melt pools are separated by a a re-solidified layer of material

(it was difficult to say whether it was metal or olivine). One can also see the red circles which track the rise of an escaped glob of molten olivine, floating to the top of the molten metal on its surface. One can also see how chaotic the molten olivine is, with a void appearing in the first frame and bubbles in the next three frames.

It became clear that creating a surface solder or weld joint was not possible with our range of possible laser parameters. We decided to instead explore a *mechanical* attachment mechanism, using the laser to drill a hole in the surface, and feed molten wire into the hole. This again goes back to the original concept of operations where the spacecraft would hover above the surface, lower the anchoring package, and form the anchor. The molten metal would then re-solidify, filling all of the cracks and irregularities in the laser-created hole, and when the spacecraft pulled on the wire, it would be locked underneath the surface.

The experiments we performed did produce anchors that did not immediately fall off as we removed the work piece from the experiment setup. In total there were seven anchors on the olivine sample (see Fig.3.18), and one each on pyroxene, serpentine, and a steel plate. Holes 3 & 4 fell off when being mounted to the universal test machine.
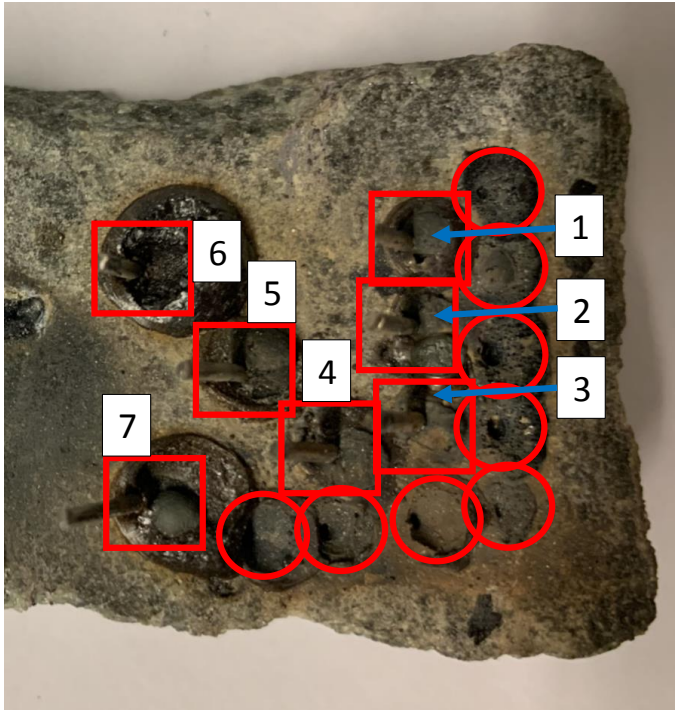
Figure 3.18: Image of the olivine sample showing successful (square) and failed (circle) anchoring attempts.

The sample was then sent to be analyzed with XMT. The analysis showed that varying the experiment duration does have effects on the depth of the anchor, with depths ranging from 1 mm to 9 mm. Further analysis showed that the wire had not melted much below the surface, and that there was some vapor and air still trapped below the anchor (see Fig. 3.19).
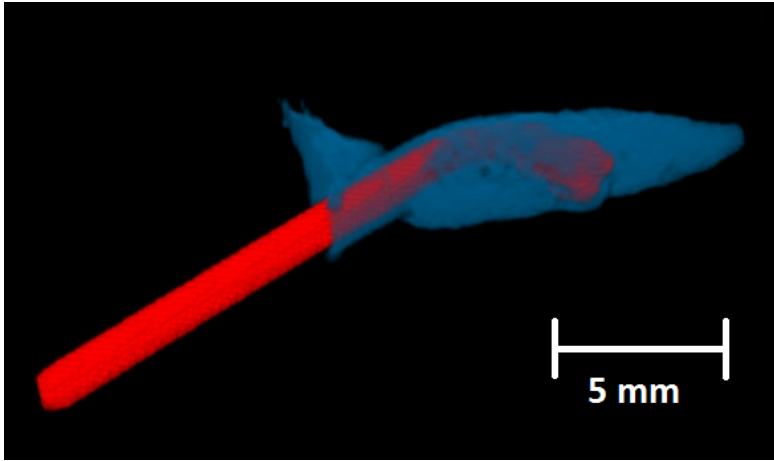
Figure 3.19: Rendering from XMT analysis of an anchor in olivine produced in the second set of experiments [81]. The red color represents the stainless steel wire, and the blue represents the air surrounding it.

After the XMT analysis, we tested the hold strength of the anchors with a tensile strength machine. The hold strengths varied depending on the laser parameters used to create the anchors. The strongest one was just over 115 N, while the weakest ones fell off when attaching the wires to the tensile strength machine. It appears that the strength of the anchor comes from the fact that the wire is bent below the surface.

CHAPTER 4

Conclusions and Future Work

4.1   Conclusions

The results of the research presented in this PhD thesis can be used to answer the research questions posed in Chapter 1, that is:

RQ1: What is the state of the art in asteroid-related technologies, and are there knowledge gaps to be filled?

RQ2: How energy efficient is laser drilling of minerals?

RQ3: How does laser drilling and laser-induced spallation compare to laser ablation in terms of asteroid redirection?

RQ4: How can a laser be used to anchor a spacecraft to a small body?

With regards to **RQ1**, a detailed literature survey proved effective at determining the state of the art in asteroid engineering. Asteroid detection capabilities are the most technologically developed, that is, they are in use today detecting thousands of asteroids per year. They do struggle, however, with detecting small (< 100-m-sized) objects, which could still be dangerous to human life. Detecting such objects requires dedicated use of large and expensive telescopes or a space-based telescope like NEO-WISE. Asteroid redirection is the next-best developed technology, though many methods remain in laboratory testing phases. The kinetic-impact method has been demonstrated in space, with further plans to measure the effects with the AIDA mission. And finally, asteroid mining remains at a relatively low technology readiness level with only a few laboratory-tested methods in development.

The literature survey showed that one knowledge gap present in all three aspects of asteroid engineering is that of determining asteroid composition. Remote observation yields information about surface composition, and requires observations in multiple wavelengths, which limits the "database" of profitable asteroids. Flyby missions could

give more detailed information, but ultimately, a "ground truth" is required to verify subsurface composition before any mining operation could begin (i.e. landing on the surface.) This, too, remains a challenge due to the micro-gravity environment. Anchoring a spacecraft with prospecting or mining equipment is no easy task.

One tool that could be implemented to address some of these challenges is a laser. As a prospecting tool, it has no moving parts, and generates no torques or forces (besides photon momentum, which is negligible). Laboratory experiments have shown that a relatively low power laser (~ 100 W) is capable of drilling well below the surface of minerals common on asteroids. When experimenting with laser drilling, we found depth penetration and volume removal energy efficiencies on the order of 1 mm/J and 10s of mm^3/kJ, respectively, answering **RQ2**. Varying laser parameters (power density, pulse length, repetition rate) has a measurable effect on processing efficiencies. The tested minerals exhibit behaviors similar to industrial metals when the power density is equivalently high. Unlike metals, however, some minerals can be induced to spallate, where solid chunks of material are removed without melting occurring. At power densities on the range of kW/cm2, pyroxene and serpentine will readily spallate, having volume removal efficiencies over twice that of the previously-tested laser drilling, answering **RQ3**.

A laser can also be used to anchor a spacecraft, which comes with several benefits. A spacecraft can lower an anchoring package, connected via fiber optic cable and wire feeder, to create an anchor with a hold strength of at least 110 N (answering **RQ4**). The spacecraft can then winch itself down and keep tension on the wire to form a strong anchor. The anchoring process involves drilling a hole with the laser, then feeding and melting the wire into the hole. This anchoring method is robust in that it can work on any type of solid surface; if the anchor breaks, the system can simply feed more wire to create another anchor; if the spacecraft wishes to relocate to a different spot on the asteroid, the anchor can be broken with the laser.

4.2   Future Work

There are a number of paths of continued research on the subject presented in this thesis. The error bars for the initial laser drilling experiments were relatively large, most likely due to composition variations. A sufficiently large set of experiments would need to be performed to find an accurate and precise value for depth penetration and volume removal efficiencies for a given set of laser parameters. The laser spallation experiments, too, could benefit from increasing the set of experiments for each given set of laser parameters. These expanded sets of laboratory data can be used to optimize the laser parameters for a given application, thus minimizing the power and mass requirements of a laser system for use on a spacecraft. The expanded data sets could also be used to develop a model based on melt dynamics, spattering, and spallation.

Another path would be to study the effects of gravity and vacuum on the processing of the minerals. Air pressure certainly affects melt pool dynamics, so running the same experiments in a vacuum chamber could isolate that effect. The experiment could be performed on a parabolic flight to simulate the micro-gravity environment, which could

affect the processing.

The results of the laser drilling papers suggest including spattering and spallation into laser-based asteroid redirection models. This would most likely take the form of a finite-element model of the tested minerals. In a similar vein, one could also take the existing high speed footage and attempt to derive an equivalent thrust by measuring each individual particle and streak and its movement over time. This would most likely be a job for machine learning, due to the overwhelming amount of small particles for a researcher to measure manually.

The processing performed in this PhD project considered only three minerals in the form of rocks (and a metal plate in the anchoring experiments). Some asteroids have a considerable layer of regolith on their surfaces. While some lasers have been demonstrated to process regolith-like material (such as LIBS or additive manufacturing), it is unclear how the tested process would behave with regolith as a target.

REFERENCES

[1] P. Schulte, L. Alegret, I. Arenillas, J. A. Arz, P. J. Barton, P. R. Bown, T. J. Bralower, G. L. Christeson, P. Claeys, C. S. Cockell, G. S. Collins, A. Deutsch, T. J. Goldin, K. Goto, J. M. Grajales-Nishimura, R. A. F. Grieve, S. P. S. Gulick, K. R. Johnson, W. Kiessling, C. Koeberl, D. A. Kring, K. G. MacLeod, T. Matsui, J. Melosh, A. Montanari, J. V. Morgan, C. R. Neal, D. J. Nichols, R. D. Norris, E. Pierazzo, G. Ravizza, M. Rebolledo-Vieyra, W. U. Reimold, E. Robin, T. Salge, R. P. Speijer, A. R. Sweet, J. Urrutia-Fucugauchi, V. Vajda, M. T. Whalen, and P. S. Willumsen, "The Chicxulub Asteroid Impact and Mass Extinction at the Cretaceous-Paleogene Boundary," *Science*, vol. 327, p. 1214, Mar. 2010.

[2] J. E. Lyne, "Origin of the Tunguska event," *Nature*, vol. 375, pp. 638–639, June 1995.

[3] O. P. Popova, P. Jenniskens, V. Emel'yanenko, A. Kartashova, E. Biryukov, S. Khaibrakhmanov, V. Shuvalov, Y. Rybnov, A. Dudorov, V. I. Grokhovsky, D. D. Badyukov, Q.-Z. Yin, P. S. Gural, J. Albers, M. Granvik, L. G. Evers, J. Kuiper, V. Kharlamov, A. Solovyov, Y. S. Rusakov, S. Korotkiy, I. Serdyuk, A. V. Korochantsev, M. Y. Larionov, D. Glazachev, A. E. Mayer, G. Gisler, S. V. Gladkovsky, J. Wimpenny, M. E. Sanborn, A. Yamakawa, K. L. Verosub, D. J. Rowland, S. Roeske, N. W. Botto, J. M. Friedrich, M. E. Zolensky, L. Le, D. Ross, K. Ziegler, T. Nakamura, I. Ahn, J. I. Lee, Q. Zhou, X.-H. Li, Q.-L. Li, Y. Liu, G.-Q. Tang, T. Hiroi, D. Sears, I. A. Weinstein, A. S. Vokhmintsev, A. V. Ishchenko, P. Schmitt-Kopplin, N. Hertkorn, K. Nagao, M. K. Haba, M. Komatsu, and T. Mikouchi, "Chelyabinsk Airburst, Damage Assessment, Meteorite Recovery, and Characterization," *Science*, vol. 342, no. 6162, pp. 1069–1073, 2013.

[4] L. T. Elkins-Tanton, E. Asphaug, J. F. Bell, H. Bercovici, B. Bills, R. Binzel, W. F. Bottke, S. Dibb, D. J. Lawrence, S. Marchi, T. J. McCoy, R. Oran, R. S. Park, P. N. Peplowski, C. A. Polanskey, T. H. Prettyman, C. T. Russell, L. Schaefer, B. P. Weiss, M. A. Wieczorek, D. A. Williams, and M. T. Zuber, "Observations, Meteorites, and Models: A Preflight Assessment of the Composition and Formation of (16) Psyche," *Journal of Geophysical Research (Planets)*, vol. 125, pp. 1–23, Mar. 2020.

[5] J. Hayes, "Organic constituents of meteorites—a review," *Geochimica et Cosmochimica Acta*, vol. 31, no. 9, pp. 1395–1440, 1967.

[6] O. Abramov and S. J. Mojzsis, "Abodes for life in carbonaceous asteroids?," *Icarus*, vol. 213, no. 1, pp. 273–279, 2011.

[7] M. Ferus, D. Nesvorný, J. Šponer, P. Kubelík, R. Michalčíková, V. Shestivská, J. E. Šponer, and S. Civiš, "High-energy chemistry of formamide: A unified mechanism of nucleobase formation," *Proceedings of the National Academy of Sciences*, vol. 112, no. 3, pp. 657–662, 2015.

[8] A. Morbidelli, J. Chambers, J. I. Lunine, J. M. Petit, F. Robert, G. B. Valsecchi, and K. E. Cyr, "Source regions and timescales for the delivery of water to the Earth," *Meteoritics & Planetary Science*, vol. 35, no. 6, pp. 1309–1320, 2000.

[9] D. Whittet, "Origins of Life," *Morgan & Claypool Publishers*, 2017.

[10] W. F. Bottke, D. D. Durda, D. Nesvorný, R. Jedicke, A. Morbidelli, D. Vokrouhlický, and H. F. Levison, "Linking the collisional history of the main asteroid belt to its dynamical excitation and depletion," *Icarus*, vol. 179, no. 1, pp. 63–94, 2005.

[11] M. Moons, "Review of the dynamics in the Kirkwood gaps," *Celestial Mechanics and Dynamical Astronomy*, vol. 65, pp. 175–204, Mar 1996.

[12] S. R. Chesley, S. J. Ostro, D. Vokrouhlický, D. Čapek, J. D. Giorgini, M. C. Nolan, J.-L. Margot, A. A. Hine, L. A. M. Benner, and A. B. Chamberlin, "Direct Detection of the Yarkovsky Effect by Radar Ranging to Asteroid 6489 Golevka," *Science*, vol. 302, no. 5651, pp. 1739–1742, 2003.

[13] N. Anthony and M. R. Emami, "Asteroid engineering: The state-of-the-art of Near-Earth Asteroids science and technology," *Progress in Aerospace Sciences*, vol. 100, pp. 1–17, June 2018.

[14] G. Fedorets, M. Granvik, and R. Jedicke, "Orbit and size distributions for asteroids temporarily captured by the Earth-Moon system," *Icarus*, vol. 285, pp. 83–94, 2017.

[15] H. Urrutxua, D. J. Scheeres, C. Bombardelli, J. L. Gonzalo, and J. Peláez, "Temporarily Captured Asteroids as a Pathway to Affordable Asteroid Retrieval Missions," *Journal of Guidance, Control, and Dynamics*, vol. 38, no. 11, pp. 2132–2145, 2015.

[16] Kwiatkowski, T., Kryszczyńska, A., Polińska, M., Buckley, D. A. H., O'Donoghue, D., Charles, P. A., Crause, L., Crawford, S., Hashimoto, Y., Kniazev, A., Loaring, N., Romero Colmenero, E., Sefako, R., Still, M., and Vaisanen, P., "Photometry of 2006 RH$_{120}$: an asteroid temporary captured into a geocentric orbit," *Astronomy & Astrophysics*, vol. 495, no. 3, pp. 967–974, 2009.

[17] G. Fedorets, M. Micheli, R. Jedicke, S. P. Naidu, D. Farnocchia, M. Granvik, N. Moskovitz, M. E. Schwamb, R. Weryk, K. Wierzchoś, E. Christensen, T. Pruyne, W. F. Bottke, Q. Ye, R. Wainscoat, M. Devogèle, L. E. Buchanan, A. A. Djupvik,

D. M. Faes, D. Föhring, J. Roediger, T. Seccull, and A. B. Smith, "Establishing Earth's Minimoon Population through Characterization of Asteroid 2020 CD$_3$," *The Astronomical Journal*, vol. 160, p. 277, nov 2020.

[18] M. Chyba, G. Patterson, G. Picot, M. Granvik, R. Jedicke, and J. Vaubaillon, "Designing rendezvous missions with mini-moons using geometric optimal control," *Journal of Industrial & Management Optimization*, vol. 10, no. 1547-5816-2014-2-477, p. 477, 2014.

[19] R. G. Martin and M. Livio, "On the evolution of the snow line in protoplanetary discs," *Monthly Notices of the Royal Astronomical Society: Letters*, vol. 425, pp. L6–L9, 09 2012.

[20] J. D. Anderson, "Feasibility of Determining the Mass of an Asteroid from a Spacecraft Flyby," *International Astronomical Union Colloquium*, vol. 12, pp. 577—583, 1971.

[21] R. L. Millis and D. W. Dunham, "Precise measurement of asteroid sizes and shapes from occultations.," in *Asteroids II* (R. P. Binzel, T. Gehrels, and M. S. Matthews, eds.), pp. 148–170, Jan. 1989.

[22] M. Delbó, A. W. Harris, R. P. Binzel, P. Pravec, and J. K. Davies, "Keck observations of near-Earth asteroids in the thermal infrared," *Icarus*, vol. 166, no. 1, pp. 116–130, 2003.

[23] A. Cellino, V. Zappalà, and P. Farinella, "Asteroid shapes and lightcurve morphology," *Icarus*, vol. 78, no. 2, pp. 298–310, 1989.

[24] M. K. Weisberg, T. J. McCoy, and A. N. Krot, *Systematics and Evaluation of Meteorite Classification*, p. 19. 2006.

[25] D. J. Scheeres, D. Britt, B. Carry, and K. A. Holsapple, "Asteroid Interiors and Morphology," *Asteroids IV*, pp. 745–766, 2015.

[26] L. Prockter, P. Thomas, M. Robinson, J. Joseph, A. Milne, B. Bussey, J. Veverka, and A. Cheng, "Surface Expressions of Structural Features on Eros," *Icarus*, vol. 155, no. 1, pp. 75–93, 2002.

[27] T. Michikami, A. M. Nakamura, N. Hirata, R. W. Gaskell, R. Nakamura, T. Honda, C. Honda, K. Hiraoka, J. Saito, H. Demura, M. Ishiguro, and H. Miyamoto, "Size-frequency statistics of boulders on global surface of asteroid 25143 Itokawa," *Earth, Planets and Space*, vol. 60, pp. 13–20, Jan 2008.

[28] A. Tsuchiyama, M. Uesugi, T. Matsushima, T. Michikami, T. Kadono, T. Nakamura, K. Uesugi, T. Nakano, S. A. Sandford, R. Noguchi, T. Matsumoto, J. Matsuno, T. Nagano, Y. Imai, A. Takeuchi, Y. Suzuki, T. Ogami, J. Katagiri, M. Ebihara,

T. R. Ireland, F. Kitajima, K. Nagao, H. Naraoka, T. Noguchi, R. Okazaki, H. Yurimoto, M. E. Zolensky, T. Mukai, M. Abe, T. Yada, A. Fujimura, M. Yoshikawa, and J. Kawaguchi, "Three-Dimensional Structure of Hayabusa Samples: Origin and Evolution of Itokawa Regolith," *Science*, vol. 333, no. 6046, pp. 1125–1128, 2011.

[29] H. Miyamoto and J. Kargel, "Lessons for the future on asteroid's surface," *SPIE Newsroom*, 01 2008.

[30] M. Grott, J. Knollenberg, M. Hamm, K. Ogawa, R. Jaumann, K. A. Otto, M. Delbo, P. Michel, J. Biele, W. Neumann, M. Knapmeyer, E. Kührt, H. Senshu, T. Okada, J. Helbert, A. Maturilli, N. Müller, A. Hagermann, N. Sakatani, S. Tanaka, T. Arai, S. Mottola, S. Tachibana, I. Pelivan, L. Drube, J.-B. Vincent, H. Yano, C. Pilorget, K. D. Matz, N. Schmitz, A. Koncz, S. E. Schröder, F. Trauthan, M. Schlotterer, C. Krause, T.-M. Ho, and A. Moussi-Soffys, "Low thermal conductivity boulder with high porosity identified on C-type asteroid (162173) Ryugu," *Nature Astronomy*, vol. 3, pp. 971–976, Nov 2019.

[31] D. S. Lauretta, D. N. DellaGiustina, C. A. Bennett, D. R. Golish, K. J. Becker, S. S. Balram-Knutson, O. S. Barnouin, T. L. Becker, W. F. Bottke, W. V. Boynton, H. Campins, B. E. Clark, H. C. Connolly, C. Y. Drouet d'Aubigny, J. P. Dworkin, J. P. Emery, H. L. Enos, V. E. Hamilton, C. W. Hergenrother, E. S. Howell, M. R. M. Izawa, H. H. Kaplan, M. C. Nolan, B. Rizk, H. L. Roper, D. J. Scheeres, P. H. Smith, K. J. Walsh, C. W. V. Wolner, D. E. Highsmith, D. Small, J.and Vokrouhlický, N. E. Bowles, E. Brown, K. L. Donaldson Hanna, T. Warren, C. Brunet, R. A. Chicoine, S. Desjardins, D. Gaudreau, T. Haltigin, S. Millington-Veloza, A. Rubi, J. Aponte, N. Gorius, A. Lunsford, B. Allen, J. Grindlay, D. Guevel, D. Hoak, J. Hong, D. L. Schrader, J. Bayron, O. Golubov, P. Sánchez, J. Stromberg, M. Hirabayashi, C. M. Hartzell, S. Oliver, M. Rascon, A. Harch, J. Joseph, S. Squyres, D. Richardson, L. McGraw, R. Ghent, R. P. Binzel, M. M. A. Asad, C. L. Johnson, L. Philpott, H. C. M. Susorney, E. A. Clouis, R. D. Hanna, F. Ciceri, A. R. Hildebrand, E.-M. Ibrahim, L. Breitenfeld, T. Glotch, A. D. Rogers, S. Ferrone, C. A. Thomas, Y. Fernandez, W. Chang, A. Cheuvront, D. Trang, S. Tachibana, H. Yurimoto, J. R. Brucato, G. Poggiali, M. Pajola, E. Dotto, E. M. Epifani, M. K. Crombie, C. Lantz, J. de Leon, J. Licandro, J. L. R. Garcia, S. Clemett, K. Thomas-Keprta, S. Van wal, M. Yoshikawa, J. Bellerose, S. Bhaskaran, C. Boyles, S. R. Chesley, C. M. Elder, D. Farnocchia, A. Harbison, B. Kennedy, A. Knight, N. Martinez-Vlasoff, N. Mastrodemos, T. McElrath, W. Owen, R. Park, B. Rush, L. Swanson, Y. Takahashi, D. Velez, K. Yetter, C. Thayer, C. Adam, P. Antreasian, J. Bauman, C. Bryan, B. Carcich, M. Corvin, J. Geeraert, J. Hoffman, J. M. Leonard, E. Lessac-Chenen, A. Levine, J. McAdams, L. McCarthy, D. Nelson, B. Page, J. Pelgrift, E. Sahr, K. Stakkestad, D. Stanbridge, D. Wibben, B. Williams, K. Williams, P. Wolff, P. Hayne, D. Kubitschek, M. A. Barucci, J. D. P. Deshapriya, S. Fornasier, M. Fulchignoni, P. Hasselmann, F. Merlin, A. Praet, E. B. Bierhaus, O. Billett, A. Boggs, B. Buck, S. Carlson-Kelly, J. Cerna, K. Chaffin, E. Church, M. Coltrin, J. Daly, A. Deguzman, R. Dubisher, D. Eckart, D. Ellis, P. Falkenstern, A. Fisher,

M. E. Fisher, P. Fleming, K. Fortney, S. Francis, S. Freund, S. Gonzales, P. Haas, A. Hasten, D. Hauf, A. Hilbert, D. Howell, F. Jaen, N. Jayakody, M. Jenkins, K. Johnson, M. Lefevre, H. Ma, C. Mario, K. Martin, C. May, M. McGee, B. Miller, C. Miller, G. Miller, A. Mirfakhrai, E. Muhle, C. Norman, R. Olds, C. Parish, M. Ryle, M. Schmitzer, P. Sherman, M. Skeen, M. Susak, B. Sutter, Q. Tran, C. Welch, R. Witherspoon, J. Wood, J. Zareski, M. Arvizu-Jakubicki, E. Asphaug, E. Audi, R.-L. Ballouz, R. Bandrowski, S. Bendall, H. Bloomenthal, D. Blum, J. Brodbeck, K. N. Burke, M. Chojnacki, A. Colpo, J. Contreras, J. Cutts, D. Dean, B. Diallo, D. Drinnon, K. Drozd, R. Enos, C. Fellows, T. Ferro, M. R. Fisher, G. Fitzgibbon, M. Fitzgibbon, J. Forelli, T. Forrester, I. Galinsky, R. Garcia, A. Gardner, N. Habib, D. Hamara, D. Hammond, K. Hanley, K. Harshman, K. Herzog, D. Hill, C. Hoekenga, S. Hooven, E. Huettner, A. Janakus, J. Jones, T. R. Kareta, J. Kidd, K. Kingsbury, L. Koelbel, J. Kreiner, D. Lambert, C. Lewin, B. Lovelace, M. Loveridge, M. Lujan, C. K. Maleszewski, R. Malhotra, K. Marchese, E. McDonough, N. Mogk, V. Morrison, E. Morton, R. Munoz, J. Nelson, J. Padilla, R. Pennington, A. Polit, N. Ramos, V. Reddy, M. Riehl, S. Salazar, S. R. Schwartz, S. Selznick, N. Shultz, and T. O.-R. Team, "The unexpected surface of asteroid (101955) Bennu," *Nature*, vol. 568, pp. 55–60, Apr 2019.

[32] R. Jaumann, N. Schmitz, T.-M. Ho, S. E. Schröder, K. A. Otto, K. Stephan, S. Elgner, K. Krohn, F. Preusker, F. Scholten, J. Biele, S. Ulamec, C. Krause, S. Sugita, K.-D. Matz, T. Roatsch, R. Parekh, S. Mottola, M. Grott, P. Michel, F. Trauthan, A. Koncz, H. Michaelis, C. Lange, J. T. Grundmann, M. Maibaum, K. Sasaki, F. Wolff, J. Reill, A. Moussi-Soffys, L. Lorda, W. Neumann, J.-B. Vincent, R. Wagner, J.-P. Bibring, S. Kameda, H. Yano, S. Watanabe, M. Yoshikawa, Y. Tsuda, T. Okada, T. Yoshimitsu, Y. Mimasu, T. Saiki, H. Yabuta, H. Rauer, R. Honda, T. Morota, Y. Yokota, and T. Kouyama, "Images from the surface of asteroid Ryugu show rocks similar to carbonaceous chondrite meteorites," *Science*, vol. 365, no. 6455, pp. 817–820, 2019.

[33] R. P. Binzel, F. E. DeMeo, E. V. Turtelboom, S. J. Bus, A. Tokunaga, T. H. Burbine, C. Lantz, D. Polishook, B. Carry, A. Morbidelli, M. Birlan, P. Vernazza, B. J. Burt, N. Moskovitz, S. M. Slivan, C. A. Thomas, A. S. Rivkin, M. D. Hicks, T. Dunn, V. Reddy, J. A. Sanchez, M. Granvik, and T. Kohout, "Compositional distributions and evolutionary processes for the near-Earth object population: Results from the MIT-Hawaii Near-Earth Object Spectroscopic Survey (MITHNEOS)," *Icarus*, vol. 324, pp. 41–76, May 2019.

[34] V. Reddy, T. L. Dunn, C. A. Thomas, N. A. Moskovitz, and T. H. Burbine, "Mineralogy and Surface Composition of Asteroids," in *Asteroids IV* (P. Michel, F. E. DeMeo, and W. F. Bottke, eds.), pp. 43–63, 2015.

[35] A. E. Rubin, "Mineralogy of meteorite groups," *Meteoritics and Planetary Science*, vol. 32, pp. 231–247, Mar. 1997.

[36] B. Foing, G. Racca, A. Marini, E. Evrard, L. Stagnaro, M. Almeida, D. Koschny, D. Frew, J. Zender, J. Heather, M. Grande, J. Huovelin, H. Keller, A. Nathues, J.-L. Josset, A. Malkki, W. Schmidt, G. Noci, R. Birki, and P. McManamon, "ESA's SMART-1 mission launched to the moon: Technology and science goals," *Science and Technology Series*, vol. 108, pp. 3–14, 01 2004.

[37] T. H. Prettyman, N. Yamashita, M. J. Toplis, H. Y. McSween, N. Schörghofer, S. Marchi, W. C. Feldman, J. Castillo-Rogez, O. Forni, D. J. Lawrence, E. Ammannito, B. L. Ehlmann, H. G. Sizemore, S. P. Joy, C. A. Polanskey, M. D. Rayman, C. A. Raymond, and C. T. Russell, "Extensive water ice within Ceres' aqueously altered regolith: Evidence from nuclear spectroscopy," *Science*, vol. 355, pp. 55–59, Jan. 2017.

[38] S.-Y. Park and I. M. Ross, "Two-Body Optimization for Deflecting Earth-Crossing Asteroids," *Journal of Guidance, Control, and Dynamics*, vol. 22, no. 3, pp. 415–420, 1999.

[39] T. J. Ahrens and A. W. Harris, "Deflection and fragmentation of near-Earth asteroids," *Nature*, vol. 360, pp. 429–433, Dec 1992.

[40] J.-M. Salotti, "Billiards Shot for Asteroid Deflection," *54th International Astronautical Congress of the International Astronautical Federation, the International Academy of Astronautics, and the International Institute of Space Law*, 2003.

[41] B. Wie, "Hypervelocity nuclear interceptors for asteroid disruption," *Acta Astronautica*, vol. 90, no. 1, pp. 146–155, 2013. NEO Planetary Defense: From Threat to Action - Selected Papers from the 2011 IAA Planetary Defense Conference.

[42] M. Bazzocchi and M. R. Emami, "A Systematic Assessment of Asteroid Redirection Methods for Resource Exploitation," *8th Symposium on Space Resource Utilization*, 2015.

[43] C. Bombardelli and J. Pelaez, "Ion Beam Shepherd for Asteroid Deflection," *Journal of Guidance, Control, and Dynamics*, vol. 34, no. 4, pp. 1270–1272, 2011.

[44] H. Urrutxua, C. Bombardelli, and J. M. Hedo, "A preliminary design procedure for an ion-beam shepherd mission," *Aerospace Science and Technology*, vol. 88, pp. 421–435, 2019.

[45] R. L. Schweickart, E. T. Lu, P. Hut, and C. R. Chapman, "The Asteroid Tugboat," *Scientific American*, vol. 289, no. 5, pp. 54–61, 2003.

[46] H. J. Melosh and I. V. Nemchinov, "Solar asteroid diversion," *Nature*, vol. 366, pp. 21–22, Nov 1993.

[47] J. Melosh, I. Nemchinov, and Y. Zetzer, "Non-nuclear strategies for deflecting comets and asteroids," vol. 1, pp. 1111–1132, Jan 1994.

[48] A. Gibbings, J.-M. Hopkins, D. Burns, M. Vasile, and I. Watson, "On Testing Laser Ablation Processes for Asteroid Deflection," *IAA Planetary Defense Conference*, 01 2011.

[49] T. H. Prettyman, W. C. Feldman, F. P. Ameduri, B. L. Barraclough, E. W. Cascio, K. R. Fuller, H. O. Funsten, D. J. Lawrence, G. W. McKinney, C. T. Russell, S. A. Soldner, S. A. Storms, C. Szeles, and R. L. Tokar, "Gamma-ray and neutron spectrometer for the Dawn mission to 1 Ceres and 4 Vesta," *IEEE Transactions on Nuclear Science*, vol. 50, no. 4, pp. 1190–1197, 2003.

[50] J. C. Sercel, C. B. Dreyer, A. Abbud-Madrid, D. Britt, R. Jedicke, L. Gertsch, and S. G. Love, *A Coordinated Research Program to Develop the Technology to Optical Mine Asteroids*, pp. 507–522.

[51] N. Anthony, J. Frostevarg, H. Suhonen, C. Wanhainen, and M. Granvik, "Laser-induced spallation of minerals common on asteroids," *Acta Astronautica*, vol. 182, pp. 325–331, 2021.

[52] L. Gertsch, A. Abbud-Madrid, C. Dreyer, R. Jedicke, A. Krot, D. L. Linne, J. Mantovani, M. Schlesinger, J. Sercel, and E. Unobe, "Producing Volatiles from Asteroid Simulants: Preliminary Results," *10th Symposium on Space Resource Utilization*.

[53] T. H. Maiman, "Stimulated optical radiation in ruby," *Nature*, vol. 187, no. 4736, pp. 493–494, 1960.

[54] C. K. N. Patel, "Continuous-Wave Laser Action on Vibrational-Rotational Transitions of CO_2," *Physical Review*, vol. 136, pp. A1187–A1193, Nov 1964.

[55] J. E. Geusic, H. M. Marcos, and L. G. Van Uitert, "Laser Oscillations in Nd-doped Yttrium-Aluminum, Yttrium-Gallium and Gadolinum Garnets," *Applied Physics Letters*, vol. 4, no. 10, pp. 182–184, 1964.

[56] K. A. Ghany, H. A. Rafea, and M. Newishy, "Using a Nd:YAG laser and six axes robot to cut zinc-coated steel," *The International Journal of Advanced Manufacturing Technology*, vol. 28, pp. 1111–1117, May 2006.

[57] L. D. Smullin and G. Fiocco, "Optical Echoes from the Moon," *Nature*, vol. 194, p. 1267, June 1962.

[58] W. M. Macek and D. T. M. Davis, "Rotation Rate Sensing with Traveling-Wave Ring Lasers," *Applied Physics Letters*, vol. 2, no. 3, pp. 67–68, 1963.

[59] R. K. Huebschman, "The MSX Spacecraft System Design," *Johns Hopkins APL Technical Digest*, vol. 17, pp. 41–48, Jan. 1994.

[60] K. Araki, Y. Arimoto, M. Shikatani, M. Toyoda, M. Toyoshima, T. Takahashi, S. Kanda, and K. Shiratama, "Performance evaluation of laser communication equipment onboard the ETS-VI satellite," in *Free-Space Laser Communication Technologies VIII* (G. S. Mecherle, ed.), vol. 2699, pp. 52–59, International Society for Optics and Photonics, SPIE, 1996.

[61] R. Z. Sagdeev and A. V. Zakharov, "Brief history of the Phobos mission," *Nature*, vol. 341, pp. 581–585, Oct. 1989.

[62] R. C. Wiens, S. Maurice, B. Barraclough, M. Saccoccio, W. C. Barkley, J. F. Bell, S. Bender, J. Bernardin, D. Blaney, J. Blank, M. Bouyé, N. Bridges, N. Bultman, P. Caïs, R. C. Clanton, B. Clark, S. Clegg, A. Cousin, D. Cremers, A. Cros, L. De-Flores, D. Delapp, R. Dingler, C. D'Uston, M. Darby Dyar, T. Elliott, D. Enemark, C. Fabre, M. Flores, O. Forni, O. Gasnault, T. Hale, C. Hays, K. Herkenhoff, E. Kan, L. Kirkland, D. Kouach, D. Landis, Y. Langevin, N. Lanza, F. LaRocca, J. Lasue, J. Latino, D. Limonadi, C. Lindensmith, C. Little, N. Mangold, G. Manhes, P. Mauchien, C. McKay, E. Miller, J. Mooney, R. V. Morris, L. Morrison, T. Nelson, H. Newsom, A. Ollila, M. Ott, L. Pares, R. Perez, F. Poitrasson, C. Provost, J. W. Reiter, T. Roberts, F. Romero, V. Sautter, S. Salazar, J. J. Simmonds, R. Stiglich, S. Storms, N. Striebig, J.-J. Thocaven, T. Trujillo, M. Ulibarri, D. Vaniman, N. Warner, R. Waterbury, R. Whitaker, J. Witt, and B. Wong-Swanson, "The ChemCam Instrument Suite on the Mars Science Laboratory (MSL) Rover: Body Unit and Combined System Tests," *Space Science Reviews*, vol. 170, pp. 167–227, Sept. 2012.

[63] P. S. Moura, B. Serpa, B. Assis, Y. Moura, V. P. Alves, K. A. Schenguer, B. L. Tumelero, A. Luz, L. G. C. Novaes, A. T. Cabral, D. V. Rotter, N. Rossini, P. M. R. Santos, T. K. Bretzke, M. de Souza, K. Morais, D. Champoski, D. Vieira, G. Spricigo, E. D. Carli, S. L. S. Taglialenha, and G. B. Hughes, "A CubeSat mission for space-environment demonstration of Remote Laser-Evaporative Molecular Absorption (R-LEMA) spectroscopy sensor system concept," in *CubeSats and NanoSats for Remote Sensing II* (T. S. Pagano and C. D. Norton, eds.), vol. 10769, pp. 164–173, International Society for Optics and Photonics, SPIE, 2018.

[64] I. F. Larsson, "Method and apparatus for drilling holes by means of a focused laser beam," no. USA, Patent Nr. US3410979A, 1964, 1964.

[65] C. M. Adams and G. A. Hardway, "Fundamentals of Laser Beam Machining and Drilling," *IEEE Transactions on Industry and General Applications*, vol. IGA-1, no. 2, pp. 90–96, 1965.

[66] T. Miyazaki, "A Study on the Mechanism of Laser Piercing Process," *Annals of the CIRP*, vol. 22, pp. 67–68, 1973.

[67] C. Lehane and H. Kwok, "Enhanced drilling using a dual-pulse Nd:YAG laser," *Applied Physics A*, vol. 73, pp. 45–48, July 2001.

[68] A. Ancona, F. Röser, K. Rademaker, J. Limpert, S. Nolte, and A. Tünnermann, "High speed laser drilling of metals using a high repetition rate, high average power ultrafast fiber CPA system," *Optics Express*, vol. 16, pp. 8958–8968, Jun 2008.

[69] M. von Allmen, "Laser drilling velocity in metals," *Journal of Applied Physics*, vol. 47, pp. 5460–5463, Dec. 1976.

[70] J. Pocorni, J. Powell, J. Frostevarg, and A. F. H. Kaplan, "Investigation of the piercing process in laser cutting of stainless steel," *Journal of Laser Applications*, vol. 29, pp. 022201–1–022201–8, May 2017.

[71] M. Schneider, L. Berthe, R. Fabbro, M. Muller, and M. Nivard, "Gas investigation for laser drilling," *Journal of Laser Applications*, vol. 19, pp. 165–169, Aug. 2007.

[72] M. Vasile, A. Gibbings, I. Watson, and J.-M. Hopkins, "Improved laser ablation model for asteroid deflection," *Acta Astronautica*, vol. 103, pp. 382–394, 2014.

[73] A. Gibbings, M. Vasile, I. Watson, J.-M. Hopkins, and D. Burns, "Experimental analysis of laser ablated plumes for asteroid deflection and exploitation," *Acta Astronautica*, vol. 90, no. 1, pp. 85–97, 2013.

[74] C. Phipps, "An Alternate Treatment of the Vapor-Plasma Transition," *International Journal of Aerospace Innovations*, vol. 3, pp. 45–50, 2011.

[75] Z. Xu, C. B. Reed, G. Konercki, R. A. Parker, B. C. Gahan, S. Batarseh, R. M. Graves, H. Figueroa, and N. Skinner, "Specific energy for pulsed laser rock drilling," *Journal of Laser Applications*, vol. 15, no. 1, pp. 25–30, 2003.

[76] J. B. Sloane and R. J. Sedwick, "Direct Force Measurement of Pulsed Laser Ablation of Asteroid Simulants," *Journal of Propulsion and Power*, vol. 36, no. 4, pp. 551–559, 2020.

[77] N. Anthony, J. Frostevarg, H. Suhonen, C. Wanhainen, A. Penttilä, and M. Granvik, "Laser processing of minerals common on asteroids," *Optics & Laser Technology*, vol. 135, p. 106724, 2021.

[78] T. Brashears, P. Lubin, G. B. Hughes, P. Meinhold, J. Suen, P. Batliner, C. Motta, J. Griswold, M. Kangas, I. Johansson, Y. Alnawakhtha, K. Prater, A. Lang, and J. Madajian, "Directed energy deflection laboratory measurements," in *Nanophotonics and Macrophotonics for Space Environments IX* (E. W. Taylor and D. A. Cardimona, eds.), vol. 9616, pp. 36–48, International Society for Optics and Photonics, SPIE, 2015.

[79] E. Hand, "Philae probe makes bumpy touchdown on a comet," *Science*, vol. 346, no. 6212, pp. 900–901, 2014.

[80] K. Zacny, P. Chu, G. Paulsen, M. Hedlund, B. Mellerowicz, S. Indyk, J. Spring, A. Parness, D. Wegel, R. Mueller, and D. Levitt

[81] N. Anthony, J. Frostevarg, H. Suhonen, and M. Granvik, "Laboratory experiments with a laser-based attachment mechanism for spacecraft at small bodies," *Acta Astronautica*, vol. Submitted, 2021.

Asteroid Engineering: A Review of Near-Earth Asteroid Science and Technology

Authors:
Niklas Anthony, M. Reza Emami

Asteroid Engineering: A Review of Near-Earth Asteroid Science and Technology

Niklas Anthony[1], M. Reza Emami[1,2,*]

1 Space Technology Division, Luleå University of Technology, Kiruna, Sweden 98128
2 Institute for Aerospace Studies, University of Toronto, Toronto, Canada M3H 5T6
*Corresponding Author, Tel: +46 (0)980 67 546, Email: reza.emami@ltu.se

Abstract

This paper presents a comprehensive review of the science and technology of accessing near-Earth asteroids (NEAs), or making them accessible, for obtaining both information and resources. The survey is divided into four major groups of NEA study, namely **a)** discovery (population estimation and detection), **b)** Exploration (identification and characterization), **c)** deflection and redirection, and **d)** mining (prospecting, excavation, processing, refining, storage.). Recent research and development advancements from both industry and academia are discussed in each group, and certain specific future directions are highlighted. Some concluding remarks are made at the end, including the need for creating new educational programs to train competent engineers and researchers for the taskforce in the new field of asteroid engineering in near future.

Keywords

Near-Earth Asteroids, Space Resource Utilization, Asteroid Mining, Asteroid detection, Asteroid Redirection, Asteroid Deflection

1. Introduction

Asteroid mining is poised to be likely the most profitable industry in the history of mankind, and has already drawn interest from private funding entities like Goldman Sachs [1]. There are millions of Near Earth Objects (NEOs), containing untold riches that can be used here on Earth or in space. The term NEO refers to any asteroid or comet that has a perihelion distance of less than 1.3 Astronomical Units (AUs), i.e., approximately 195 million km. This paper will focus on Near-Earth Asteroids (NEAs,) as near-Earth comets tend to spend most of their orbits very far away from Earth. While humans have been mining resources on Earth for millennia, technology to prospect, extract and refine resources in the zero-gravity, vacuous environment of space has yet to be developed.

There are three main drivers behind the interest in NEAs: the expected scientific return, planetary defense, and mining. Scientists can glean information about the formation of the Solar System by studying the composition and structure of NEAs. Most of NEAs have peculiar orbits that scientists study to reveal orbital change processes. These objects might also contain organic compounds that could have kick-started life on Earth [2]. In addition to originating life, they could also destroy it. It is evident that a ten-kilometer-wide impactor caused the Cretaceous-Paleocene extinction event, when it made the Chicxulub crater over 64 million years ago [3]. More recently, the Chelyabinsk bolide in February 2013, which caused massive property damage and injured around 1500 people, was only 20 m wide, weighed 12,000 metric tons, and entered our atmosphere at a relative speed of 19 km/s [4]. It is imperative that technologies be developed to divert these objects away from collision courses with Earth, ideally into a stable orbit around Earth. Countless science fiction tales and scientific papers alike rely on using materials from asteroids to build the infrastructure necessary for mass exploration and colonization of the Solar System. The company Deep Space Industries (DSI) believes that NEA 2012 DA14 could be worth up to $195 billion, for example [5]. The asteroid passed within geostationary orbit distance in 2013, and it is estimated to be 45 m wide [6].

To facilitate the emergence of these technologies, it has been argued that a new field of asteroid engineering must be founded, characterized as "the science and technology of exploring, accessing asteroids and/or making them accessible to avoid collision with Earth and to retrieve and process both information and raw materials from them for scientific activities as well as Earth and space developments" [7].

Asteroids are best found by using wide-angle optical or infrared (IR) telescopes using streak-detection software. There are fundamental limitations when looking for small, dim, and distant objects using ground-based telescopes; not only are they difficult to find, the information about these NEAs is incredibly limited as well. There are methods to remotely determine a NEA's physical properties, but their requirements limit the number of investigable asteroids to close-approaching or well-observed ones. To reliably gather

detailed information about a NEA, a spacecraft must be sent to explore it. Only then can we accurately determine the NEA's size, shape, spin-vector, mass distribution, and composition. In-situ exploration of an asteroid can be done through either rendezvousing with the asteroid in its natural orbit, which is typically unstable and far from Earth, or first bringing the asteroid into a closer and more stable orbit in the Earth-Moon system before the exploration phase, a mission called asteroid redirection.

Many unique asteroid redirection methods have been suggested over the years, ranging from landing rockets on an asteroid's surface to detonating a nuclear warhead near, on, or in an asteroid. As of 2016 though, there is no developed technology to carry out any of those redirections, but there are a few promising plans. For instance, NASA's Asteroid Redirect Robotic Mission (ARRM) seeks to physically grab a boulder from a large asteroid and bring it to a distant retrograde orbit around the Moon in 2021. It will then be the target of a human exploration phase as the next step in getting humans to Mars [8]. Companies like DSI and Planetary Resources are interested in moving asteroids around in the future, but do not have any redirection missions planned yet.

The country of Luxembourg announced in early 2016 that it plans to invest several hundred million euros into the asteroid mining industry [9]. Later that year, they invited asteroid mining companies and interested parties to a workshop to answer questions about the future use of space resources [10]. The general science gaps that they identified were centered on detecting a large enough sample size, figuring out what they were made of before sending a spacecraft to asteroid, and regolith dynamics. What is clear among almost every extra-terrestrial mining operation is that water is the desired resource. There are countless papers on extracting and using or selling water from asteroids, the Moon, and even Mars. While asteroids might contain promising platinum-group metals, there is no technology capable of refining these metals in space.

This paper will be organized into four sections; **Section 1** will discuss the latest NEA detection capabilities, **Section 2** will review the most promising asteroid redirection methods, **Section 3** will analyze various asteroid mining technologies, and **Section 4** will convey some conclusions and suggestions.

Section 1 – Asteroid Discovery

Astronomers have been discovering asteroids since the 1800s, with Giuseppe Piazzi's discovery of 1 Ceres, an object in the main asteroid belt with a diameter of nearly 1000 km, in 1801. However, it was not until early 1970s when NASA began to take interest in NEOs by sending Pioneer 10 to Jupiter through the main asteroid belt [11]. Most NEOs appear to have originated from the main asteroid belt through a combination of processes, including planetary perturbations, collisions, thermal forces, and solar wind pressure. Such processes could have shifted asteroids into resonant orbits with planets, most notably Jupiter, which can drastically change their orbit and send them into the Near-Earth environment [12].

In 1994, the US Congress mandated NASA to "identify and catalogue within 10 years the orbital characteristics of all comets and asteroids that are greater than 1 kilometer in diameter and are in an orbit around the sun that crosses the orbit of the Earth" [13]. This mandate was completed two years after NASA started its NEO Observations Program in 1998 [14]. The Congress further mandated NASA in 2005 to "detect, track, catalogue, and characterize the physical characteristics of near-Earth objects equal to or greater than 140 meters in diameter in order to assess the threat of such near-Earth objects to the Earth. It shall be the goal of the Survey program to achieve 90 percent completion of its near-Earth object catalogue (based on statistically predicted populations of near-Earth objects) within 15 years after the date of enactment of this Act" [15]. Both mandates revolve around absolute size, in meters, of NEOs, which is an indirect metric because when any extraterrestrial object is detected it appears as a bright dot or streak, the intensity of which is given by a metric known as absolute magnitude. Absolute magnitude (H) is a measure of how bright an object is if it were 1 AU from Earth and 1 AU from the Sun (the L4 or L5 Lagrange points), with larger values representing dimmer objects in a logarithmic scale. This metric can be used to estimate an object's size, but is also dependent on the object's albedo, i.e., the percentage of light that the object reflects, depending on its size, shape, spin rate, and composition. Most asteroids' bolometric luminosity is concentrated in the IR spectrum [16], which is why optical and IR telescopes are used to search for them. Larger asteroids that rotate quickly, or have high thermal inertias, exhibit IR profiles similar to smaller objects [17]. By studying data on 419 NEAs from the 2010 Wide-field Infrared Survey Explorer (WISE) mission and follow-up optical observations, it was found that there are two average albedos for NEAs: 25.3% of studied NEAs have albedos centered at 0.030 and the remaining 74.7% are centered around 0.168 (3% and 16.8%

albedos, respectively) [18]. An object's diameter can be estimated using its absolute magnitude and albedo in the following equation [19]:

$$D = 10^{0.5*(6.259 - \log_{10} a - 0.4*H)}$$

(1)

which can be simplified as:

$$D = \frac{1347}{\sqrt{a}} 10^{-0.2*H}$$

(2)

where D is the diameter of the object in km, a is the object's albedo, and H is absolute magnitude. Equation (1) assumes that the object is a perfect sphere with a homogenous composition.

In 2016, NASA created the Planetary Defense Coordination Office, tasked with ensuring the early detection of Potentially Hazardous Objects (PHOs) [20]. The current definition of a PHO is any NEO that passes within 0.05 AU of Earth and has $H \geq 22$ [21]. A NEO with an $H = 22.0$ can have a diameter between 129 and 305 m using the two average values (3% and 16.8%); NASA uses an average albedo of 14% on its Center for NEO Studies (CNEOS) website to equate an absolute magnitude of 22.0 to a diameter of around 140 m. For comparison, kilometer-sized NEAs would have a corresponding absolute magnitude of 18, and 30-50 m NEAs would have an absolute magnitude of roughly 25. An average albedo of 14% is used throughout this paper.

1.1 Asteroid Population Estimation

In order to determine the proportion of discovered NEAs to their entire population and, hence, make a better assessment of discovery efforts, proper models should be developed for the distribution of small bodies in the Solar System. Several researchers have created models for the Size-Frequency Distributions (SFD) of NEAs in recent years, including Mainzer et al., 2011 [22], Harris et al., 2015 [23], Granvik et al., 2016 [24], and Tricarico, 2017 [25].

The estimation models in [22], [23] and [25] are based on randomly generating a large population of synthetic near-Earth asteroids, in the range of hundred thousand to one million, and simulating their evolution during a certain period of time (20 years in [23] and [25] but shorter in [22]). A simulated survey, in the form of a Monte Carlo simulation, then determines the asteroids detectability based on the detection efficiency of some of the real survey campaigns (see Section 2.2), while randomly assigning to the asteroids different absolute magnitudes, ranging from 8 to 30, in multiple runs. Several factors are considered for having a realistic detection ratio in the simulation, including survey trailing losses, viewing angles, galactic background, and NEA redetections. The obtained ratio of detectable synthetic asteroids to their total population is then used for estimating the total population of real asteroids from the discovered ones.

While these works create synthetic asteroids in near-Earth orbits, the study in [22] generates 70,708 synthetic NEA orbital distribution by simulating the evolution of known main-belt asteroids (prior to January 1, 2012), with an absolute magnitude of lower than 14.4 and 15.9 in two groups, over the next 100 million years, taking into account the gravity effect of 8 planets, from Mercury through Neptune, and a simple Yarkovsky drift factor. Rather than employing a Monte Carlo approach to their survey simulation, the researchers numerically integrate the nightly bias given by Catalina Sky Survey (see Section 2.2), as the sum of detection efficiencies over telescope pointings, and use the bias to obtain the ratio of detectable synthetic asteroids to their total population. The work also points to a lack of real-world NEAs with low perihelion distances, and thus includes a "disruption model," so that any asteroid that passed within 0.076 AU from the Sun was destroyed and removed from the results.
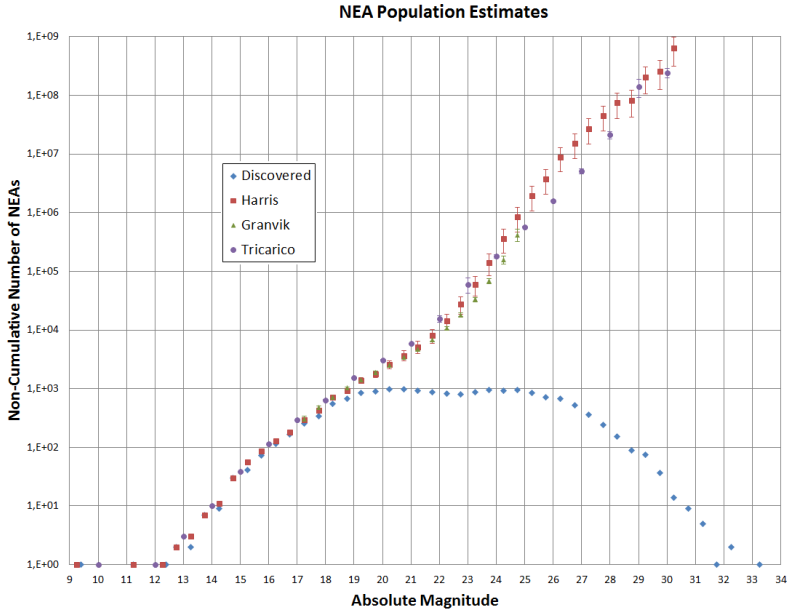
Figure 1: NEA Population Estimation (Discovered as of Oct 11, 2017)

NEA Population Estimates
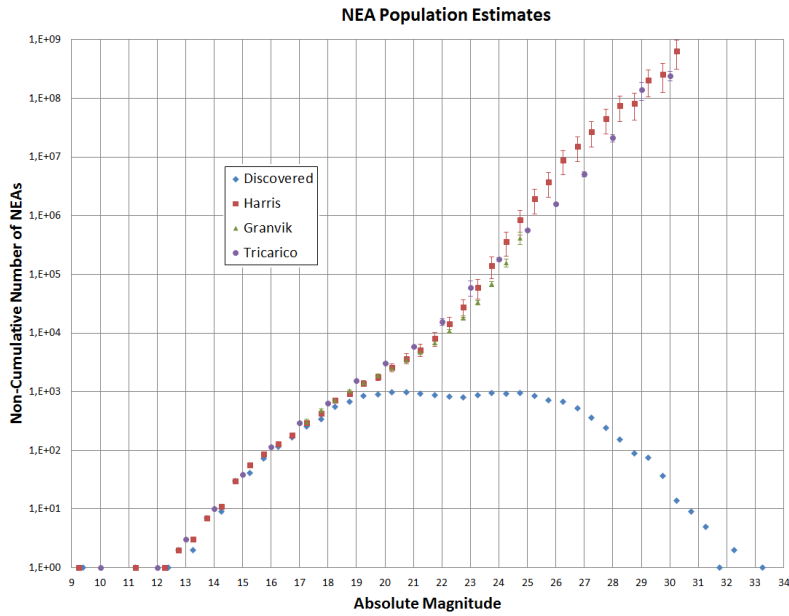
Figure 1 shows a comparison between the current distribution of discovered NEAs and their estimated population by the above-mentioned models. Regardless of the modeling method, the figure clearly depicts the divergence between the number of detected NEAs and estimated number of asteroids with absolute magnitudes greater than about 19, i.e., smaller than nearly 570 m in diameter. While the number of detections has been increasing over the past few years, the discovery rate has remained around 1,500 per year. Table 1 lists discovered NEAs with a notable diameter compared to their estimated populations. Approximately 94% of NEAs larger than 1 km have been discovered. However, only 29% of NEAs with a diameter larger than 140 m have been detected so far, and at a rate of 500 detections per year the discovery of such asteroids will extend the second congressional mandate deadline by 33 years. For objects between 10 and 50 meters, such as the 20m Chelyabinsk bolide [4], only about 4,600 NEAs of the estimated 29 million have been discovered, less than two tenths of one percent [25].

1.2 Asteroid Detection

Asteroids are detected by studying wide-angle images of the night sky at the optical and IR wavelengths. Charge-Coupled Devices (CCDs) at the focal points of such telescopes are exposed to around 30 seconds of incident light, which are then read out and stored as images. The automated tracking movement of robotic telescopes will ensure that large and distant objects, such as stars and galaxies, remain in the same location in a single image. Asteroids, on the other hand, move relatively quickly across the sky, some as quickly as 10 degrees per day [26]. The total amount of light received from an asteroid in one frame is spread

NEA Size	> 1 km	> 140 m	All Sizes
Discovered Population	875	8,537	16,188 (H < 33.2)
Estimated Total [25]	920 ± 10	27,116 ± 2,206	413 ± 100 million (H < 30.0)
Discovered in 2016	7	568	1,889
Discovered in 2015	9	527	1,572
Discovered in 2014	12	507	1,477

Table 1: NEA Discovery Statistics (as of October 2017) [207]

across several pixels, in a process known as "trailing loss," which makes detecting them even more difficult. To solve this problem, multiple sequential images are analyzed; a group of three or more sequential images is known as a "tracklet." Until recently, astronomers had to study these tracklets to see if anything seemed to move an outstanding distance over several frames; now, advanced algorithms and super computers are used to find asteroid *streaks* in these tracklets, but still need to be confirmed by a human observer. A streak is the pattern formed by an asteroid's trajectory in tracklets. This process can be formalized as the Blind Search Streak Detection (BSSD) problem.

A summary of various asteroid detection techniques is reviewed recently in [27], including spectrophotometry, radiometry, spectro-polarimetry, hyper-spectral imaging, and thermal modelling. The thesis also discusses a few water and metal mining methods.

1.2.1 Detection Methods

A conventional approach to the BSSD problem is the "shift-and-add" method, which was first introduced in 1992 for finding faint, trans-Neptunian objects [28]. After removing bright and stationary objects from the images, the algorithm shifts the pixels in the image frames of the tracklet relative to each other successively and co-adds the frames of each tracklet, as shown in Figure 2. This will create a simulated long-exposure image analogous to physical tracking of an object by the telescope. If the shifting direction is consistent with the object's movement, the synthetic image will show a bright spot. To examine all possible directions of the object's movement in a tracklet, the shifting action must be carried out in all directions in the frames, which a computationally intensive process. Several methods are suggested in the literature to make the search process more efficient, including Fourier volume rendering [29], Approximate Discrete Radon Transforming (ADRT) [30], Tilt and 3DRT [31]. A review of these methods can be found in [31].

Smaller NEAs can only be detected when they are very close to Earth, but this will also make them viewed as very fast-moving objects across the sky. Consequently, conventional 30-second exposures are not able to keep up with such objects, making their follow-up observations very difficult. Several advanced implementation of synthetic, or digital, tracking have been suggested recently, which use the shift-and-add

method but with shorter exposure times, enabling search algorithms to find much dimmer and faster-moving NEAs than those with traditional methods [26] [32]. Synthetic tracking enables rapid detection and coverage, giving more accurate astronomical data and wider follow-up observation windows. However, the method requires special CCDs capable of high framerates and low read-out noise. One NEA has already been detected using this method, utilizing the Caltech high-speed multi-color camera (CHIMERA) instrument with the Palomar's 200-inch telescope at Palomar Observatory. Through studying 501 frames over a 30-second period, the researchers found a (small) NEA with H=29, which was traveling at a rate of 6.32 degrees/day [33].
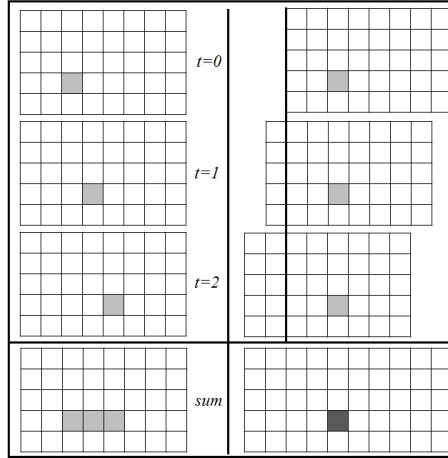

Figure 2: Shift-and-Add (Synthetic Tracking) Method. The left column represents an NEA's motion across the sky as seen from a telescope. The sum of the three frames is what a traditional long-exposure survey sample would see (assuming the light grey is undetectable or confused as noise by the survey). The right column represents a shift-and-add (or synthetic tracking) vector of negative one. By shifting each subsequent frame to the left by one, and THEN summing the pixel values, a dark grey spot appears (assume this darker grey is detectable by the survey). A shift in any other direction or magnitude would not produce a dark grey spot; the shift MUST correspond to the motion of the NEA.

Optical interferometry is also used for blind-search surveys of NEAs. By pointing multiple telescopes at the same patch of sky and combining their images, it is possible to detect fainter objects than a single telescope can. Further, unlike most of the single-telescope blind-search survey methods that need to make assumptions about the point-like characteristics of the objects, multiple-telescope approaches use many (small) apertures and fuse their images using statistical techniques, thus becoming independent from the shape of the object. Consequently, such survey methods can be used in more robust climates [34].

In 1995, the US Air Force created the Raven program for tracking satellites, asteroids and debris. It developed a system of small telescopes, using commercial off-the-shelf parts, to mimic the performance of a single large-aperture telescope [35]. Following the program's success, development of a new Raven-style network of telescopes dedicated to NEA-detection has been proposed [34] [36]. The primary advantage of Raven-style surveys is cost efficiency. It is estimated that a system of sixty 16-inch telescopes for $12.5 million can detect objects as faint as $H = 22.6$ by combining Poisson and Gaussian noise reduction algorithms [34], which is at least one order of magnitude less expensive than building and operating a single, large-aperture telescope with similar performance [37]. For example, the 8.4-m Large Synoptic Survey telescope (LSST), whose construction started in 2014 with the expected completion in 2022, will cost around $390 million upon completion [38]. More recently, a team from the Georgia Institute of Technology has developed a Raven-style telescope system to search for faint, transient events like NEOs, gamma ray bursts and supernovae, which is currently tested in Svalbard, Norway [36].

Another method for detecting small, fast-moving objects is developed in the Sloan Digital Sky Survey (SDSS), which uses multi-wavelength CCD scans with a small time separation between the wavelength components [39]. A fast-moving object appears in different locations in various wavelength components of the same image.

1.2.2 Automated Telescopes

Telescope movements are automated, both to maintain the telescope pointed at the same patch of sky during long exposures and to ensure that frame-to-frame scanning is precise and accurate. Some programs use automated follow-up scheduling to confirm the orbits of potential NEAs. Setting up and pointing a telescope require certain skills; however, it is now possible to use servo mechanisms with proper control software to ensure that the telescope is pointed reliably and accurately in the correct direction. Such automated systems alleviate the need for professionals to constantly be on-site, facilitating more astronomers to perform research. They also allow the telescopes to constantly produce scientific data, which can pay back the initial capital investment more rapidly. They are also particularly useful in education, as schools do not usually operate over night, when telescopes are often used [40].

The Small Autonomous Robotic Optical Nightwatcher (SAURON) is an 11-inch autonomous telescope at MIT's Wallace, Jr. Astrophysical Observatory [41]. They equipped the telescope with a COTS actuator system (Paramount ME II) for steering. The team uses TheSkyX software [42] to control the telescope, which includes initialization and periodic error corrections, MasterSync software [43] to ensure accurate GPS timing, and CCDAutoPilot software [44] to schedule the telescope and dome movements, download weather data, and automate observations.

A team at the Automation and Control Institute in Vienna developed a system of servo controllers for a 12-inch telescope using two direct-drive permanent-magnet synchronous motors as actuators and optical encoders as sensors. They were able to achieve a maximal error of 1.3 arcseconds in the declination axis and 0.5 arcseconds in the right-ascension axis at a rate of up to 5°/s, which is enough to track the International Space Station (ISS) [45].

The DEMONEXT telescope, operated by the Ohio State and Vanderbilt Universities, is a low-cost, automated 20-inch telescope used to follow up exoplanet transits and other transient events. The team uses Python to automate the telescope, including a screw-driven focuser and filter wheel. The automation software begins by looking at the results of the Kilodegree Extremely Little Telescope (KELT) survey, another automated telescope with a 4.2-cm aperture, and selecting targets based on viewing conditions and ephemerides of the candidates for the upcoming night. The telescope is calibrated using eleven bias and dark frames. A software application, called PWI3 [46], is used to calibrate the focuser by stepping through every focus of a few images. The nightly observation begins when the sun is 18 degrees below the horizon; if no exoplanet transients are scheduled, the software checks a list of monitor program targets to schedule pointings. Targets are given merits based on software called Remote Telescope System 2 [47]. Their reported design includes a wiring diagram, seen below in Figure 3, which illustrates how an automated telescope system is set up [48].
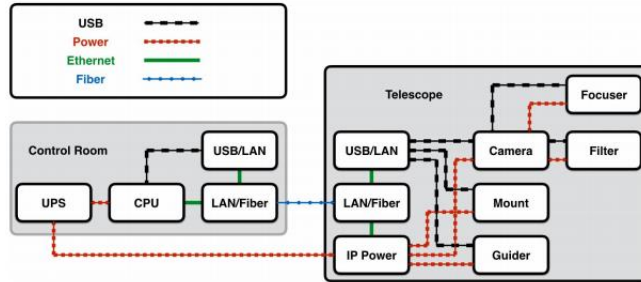
Figure 3: Wiring Diagram of DEMONEXT. Control Room is 40 feet from telescope [48].

There are several global networks of automated telescopes that allow a user to remotely operate them or passively collect data from them. To name a few, the Las Cumbres Observatory Global Telescope Network will have two 2-m, seventeen 1-m, and twenty-three 0.7-m telescopes to study UV-to-IR-wavelengths around the world [49]. Skynet Robotic Telescope Network has sixteen automated telescopes currently operational [50]. The iTelescope network has twenty telescopes in the US, Spain, and Australia [51].

1.2.3 Ground-based NEA Surveys

1.2.3.1 Catalina Sky Survey

The Catalina Sky Survey (CSS) consists of three unique surveys: the CSS Schmidt telescope, the Sliding Spring Survey (SSS), and the Mt. Lemmon Survey (MLS). The CSS Schmidt is the USA's second largest Schmidt telescope, at 0.7 m in aperture size. The SSS is a sister survey in New South Wales, Australia that consists of a 0.5m Schmidt telescope with the same camera as the CSS's. The MLS is the largest and most productive of the surveys, using a 1.5m telescope, capable of seeing objects with absolute magnitudes (H) less than 22. The MLS conducts discovery and follow-up observations of potential impactors, using photometry to determine size, shape, and spin vectors, and using spectrophotometry to determine composition and albedo of the NEAs [52].

1.2.3.2 Pan-STARRS

The Panoramic Survey Telescope and Rapid Response System (Pan-STARRS) consists of two 1.8m Ritchey-Chretien telescopes that observe three quarters of the sky in five optical filters: g (4866 Å), r (6215 Å), i (7545 Å), z (8679 Å), and y (9633 Å). For NEAs, it uses a wide filter, w, which spans g, r, and i ranges to observe the solar ecliptic plane [53]. It is stated that the survey would detect two ARM targets for NASA every year [54].

1.2.3.3 LINEAR

The Lincoln Near-Earth Asteroid Research Program (LINEAR) consists of two 1m GEODDSS telescopes, capable of detecting objects as faint as H=20. In 2013, LINEAR acquired DARPA's Space Surveillance Telescope (SST), a 3.5m Mersenne-Schmidt optical telescope, which was designed to detect space debris in geostationary orbit. It is now being used to discover and track both large NEAs that can satisfy the 2005 mandate and small NEAs that could be targets for ARM targets. In 2015, the telescope was moved from its home in New Mexico, USA, to Western Australia [55], and should be operational again by 2020 [56].

1.2.3.4 Future Ground Surveillance

The Asteroid Terrestrial-impact Last Alert System (ATLAS) Survey consists of one functioning 50cm Wright-Schmidt telescope, which can detect a 10m-wide object at a distance of 10 LD (Lunar

Distance). It was commissioned in 2015, and will consist of two identical telescopes spaced 100 miles apart. It is designed to complement Pan-STARRS by observing the entire sky every night [57].

The Large Synoptic Survey Telescope (LSST) will be a 8.4m telescope using six filters between 350 and 1100 nm [58]. It will use a 3.2 GP CCD camera, the largest in the world, and will be able to half the trailing loss compared to current NEA surveys. It began construction in 2014 in northern Chile, and is expected to achieve first science light by 2021 [59]. While the LSST will not be used exclusively for NEA searches, it will provide a significant contribution to the search at a fraction of the cost of a dedicated system.

1.2.4 Space-based NEA Surveys

In order to prevent damage to telescope's optics and hardware, NEA surveys have to operate when the observatory is facing away from the Sun. To overcome this limitation, space-based observatories can be deployed to increase the observation window.

The NASA report that led to the 2005 Congressional mandate states that current technology, as of 2003, was capable of finding orders of magnitude more objects by combining existing observation campaigns with a space-based observation platform dedicated to NEA detection [37]. Their suggestion was to place a 50cm IR telescope in a near-Venus orbit, which would orbit the Sun faster than Earth, and could see the space between Venus and Earth which is currently non-viewable by surface-based surveys, and would double the discovery rate of NEAs. The detection proportion from Erath and Venus orbits is illustrated in Figure 4 [60].
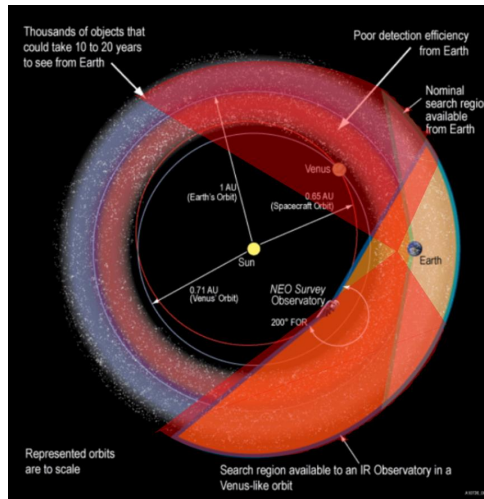
Figure 4: Detecting NEOs from a near-Venus orbit [60]. Top two text boxes are referring to an Earth-based-only

system. The red overlay represents the new NEOCam proposal.

This mission concept has since changed to an Earth-Sun L1 or L2 observatory, and named Near-Earth Object Camera (NEOCam); and has received extended Phase A funding in January 2017 [61]. Placing the spacecraft in the L1 or L2 point will yield the same survey completeness that a Venus-like orbit would; the Venusian observatory could potentially detect more objects, but is 30-170 times farther away from Earth than a Lagrangian observatory [16]. The NEOCam mission plans to detect two-thirds of NEAs larger than 140 m within four years of launch by using a 50cm telescope and two IR filters [62].

The only space-based telescope that has been used to detect NEAs is NASA's WISE mission, launched in 2009. It has a cooled 0.4m telescope that can detect four bands of IR, centered at 3.3, 4.7, 12, and 23 µm. The mission was designed to take a full-sky survey for six months, with eight passes over every region of the sky [63]. It orbits Earth at just under 500 km in a Sun-Synchronous orbit. Currently, its coolant has run out, and is now running in an extended mission mode, known as NEOWISE. As of March 2017, the telescope has discovered over 600 NEAs, and the project is reprocessing the primary mission data to look for more [64].

Both Canada and Germany attempted to fly small space-based telescopes for the explicit purpose of discovering new NEAs, but both failed. The Canadian Space Agency launched their Near Earth Object Surveillance Satellite (NEOSSat) in February 2013 to detect asteroids and comets, as well as monitor space debris. The optical CCD had irreparable damage, and could not produce accurate scientific images [65]. The German Asteroid Finder mission was cancelled in 2012, due to the excessive cost increase [66]. It was to use a 20cm telescope to detect objects that were between the Earth and Sun [67].

Section 2 – Asteroid Exploration

Once the orbit of a NEA is determined, researchers can study its physical properties such as size, shape, mass, spin, structure, and composition. Objects that are passing close to Earth and moving relatively slowly across the sky can be studied with optical or IR telescopes or by using radars. Most NEAs do not meet these criteria, so our knowledge of their physical properties is limited. A proven way to get high-resolution imagery and data from distant NEAs is to send a spacecraft to or by the asteroid.

2.1 Asteroid Identification

Asteroids are classified based on spectral absorption features from data obtained in the 2002 Small Main-Belt Asteroid Spectroscopic Survey (SMASS) [68], which analyzed visible- and near-IR-wavelength spectra for 1,341 asteroids in the Main Belt, between Mars and Jupiter, as well as 106 NEAs. Most of the data comes from the 2.4-m Hiltner telescope at the Michigan Dartmouth MIT (MDM) Observatory in Arizona, and covers wavelengths between 400 to 1000 nm. The survey defines three major groups of asteroids: S-type (stony/silicate), C-type (carbonaceous), and X-type (the rest). Twenty-six unique classes are split among the three groups based on their slopes and absorption windows in the visual/IR spectrum. The exact spectral properties are then compared against meteorite sample responses to estimate the composition of the asteroid. However, asteroids are constantly bombarded by meteorites and solar wind, which can alter their surface composition [69]. This means that studying surface properties of a NEA may not accurately reflect its subsurface composition and structure.

Major Taxonomic Types	Reflectance Spectrum (0.4-0.9 um)	Visible Albedo	Suspected Composition
D (D,T)	Blue → Red	0.02-0.06	Primitive carbonaceous Organic-rich compounds Hydrated minerals
C (C,B,F,G)	Blue → Red	0.03-0.10	Hydrated minerals Silicates Organics
X (E,M,P)	Blue → Red	E: 0.18-0.40 M: 0.10-0.18 P: 0.03-0.10	E: Enstatite-rich M: metallic, Nickel-Iron P: Carbonaceous, Organics
S (S,Q,A,K,L)	Blue → Red	0.10-0.22	Stony composition Magnesium Iron silicates
V	Blue → Red	0.20-0.60	Volcanic basalts Plutonic rocks

Figure 5: IR Profiles for Asteroids (Adapted from [69]).

In addition to studying spectral responses of asteroids, researchers study their brightness over time, the plot of which is called a "light curve." This can reveal several physical properties such as shape, spin vector, size, and potential moons. Since 2001, astronomers have been able to inverse light curve data to determine an object's general shape and spin vector [70]. The method requires high quality data from multiple viewing angles, in terms of sampling frequency, which is only available for a small number of NEAs. Light curves alone cannot determine the absolute size of the object either, and must be augmented with time chord data or direct observations from radar to scale the size of the object [71]. Asteroids in binary and triple-asteroid systems will often occult and eclipse each other, which will show up in the light curve data [72]. The Palmer Divide Observatory (PDO) in California uses a 1.5-m and a 5-m telescope to detect and characterize asteroids by their light curves [73]. Data from the PDO also shows that there is a limit to how fast an asteroid can rotate, depending on its size, without tearing itself apart due to centripetal force (roughly 2-hour periods for objects hundreds of meters in size) [74]. This is highly dependent on its internal structure, which could be a regolith pile, rubble pile, monolithic, or porous monolithic, which can hardly be determined remotely.

Delay-doppler radar is the best method for remote characterization of NEA surface structure [75] [76]. The Arecibo Observatory in Puerto Rico and the Goldstone Solar System Radar in California observe around 70-80 NEAs per year to determine size and shape within 2 meters, orbital data, spin vector, and surface density and roughness [77]. They are limited, however, to slow-moving objects that pass very close to Earth, subject to scheduling constraints, and require massive power to operate [78].
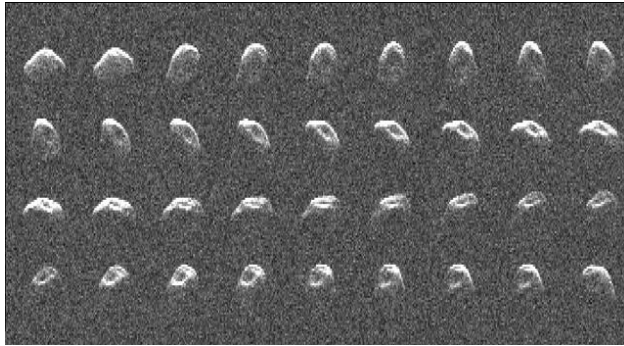
Figure 6: Goldstone Radar reconstruction of NEA 2010 JL33 at a distance of 8.5 million km (NASA JPL-Caltech).

Interferometry can also be used to determine the size of parent asteroids in multi-body systems as well as the semi-major axes of any moons [79].

The size of asteroids can be determined without knowledge of shape or composition when they pass by radio sources. Bright radio sources in the sky are pretty well understood, and they have distinct shapes caused by Fresnel-Kirchoff diffraction; when they are occulted by an asteroid, the shapes are distorted and their measured magnitude decreases, which can give an accurate size measurement within 2 km at 5 Ghz [80].

Some NEAs appear to orbit Earth in unusual ways; co-orbital objects share nearly the same orbital parameters as Earth, but are far enough away not to be captured by the Earth's gravity. They include quasi- or retrograde- satellites, Trojans or tadpoles, and horseshoe satellites [81]. Sometimes, NEAs come close enough that the Earth's gravity captures the object, making it a Temporarily Captured Object (TCO), colloquially known as "mini-moons." These objects make excellent candidates for technology demonstration missions regarding asteroid redirection and mining, due to their small size and their proximity to Earth [82] [83]. There are only one or two 1-2m objects in the steady state TCO population at any given time, plus a dozen objects around 50 cm in diameter; larger objects can be captured, but they are much less frequent events [84]. It is

suggested that TCOs as small as half a meter wide can be detected by a dedicated NEA survey with the 8.2-m Subaru Telescope in Hawaii [85].

2.2 Asteroid Characterization

To definitively determine the physical properties of distant NEAs, a robotic or manned spacecraft must be flown to the object for detailed studies.

The first images of an asteroid were taken in 1991 from NASA's Galileo spacecraft. It flew within 1600 km of the Main Belt asteroid 951 Gaspra at a relative speed of 8 km/s, and managed to take pictures of 80% of its surface. It showed a far larger number of craters than was predicted, and thus asteroid collision models had to be updated. Images from the onboard camera were synchronized with measurements from the infrared spectrometer to determine the mineral phases of the surface composition. A weak magnetic field was detected with the onboard magnetometer, implying the core had some ferromagnetic materials in it. Later in Galileo's mission, it rendezvoused with Main Belt asteroid 243 Ida, where it found a "small" kilometer-sized moon orbiting the main body, providing the first proof that asteroids can be binary or multi-body systems [86]. Since then, there have been several fly-bys of asteroids, but the first mission to enter "orbit" around an asteroid was NEAR at the 433 Eros NEA in year 2000. Astronomers were able to image boulders on the surface, most likely ejecta from the ancient craters. They were also able to determine the absolute size, mass and density from the spacecraft's GNC sensors, which revealed a porous substructure.

The prospecting company Gedex Inc. is working with SP Systems, and the University of Toronto's Space Flight Laboratory (SFL) to create a small satellite (<20 kg) capable of measuring the density of NEAs. They designed a 12U cubesat, called "Gravimetric Asteroid Surface Probe" (GRASP), capable of determining the density distribution and total mass of asteroids between 100 and 1000 m in diameter. Once it is deployed from a mothership already at a target NEA, it will use a small propulsion system to land on the surface. It will then use linear actuators and its attitude control system to move around the surface to take gravimeter and accelerometer readings at various points on the surface to map the gravity field and density distribution of the asteroid. It can also determine the exact mass of a surface boulder, for the NASA ARRM, for example. For small asteroids, the total size can be reduced to 3U by removing the attitude control, propulsion, and navigation subsystems [87].

The surface roughness of asteroid Vesta was analyzed by using the communication antennae of NASA's Dawn spacecraft. The bistatic radar experiment used NASA's 70-m Deep Space Network (DSN) dishes to listen while Dawn transmitted. Astronomers compared the surface roughness to that of the Moon by analyzing the Doppler spreading and power of the return signals [88].

The JAXA "Hayabusa" spacecraft, launched in May 2003, made history when it returned 1500 particles of surface dust from the asteroid 25143 Itokawa in June 2010 [89]. Scientists observed that the asteroid had low bulk density and several surface boulders and pillars, and concluded that it was subject to a catastrophic collision and reformation into the rubble pile they see today [90]. By studying the oxygen isotope distribution from the returned sample, scientists confirmed that each asteroid class has its own oxygen isotope profile [91]. Studies on the shapes of regolith particles from Itokawa also showed that meteoroid impacts formed the regolith particle shapes and seismic sifting abraded them over time. It was also observed that the regolith particle shapes differed from Lunar regolith particle shapes [92]. The samples were studied for element composition using X-rays [93], noble gasses [94], and soluble organic compounds [95].

There are two missions that are in development to rendezvous with a NEA, collect science and physical samples, and return to Earth with them. The OSIRIS-REx mission, run by NASA, will rendezvous with NEA 1999 RQ_{36}, colloquially known as Bennu, and study it with five different instruments as well as with its radio antenna. It will determine the size, shape, gravity field, spin vector, and surface composition, and select four potential landing sites for its sample collection phase. The spacecraft will approach within meters of the asteroid, and fire nitrogen gas at the surface. The lofted regolith will be collected and returned to Earth for future studies [96]. The other mission in development is Hayabusa 2, a sequel spacecraft to the Hayabusa mission by JAXA, which will visit asteroid 162173 Ryugu (1999 JU_3) and study the object for a year and a half before taking a sample of the surface regolith and returning to Earth by 2020. It is carrying an explosive impactor, which the main craft will study when it collides with the object at 2 km/s. The mission also has a lander, the Mobile Asteroid Surface Scout (MASCOT), which has an infrared spectrometer, a

magnetometer, a radiometer, and a camera, and is capable of moving around the surface to study different points [97].

Section 3 – Asteroid Deflection and Redirection

Several works have studied deflection and/or redirection of asteroids. Deflection methods seek to only change the asteroid trajectory to avert a potential impact with Earth, whereas redirection methods imply a controlled change of asteroid orbit for future use. Different methods of redirecting a NEA have been theorized, which pose their own strengths and weaknesses with regard to factors such as fuel requirements, mission and development time, and cost. Technologies that are developed to de-orbit or otherwise remove orbital debris also push the similar technologies required for asteroid deflection and redirection.

A 2006 analysis by the University of Glasgow studies various deflection and redirection methods, including solar collector, nuclear blast, kinetic impactor, low-thrust propulsion, and mass driver [98]. They compare these various methods by studying their achieved miss distance at Earth (given as the MOID,) the warning time (difference between time of impact and full redirection mission implementation,) total mass of redirection system at launch, and the Technology Readiness Level (TRL.) They then run an optimization function to find a set of Pareto optimal solutions that minimize system mass and warning time, and maximize deflection distance. They conclude that solar collector and nuclear blast are "best" if TRL is not taken into account, and kinetic impact becomes competitive when TRL is taken into account.

The Keck Institute for Space Studies published a report in 2012, with the help of NASA's JPL, which outlines a full asteroid retrieval mission, similar to the ARRM concept. The report discusses asteroid selection, spacecraft design, and mission and orbit design. It suggests that a $2.65 billion spacecraft could redirect a 500,000-kg boulder to high lunar orbit by 2025. It also recommends the development of a 40-kW-class ion engine to deliver an "instrument pre-package" to an asteroid for use by human explorers after it is redirected to the Earth-Moon system [99].

While NASA's ARRM mission was in development, the JPL made a summary in 2015 of some similar methods, such as kinetic impactor, ion beam deflection, gravity tractor, enhanced gravity tractor, and laser ablation [100]. They required the object to miss Earth by 2 Earth radii, and studied the effectiveness of these methods for objects between 50 m and 1 km in size over a warning time span of 5 to 30 years (that is build, rendezvous, and deflection time.) The asteroids were assumed with S-type composition, spherical in shape, 2 kg/m3 in density, and without any rotation. They found that for objects less than 300 m in diameter, a single kinetic impact can divert a NEA off its collision trajectory in the least amount of warning time. By launching three separate kinetic impact missions, objects up to 600 m in diameter can be deflected in minimal time, as well. For larger objects, laser ablation was found to be most effective, but is currently low in TRL and is incompatible with metallic objects (laser would reflect, not ablate.)

Another analysis by the University of Toronto was conducted in 2016 on ion beam shepherd, tugboat, gravity tractor, laser sublimation, and mass ejector [101]. They compared each redirection method using the following criteria: system mass, system volume, TRL, delta-v of the target asteroid, mission risk, system cost, average power requirement, robustness (a Monte Carlo simulation of varying delta-v values for each method, alteration of the shape or structure of the asteroid, and long-term value in terms of reusability and system extensibility. They found that ion beam redirection performed best with tugboat and gravity tractor close behind. Mass ejector destroyed too much of the asteroid to be useful for scientific purposes, and laser ablation was not effective on rotating or metallic targets.

This survey will highlight two deflection methods and five redirection techniques: kinetic impactor and nuclear blast deflection methods and gravity tractor, ion-beam redirection, tugboat, laser sublimation, and mass driver redirection methods.

3.1 Deflection Techniques

3.1.1 Kinetic Impactor

The most primitive and technologically ready method for deflecting an asteroid is to fly into it; the momentum transfer during the impact provides enough energy to divert the asteroid from collision with Earth. A 1992 study [102] showed that kinetic deflection is most effective along its original orbit at perihelion; it

also noted that the energy/momentum transfer from a kinetic impact is much more efficient than a nearby nuclear charge detonation.

A kinetic impact redirection mission has already been conducted. The Deep Impact mission, launched in January 2005 sought to study the interior composition of a comet by creating an artificial impact (lofting the surface regolith and revealing the subsurface substrate). While redirecting the comet was not the primary purpose of the mission, it nonetheless demonstrated that a small body can be deflected by steering a spacecraft into it. The impactor spacecraft had a mass of 370.5 kg and collided with comet Tempel 1 at a relative speed of 10.3 km/s. If we assume a perfectly inelastic collision and the comet as the reference frame center, the comet's orbital velocity was altered by about half a micrometer per second relative to the impact direction.

$$(m_{sc,i} * v_{sc,i}) + (m_{c,i} * v_{c,i}) = (m_{sc,i} + m_{c,i}) * v_{c,f}$$

$$(370.5 kg * 10.3 * 10^3 m/s) + (6.78 * 10^{10} kg * 0 m/s) = (6.78 * 10^{10} \ kg) * v_{c,f}$$

$$v_{c,f} = 5.6 * 10^{-5} \ m/s$$

where $m_{sc,i}$ is the mass of the spacecraft, $v_{sc,i}$ is the velocity of the spacecraft relative to the comet upon impact, $m_{c,i}$ the the mass of the comet before impact, $v_{c,i}$ is the initial comet velocity, set to zero as it is the origin of reference frame, and $v_{c,f}$ is the velocity of the comet and spacecraft mass after the collision. The total mass of the comet was determined by multiplying the average core density of 600 kg/m3 by its volume (assumed 6-km-wide sphere) [103].

Another kinetic impact mission is in development today: the Asteroid Impact and Deflection Assessment (AIDA) mission, a collaboration between NASA and ESA, involves sending an impactor spacecraft to deflect the smaller body in the Didymos binary system in 2022 [104]. Both space agencies will be developing their own independent spacecraft to be launched together: the Double Asteroid Redirection Test (DART) spacecraft will be built by NASA to collide with the smaller body at 6 km/s using onboard cameras and navigation systems, and the Asteroid Impact Mission (AIM) spacecraft, developed by ESA, will study the motion of both bodies in the system before and after the impact, as well as the properties and composition of the plume of ejected material created after the impact.

A second kinetic impact method would be to redirect another asteroid or comet to collide with the dangerous NEO, rather than destroying an expensive spacecraft. One study suggests using a solar sail to impart a total of 60 km/s of delta-v to a 2-km-wide asteroid, putting it on a retrograde orbit relative to Earth, which would give it maximal relative velocity for a kinetic impact [105].

One risk with both kinetic impact and nuclear blast is the fragmentation of the original body into smaller, potentially dangerous chunks. A study was conducted to analyze the effects of kinetic impact at various velocities (1-30km/s) on various structures of asteroid [106]. Another risk is that the navigation computer of the impactor failing to correctly calculate the impact trajectory, and missing the object completely. One team ran Monte Carlo simulations on the AutoNav onboard autonomous navigation system used on Deep Impact to determine its efficiency at conducting its mission on smaller targets (100-300m in diameter) and at varying speeds (7.5-20km/s) [107]. They found a high probability for success (>90%) in most cases, and that impact chance is highly related to the quality of the onboard gyroscopes; they also ran a simulation for their own Impactor for Surface and Interior Science (ISIS) mission with successful results [108].

3.1.2 Nuclear Blast

Another deflection technique would be to detonate a nuclear warhead near, on, or under the surface of a NEA. Detonation of a nuclear charge remains the only solution to deflecting a NEA given very short warning times (several months to a few years). Most monolithic or low-porous monolithic asteroids will not be fragmented by a surface nuclear blast, but for smaller objects (under 300 meters) fragmentation will probably occur [109]. As of 2013, nuclear charges will be prematurely destroyed by impacts greater than 300 m/s, but various solutions to very high speed nuclear impacts are being studied and developed at the Iowa State University (ISU) [110] [111]. Multiple nuclear fragmentation models and orbital dispersions have been developed at ISU, as well [112] [113] [114] [115]. A study by Russian scientists, published in 2016 [116],

calculated the effects a one-megaton nuclear charge would have at varying distances to a large asteroid. In the initial phase of the nuclear explosion, the matter surrounding the charge was instantly vaporized, and the surrounding matter was superheated by a thermal wave, followed by a shock wave that deformed the asteroid material. Objects under 25 m in diameter would be instantly destroyed, while objects between 25 m and up to 200 m would splinter into smaller objects no larger than 10 m.

A key risk in this method is the warning time. While a nuclear charge has never been detonated in deep space, a few have been detonated in Earth's upper atmosphere, causing Electromagnetic Pulses (EMPs) that interfered with power grids and other systems, and ionized the surrounding atmosphere, which was then pulled around by the Earth's magnetic field. If the asteroid is obliterated close to Earth, the radioactive fragments would collide with Earth. However, if the asteroid is detected well enough in advance, the fragments will have enough time to "cool off," and might pass by Earth completely.

3.2 Redirection Methods

3.2.1 Gravity Tractor

The simplest redirection method involves using the law of gravity to pull on an object. A spacecraft positions itself near a target NEA, and the two objects will then begin to slowly attract each other; without added energy, the two bodies will eventually touch, so some station keeping is necessary. This method was first suggested in 2005, proposing to use a 20-ton spacecraft with nuclear-powered ion engines to apply 1-N of equivalent pull on a 200-m asteroid for one year given 20 years of warning time [117]. Rather than using a complex nuclear system, the tractor spacecraft could be equipped with solar sails [118]. It is found to be most efficient when multiple spacecraft are flown in a singular halo orbit near a NEA; the asteroid's acceleration vector would be in the same direction as the orbital normal vector [119] [120]. More spacecraft can be flown in other halo orbits to further multiply the net force.

The limiting factor in this method is the masses involved. Massive asteroids require more massive spacecraft to generate an equivalent net acceleration. The maximum mass a single launch vehicle can put into LEO is the Falcon Heavy (at 63.8 metric tons, as of 2017 [121].) The spacecraft will also slowly be losing mass over time due to their engines using fuel to maintain position, further reducing the force the object feels. The spacecraft need to also ensure the plume of exhaust does not contact the object, as that would negate the net force.

One study suggested charging a target asteroid with Polonium, and a tractor spacecraft by emitting electrons or ions to create an electrostatic force between them [122]. They suggest that for small objects (around 10-m in diameter) electrostatic forces at 20 kV would dominate gravitational ones. Another work studies how to generate electric fields to use with such a method [123]. Another study suggests using electromagnets to push or pull an asteroid [124]. A spacecraft would rendezvous with a NEA, launch magnetic projectiles at the surface, which would interact with the spacecraft's magnet(s), either pushing or pulling it depending on the polarization of the spacecraft's magnets.

3.2.2 Ion Beam

The ion beam redirection method (IBRM) involves pointing an active ion thruster at a NEA, using the exhaust plume to push on the object. The method was first patented in 2010 [125], and described in 2011 [126] as an "Ion Beam Shepherd," adapted from another report that sought to deorbit space debris using the same method [127]. The IBRM spacecraft must also have a thruster pointing in the exact opposite direction to maintain the spacecraft's position relative to the NEA. The spacecraft's distance to the asteroid must be within the beam divergence of the thruster, which can be as low as 15 degrees [126], otherwise the exhaust ions will pass by the NEA, unable to impart force on the object.

The primary advantage to using the IBRM is that its technology is at the state-of-the-art level, and can be built using COTS parts. Ion engines have been flying in space since the SERT-1 mission in the mid-60's; the SERT-1 mission's Kaufman ion thruster used 1.4 kW of electrical energy to produce around 28 mN of thrust at a specific impulse of 4900 s [128]. Another advantage of the IBRM is its applicability to any object: knowledge of the size, shape, spin, and composition of the asteroid is not required for the mission to be a success. The primary drawback to using the IBRM is the thrust-to-power ratio requirement, which has

not increased much since SERT-1 mission. For instance, NASA's latest gridded ion engine, the NEXT, uses 6.9 kW of energy to produce 230 mN of thrust with a specific impulse of 4190 s [129].

Some risks with the spacecraft itself include high power requirements, very long thruster operation times, attitude and position control failure, and high fuel requirements. Other risks involving the asteroid include: charging the asteroid by accumulation of ions, structural integrity threatened by the plume, contamination of the thrusters and solar panels by a potentially dusty environment.

3.2.3 Tugboat

The tugboat redirection method, first published in 2003 [130], involves landing one or several spacecraft on the surface of an asteroid and using thrusters facing outward to push the NEA. For instance, a 5-ton, low-thrust lander with a gimballed thruster can protect Earth from objects under 170 m, as well as apply a controlled enough force to redirect an asteroid into the EMS [131]. Using gimballed thrusters or flexible landing legs, the thrust vector from the spacecraft must be aligned with the center of mass, otherwise moments would be applied, and the NEA would begin to spin. The spacecraft could go out of line-of-sight with Earth, thus it must be capable of autonomous operations; it could also become eclipsed, rendering solar panel power generation ineffective, and would require either a mothership providing it with power or a secondary power source for use during eclipses.

One of the most important technologies associated with this method is the landing/attachment mechanism. Near-Earth asteroids have very low surface gravity, thus very low escape velocities. Any downward anchoring force would also push the spacecraft away, potentially escaping the gravity well of the object. Little is known about the surface consistencies of the discovered NEAs. They can vary from loose packed regolith or flour-like dust [132] to rubble piles of stone [90]. Certain landing mechanisms only function on solid rock or magnetic substances or dense regolith.

A recent work, published in January 2018, studied the viability of the tugboat redirection method using multiple landers [133]. The paper considers C-type NEAs that pass within 0.05 AU of the Earth and are no larger than H = 22.0. It investigates the feasibility of 10,000 different variations of return delta-V (1 – 2,370 m/s) and asteroid diameters (1 – 150 m) using a net present value method and implementing a genetic algorithm to optimize the number of spacecraft and power requirement for each. The study concludes that asteroids between 5 and 40 m with delta-V values less than 200 m/s are ideal candidates for return. For example, NEA 2009 BD (a small <5 m asteroid) can be redirected with 127.4 m/s of delta-V within 2.4 years; the two spacecraft would weigh 360kg and consume 3 kW of power each. The mission is estimated to cost $276 million with an 18% return-on-investment.

3.2.4 Ablation/Sublimation

If a small pinpoint-sized area of the surface of a NEA is subjected to intense energy, be it via solar collector or laser, the material will vaporize and/or sputter at escape velocity; this momentum transfer acts as a thruster, pushing the asteroid in the opposite direction of the plume. Solar concentrators were first suggested in 1993 to divert asteroids on collision courses with Earth [134]. More recent studies have suggested using a series of spacecraft equipped with mirrors to sublimate the surface of NEAs [135] [136].

A summary of the state of the art in laser ablation technologies (not just asteroid redirection) is presented in a 2012 report [137]. A thesis published in 2014 reviews redirection methods and orbital dynamics, and contains a detailed design of a laser sublimation spacecraft, which uses a 860- or 1032-W laser centered on 1070 nm and weighing 24 kg [138]. The dissertation also reports several physical experiments in a laboratory, which tested a 90-W 808 nm laser on three meteorite samples: a LL6 ordinary chondrite, a CV3 carbonaceous chondrite, and a metallic H4/5 ordinary chondrite.

The designers of the LightTouch[2] mission, funded by ESA's General Studies Programme, suggest launching a small satellite after 2025 capable of deflecting a 4-m-wide object by at least 1 m/s using laser ablation [139].

An experiment conducted in 2013 [140] shows that a 90-W laser can create a plume of ejecta on a sample of olivine. The thrust dropped by an order of magnitude after 10 minutes, due to an assumed loss of focus of the laser. The laser was not hot enough to vaporize certain materials that were mixed in the olivine, which could block further progress of the laser. Most of the thrust comes from the vaporized material, not sputtering. The study concludes that it could be an effective means of tunneling into an object (assuming a powerful enough laser,) extracting materials via an exhaust plume of deep-seated materials, otherwise inaccessible by traditional sampling techniques. The study later created better laser ablation simulation models to match the experimental results [141].

One drawback with the ablation/sublimation method is with respect to rotating asteroids. The plume should be in line with the center of mass to prevent torque buildup, as such the spacecraft needs to be able to maintain laser focal length and spot control as the asteroid spins. One work suggests using this method to actively control the rotation rate of the asteroid as to minimize the mission time spent on firing the laser [142]. To alleviate this issue, multiple spacecraft can be used in formation to maintain constant thrust taking benefit from redundancy and fault-tolerance [143] [144].

While most laser ablation missions assume a long-term, low-thrust operating style, one work studied how powerful of a laser would be required to divert an asteroid one orbital period [145]. The report concludes that for a 130-m asteroid, a 295-kW laser would be required to avoid an Earth impact; for a 300-m asteroid, that requirement increases to 8.52 MW.

3.2.5 Mass Driver

The mass driver redirection method involves throwing off materials from the asteroid faster than its escape velocity; the momentum exchange will then propel the asteroid forward. The mass driver system was theorized by the science fiction writer Arthur C. Clarke in his 1953 book "Childhood's End" [146], and first technically published in 1977 as a means of extracting 600,000 tons of Lunar material off of the Moon's surface per year with an electromagnetic rail gun [147]. In 1980, the mass driver method was suggested to be used for redirecting asteroids [148] or for sending processed asteroid materials back to an Earth orbit.

If an asteroid contains magnetic materials, an electromagnetic rail gun could be used to eject the matter at very high speeds, imparting more momentum than a mechanical system would. A study in 2007 suggests using several landers with timed ejections to produce thrust [149].

This method is the most technologically difficult, as it involves a spacecraft capable of landing on an asteroid, gathering and processing materials, as well as a mechanism capable of launching material. Further, the concern about space debris around Earth is also valid everywhere else in space. By flinging small objects from the asteroid, we may eventually create an unsustainable environment for future explorations.

3.3 Orbit Considerations

To measure the effectiveness of deflection and redirection methods, one must consider the resulting or final orbital path of the moved asteroid. For a deflection mission, "not hitting Earth" is an acceptable outcome; for redirection missions, however, the goal is to alter the orbit in such a way that the asteroid either will never return to Earth again or will be easily accessible from Earth. In this regard, many papers have been written on the orbital dynamics of small body capture.

To reduce the amount of fuel required for a spacecraft (or an asteroid) to enter orbit around a planet, a flyby of one of its moons can be done, a method first published in 1979 [150]. The Galileo [151] and Cassini [152] missions both used a moon of the parent body (Jupiter and Saturn, respectively) to decrease their required insertion burn fuel requirements. One paper suggests capturing asteroids by using the Moon as a gravitational sling by analyzing various Jacobi constants [153]. Another paper studies the orbital dynamics of moving small asteroids to the Earth-Sun L2 point [154]. The results of ESA's Asteroid Retrieval Project are presented in [155], creating low-thrust trajectories for the 17 closest NEAs. There have been many alterations to NASA's ARRM mission, but a destination of a Lunar Distant Retrograde Orbit (DRO) is common. For a sample Asteroid 2009 BD, capture would require 165 m/s of delta-V to enter an unstable DRO at the Earth-Moon L1 or L2 point, after which an additional 16 m/s would be required to trim the orbit into a stable one [156].

Every method, save for nuclear blast, causes relatively slow acceleration ($\mu m/s^2$ range), which, while not useful in an emergency situation, can be used to preemptively move an object out of its "keyhole," region in space where some NEAs might enter leading them to collide with Earth on a future close approach. It has been shown that altering the radial orbital parameters on a close-approaching NEA is five times more efficient with regard to the required delta-V change of the asteroid than making alterations to its in-orbit motion [157].

Low-thrust orbital maneuvers require optimization, either mathematically or heuristically. For instance, a model using a minimized form of Gauss' variational equations is used in [158] to determine the available trajectories for Arjuna-type asteroid redirection. Another method, known as "pseudo-equinoctial shaping", first suggested in 2007 [159], is used to determine an initial first-guess as to the optimal return trajectory. This method is applied to the return trajectories of NEAs, specifically Arjuna-type asteroids [160]. The work ran a genetic algorithm on the return profiles of Asteroid 2013 RZ_{53} to minimize the delta-V required to redirect the NEA to the Earth-Moon system.

Section 4 – Asteroid Mining

Asteroid mining was first suggested in 1898 in the novel "Edison's Conquest of Mars," where gold was mined from an asteroid [161]. It remained in the realm of science fiction until the late 70s, such as when the US Congress approved funding for NASA to study "solar power satellites" and the feasibility of building them with lunar and asteroidal materials [162]. Since then, many asteroid mining infrastructures, roadmaps, systems, and architectures have been suggested.

One study in 2013 developed such a framework by describing what resources are accessible, the economics of those resources, developing a mission and spacecraft designs, i.e., the Robotic Asteroid Prospector (RAP), and reviewing asteroid mining technology. The study suggested that there are three key target resources in NEAs: water, Platinum-Group Metals (PGMs), and bulk regolith. Water would be the first commodity sold to in-space customers, primarily as a fuel, and for use in life support systems. Bulk regolith, also to be sold to in-space customers, could be shaped to provide radiation protection or used for space additive manufacturing to construct large-scale structures that are impossible to launch from Earth. The PGMs are most likely to be sold to clients on Earth, and are the most complicated to mine. The study concludes that an asteroid mining mission is not feasible unless the resources are processed in-situ before being sent back to the Earth system [163].

In life support systems, water could be used as-is for drinking, or electrolyzed to produce O_2 for breathing. As for fuel: the company DSI has developed the Comet-1 thruster for cubesats, which uses water as a propellant [164], with the anticipation of future larger spacecraft needing to be refueled in LEO. Water can also be electrolyzed to produce hydrogen and oxygen gasses, which can be combined in a combustion reaction to produce thrust. The company Tethers Unlimited Incorporated has developed the HYDROS thruster for nanosatellites and microsatellites, which electrolyzes water in orbit, being able to produce over 1.5 N of thrust at over 310 s of ISP [165].

A new book, published in January 2018, studies how space resource utilization can be beneficial to emerging countries [166]. The book has a short section on technical space mining methods, but mostly focuses on the economic, political, legal, and social state-of-the-art frameworks, in terms of developed space-faring nations.

The overall process of mining asteroids can be broken down to several phases similarly to the mining operations here on Earth's surface. Table 2 below lists the high-level phases of mining in space [163].

Phase	Detail
Prospecting	Scanning, probing, or mapping an asteroid to determine how much and where target materials are located
Excavation	Removing target materials from the asteroid
Processing	Transforming raw products from excavation process into shapes or forms needed for the refinement process
Refining	Extracting important products from the processed asteroid materials
Storage	Turning the extracted products into a stable, useable, transferable, and storable form

Table 2: Asteroid Mining Phases (adopted from *[163]*)

The International Space University (ISU) organized a multidisciplinary international team in the 2010 Space Studies Program to produce a report titled ASTRA (ASteroid mining Technologies, Roadmap, and Applications) which combined physical sciences, engineering, space law, business, and life sciences to identify challenges with a commercial asteroid mining system and to suggest possible solutions [167]. They concluded that mass characterization of NEAs is the first step in the asteroid mining industry.

4.1 - Prospecting

Prospecting is defined as searching for mineral resources. The surface composition can be estimated by comparing optical and IR images of an NEA to meteorite samples and other Earth-based proxies, but space weathering and collisions may alter the composition of the surface of the object. X-ray and gamma-ray spectroscopes can be used to determine the presence of many chemicals [78]. Estimates can be made about the composition beneath the surface using a density map, but for an accurate model, sampling of materials under the surface must be conducted. Traditionally, a single lander with a comprehensive set of sensors and sampling technologies would be sent to the NEA, where it would either land in one spot and conduct extensive science, or attempt to rove around the asteroid, collecting data from various points; an example of this would be the Philae lander. A newer approach would be to use a heterogeneous team of small and redundant satellites, including landers, rovers, orbiters, tumblers, etc., with simple sampling mechanisms to compile a detailed model of the inside of the NEA. Asteroid Initiatives LLC are developing femtosatellites called Pixies, roughly the size of a modern smartphone, to swarm around a NEA and take pictures of it [168].

Regardless of the number of landers, it is vital that the surface consistency be determined before designing a landing mechanism for a potential lander craft. Several landing mechanisms include drills, harpoons, magnets, glue, and envelopment have been explored in a NASA/Honeybee Robotics analysis [169]. Specifically, they tested weight-on-bit (WOB) drilling, nail hammering, described liquid adhesive footpads, a Cadtrak self-opposing drill anchor system, Honeybee's self-opposing multi-mode anchor, and NASA's self-opposing microspine anchors. If a NEA possesses magnetic materials, a magnetic anchor could be used.

Water cannot exist as ice or snow in space within 2.7 AU from the Sun, as it is too hot; this is known as the "snow line" [170]. Instead, it usually exists in hydrated regolith or is chemically bound to other materials. Water and/or hydroxyl (OH-) were detected on asteroid 16 Psyche by studying the $3\mu m$ absorption band [171]. Sufficient water for commercial utilization in space is estimated to be in 1 out of about 1100 NEAs [172], which puts the estimated total at over 9,000, considering the estimated 10 million NEAs greater than 18 m in diameter [23]. Planetary Resources has developed a mid-wave infrared camera for detecting water on NEAs, and it is in use in space now to image water features on the Earth's surface [173].

Humans are scheduled to conduct Extra-Vehicular Activities (EVAs) on the asteroid redirected by NASA's ARRM mission. Astronauts aboard the ISS have trouble with stabilization and tool utilization, due to

the microgravity. Since July 2016, NASA has been working on developing tools and systems to enable safe and effective sampling of materials and human movement about a NEA, including chip, float, regolith, and surface samplers, drills, stabilizers, anchors, and cameras [174]. A tool called the Portable Asteroid Lift and Lock Aggregate System (PALLAS) was developed for $262.45, which will allow astronauts to grab loose or floating rocks from a NEA [175].

Another method of determining sub-surface composition is to make and study craters. The Hayabusa mission fired a 5-gram tantalum pellet at 300 m/s into the surface of the NEA Itokawa, and captured some 1500 grains from the impact, which were returned to Earth for study. A study of low-velocity, low-gravity impacts into loose granular media shows that the penetration depth scales linearly with velocity, and that no rebounding was observed in any of the experiments [176]. A team at the University of Colorado, Boulder, are developing a dust-capture instrument for use after a kinetic or explosive impact. They have concluded that dust does not remain lofted for long after an impact, and must be captured quickly [177].

Optical and X- and gamma-ray spectroscopy suffer from spectral deconvolution difficulties, low spatial resolution, and thermal/matrix effects; X-ray fluorescence spectroscopy and alpha particle X-ray spectroscopy are limited by the detectability of Hydrogen and Carbon and of the time/complexity of the sampling process itself [178]. A new method, Laser-Induced Breakdown Spectroscopy (LIBS), can circumvent these issues, and has even been demonstrated in-situ: the Curiosity rover uses LIBS by the ChemCam instrument to study the concentrations of Hydrogen, Carbon, Nitrogen, and Oxygen on the Martian surface. The next iteration of the ChemCam instrument, Laser-Induced Remote Analysis (LIRA), was verified in a laboratory, and can conduct sampling at a distance of 10 meters. Long-distance LIBS would make a very effective prospecting tool.

4.2 Excavation

When using a drill in microgravity, the counter-torque applied to the spacecraft needs to be stabilized and removed, with either a second counter-spinning drill or onboard reaction wheels. A repulsive force is also felt by the spacecraft as the drill makes its way down, which requires some means of dissipation, whether it be through landing legs or using the ship's onboard thrusters to apply a "weight" to the drill bit. The weight on the bit and the speed at which it turns can be precisely controlled to increase performance of the drill; a percussive or hammer-drill system uses more power, but can allow for greater effective weight-on-bit [179]. It could also be increased by using microwaves to heat and weaken the substrate at the drill site [180] [181] [182]. Bit force can be reduced by stimulating piezoceramic materials to vibrate the bit at ultrasonic (~20 kHz) frequencies [183]. Researchers at the University of Glasgow designed and developed a core-sample-retrieval drill, integrated it to a rover, and studied the performance of the drill and the holes and samples it took [184]. Deltion Innovations has conducted thermal-vacuum tests on their DESTIN instrument, a drill on lunar-style regolith [185].

If the surface gravity is sufficient and the surface regolith soft enough, it is possible to use a bucket wheel system on a rover, such as the one tested at the University of Arizona in 2016 [186]. One of NASA's old Lunar regolith production and excavator/drilling technologies was re-analyzed in 2016, but no official publication of the results yet exists [187]. If the regolith is loose, light and magnetic, an electromagnetic "vacuum" system can be used to suck up the regolith. Several teams have been working on electromagnetic surface regolith samplers to loft and capture magnetic regolith [188] [189].

A team from the University of Tokyo studied the thermodynamics involved in encapsulating a TCO and using solar energy to heat the object to extract water vapor [190].

A team from the Georgia Institute of Technology proposed a 3.6-billion-dollar spacecraft capable of creating 20-cm blocks from a NEA. Their spacecraft would rendezvous with a NEA, attach itself, and use a combination of plasma and laser cutters to extract cubes for resource extraction or habitat building [191].

Terrestrial mining utilizes chemical explosives to loosen rock, which could be applied to asteroid mining as well. Apollo 16 astronauts detonated HNS/Teflon explosives and studied the craters, which were much larger in the reduced gravity [192].

4.3 Processing

The TransAstra Corporation has prototyped a solar concentrator that focuses solar energy to heat and spall asteroid simulants [193]. The heating releases volatile gases and the spalling transforms the ore into potential refining-sized fragments.

Researchers at the Advanced Space Concepts Laboratory of the University of Strathclyde in Glasgow published a paper in 2014 suggesting that solar radiation pressure can be utilized to sort grains by size. The constant force will accelerate smaller, less massive particles to faster velocities than larger, more massive ones. The report suggests two ways of collecting the material, both involve one lofting rover and one collecting craft. The first is to loft the dust high enough such that a nearby hovering/orbiting spacecraft could collect it; sorting the material over time by mass/size with every pass. The second way is to let the lofted dust land back on the asteroid, where lighter particles would have travelled further in orbit around the asteroid than the heavier ones. A second rover would then be able to sort the regolith by distance, rather than time [194].

4.4 Refining

Water ice was extracted from various regolith simulants by heating it above 500° C in a study published in early 2017 [195]. The researchers heated three simulants and a meteorite sample in a vacuum, resulting in vaporization of volatile gases, which they measured with a mass spectrometer. They then used a liquid-nitrogen-cooled condenser to gather the gasses, and weighed the formed ices. As gravity has little effect on the process, it is safe to assume that the extraction process would work similarly in space as well.

A team from NASA's Space Technology Mission Directorate has developed a Carbonaceous Asteroid Volatile Recovery System (CAVoR) that is capable of retrieving water and several gases (hydrogen, carbon monoxide and dioxide, and methane) from simulants prepared from organic constituents. They give a table of estimated power requirements for processing roughly 50 kg of simulant per day, as well as a 200kg system mass estimate (including an electrolyser). They claim that CAVoR can produce 10 kg of water, oxygen, and methane per day from the 50kg simulant [196].

4.5 Storage

A concept that is common amongst many roadmaps to massive Solar System exploration is the orbital refueling station; similar to a terrestrial gas station, these orbiting depots would store fuel, water, or other raw materials for spacecraft to purchase and use. These concepts have been suggested since the space race first began by Wernher von Braun in the 1950s [197].

Liquid oxygen (LOX) and liquid hydrogen (LH2) are used consistently in upper-stage rockets; they are very volatile and difficult to contain; the state-of-the-art ability to store these materials in a space environment is nine hours as of 2012 [198]. One solution is to store water, which can be electrolyzed into oxygen and hydrogen, and later processed. By creating a water depot in the L1 point of the Earth-Moon system, the necessity to develop long-term LOX and LH2 storage can be minimized [198]. A problem to note when storing either LOX/LH2 or liquid water is how the liquid moves around, or sloshes; sloshing of volatile liquids has caused several rockets to fail catastrophically here on Earth. A team from the Florida Institute of Technology has teamed up with NASA in 2015 to develop a model of slosh dynamics for liquid fuel storage. They conducted numerical, analytical, and experimental models of liquid water and cryogenic liquid nitrogen for a 30cm diameter spherical tank to characterize damping, slosh mode frequencies and forces [199].

In 2008, NASA contracted with Ball Aerospace to design a system capable of keeping LOX and liquid methane (LCH4) for the Orion spacecraft. They were unable to design a system with passive cooling or actively consuming propellant to achieve Zero-Boil-Off (ZBO). They had to implement an active cooling system of cryocoolers (gaseous helium) to achieve ZBO [200]. Later in 2013, ESA contracted with Thales Alenia Space-Italia to develop a water, nitrogen, and oxygen storage and distribution system for the Orion spacecraft. Both the water and gas delivery systems must provide potable water and air to the main capsule from a simple ISS mission to a lengthy Lunar mission. As of July 2017, the project is in phase-D, with a new design for both the water and gas tanks and the system has undergone several critical design reviews [201].

In early 2017, a team from Florida Institute of Technology, United Launch Alliance (ULA), NASA, and the Embry-Riddle Aeronautical University published their work on designing and testing a propellant

storage and transfer system for the Centaur upper-stage craft. Their system uses a pair of rotating tanks, 9.6 m and 16.3 m long, to separate and transfer LOX and LH2, respectively, with gaseous helium and oxygen pressurants. They have succeeded in demonstrating smaller prototypes in a laboratory environment and on a low-gravity parabolic flight. They have developed computational models and simulations in parallel with the physical experiments to test the scalability of the concept. They plan on testing their system on both a sub-orbital trajectory with Virgin Galactic's SpaceShipTwo and in-orbit onboard the ISS [202].

Section 5 - Conclusions

A review of the current literature in asteroid engineering was presented in this paper, with a focus on the discovery, exploration, deflection and redirection, and mining of near-Earth asteroids. Some concluding remarks can be made, as follows:

1) **Current asteroid discovery paradigms may not be sufficient for detecting the vast number of NEAs below 140 m in diameter.** There is a need for a significant increase in funding towards NEA discovery, including the dedication of existing telescopes, as well as building new ones, to explicitly search for small NEAs, in order to eventually consider our near-space environment as "safe."
2) **The current understanding of NEA composition is quite limited.** The ability to characterize a NEA is currently mainly limited to remote observations of surface reflectivity. More flyby missions need to be conducted, at low costs and fast development paces, to perform gravity mapping and study subsurface composition, in order to accurately describe what a NEA is made of.
3) **A key technology of NEA redirection and/or prospecting is the ability to land and anchor on a NEA.** More research is needed for developing robust landing mechanisms on unknown surfaces in low-gravity environments, which will lead to more effective redirection approaches, such as tugboat, as well as more detailed prospecting of potential resources on NEAs.
4) **Microgravity surface operations is an emerging subject of research.** While notable research has been done into developing rovers, drilling mechanisms and large-scale systems similar to terrestrial mining machines for use on the Moon and Mars, performing such operations in microgravity introduces new challenges that must be addressed specifically.
5) **Comprehensive and multidisciplinary academic curricula should be developed, at both undergraduate and graduate levels, to train future engineers and researchers for the field.** The field of asteroid engineering is rapidly evolving to a state where formal training systems are needed to be put in place to generate sufficient task force for the field. While asteroid engineering can be considered as a subject within the domain of space science and engineering, the extent of the required knowledge from a wide variety of other disciplines, such as astronomy, astrophysics, Earth and planetary geology, mining engineering, computer, electrical and systems engineering, etc., necessitates the inception of an independent educational programs for asteroid engineering. A few universities have recently initiated such programs: the Colorado School of Mines has a Space Resources Program, offering post-graduate certificates and Master's and Ph.D. degrees, which seeks to expand their terrestrial mining expertise to space resources, including asteroids, the Moon and Mars [203]. The Luleå University of Technology in Sweden is also planning for the establishment of an asteroid engineering program offering undergraduate and post-graduate degrees [7]. Further, several academic research centers have focused on some aspects of asteroid engineering. Some notable examples include Iowa State University's Asteroid Deflection Research Center, established in 2008, which conducts research in how to deflect or disrupt asteroids that could potentially cause global catastrophic impacts [204]. The University of Strathclyde operates an aerospace center of excellence, called the Advanced Space Concepts Laboratory, which focuses on space situational awareness and minor body exploration, exploitation, and manipulation [205]. The University of Glasgow has a Space Systems department with a research area of potentially hazard asteroid threat mitigation [206].

References

[1]   J. Edwards, "Goldman Sachs says space-mining for platinum with asteroid-grabbing spacecraft is 'more realistic than perceived'," Goldman Sachs, 06 April 2017. [Online]. Available:

http://nordic.businessinsider.com/goldman-sachs-space-mining-asteroid-platinum-2017-4?r=UK&IR=T. [Accessed 19 February 2018].

[2]   J. C. Castillo-Rogez, M. Pavone, I. A. D. Nesnas and J. A. Hoffman, "Expected Science Return of Spatially-Extended In-Situ Exploration at Small Solar System Bodies," in *IEEE Aerospace*, Big Sky, MT, USA, 2012.

[3]   R. A. F. Grieve, "Logan Medallist 4. Large-Scale Impact and Earth History," *Journal of the Geological Association of Canada,* vol. 44, no. 1, 2017.

[4]   O. P. Popova, "Chelyabinsk Airburst, Damage Assessment, Meteorite Recovery, and Characterization," *Science,* vol. 342, pp. 1069-1073, 2013.

[5]   D. Gump, "Coming Asteroid Could be Worth $195 Billion," Deep Space Industries, 12 February 2013. [Online]. Available: https://deepspaceindustries.com/wp-content/uploads/2013/02/DSIPR_Asteroid195bil_20130213.pdf. [Accessed 19 February 2018].

[6]   P. Chodas and D. Yeomans, "Asteroid 2012 DA14 To Pass Very Close to the Earth on February 15, 2013," NASA's Near Earth Object Program, 1 February 2013. [Online]. Available: http://neo.jpl.nasa.gov/news/news177.html. [Accessed 19 February 2018].

[7]   M. R. Emami, "Asteroid Engineering: Are We There Yet?," *Pan-European Networks - Science and Technology,* pp. 100-103, April 2017.

[8]   D. E. Steitz, "NASA Announces Next Steps on Journey to Mars: Progress on Asteroid Initiative," NASA Asteroid Redirect Mission, 7 August 2017. [Online]. Available: https://www.nasa.gov/press/2015/march/nasa-announces-next-steps-on-journey-to-mars-progress-on-asteroid-initiative. [Accessed 19 February 2018].

[9]   E. Schneider and J. Dordain, *Space Resources - Press Conference,* Luxembourg: Ministry of Economy of Luxembourg, 2016.

[10]   A. Graps, P. Blondel, G. Bonin, D. Britt, S. Centuori and e. al., *In-Space Utilization of Asteroids: "Answers to Questions from the Asteroid Miners",* Luxembourg City, Luxembourg: Asteroid Science Intersections with In-Space Mine Engineering 2016, 2017.

[11]   R. K. Soberman, S. L. Neste and K. Lichtenfeld, "Particle Concentration in the Asteroid Belt from Pioneer 10," *Science,* vol. 183, no. 4122, pp. 320-321, 1974.

[12]   G. W. Wetherill, "Steady State Populations of Apollo-Amor Objects," *Icarus,* vol. 37, pp. 96-112, 1979.

[13]   "Aeronautics and Space Policy Act of 1994," United States House of Representatives, Washington DC, USA, 1994.

[14]   T. Talbert, "Planetary Defense Coordination Office," NASA, 29 August 2017. [Online]. Available: https://www.nasa.gov/planetarydefense/overview. [Accessed 19 February 2018].

[15]   "National Aeronautics and Space Administration Authorization Act of 2005," 109th United States Congress, Washington DC, 2005.

[16]   A. Mainzer, T. Grav, J. Bauer, T. Conrow, R. M. Cutri and e. al., "Survey Simulations of a New Near-Earth Asteroid Detection System," *The Astronomical Journal,* vol. 149, no. 172, 2015.

[17]   N. Myhrvold, "Comparing NEO Search Telescopes," *Publications of The Astronomical Society of the Pacific,* vol. 128, no. 962, 2016.

[18]   E. L. Wright, A. Mainzer, J. Masiero, T. Grav and J. Bauer, "The Albedo Distribution of Near Earth Asteroids," *The Astronomical Journal,* vol. 152, no. 4, 2016.

[19]   P. Chodas, "Asteroid Size Estimator," NASA JPL Center for Near Earth Object Studies, [Online]. Available: https://cneos.jpl.nasa.gov/tools/ast_size_est.html. [Accessed 19 February 2018].

[20]   D. Daou, L. Johnson, K. E. Fast, R. Landis, V. P. Friedensen and e. al., "NASA's Planetary Defense Coordination Office at NASA HQ," *European Planetary Science Congress 2017,* vol. 11, no. 1024, 2017.

[21]   P. Chodas, "Glossary," NASA JPL Center for Near Earth Object Studies, [Online]. Available: http://cneos.jpl.nasa.gov/glossary/PHA.html. [Accessed 19 February 2018].

[22]   A. Mainzer, T. Grav, J. Bauer, J. Masiero, R. McMillan and e. al., "NEOWISE OBSERVATIONS OF NEAR-EARTH OBJECTS: PRELIMINARY RESULTS," *The Astrophysical Journal,* vol. 743, no. 156, 2011.

[23]   A. W. Harris and G. D'Abramo, "The population of near-Earth asteroids," *Icarus,* vol. 257, pp. 302-312, 2015.

[24]   M. Granvik, A. Morbidelli, R. Jedicke, B. Bolin, W. F. Bottke and e. al., "Super-catastrophic disruption of asteroids at small perihelion distances," *Nature,* vol. 530, pp. 303-306, 2016.

[25]   P. Tricarico, "The near-Earth asteroid population from two decades of observations," *Icarus,* vol. 284, pp. 416-423, 2017.

[26]   M. Shao, B. Nemati, C. Zhai, S. G. Turyshev, J. Sandhu and e. al., "Finding Very Small Near-Earth Asteroids Using Synthetic Tracking," *The Astrophysical Journal,* vol. 782, no. 1, 2014.

[27] V. Hellgren, "Asteroid Mining: A Review of Methods and Aspects," Lund University Department of Physical Geography and Ecosystem Science (INES NGEK01 20161), Lund, Sweden, 2016.

[28] J. A. Tyson, P. Guhathakurta, G. M. Bernstein and P. Hut, "Limits on the Surface Density of Faint Kuiper Belt Objects," *Bulletin of the American Astronomical Society,* vol. 181, no. 24, p. 1127, 1992.

[29] M. Levoy, "Volume Rendering Using the Fourier Projection-Slice Theorem," Computer Systems Laboratory, Stanford, CA, USA, 1992.

[30] M. L. Brady, "A Fast Discrete Approximation Algorithm for the Radon Transform," *SIAM Journal on Computing,* vol. 27, no. 1, pp. 107-119, 1998.

[31] J. Brown, "ROAD: Rapid Optical Asteroid Detection," Massachusetts Institute of Technology, Baltimore, MD, USA, 2016.

[32] A. N. Heinze, S. Metchev and J. Trollo, "Digital Tracking Observations can Discover Asteroids 10 Times Fainter than Conventional Searches," *The Astronomical Journal,* vol. 150, no. 125, 2015.

[33] C. Zhai, M. Shao, B. Nemati, T. Werne, H. Zhou and e. al., "Detection of a Faint Fast-Moving Near-Earth Asteroid Using the Synthetic Tracking Technique," *The Astrophysical Journal,* vol. 792, no. 60, 2014.

[34] S. C. Cain and A. MacDonald, "Improved Near-Earth Orbiting Asteroid Detection via Statistical Image Fusion," in *IEEE Aerospace*, Big Sky, MT, USA, 2007.

[35] C. Sabol, K. K. Luu, P. Kervin, D. Nishimoto, K. Hamada and e. al., "Recent developments of the Raven small telescope program," *Advances in the Astronautical Sciences,* vol. 112, pp. 397-416, 2002.

[36] M. Grotte, S. Virani, M. Holzinger, A. Register, C. Perez and e. al., "All-Sky Image Fusion for a Synoptic Survey Telescope in Arctic and Antarctic Domains," in *Proceedings of the Advanced Maui Optical and Space Surveillance Technologies Conference*, Wailea, HI, USA, 2016.

[37] G. H. Stokes, D. K. Yeomans, W. F. Bottke, S. R. Chesley, J. B. Evans and e. al., "Study to Determine the Feasibility of Extending the Search for Near-Earth Objects to Smaller Limiting Diameters," 22 August 2003. [Online]. Available: https://cneos.jpl.nasa.gov/doc/neoreport030825.pdf. [Accessed 19 February 2018].

[38] "Construction Project Status," LSST Corporation, November 2016. [Online]. Available: https://www.lsst.org/about/project-status. [Accessed 19 February 2018].

[39] J. Melton, "Asteroid detection using a single multi-wavelength CCD scan," in *Applications of Digital Image Processing 39*, San Diego, CA, USA, 2016.

[40] E. L. Gomez and M. T. Fitzgerald, "Robotic telescopes in education," *Astronomical Review,* vol. 13, no. 1, pp. 28-68, 2017.

[41] M. Kosiarek, M. Mansfield, T. Brothers, H. Bates, R. Aviles and e. al., "SAURON: The Wallace Observatory Small AUtonomous Robotic Optical Nightwatcher," *Publications of the Astronomical Society of the Pacific,* vol. 129, no. 977, 2017.

[42] "TheSkyX Professional Edition," Software Bisque, 2017. [Online]. Available: http://www.bisque.com/sc/pages/TheSkyX-Professional-Edition.aspx. [Accessed 19 February 2018].

[43] "MasterSyncPC Software," Masterclock, 2017. [Online]. Available: https://www.masterclock.com/products/software/mastersyncpc. [Accessed 19 February 2018].

[44] "Introducing CCDAutoPilot 5.0," CCDWare, 2010. [Online]. Available: http://www.ccdware.com/products/ccdap5/. [Accessed 19 February 2018].

[45] T. Riel, R. Saathof, A. Katalenic and G. Schitter, "Tracking Performance Analysis and Control of a Small Robotic Telescope System," in *Proceedings of the Advanced Maui Optical and Space Surveillance Technologies Conference*, Wailea, HI, USA, 2016.

[46] "Software and Updates," Planewave Instruments, 2017. [Online]. Available: http://planewave.com/downloads/software/. [Accessed 19 February 2018].

[47] P. Kubanek, "RTS2 - The Remote Telescope System," *Advances in Astronomy,* vol. 2010, 2010.

[48] S. J. Villanueva, J. Eastman, B. Gaudi, R. Pogge, K. Stassun and e. al., "DEdicated MONitor of EXotransits and Transients (DEMONEXT): a low-cost robotic and automated telescope for followup of exoplanetary transits and other transient events," in *Ground-Based and Airborne Telescopes VI*, Edinburgh, Scotland, 2016.

[49] T. M. Brown, N. Baliber, F. B. Bianco, M. Bowman, B. Burleson and e. al., "Las Cumbres Observatory Global Telescope Network," *Publications of the Astronomical Society of the Pacific,* vol. 125, no. 931, 2013.

[50] "Skynet Robotic Telescope Network," University of North Carolina, 2016. [Online]. Available: https://skynet.unc.edu/skynet/default/index. [Accessed 19 February 2018].

[51] "Telescope Information," iTelescope Network, 2017. [Online]. Available: http://www.itelescope.net/telescope-information. [Accessed 19 February 2018].

[52]   "Facilities," Catalina Sky Survey, 2018. [Online]. Available: http://www.lpl.arizona.edu/css/css_facilities.html. [Accessed 19 February 2018].

[53]   K. C. Chambers, E. A. Magnier, N. Metcalfe, H. A. Flewelling, M. E. Huber and e. al., "The Pan-STARRS1 Surveys," arXiv:1612.05560v3, 2016.

[54]   E. Schunova-Lilly, R. Jedicke, P. Veres, L. Denneau and R. J. Wainscoat, "The size-frequency distribution of H>13 NEOs and ARM target candidates detected by Pan-STARRS1," *Icarus,* vol. 284, pp. 114-125, 2017.

[55]   H. E. M. Viggh, G. Ushomirsky, G. Stokes, M. Cornell, J. D. Ruprecht and e. al., "Initial asteroid detection results using the Space Surveillance Telescope," in *IEEE Aerospace*, Big Sky, MT, USA, 2015.

[56]   L. Millard, Interviewee, *DARPA hands over space tracking telescope to the Air Force.* [Interview]. 19 October 2016.

[57]   "ATLAS: How it Works," The ATLAS Project, 2017. [Online]. Available: http://www.fallingstar.com/how_atlas_works.php. [Accessed 19 February 2017].

[58]   N. R. Council, Defending Planet Earth: Near-Earth Object Surveys and Hazard Mitigation Strategies, Washington DC, USA: National Academies Press, 2010.

[59]   "LSST Project Schedule," Large Synoptic Survey Telescope Corporation, [Online]. Available: https://www.lsst.org/about/timeline. [Accessed 19 February 2018].

[60]   H. Reitsema and R. Arentz, "Lunar and Planetary Institute," 2017. [Online]. Available: http://www.lpi.usra.edu/decadal/sbag/topical_wp/RobertFArentz.pdf. [Accessed 19 February 2018].

[61]   D. Brown and L. Cantillo, "NASA Selects Two Missions to Explore the Early Solar System," NASA Discovery Program, 4 January 2017. [Online]. Available: https://www.nasa.gov/press-release/nasa-selects-two-missions-to-explore-the-early-solar-system. [Accessed 19 February 2018].

[62]   "NEOCam," NASA JPL, 2018. [Online]. Available: http://neocam.ipac.caltech.edu/page/mission. [Accessed 19 February 2018].

[63]   I. I. Shapiro, F. Vilas, M. A'Hearn, A. F. Cheng and F. J. e. a. Culbertson, Near-Earth Object Surveys and Hazard Mitigation Strategies, Washington D.C.: The National Academies Press, 2009.

[64]   A. Mainzer, "The NEOWISE Project," NASA JPL, March 2017. [Online]. Available: http://neowise.ipac.caltech.edu/. [Accessed 19 February 2018].

[65]   "Evaluation of the Near Earth Object Surveillance Satellite (NEOSSat) Project," Audit and Evaluation Directorate of Canadian Space Agency, Ottawa, Canada, 2014.

[66]   O. Mierheim, "Asteroid Finder Handout," [Online]. Available: http://www.dlr.de/fa/Portaldata/17/Resources/dokumente/abt_17/projekte/Handout_Asteroid_Finder.pdf. [Accessed 19 February 2018].

[67]   J. F. Pedersen, O. Essmann, R. Findlay, H. Hoffmann, G. Messina and e. al., "AsteroidFinder: A Small Satellite to Characterize the IEO Population," in *25th Annual AIAA/USU Conference on Small Satellites*, Logan, UT, USA, 2011.

[68]   S. J. Bus and R. P. Binzel, "Phase II of the Small Main-Belt Asteroid Spectroscopic Survey - A Feature-Based Taxonomy," *Icarus,* vol. 158, no. 1, pp. 146-177, 2002.

[69]   J. G. Bodnarik, J. S. Schweitzer, A. M. Parsons, L. G. Evans and R. D. Starr, "PING Gamma Ray and Neutron Measurements of a Meter-Sized Carbonaceous Asteroid Analog," in *IEEE Nuclear Science Symposium*, Valencia, Spain, 2011.

[70]   M. Kaasalainen and J. Torppa, "Optimization Methods for Asteroid Lightcurve Inversion: I. Shape Determination," *Icarus,* vol. 153, no. 1, pp. 24-36, 2001.

[71]   T. Santana-Ros, G. Dudzinski and P. Bartczak, "Shape Models and Physical Properties of Asteroids," in *Assessment and Mitigation of Asteroid Impact Hazards: Proceedings of the 2015 Barcelona Asteroid Day*, Springer International Publishing, 2017, pp. 55-71.

[72]   J. Margot, P. Pravec, P. Taylor, B. Carry and S. Jacobson, "Asteroid Systems: Binaries, Triples, and Pairs," in *Asteroids IV*, Tucson, AZ, USA, The University of Arizona Press, 2015, pp. 355-374.

[73]   B. D. Warner, "Asteroid Lightcurve Research at Palmer Divide Observatory," BDW Publishing, 16 May 2010. [Online]. Available: http://www.minorplanetobserver.com/PDO/PDOLightcurves.htm. [Accessed 19 February 2018].

[74]   C. Chang, L. Hsing-Wen, I. Wing-Huen, T. A. Prince, S. R. Kulkarni and e. al., "Asteroid spin-rate studies using large sky-field surveys," *Geoscience Letters,* vol. 4, no. 17, 2017.

[75]   A. K. Andrews, R. S. Hudson and D. Psaltis, "Optical-radar imaging of scale models for studies in asteroid astronomy," *Optics Letters,* vol. 20, no. 22, pp. 2327-2329, 1995.

[76]   M. W. Busch, Shapes and Spins of Near-Earth Asteroids, Boca Raton, FL, USA: Dissertation.com, 2010.

[77] L. Johnson, "NASA NEO Program AGC Seminar," NASA Asteroid Grand Challenge, 28 February 2014. [Online]. Available: https://ac.arc.nasa.gov/p8tyk487hvm. [Accessed 19 February 2018].

[78] M. Elvis, "Prospecting Asteroid Resources," in *Asteroids: Prospective Energy and Material Resources*, Berlin, Germany, Springer-Verlag Berlin Heidelberg, 2013, pp. 81-129.

[79] M. Delbo, P. Tanga, G. Van Belle, A. Matter, B. Carry and e. al., "Long Baseline Interferometric Observations of Asteroids: Physical Characterization of Binary Systems," in *Resolving The Future Of Astronomy With Long-Baseline Interferometry*, Socorro, NM, USA, 2014.

[80] K. Lehtinen, U. Bach, K. Muinonen, M. Poutanen and L. Petrov, "Asteroid Sizing by Radiogalaxy Occultation at 5 Ghz," *The Astrophysical Journal Letters,* vol. 822, no. 21, 2016.

[81] C. F. Marcos and R. F. Marcos, "Asteroid (469219) 2016 HO3, the smallest and closest Earth quasi-satellite," *Monthly Notices of the Royal Astronomical Society 462,* pp. 3441-3456, 8 August 2016.

[82] M. Granvik, R. Jedicke, B. Bolin, M. Chyba, G. Patterson and e. al., "Earth's Temporarily-Captured Natural Satellites - The First Step towards Utilization of Asteroid Resources," in *Asteroids, Prospective Energy and Material Resources*, Berlin, Germany, Springer-Verlag Berlin Heidelberg, 2013, pp. 151-167.

[83] H. Urrutxua, D. J. Scheeres, C. Bombardelli, J. L. Gonzalo and J. Pelaez, "Temporarily Captured Asteroids as a Pathway to Affordable Asteroid Retrieval Missions," *Journal of Guidance, Control, and Dynamics,* vol. 38, no. 11, 2015.

[84] R. Jedicke, B. Bolin, W. F. Bottke, M. Chyba, G. Fedorets and e. al., "Small asteroids temporarily captured in the Earth-Moon system," in *IAU Symposium No. 318 (Asteroids: New Observations, New Models)*, Honolulu, HI, USA, 2015.

[85] B. Bolin, R. Jedicke, M. Granvik, P. Brown, E. Howell and e. al., "Detecting Earth's temporarily-captured natural satellites—Minimoons," *Icarus,* vol. 241, pp. 280-297, 2014.

[86] I. Bertini, "Asteroids Close-Up: What We Have Learned from Twenty Years of Space Exploration," in *Asteroids: Prospective Energy and Material Resources*, Berlin, Germany, Springer-Verlag Berlin Heidelberg, 2013, pp. 1-33.

[87] K. A. Carroll, H. Spencer and R. E. Zee, "An Asteroid Lander/Rover for Asteroid Surface Gravity Surveying," in *30th Annual AIAA/USU Conference on Small Satellites*, Logan, UT, USA, 2016.

[88] E. M. Palmer, E. Heggy and W. Kofman, "Exploring the Surface Roughness of Asteroid Vesta using Bistatic Radar Observations by the Dawn Mission," in *IAU General Assembly Meeting 29*, Honolulu, HI, USA, 2015.

[89] "Identification of origin of particles brought back by Hayabusa," JAXA, 16 November 2010. [Online]. Available: http://global.jaxa.jp/press/2010/11/20101116_hayabusa_e.html. [Accessed 19 February 2018].

[90] A. Fujiwara, J. Kawaguchi, D. K. Yeomans, M. Abe, T. Mukai and e. al., "The Rubble-Pile Asteroid Itokawa as Observed by Hayabusa," *Science,* vol. 312, no. 5778, pp. 1330-1334, 2006.

[91] H. Yurimoto, K. Abe, M. Abe, M. Ebihara, A. Fujimura and e. al., "Oxygen Isotopic Compositions of Asteroidal Materials Returned from Itokawa by the Hayabusa Mission," *Science,* vol. 333, no. 6046, pp. 1116-1119, 2011.

[92] A. Tsuchiyama, M. Uesugi, T. Matsushima, T. Michikami, T. Kadono and e. al., "Three-Dimensional Structure of Hayabusa Samples: Origin and Evolution of Itokawa Regolith," *Science,* vol. 333, no. 6046, pp. 1125-1128, 2011.

[93] H. Yabuta, M. Uesugi, H. Naraoka, M. Ito, A. L. D. Kilcoyne and e. al., "X-ray absorption near edge structure spectroscopic study of Hayabusa category 3 carbonaceous particles," *Earth, Planets, and Space,* vol. 66, no. 156, 2014.

[94] K. Nagao, R. Okazaki, T. Nakamura, Y. N. Miura, T. Osawa and e. al., "Irradiation History of Itokawa Regolith Material Deduced from Noble Gases in the Hayabusa Samples," *Science,* vol. 333, no. 6046, pp. 1128-1131, 2011.

[95] H. Naraoka, H. Mita, K. Hamase, M. Mita, H. Yabuta and e. al., "Preliminary organic compound analysis of microparticles returned from Asteroid 25143 Itokawa by the Hayabusa mission," *Geochemical Journal,* vol. 46, no. 1, pp. 61-72, 2012.

[96] D. S. Lauretta, E. Acton, A. Adams, L. Adelman, T. Ajluni and e. al., "An Overview of the Osiris-Rex Asteroid Sample Return Mission," in *43rd Lunar and Planetary Science Conference*, The Woodlands, TX, USA, 2012.

[97] Y. Tsuda, M. Yoshikawa, M. Abe, H. Minamino and S. Nakazawa, "System design of the Hayabusa 2- Asteroid sample return mission to 1999 JU3," *Acta Astronautica,* vol. 91, pp. 356-362, 2013.

[98] C. Colombo, J. P. S. Cuartielles, M. Vasile and G. Radice, "A Comparative Assessment of Different Deviation Strategies for Dangeros NEO," in *57th International Astronautical Congress*, Valencia, Spain, 2006.

[99] J. Brophy, F. Culick, L. Friedman, C. Allen, D. Baughman and e. al., "Asteroid Retrieval Feasibility Study," Keck Institute for Space Studies, Pasadena, CA, USA, 2012.

[100] C. Weisbin, W. Lincoln, B. Wilcox, J. Brophy, P. Chodas and e. al., "Comparative Analysis of Asteroid-Deflection Approaches," in *IEEE Aerospace*, Big Sky, MT, USA, 2015.

[101] M. C. F. Bazzocchi and M. R. Emami, "Comparative analysis of redirection methods for asteroid resource exploitation," *Acta Astronautica,* vol. 120, pp. 1-19, 2016.

[102] T. J. Ahrens and A. W. Harris, "Deflection and fragmentation of near-Earth asteroids," *Nature,* vol. 360, no. 6403, pp. 429-433, 1992.

[103] M. F. A'Hearn, M. J. S. Belton, W. A. Delamere, J. Kissel and K. P. e. a. Klaasen, "Deep Impact: Excavating Comet Tempel 1," *Science,* vol. 310, no. 5746, pp. 258-264, 2005.

[104] A. F. Cheng, P. Michel, C. Reed, A. Galvez and J. Carnelli, "DART: Double Asteroid Redirection Test," *European Planetary Science Congress,* vol. 935, no. 1, 2012.

[105] C. R. McInnes, "Deflection of near-Earth asteroids by kinetic energy impacts from retrograde orbits," *Planetary and Space Science,* vol. 52, no. 7, pp. 587-590, 2004.

[106] M. B. Syal, J. M. Owen and P. L. Miller, "Deflection by kinetic impact: Sensitivity to asteroid properties," *Icarus,* vol. 269, no. 1, pp. 50-61, 2016.

[107] S. Bhaskaran and B. Kennedy, "Closed loop terminal guidance navigation for a kinetic impactor spacecraft," *Acta Astronautica,* vol. 103, pp. 322-332, 2014.

[108] S. Chelsey, J. Elliot, S. Bhaskaran, T. Lam, P. Abell and e. al., "The ISIS mission concept: an impactor for surface and interior science," in *Planetary Defence Conference*, Flagstaff, AZ, USA, 2013.

[109] M. B. Syal, D. S. P. Dearborn and P. H. Schultz, "Limits on the use of nuclear explosives for asteroid deflection," *Acta Astronautica,* vol. 90, no. 1, pp. 103-111, 2013.

[110] B. Wie, "Hypervelocity nuclear interceptors for asteroid disruption," *Acta Astronautica,* vol. 90, no. 1, pp. 146-155, 2013.

[111] B. Kaplinger, P. Premaratne, C. Setzer and B. Wie, "GPU Accelerated 3D Modeling and Simulation of a Blended Kinetic Impact and Nuclear Subsurface Explosion," in *AIAA Guidance, Navigation, and Control (GNC) Conference*, Boston, MA, USA, 2013.

[112] B. Kaplinger and B. Wie, "Preliminary Results for High-Fidelity Modeling and Simulation of Orbital Dispersion of Asteroids Disrupted by Nuclear Explosives," in *AIAA/AAS Astrodynamics Specialist Conference*, Toronto, Canada, 2010.

[113] B. Kaplinger, B. Wie and D. Dearborn, "Nuclear fragmentation/dispersion modeling and simulation of hazardous near-Earth objects," *Acta Astronautica,* vol. 90, no. 1, pp. 156-164, 2013.

[114] B. Kaplinger, B. Wie and D. Dearborn, "Earth-Impact Modeling and Analysis of a Near-Earth Object Fragmented and Dispersed by Nuclear Subsurface Explosions," *The Journal of the Astronautical Sciences,* vol. 59, no. 1-2, pp. 101-119, 2014.

[115] P. Premaratne, B. J. Zimmerman, C. Setzer, J. Harry and B. Wie, "Nuclear explosion energy coupling models for optimal fragmentation of asteroids," *Advances in the Astronautical Sciences,* vol. 152, pp. 1233-1250, 2014.

[116] A. G. Aleksandrova, T. Y. Galushina, A. B. Prishchepenko, K. V. Kholshevnikov and V. Chechetkin, "The Preventive Destruction of a Hazardous Asteroid," *Astronomy Reports,* vol. 60, no. 6, pp. 611-619, 2016.

[117] E. T. Lu and S. G. Love, "Gravitational tractor for towing asteroids," *Nature,* vol. 438, no. 10, pp. 177-178, 2005.

[118] B. Wie, "Hovering Control of a Solar Sail Gravity Tractor Spacecraft for Asteroid Deflection," in *Planetary Defense Conference*, Washington DC, USA, 2007.

[119] B. Wie, "Dynamics and Control of Gravity Tractor Spacecraft for Asteroid Deflection," in *AIAA/AAS Astrodynamics Specialist Conference and Exhibit*, Honolulu, HI, USA, 2008.

[120] Y. Ketema, "Asteroid deflection using a spacecraft in restricted keplerian motion," *Acta Astronautica,* vol. 136, pp. 64-79, 2017.

[121] "Falcon Heavy," SpaceX, 2017. [Online]. Available: http://www.spacex.com/falcon-heavy. [Accessed 19 February 2018].

[122] N. Murdoch, D. Izzo, C. Bombardelli, I. Carnelli, A. Hilgers and e. al., "Electrostatic Tractor for Near Earth Object Deflection," in *59th International Astronautical Congress*, Glasgow, Scotland, 2008.

[123] E. A. Gonzaga, "A Method of Controlling Asteroid Collision with the Earth," *Cosmic Research,* vol. 48, no. 5, pp. 459-466, 2010.

[124] W. Brown, "A novel Push-Pull Asteroid Magnetic Tractor (MT)," in *AIAA/AAS Astrodynamics Specialist Conference*, Long Beach, CA, USA, 2016.

[125] C. Bombardelli and J. Pelaez, "Sistema de Modicación de la Posición y Actitud de Cuerpos en Órbita por Medio de Satélites Guía". Spain Patent Spanish Patent No. P201030354 PCT Patent App. PCT/ES2011/000011, 11 March 2010.

[126] C. Bombardelli and J. Pelaez, "Ion Beam Shepherd for Asteroid Deflection," *Journal of Guidance, Control, and Dynamics,* vol. 34, no. 4, pp. 1270-1272, 2011.

[127] C. Bombardelli and J. Pelaez, "Ion Beam Shepherd for Contactless Space Debris Removal," *Journal of Guidance, Control, and Dynamics,* vol. 34, no. 3, pp. 916-920, 2011.

[128] J. S. Sovey, V. K. Rawlin and M. J. Patterson, "Ion Propulsion Development Projects in U. S.: Space Electric Rocket Test 1 to Deep Space 1," *Journal of Propulsion and Power,* vol. 17, no. 3, pp. 517-526, 2001.

[129] M. J. Patterson and S. W. Benson, "NEXT Ion Propulsion System Development Status and Performance," in *43rd AIAA/ASME/SAE/ASEE Joint Propulsion Conference & Exhibit*, Cincinnati, OH, USA, 2007.

[130] R. L. Schweickart, E. T. Lu, P. Hut and C. R. Chapman, "The Asteroid Tugboat," *Scientific American,* vol. 289, no. 5, pp. 54-61, 2003.

[131] J. P. Sanchez and C. R. McInnes, "Synergistic approach of asteroid exploitation and planetary protection," *Advances in Space Research,* vol. 49, no. 4, pp. 667-685, 2012.

[132] J. M. H. J. Richardson, C. M. Lisse and B. Carcich, "A ballistic analysis of the Deep Impact ejecta plume: determining Tempel 1's gravity, mass, and density," *Icarus,* vol. 190, pp. 357-390, 2007.

[133] M. C. F. Bazzocchi and M. R. Emami, "Asteroid Redirection Mission Evaluation Using Multiple Landers," *Journal of Astronautical Science,* pp. 1-22, 2018.

[134] J. Melosh, I. V. Nemchinov and Y. I. Zetzer, "Non-nuclear strategies for deflecting comets and asteroids," in *Hazard due to comets and asteroids*, Tuscon, AZ, USA, University of Arizona Press, 1994, pp. 1111-1132.

[135] C. Maddock, J. P. S. Cuartielles, M. Vasile and G. Radice, "Comparison of Single and Multi-Spacecraft Configurations for NEA Deflection by Solar Sublimation," *American Institute of Physics Conference Proceedings,* vol. 886, no. 303, 2007.

[136] C. Maddock, M. Vasile and L. Summerer, "Conceptual design of a multi-mirror system for asteroid deflection," in *27th International Symposium on Space Technology and Science*, Tsukuba, Japan, 2009.

[137] A. L. Gibbings, M. Vasile, J. Hopkins, D. Burns and I. Watson, "Potential of laser-induced ablation for future space applications," *Space Policy,* vol. 28, no. 3, pp. 149-153, 2012.

[138] A. L. Gibbings, "Laser ablation for the deflection, exploration and exploitation of near Earth asteroids," Univeristy of Glasgow, Glasgow, Scotland, 2014.

[139] M. Vetrisano, J. Branco, D. G. Yarnoz, J. P. S. Cuartielles and M. Vasile, "Deflecting Small Asteroids Using Laser Ablation- Deep Space Navigation and Asteroid Orbit Control for LightTouch2 Mission.pdf," in *AIAA Guidance, Navigation, and Control (GNC) Conference*, Boston, 2013.

[140] A. L. Gibbings, M. Vasile, I. Watson, J. Hopkins and D. Burns, "Experimental analysis of laser ablated plumes for asteroid deflection and exploitation," *Acta Astronautica,* vol. 90, no. 1, pp. 85-97, 2013.

[141] M. Vasile, A. Gibbings, I. Watson and J. Hopkins, "Improved laser ablation model for asteroid deflection," *Acta Astronautica,* vol. 103, pp. 382-394, 2014.

[142] M. Vetrisano, C. Colombo and M. Vasile, "Asteroid rotation and orbit control via laser ablation," *Advances in Space Research,* vol. 57, no. 8, pp. 1762-1782, 2016.

[143] M. Vasile and C. A. Maddock, "Design of a formation of solar pumped lasers for asteroid deflection," *Advances in Space Research,* vol. 50, no. 7, pp. 891-905, 2012.

[144] N. Thiry, M. Vasile and E. Monchieri, "Mission and system design for the manipulation of PHOs with space-borne lasers," in *IEEE Aerospace*, Big Sky, MT, USA, 2016.

[145] Y. Song and S. Park, "Estimation of necessary laser power to deflect near-Earth asteroid using conceptual variable-laser-power ablation," *Aerospace Science and Technology,* vol. 43, pp. 165-175, 2015.

[146] C. Gritzner and R. Kahle, "Mitigation technologies and their requirements," in *Mitigation of Hazardous Comets and Asteroids*, Cambridge, UK, Cambridge University Press, 2004, p. 179.

[147] G. K. O'Neill, S. Cheston, B. Zeitman, J. Spurlock, W. Cooper and e. al., "Space Resources and Space Settlements," NASA Ames Research Center, Moffett Field, CA, USA, 1977.

[148] J. Pearson, "Asteroid Retrieval by Rotary Rocket," in *AIAA 18th Aerospace Sciences Meeting*, Pasadena, CA, USA, 1980.

[149] J. Olds, A. Charania and M. Schaffer, "Multiple Mass Drivers as an Option for Asteroid Deflection Missions," in *AIAA Planetary Defense Conference*, Washington DC, USA, 2007.

[150] J. K. Cline, "Satellite aided capture," *Celestial mechanics,* vol. 19, no. 4, pp. 405-415, 1979.

[151] L. A. D'Amario, L. A. Bright and A. A. Wolf, "Galileo trajectory design," *Space Science Reviews,* vol. 60, no. 1-4, pp. 23-78, 1992.

[152] F. Peralta and S. Flanagan, "Cassini interplanetary trajectory design," *Control Engineering Practice,* vol. 3, no. 11, pp. 1603-1610, 1995.

[153] S. Gong and J. Li, "Asteroid capture using lunar flyby," *Advances in Space Research,* vol. 56, no. 5, pp. 848-858, 2015.

[154] N. Llado, Y. Ren, J. J. Masdemont and G. Gomez, "Capturing small asteroids into a Sun-Earth Lagrangian point," *Acta Astronautica,* vol. 95, pp. 176-188, 2014.

[155] J. P. Sanchez and D. G. Yarnoz, "Asteroid retrieval missions enabled by invariant manifold dynamics," *Acta Astronautica,* vol. 127, pp. 667-677, 2016.

[156] B. K. Muirhead and J. R. Brophy, "Asteroid Redirect Robotic Mission feasibility study," in *IEEE Aerospace*, Big Sky, MT, USA, 2014.

[157] R. Kahle, G. Hahn and E. Kuhrt, "Optimal deflection of NEOs en route of collision with the Earth," *Icarus,* vol. 182, no. 2, pp. 482-488, 2006.

[158] M. C. F. Bazzocchi and M. R. Emami, "Study of Arjuna-Type Asteroids for Low-Thrust Orbital Transfer," *Journal of Spacecraft and Rockets,* vol. 55, no. 1, pp. 37-48, 2018.

[159] M. Vasile, P. De Pascale and S. Casotto, "On the optimality of a shape-based approach on pseudo-equinoctial elements," *Acta Astronautica,* vol. 61, no. 1, pp. 286-297, 2007.

[160] M. C. F. Bazzocchi, N. de Decker and M. R. Emami, "Application of pseudo-equinoctial shaping to Near-Earth asteroid orbital transfer," in *IEEE Aerospace Conference*, Big Sky, MT, USA, 2017.

[161] G. P. Serviss, Edison's Conquest of Mars, Los Angeles, CA, USA: Carcosa House, 1898.

[162] D. Dickinson, "Congress approves solar power satellites-and asteroid mining," *Nature,* vol. 274, no. 5666, p. 3, 1978.

[163] K. Zacny, P. Chu, J. Craft, M. M. Cohen, W. W. James and e. al., "Asteroid Mining," in *AIAA Space*, San Diego, CA, USA, 2013.

[164] "Comet Water Thruster by Deep Space Industries," August 2016. [Online]. Available: http://deepspaceindustries.com/wp-content/uploads/2016/08/DSI_Comet1_Thruster_Specs_4.pdf. [Accessed 19 February 2018].

[165] "HYDROS Thruster by Tethers Unlimited Inc.," [Online]. Available: http://www.tethers.com/SpecSheets/Brochure_HYDROS.pdf. [Accessed 19 February 2018].

[166] A. (. Froehlich, Space Resource Utilization: A View from an Emerging Space Faring Nation - Studies in Space Policy, Vol. 12, Springer, January 2018.

[167] G. Alotaibi, J. Boileau, H. Bradshaw, R. Chalex, J. Chun and e. al., "Asteroid Mining, Technologies Roadmap, and Applications," International Space University, SSP 2010, Illkirch-Graffenstaden, France, 2010.

[168] T. M. Eubanks, *Asteroid Mining: The State of Play in 2016,* Fairfax, VA, USA: George Mason University, 2016.

[169] K. Zacny, P. Chu, G. Paulsen, M. Hedlund, B. Mellerowicz and e. al., "Asteroids: Anchoring and Sample Acquisition Approaches in Support of Science, Exploration, and in-situ Resource Utilization," in *Asteroids: Prospective Energy and Material Resources*, Berlin, Germany, Springer-Verlag Berlin Heidelberg, 2013, pp. 287-343.

[170] R. G. Martin and M. Livio, "On the Evolution of the Snow Line in Protoplanetary Discs," *Monthly Notices of the Royal Astronomical Society,* pp. L6-L9, Vol 425 2012.

[171] D. Takir, V. Reddy, J. A. Sanchez, M. K. Shepard and J. P. Emery, "Detection of Water and/or Hydroxyl on Asteroid (16) Psyche," *The Astronomical Journal,* vol. 153, no. 31, p. 6, 2017.

[172] M. Elvis, "How many ore-bearing asteroids?," *Planetary and Space Science,* vol. 91, pp. 20-26, 2014.

[173] H. R. Goldberg, M. Beasley and C. Voorhees, "Asteroids to Agriculture: Carving a Niche in Earth Observation Using Asteroid Prospecting Instruments on an Earth-Orbiting CubeSat Constellation," in *Small Satellite Conference*, Menlo Park, CA, USA, 2016.

[174] A. J. Naids, A. D. Hood, P. Abell, T. Graff and J. Buffington, "A Geology Sampling System for Small Bodies," in *46th International Conference on Environmental Systems*, Vienna, Austria, 2016.

[175] C. J. Kiang, J. L. Ly, E. W. Berg, P. N. Cancar, H. R. Rudin and e. al., "PALLAS: A Portable Asteroid Lift and Lock Aggregate System," in *AIAA Space*, Long Beach, CA, USA, 2016.

[176] N. M. I. A. Murdoch, C. Sunday, E. Zenou, O. Cherrier and e. al., "An experimental study of low-velocity impacts into granular material in reduced gravity," University of Toulouse, Toulouse, France, 2017.

[177] J. W. McMahon and B. Cheetham, "Lofted Regolith Sampling of Small Bodies," in *Space Resources Roundtable*, Golden, CO, USA, 2016.

[178] V. Latendresse, R. V. Kruzelecky, P. Murzionak, J. Lavoie, E. Wallach and e. al., "LIRA LIBS for Stand-Off Planetary and Asteroid Resource Prospecting," in *Earth and Space*, Orlando, FL, USA, 2016.

[179] K. Zacny, Y. Bar-Cohen, M. Brennan, G. Briggs, G. Cooper and e. al., "Drilling systems for extraterrestrial subsurface exploration," *Astrobiology,* vol. 8, no. 3, pp. 665-706, 2008.

[180] P. Nekoovaght, N. Gharib and F. Hassani, "Microwave Assisted Rock Breakage for Space Mining," in *Earth and Space*, St. Louis, MO, USA, 2014.

[181] H. Satish, J. Ouellet, V. Raghavan and P. Radziszewski, "Investigating microwave assisted rock breakage for possible space mining applications," *Mining Technology,* vol. 115, no. 1, pp. 34-40, 2006.

[182] H. Satish, "Exploring microwave assisted rock breakage for possible space mining applications," McGill University, Montreal, Canada, 2005.

[183] X. Li, K. Worrall, P. Harkness, R. Timoney, A. Bolhovitins and e. al., "A motion control system design for an Ultrasonic Planetary Core Dril (UPCD) unit," in *AIAA Space*, Pasadena, CA, USA, 2015.

[184] P. Harkness, M. McRobb, Y. W. Loh, M. Hyde and M. Lucas, "A Rock-Coring Campaign in an Analogue Environment," in *AIAA Space*, San Diego, CA, USA, 2014.

[185] S. Schmidt and D. Boucher, "Thermal Vacuum Testing of a Lunar Rated Sample Drill," in *Space Resources Roundtable*, Golden, CO, USA, 2016.

[186] R. T. Nallapu, A. Thoesen, L. Garvie, E. Asphaug and J. Thangavelautham, "Optimized Bucket Wheel Design for Asteroid Excavation," in *67th International Astronautical Congress*, Guadalajara, Mexico, 2016.

[187] N. Zeitlin, J. Mantovani, A. Swanger and I. Townsend, "Asteroid Icy Regolith Excavation and Volatile Capture Project," NASA TechPort, Titusville, FL, USA, 2016.

[188] M. Adachi, R. Obata, A. Shigeta and H. Kawamoto, "Sampling of Regolith from Asteroids Utilizing Magnetic Force," in *54th AIAA Aerospace Sciences Meeting*, San Diego, CA, USA, 2016.

[189] S. D. Covey, "An Electromagnetic Asteroid Regolith Excavator—Preliminary Results," in *Earth and Space*, Orlando, FL, USA, 2016.

[190] S. Nomura, M. Tomooka and R. Funase, "Initial Design and Analysis of a System Extracting and Collecting Water from Temporarily Captured Orbiters," in *10th Symposium on Space Resource Utilization*, Grapevine, TX, USA, 2017.

[191] N. Komerath, T. Rangedera and S. Bennett, "Extracting Asteroidal Mass for Robotic Construction," in *Asteroids: Prospective Energy and Material Resources*, Berlin, Springer-Verlag Berlin Heidelberg, 201, pp. 365-378.

[192] M. R. Cooper, R. L. Kovach and J. S. Watkins, "Lunar Near-Surface Structure," *Reviews of Geophysics and Space Physics,* vol. 12, no. 3, 1974.

[193] J. C. Sercel, C. B. Dreyer, A. Abbud-Madrid, D. Britt, R. Jedicke and e. al., "A Coordinated Research Program to Develop the Technology to Optical Mine Asteroids," in *Earth and Space*, Orlando, FL, USA, 2016.

[194] D. G. Yarnoz, P. S. Cuartielles and C. R. McInnes, "Passive Sorting of Asteroid Material Using Solar Radiation Pressure," *Journal of Guidance, Control, and Dynamics,* vol. 37, no. 4, pp. 1223-1235, 2014.

[195] L. Gertsch, E. Unobe, M. Schlesinger, A. Abbud-Madrid, C. Dreyer and e. al., "Producing Volatiles from Asteroid Simulants: Preliminary Results," in *AIAA 10th Symposium on Space Resource Utilization*, Grapevine, TX, USA, 2017.

[196] M. Berggren, "Carbonaceous Asteroid Volatile Recovery System," in *Space Resources Roundtable: Planetary & Terrestrial Mining Sciences Symposium*, Golden, CO, USA, 2016.

[197] W. Von Braun and C. Ryan, "Can We Get to Mars?," *Collier's,* vol. 133, no. 13, pp. 22-29, 1954.

[198] W. Notardonato, W. Johnson, A. Swanger and W. McQuade, "In-Space Propellant Production Using Water," in *AIAA Space*, Pasadena, CA, USA, 2012.

[199] J. M. Storey, D. Kirk, H. Gutierrez, B. Marsell and P. Schallhorn, "Experimental, Numerical and Analytical Characterization of Slosh Dynamics Applied to In-Space Propellant Storage and Management," in *51st AIAA/SAE/ASEE Joint Propulsion Conference*, Orlando, FL, USA, 2015.

[200] C. H. McLean, G. L. Mills, M. E. Riesco, M. L. Meyer, D. W. Plachta and e. al., "Long Term Space Storage and Delivery of Cryogenic Propellants for Exploration," in *44th AIAA/ASME/SAE/ASEE Joint Propulsion Conference & Exhibit*, Hartford, CT, USA, 2008.

[201] M. Lamantea, O. Faure and F. Bouckaert, "The Orion MPCV-ESM Consumables Storage Subsystem," in *47th International Conference on Environmental Systems*, Charleston, SC, USA, 2017.

[202] V. Nazario, J. Ramirez, M. Kulkarni, S. Gangadharan, D. Kirk and e. al., "Mass Gauging and Validation of a Novel In-Space Propellant Storage and Transfer using CFD," in *AIAA Space*, Orlando, FL, USA, 2017.

[203] A. Abbud-Madrid, "Space Resources Program," Colorado School of Mines, [Online]. Available: http://space.mines.edu/. [Accessed 19 January 2018].

[204] B. Wie, "Asteroid Deflection Research Center," Iowa State University, 2018. [Online]. Available:
       https://www.adrc.iastate.edu/. [Accessed 19 February 2018].

[205] "The Aerospace Centre of Excellence," University of Strathcylde, 2014. [Online]. Available:
       https://www.strath.ac.uk/research/subjects/mechanicalaerospaceengineering/aerospace/. [Accessed 19 February
       2018].

[206] G. Radice, "Space Systems," University of Glasgow, [Online]. Available:
       https://www.gla.ac.uk/schools/engineering/research/divisions/aerospace/researchthemes/spacesciencesandengine
       ering/. [Accessed 19 February 2018].

[207] P. Chodas, "NEO Discovery Statistics," NASA JPL Center for Near Earth Object Studies, [Online]. Available:
       http://cneos.jpl.nasa.gov/stats/. [Accessed 19 February 2018].

PAPER B

Laser processing of minerals common on asteroids

Authors:
Niklas Anthony, Jan Frostevarg, Heikki Suhonen, Christina Wanhainen, Antti Penttilä, Mikael Granvik

Laser processing of minerals common on asteroids

Niklas Anthony[a,*], Jan Frostevarg[b], Heikki Suhonen[c], Christina Wanhainen[d], Antti Penttilä[c], Mikael Granvik[a,c]

[a]*Asteroid Engineering Laboratory, Onboard Space Systems, Luleå University of Technology, Box 848, 98128 Kiruna, Sweden*
[b]*Department of Engineering Sciences and Mathematics, Luleå University of Technology, 97187 Luleå, Sweden*
[c]*Department of Physics, P.O. Box 64, 00014 University of Helsinki, Finland*
[d]*Division of Geosciences and Environmental Engineering, Luleå University of Technology, 97187 Luleå, Sweden*

Abstract

Asteroid mining and redirection are two trends that both can utilize lasers, one to drill and cut, the other to ablate and move. Yet little is known about what happens when a laser is used to process the types of materials we typically expect to find on most asteroids. To shed light on laser processing of asteroid material, we used a 300-W, pulsed Ytterbium fiber laser on samples of olivine, pyroxene, and serpentine, and studied the process with a high-speed camera and illumination laser at 10 000 frames per second. We also measure the sizes of the resulting holes using X-ray micro-tomography to find the pulse parameters which remove the largest amount of material using the least amount of energy. We find that at these power densities, all three minerals will melt and chaotically throw off spatter. Short, low-power pulses can efficiently produce thin, deep holes, and long, high-power pulses are more energy efficient at removing the most amount of material.

Keywords: Laser Drilling, High-Speed Imaging, X-ray Micro-Tomography, Asteroid Mining

---

Abbreviations

DE = Depth Efficiency
VE = Volume Efficiency
XMT = X-Ray Micro-Tomography
fps = frames per second

1. Introduction

Asteroid mining has the potential to be a very profitable industry [1]. Sourcing nickel-iron family metals from asteroids has gained interest since 1977 [2], and it was

---

shown to be as economically competitive as extracting the metals from the Moon [3]. Volatiles like water can be extracted from asteroids and used as rocket fuel [4] and even raw, unprocessed material can be used as radiation shielding [5]. The only feasible way to thoroughly prospect an asteroid is to study it with a robotic spacecraft, capable of getting below the surface. Although remote analysis methods like X-ray spectroscopy have been space-proven by the Dawn mission [6], their findings have some ambiguity that should be resolved by in-situ verification.

Using a drill or shovel would require landing on a small body, which presents several challenges such as the lack of knowledge of surface strength (i.e., powdery or stoney) and accounting for rotation or even tumbling. A summary of some landing/anchoring and sampling technologies with advantages and disadvantages is given in [7]. One solution to these challenges would be to use a laser to drill beneath the surface. Because there are no moving parts, it produces negligible counter-torques, and will not get stuck. It also has the advantage of being able to function on a diverse range of targets, from dust to solid metal; see Section 3 of [8] for publications related to various materials. They could even be used without having to land: a diffraction-limited Nd:YAG laser (wavelength 1070 nm) with a 34-cm aperture can make a 1-mm spot at a distance of 1 km.

The first laser was built in 1960 [9], and the first patent on laser drilling was filed in 1964 [10]. The first mathematical model of the drilling process was developed in 1976, which studied hole size and drilling rate on a copper plate [11]. Since then, High-Speed Imaging (HSI) has been useful in understanding the processes occurring when drilling, piercing, and cutting metals, such as spatter [12], melt dynamics, [13] and the gas effect [14], to name a few. By properly tuning the laser repetition rate and pulse width, the drilling efficiency has been shown to improve by a factor of 27 [15]. Lasers have also been tested on natural materials such as shale and sandstone [16], granite [17], and slate [18]. These were mostly for industrial purposes like cutting or engraving, and did not study the process in detail. Lasers have been used to process bauxite and red mud in [19], gold ores in [20], and is also used as a sampling tool when studying trace element chemistry of sulfides by mass spectrometry [21].

The first laser intended for use in space was the LIMA-D instrument on the Phobos 1 and 2 spacecraft launched in 1988 [22]. It was supposed to perform laser-ablated mass spectroscopy to determine the surface composition of the Martian moon, but unfortunately the mission was unable to reach this phase, and the instrument went unused. A laser is currently in use on the Mars, via the Curiosity rover, conducting Laser-Induced Breakdown Spectroscopy (LIBS) experiments on the natural materials on the Martian surface [23]. A similar process is also being suggested to determine asteroid composition using small satellites [24].

The majority of asteroids in the main belt and in the near-Earth region have spectral types S ($\sim$60%) or C ($\sim$20%), that stand for siliceous and carbonaceous, respectively [25]. Olivine and pyroxene are thought to be the dominant minerals for S and C types [26], and were therefore selected for the present study. Serpentine was also selected, because serpentine-group minerals are the most common hydrated minerals in meteorites [27]. Table 1 provides the main chemical and physical characteristics of the samples following [28]. The specific heat capacities for olivine, pyroxene, and serpentine are roughly 1.5, 1.1, and 1.3 kJ kg^{-1} K^{-1}, respectively. Iron-rich olivine (fayalite) begins to melt at 1763 K, while magnesium-rich olivine (forsterite) does not begin to melt until 2436 K [29]. In liquid form, gases like MgO, FeO, and SiO$_2$ begin to appear, so it is difficult

to say at what temperature olivine begins to vaporize, if at all in its full mineral form [30]. As olivine is one of the first minerals to crystalize while cooling, we will assume the melting temperatures for our pyroxene and serpentine samples are below that of olivine.

Laser-induced ablation has also been suggested as a method of redirecting potentially dangerous asteroids since 1994 [31]. They simulated a solar concentrator by using a laser on a sample of basalt and studied the evaporation force using a pressure plate. Experiments with olivine were conducted to test the usefulness of a laser for asteroid redirection [32]. Force measurements on pyroxene as well as high-fidelity asteroid simulant powder were performed with sub-nanosecond pulses, also for the purpose of asteroid redirection [33].

Table 1: The main chemical and physical characteristics of test samples: olivine, pyroxene (clino-), and serpentine [28]. The letter M_1 can be Mg or Fe, M_2 can be Ca or Na, M_3 can be Mg, Fe, or Al, M_4 can be Mg, Fe, Ni, Mn, or Zn, and M_5 can be Si, Al, or Fe.

Mineral group	Chemical composition	Mohs hardness	Specific gravity
Olivine	$(M_1)_2SiO_4$	6.5–7.0	3.2–4.4
Pyroxene	$(M_2)(M_3)Si_2O_6$	5.0–6.5	3.2–3.6
Serpentine	$(M_4)_3(M_5)_2O_5(OH)_4$	3.0–6.0	2.5–2.6

The main purpose of our research is two-fold: first, to understand how natural materials respond to laser irradiation, and second, to explore how varying laser pulse parameters affects the hole depth and the volume removed. We use millisecond pulses, which we believe is most suitable for a piercing experiment, whereas nano- to femto-second pulses mostly operate in a shallow ablation mode. By studying the process with HSI, we are able to see exactly what processes occur, be they melting, vaporization, explosion, etc, and how, exactly, the process differ from one mineral to the next. By studying the hole depths and volumes, the question how pulse parameters affect the depth and the volume removed can be answered.

2. Methodology

First, the three samples—olivine, pyroxene, and serpentine—were cut into roughly 1 cm thick slices to perform experiments on. A reflectance spectra was obtained of each sample, and in addition, thin sections of each rock were taken for petrographic analysis. During each experiment, HSI was applied at the laser beam-surface interaction point. Once the experiments were finished, the samples were further cut and analyzed with an X-ray Micro-Tomography (XMT) device. We describe the methodology in greater detail in the following subsections.

2.1. Sample characterization

Reflectance spectra of the samples were measured over the visual and near-infrared wavelengths 450–1150 nm. The measurements were carried out using a Light Tec Reflet 180S goniometer in a measurement geometry with 8° incidence and 0° measurement angles. The spot size from the incident illumination on the sample was about 1 cm in diameter. The reflected signal was recorded with an Ocean Optics Maya2000 Pro

spectrometer and the calibration of the measured signal was done using a LabSphere Spectralon diffuse reflectance standard. Two spots from each of the three samples were selected from the most prominent phase of the material. All the materials are measured with the same settings and calibrated against a diffuse reflectance standard, so their absolute reflectance levels can be compared.

Petrographic studies were carried out to characterize the test samples and to provide further compositional and textural information that could be relevant for the laser performance (impurities, cleavage planes, etc). The polished thin sections were prepared by Precision Petrographics Ltd (Canada) and were studied in an optical microscope (Nikon ECLIPSE E600 POL) using cross-polarized light.

The XMT measurements to characterize the resulting holes were carried out with a GE phoenix nanotom s system. The samples were imaged at 25 µm voxel size, with X-ray generator settings at 100 kV and 150 µA, using a 0.5 mm Cu filter. A total of 1000 projection images were recorded over a 360° rotation of the sample (0.36° step) with 1.5 s exposure time for each projection. The 3D volume data was reconstructed from these data sets using datos|x reconstruction software version 2.4.0.1199 (GE phoenix).

The 3D volumetric data was analysed using the free software Fiji (ImageJ) by first manually choosing and labeling the locations of the holes in the 3D volumes [34], [35]. The grayscale voxel data (corresponding to "radiodensity" which is a function of density and the average atomic number) was then filtered with a 3D median filter and thresholded using a value selected to be $I_{th} = I_{bg} + 0.7 \cdot (I_{mat} - I_{bg})$, where I_{bg} and I_{mat} are the average grayscale values in the background (surrounding air) and the matrix of the sample (excluding metal impurities), respectively. Binary image operations to clean and join isolated objects were then applied before the volumes and lengths of each hole were printed to a file for further analysis. The uncertainties for the measurements for both volume and depth were less than 2%.

2.2. Laser experiment and observation

The experiments were conducted with a YLR-300-MM-AC Ytterbium fiber laser, in an autonomous mode, from IPG Photonics, with capabilities given in Table 2. The laser head was mounted in a fume hood and connected via fiber-optic cable to the source located outside the hood. To better simulate the effects of zero gravity, the experiment was conducted horizontally, to prevent molten material from pooling in the bottom of the hole. The laser head was angled 10° from horizontal to prevent reflected processing light and ablated material from damaging the optics. A shielding gas of Argon was placed near the surface of the targets to prevent oxidation of the experiment samples. The target was mounted to a moving platform (CNC machine) capable of re-positioning between experiments and controlling the focal distance. The surface of the samples were placed in the focal plane, which allowed for power densities up to 954.9 kW/cm^2.

4

Table 2: Laser parameters.

Parameter	Value
Wavelength	1070 nm
Source power	< 300 W
Pulse frequency	< 500 Hz
Spot width	100 µm
Beam quality	8 mm mrad
Focal length	220 mm

The HSI system used in this experiment is based on the one used in [13]. A high-speed camera (FASTCAM Mini UX100 type 800-M-16G) running at 10 000 frames per second (fps) was used to study what physical processes happen during illumination. The light produced during processing over-saturated the CCD detector in the camera, thus a filter allowing only 810 nm light through was placed in front of the lens of the camera to reduce the processing light. An illumination laser of the same wavelength (810 nm) (CaviLux HF) was configured to illuminate the target area, which provided a clear view of the behavior of the material. The illumination laser was configured to have 10 µs pulses at 10 kHz, and the camera had an exposure time of 4 µs. An overview of the entire experiment setup is given in Fig. 1.
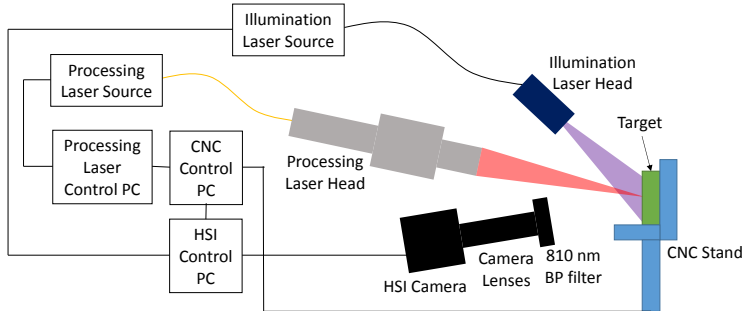

Figure 1: Experiment setup.

There were three independent variables in the experiments: laser power, pulse width, and repetition rate. The power was varied from 100 W to 300 W, the pulse widths from 1 ms to 16 ms, and the repetition rate from 53 Hz to 500 Hz. The repetition rate was selected to give integer values of pulse gaps from 1 ms to 4 ms. As it is assumed that olivine is the most abundant mineral of the three, it was selected for a wide range of experimental parameters. The pyroxene and serpentine had a narrower, and more specific range of parameters, based on iterative analysis of high-speed footage viewed while performing the experiments. We started with a regular matrix of parameters, but it turned out that many of the chosen parameters would not provide useful results. So we decided to use the pulse settings that seemed to produce the largest amount of spatter

during the initial olivine experiments also on the other two samples. A summary of the pulse settings space is given in Fig. 2. In addition, several "continuous mode" experiments were run to observe long-term behavior, each lasting ∼350 ms.

			Pulse gap (ms)											
			1			2			3			4		
Power (W)			100	200	300	100	200	300	100	200	300	100	200	300
	Olivine	1		■	■					■	■			
		2		■	■	■	■			■	■			
		4		■	■	■	■			■	■	■		
		8		■	■					■	■			
		16		■	■					■	■		■	■
Pulse length (ms)	Pyroxene	1	■	■	■									
		2												■
		4			■						■			
		8												
		16			■						■			
	Serpentine	1	■	■	■									
		2												
		4			■						■			
		8												
		16									■			

Figure 2: Overview of which laser parameters (power, pulse length, and pulse gap) were used in the experiments. The grey boxes indicate an experiment was performed at the corresponding pulse parameters, and white boxes indicate no experiment was performed.

The pulse parameters were set using the software provided with the laser itself, and an on-off trigger signal was sent from the CNC controller PC. Pulse modulation is done via selective voltage control (power modulation). Before the on signal was sent, the CNC PC would also toggle the crossjet and shielding gases and send a trigger signal to the HSI PC. The HSI PC, running Photron FASTCAM Viewer software, would then activate the illumination laser and begin recording for approximately 1 second, which is longer than all the experiment durations. After the laser-off signal was sent by the CNC PC, the gases and lasers would be shut off. The HSI PC ws then used to clip and save the experiment from the 1-second recording.

An important note is that the number of pulses varied for each experiment due to the synchronization signals having delays. Some experiments were repeated multiple times in order to test how sensitive the results were to local variations in the material composition and structure. The samples were not uniform crystals so their compositions and structures varied across their surfaces, especially for pyroxene and serpentine.

3. Results

The results are grouped into three parts. The first part concerns the characterization of the samples, which include images to show the overall characteristics of the samples. It also includes the results of the spectral analysis and petrographic studies. The second part is about the HSI, showing the processes that occur on each sample at varying depths. The third part is a study of the size and shape of the holes, including processing efficiencies.

3.1. Sample pre-characterization

Imaging in visual wavelengths reveals the overall variation between and on the samples (Fig. A.1). The olivine sample shows evenly distributed dark and light lithologies, with what looks like metallic iron or iron sulfide near the middle bottom. The pyroxene sample has an overall smooth grey/white/blue color, with some characteristic cleavages throughout the surface. The serpentine contains brown, yellow, and green regions, with spots and cracks all over the surface. There is a dark blue region in the bottom as well.

The reflectance spectra is shown in Fig. A.2. Both the olivine and pyroxene materials are showing the absorption band (pyroxene) or overlapping bands (olivine) around $\sim$ 1000 nm. It can be noted, that the reflectance levels of the serpentine material are clearly higher compared to the olivine and pyroxene materials at the wavelength of the laser, at 1070 nm. With the assumption that all the three materials have quite similar, diffuse angular scattering profiles, we can argue that the higher reflectance of serpentine indicates also lower absorption in the material, which also indicates that a smaller fraction of incident power is available for material heating.

The petrographic analysis reveals the microstructure of segments of the samples (Fig. 3). The olivine thin section reveals olivine crystals with diagnostic cracks and third-order interference colors. The sample is slightly mica altered, meaning a small amount of the olivine converted to mica, and contains accessory iron sulfides and iron oxides. The pyroxene thin section contains pyroxene crystals with second-order interference colors and small parts altered to calcite. The left part of the pyroxene image shows the 87° cleavage intersection usually associated with pyroxene. The serpentine thin section shows typical low first-order interference colors and mesh texture. Iron oxides/hydroxides are present in the sample as is a relict olivine crystal in the top right corner of the image.
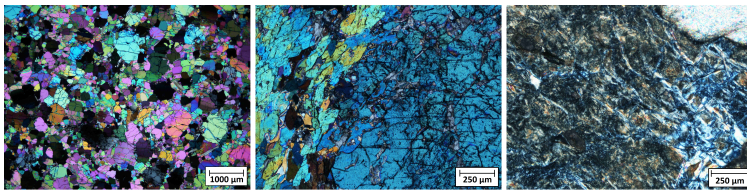

Figure 3: Photomicrographs taken in cross-polarized light of olivine (left), pyroxene (middle) and serpentine (right) test samples.

7

3.2. High-speed imaging analysis

High-speed footage revealed a number of intriguing processes occurring during inter-
action of the processing laser beam and the minerals. The olivine and pyroxene samples
rapidly ejected small (sub-millimeter-sized) particles in the initial moments of illumi-
nation (Fig. 4). At t_0, the laser begins irradiating the pyroxene surface. After 0.3 ms,
particles have already reached the far left part of the image, a distance of roughly 7 cm.
We estimate that these particles travel at over 230 m/s, the escape velocity of a 360-
km-wide asteroid. The opening angle of the stream is $\sim$25° and the rapid outburst lasts
roughly 1.5 ms.
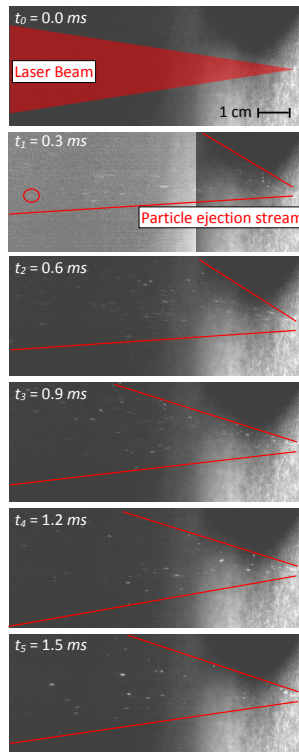
Figure 4: High-speed footage of pyroxene during the initial moments of the first pulse. Laser power was
300 W with 4 ms on time and 1 ms off time. The left side of the second frame has been brightened to
show the furthest discernible particle.

As the cavity depth increases and heat accumulates, the material begins to melt. The

rapid ejection of material then stops, most likely due to the surface tension of the melt pool, and is replaced by a different process where molten material is cast off in larger chunks (over 1 mm in size) at slower speeds, ranging from 5 m/s to 30 m/s (5 m/s is the escape velocity of a 7.5-km-wide asteroid), and in all directions. This can be demonstrated with an experiment on pyroxene, where the power is 300 W, pulse width of 4 ms, and repetition rate of 200 Hz (Fig. 5). The figure is divided into three phases: early, middle and late. The "early" series starts at the third pulse, showing a relatively small melt area, 1–2 mm in width, and ejection of relatively small spatters, less than 1 mm in size. By the time the ninth pulse is over (the beginning of the "middle" phase), the melt pool has increased in size to 2–3 mm, and is ejecting more and larger spatter, up to 1 mm in diameter. The "late" series shows the 19th pulse, where the melt area is relatively large, roughly 4–5 mm, and the ejected spatter is also relatively large, 1–2 mm in size. The same overall behavior was observed for olivine and serpentine (Figs. A.3 and A.4, respectively), except that the initial outburst was not seen for serpentine.
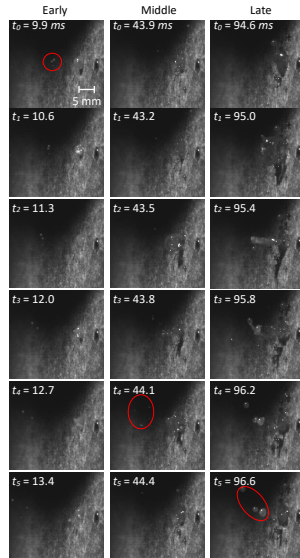

Figure 5: Selected frames showing the behavior of pyroxene under laser irradiation over time. The pulse settings are 4 ms on and 1 ms off at 300 W. The frames in the near-surface, mid-depth, and deep series are 0.7, 0.3, and 0.4 ms apart, respectively. The red circles highlight the spatter for each series.

An interesting phenomenon seen in olivine and pyroxene is a tendril-like formation, which extended roughly 1 cm from the melt pool before emitting a large (1–2-mm) particle at the tip, and then retracted back. An example of this phenomenon is seen at t_0 in the late series in Fig. A.3, and another less pronounced one at t_1 in the middle

9

series.

The continuous-mode experiments showed similar behaviors to pulsed experiments (Fig. 6). In the olivine sample, a melt pool of material extending roughly 1 mm above the surface formed and slowly grew to 5 mm in diameter. It undulated vertically from the surface, but did not throw off much spatter. The pyroxene exhibited a similar bulge above the surface, but threw off large pieces (1–2 mm in diameter) of spatter frequently (roughly 1 per millisecond) throughout the experiment. One can also see evidence of the tendril like formation. The serpentine did not have a large melt pool extending above the surface, but threw off spatter of small (micrometer-sized) and medium (1-mm-sized) pieces nearly constantly throughout the entire experiment.
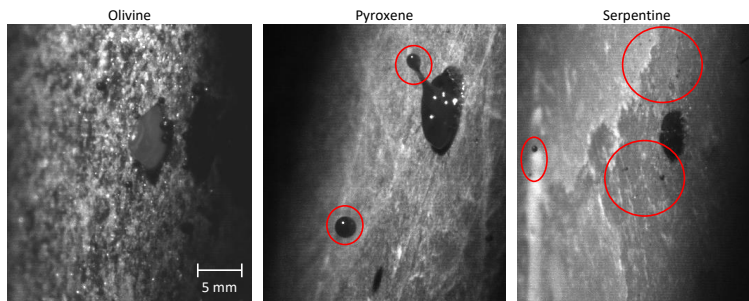
Figure 6: Images from the continuous-mode experiments. From left to right are olivine, pyroxene, and serpentine. No ejection is visible from olivine, and red circles show large spatter from pyroxene, and fine spatter from serpentine.

On all three samples, after the laser was switched off, the melt pools rapidly increased in size, forming semi-translucent bubbles and ejecting material, until it cooled completely (Fig. A.5), though the serpentine sample's bubbles were not as large.

3.3. Hole Sizes and Shapes

After the laser experiments, the samples were cut again to be better suited for the XMT studies. Each of the resulting XMT images is oriented that the surface of the sample is in the top left of each image, and drilling "down" is in the bottom-right direction. Due to the fact that the number of pulses varied between experiments and between samples, it is difficult to directly compare the shapes, structure, and sizes of the holes. There were, however, a few comparable situations. For instance, there is a clear increase in volume removed when increasing the pulse length while maintaining the power (300 W), gap between pulses (3 ms), and total energy (9.6 J) (Fig. 7).

Another interesting thing can be seen comparing the holes of the continuous-mode tests (Fig. A.6); the holes are roughly the same depth (11 mm), but the serpentine hole is nearly twice as wide near the bottom. The difference in shape could be due to the sheet-like structure of serpentine, which funneled energy sideways instead of downward. The pyroxene hole was larger than the others, possibly due to the cleavages breaking off, instead of a smooth melt.
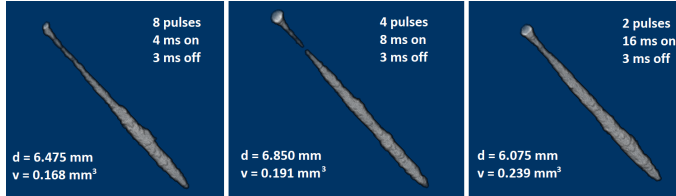
Figure 7: XMT images of three holes in the olivine sample. Each hole was created by 9.6 J of energy at the 300-W power setting. Shown are the pulse parameters, number of pulses, d for depth, and v for volume removed.

Eleven out of 36 holes in the olivine sample had discontinuities close to the surface (Fig. A.7). There seems to be no correlation to laser power or pulse settings. The discontinuities could be caused when liquid from the bottom cools and solidifies before it exits the hole, sometimes even closing the hole.

Accurate numbers of laser pulses were derived by analyzing the high-speed video footage. The total energy that was injected into the rocks was calculated by multiplying the energy per pulse (multiply the laser power by the pulse duration) by the number of pulses. The volume and depth for each hole is divided by the total energy of the experiment to find volume efficiency (VE) and depth efficiency (DE), respectively. These values can then be compared to the corresponding pulse parameters. The values for the experiments that were run more than once are the averages. The measurement values for groups of data (i.e. all olivine experiments) are the averages and the standard deviations.

The DE results suggest that olivine is the easiest to process , having an average DE of 0.722 ± 0.336 mm/J, and serpentine the most difficult , averaging 0.492 ± 0.080 mm/J, with pyroxene in between with an average DE of 0.589 ± 0.286 mm/J (Fig. 8). In general, our results suggest the shorter the pulse is, the more energy efficient the depth processing is, see the dotted line in Fig. 9. Allowing a longer gap, that is, reducing the repetition rate, also seems to increase the efficiency. For experiments with a 1-ms gap, the average DE was 0.586 ± 0.205 mm/J, while those with a 3-ms gap had an average of 0.663 ± 0.291 mm/J. The averages of the 200-W and 300-W experiments were 0.735 ± 0.327 mm/J and 0.713 ± 0.234 mm/J, respectively.

			Pulse gap (ms)			
			1	2	3	4
	Ol. 200 W	1	0.79		0.975	
		2	0.745	0.292	1.008	
		4	0.828	1.484	0.906	
		8	0.697		0.598	
		16	0.492		0.467	
	Ol. 300 W	1	0.895		0.907	
		2	0.756	0.986	1.031	
		4	0.564		0.674	
Pulse Length (ms)		8	0.441		0.714	
		16	0.327		0.633	
	Py. 300 W	1	1.049			
		2				0.994
		4	0.320		0.891	
		8				
		16	0.420		0.405	
	Se. 300 W	1	0.563			
		2				
		4	0.451		0.559	
		8			0.466	
		16			0.413	

Figure 8: Hole depth in mm per joule added for pulsed experiments. Color increases in intensity with an increase in depth. Blank cells indicate no experiment was performed with the corresponding pulse parameters.
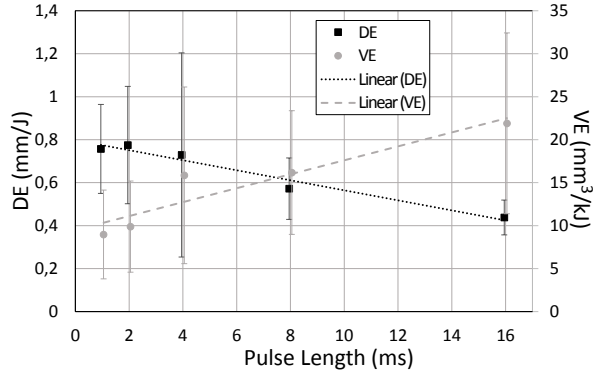
Figure 9: Depth (DE) and volume (VE) processing efficiencies by pulse length.

The VE results seem to paint a different picture, suggesting that pyroxene is the easiest to process , having an average VE of 22.3 ± 13.0 mm^3/kJ, and olivine is the most difficult , with an average VE of 11.9 ± 6.8 mm^3/kJ; serpentine was in the middle with an average 16.2 ± 6.7 mm^3/kJ (Fig. 10). The difference in VE could be due to the cleavages associated with pyroxene, where chunks of the mineral could be broken off from the sides of the processing hole. It appears that the longer the pulse, the more efficiently the material is removed, see the dashed line in Fig. 9.   Pulses with 1-ms gaps had an average VE of 16.8 ± 11.3 mm^3/kJ, and 3-ms gaps had 15.2 ± 9.0 mm^3/kJ. The 200 W experiments clearly performed less efficiently than the 300 W ones , having average VE values of 8.9 ± 4.0 mm^3/kJ and 17.9 ± 5.8 mm^3/kJ, respectively.

		Pulse gap (ms)			
		1	2	3	4
Ol. 200 W	1	5.400		5.500	
	2	9.327	2.083	5.000	
	4	8.281	17.188	8.750	
	8	9.375		10.651	
	16	7.891		9.609	
Ol. 300 W	1	13.684		4.912	
	2	19.359	11.667	15.208	
	4	16.154		17.500	
	8	25.243		19.896	
	16	24.000		24.896	
Py. 300 W	1	17.222			
	2				11.190
	4	31.081		17.917	
	8				
	16	28.472		36.736	
Se. 300 W	1	15.667			
	2				
	4	21.771		20.139	
	8			23.229	
	16			17.465	

Figure 10: Volume removed in mm^3 per kilojoule added for pulsed experiments. Color increases in intensity with an increase in volume removed.   Blank cells indicate no experiment was performed with the corresponding pulse parameters.

The few experiments performed with a laser power of 100 W show DE values comparable to the higher power levels , an average of $0.648 \pm$ mm/J, but much lower VE values , an average of $4.9 \pm$ mm^3/kJ (Table 3).

The processing efficiencies of the continuous-mode experiments show that DE suffers greatly even compared to the lowest values produced by pulsed experiments (average DE for continuous-mode was 0.114 ± 0.013 mm/J, and the lowest pulsed-mode was 0.236 mm/J) whereas the VE values are comparable to their pulsed counterparts , with an average VE of 18.2 ± 6.837 mm^3/kJ (Table 4).

The experiments that were duplicated show that wide scatter is possible for all three samples (Table 5).   In terms of relative deviations, the results suggest that values for

Table 3: Processing efficiencies for the pulsed experiments with a laser power of 100 W. VE stands for volume efficiency and DE stands for depth efficiency.

Material	Pulse width (ms)	Pulse gap (ms)	VE (mm^3/kJ)	DE (mm/J)
Oliv.	2	2	5.833	0.417
Oliv.	4	2	5.625	1.063
Oliv.	4	4	5.000	0.359
Pyrox.	1	1	4.211	0.434
Serp.	1	1	2.857	0.554

Table 4: Processing efficiencies for continuous-mode experiments. VE stands for volume efficiency and DE stands for depth efficiency.

Material	Power (W)	Duration (ms)	VE (mm^3/kJ)	DE (mm/J)
Oliv.	200	376	8.684	0.127
Oliv.	300	313	19.375	0.121
Pyro.	300	380	23.219	0.098
Serp.	300	380	19.404	0.098

DE can vary from 3.4% to 104.0% for olivine, 8.6% to 37.1% for pyroxene, and 12.3% for serpentine. The VE values vary from 1.0% up to 78.6% for olivine, 43.3% to 54.5% for pyroxene, and 23.0% for serpentine.

Table 5: Average efficiencies and standard deviations for duplicate experiments. The letter c is for the continuous-mode experiment, which is 1 pulse 313 ms in length. VE stands for volume efficiency, DE for depth efficiency, and SD for standard deviation.

Material	Power (W)	Pulse width (ms)	Rep. rate (Hz)	Average VE (mm^3/kJ)	Std. Dev. VE (mm^3/kJ)	Average DE (mm/J)	Std. Dev. DE (mm/J)
Oliv.	100	4	167	5.625	4.419	1.063	1.105
Oliv.	200	2	333	9.327	0.408	0.745	0.136
Oliv.	200	8	91	10.651	2.429	0.598	0.163
Oliv.	300	8	111	25.243	0.246	0.441	0.015
Oliv.	300	c	c	19.375	7.496	0.121	0.005
Pyrox.	300	4	200	31.081	16.934	0.320	0.119
Pyrox.	300	16	59	28.472	12.339	0.420	0.036
Serp.	300	16	53	17.465	4.016	0.413	0.051

The shape, color, and width of the holes were different between samples, as well as different on each sample too (Fig. 11). The top two rows are olivine, the third row is pyroxene, and last row is serpentine. The olivine mostly has dark/metallic holes, with the exception of two of them, the hole second from the right on the bottom row, and sixth from the left on the bottom row. The pyroxene mostly has yellow holes, with the exception of the second from the left, which is white. Each of the non-white holes has

a glassy coating. The serpentine holes vary the most, with white holes and brown holes over different regions of the material.
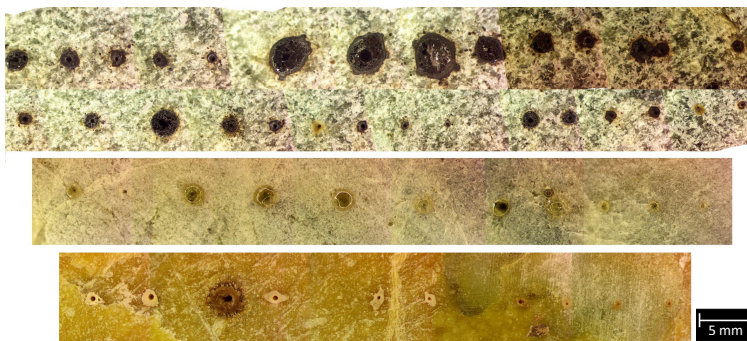

Figure 11: View of holes on all three samples. The top panel is olivine, the middle panel is pyroxene, and bottom panel is serpentine. Individual images were taken of each hole under a microscope that were then stitched together. The images have the same size scale and can thus be directly compared to each other. Continuous-mode experiments are the largest of the series: middle center for olivine and 3rd from left on pyroxene and serpentine. Small holes on the far right were made by 100-W settings.

Comparing the wide range of settings used to make holes in the olivine sample, there appears to be a linear relationship between the total energy of the experiment and the volume of material removed from the hole (Fig. 12). The slope of the line increases relative to higher laser power, i.e., the higher the power, the steeper the slope. There is no 100-W trend line as there were only four experiments, and thus the trend cannot be accurately modelled. Although we note that they appear at the bottom left of the plot with some of the lowest volumes removed.
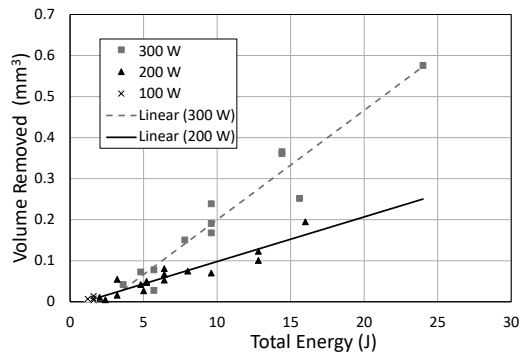
Figure 12: Plot of volume removed against the total energy for the experiment for the olivine sample.

Another trend is a decreasing logarithmic relationship between the total energy and the depth of the hole (Fig. 13). The same logarithmic relationship between energy and depth holds true for the other three samples, where olivine appears to be be easiest to process, followed by pyroxene and then serpentine (Fig. 14). In addition, it is clear that higher laser power produces deeper holes (Fig. 15).
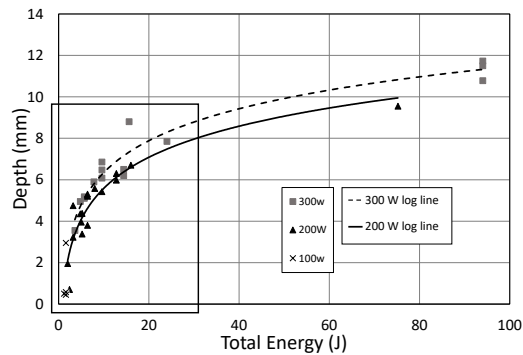

Figure 13: Plot of the depth of the holes made in olivine versus how much total energy was used to make them. The box shows the region of experiments with pulsed settings, and the data points outside the box correspond to continuous-mode irradiation.
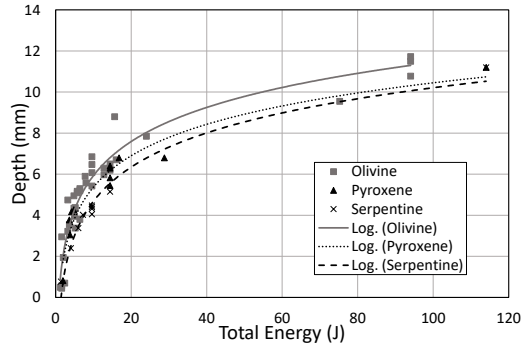
Figure 14: Plot of depth of the holes made in all three samples versus how much total energy was used to make them. The depths for the pyroxene and serpentine were the same, so the data points overlap.
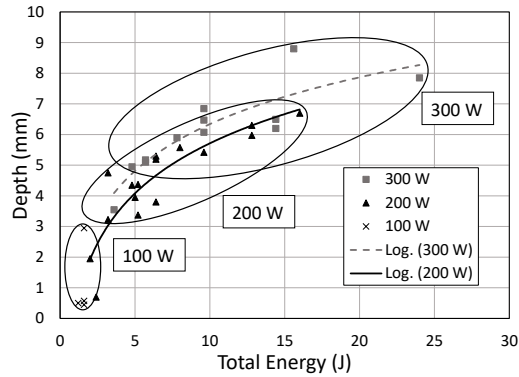
Figure 15: Plot of the depth of the holes made in olivine versus how much total energy was used to make them. Here we only consider pulsed laser.

4. Discussion and Additional Analysis

In general, serpentine had smaller holes than olivine and pyroxene. The size difference could be due to the fundamental difference in crystal structure and chemical composition of the materials. Unlike olivine and pyroxene, serpentine contains water, which is located between layers of SiO_4 tetrahedra and AlO_6 octahedra. The energy entering the mineral

17

might be absorbed by the water and dissipated from the hole area, if not simply expanding between the layers without melting or breaking. The distinct spattering behavior of serpentine may thus be due to its water content in combination with its layered structure, and in particular the dehydroxylation process at high temperatures.

The specific energy (reciprocal of VE) for slate and sandstone are in the range of 1 to 2 kJ/cm^3 at power densities of roughly 1 kW/cm^3 [16]. The minimum values we calculated for olivine, pyroxene, and serpentine were 36.5, 23.2, and 43.0 kJ/cm^3, respectively, but our power densities were on the order of 900 kW/cm^3. Slate and sandstone are "weaker" rocks, and would thus have lower specific energies overall. The specific energies for different rocks are within about one order of magnitude of each other, so there does not appear to be a radical difference between the energies required to process various stones. Another finding from [16] was that increasing the repetition rate reduced the specific energy. We cannot confirm this relationship, as only six of 13 instances showed such a trend. This could be due to the difference in power intensities and the corresponding difference in removal mechanisms (i.e. spallation vs spattering). We can also estimate the temperatures achieved in the experiment using the specific energy and specific heat capacities; the temperatures varied quite a lot, between 5 254 K and 141 414 K, but averaged at 22 423 K.

Results from [32] showed mass removal rates near the "beginning" of their experiments of 2.1×10^{-7} kg/s, and near the "end" it was down to 2.5×10^{-8} kg/s. Their experiments ran for 10 minutes in continuous mode, and it is not clear exactly how they define the beginning of their experiments. We note that their model only considered sublimation, not spallation or melt ejection. The maximum removal rate in our experiments was 4.1×10^{-5} kg/s; the significant difference in magnitude suggests that a vast majority of material is ejected in the initial moments of laser beam irradiation.

The experiments by [32] were performed in a vacuum chamber, where atmospheric disturbances could not affect the processing. These disturbances could include melt pool pressure, turbulence, or eddy currents; lower ambient pressure could also allow vapour in the hole to escape easier, perhaps creating narrower holes. The spatter may behave differently, as it is unclear from the HSI whether the bubbles formed contained atmospheric gas or vapor from the processing.

The time required to ablate material has a considerable impact on mission design, primarily regarding whether or not a spacecraft is required to land on the surface or if it can stay in orbit near the asteroid. The ability to maintain the location of the focal point of the laser on the asteroid surface is difficult from orbit, and would require highly precise control equipment, whereas a lander would have little issue with spot control. Our results suggest that, if the aim is to redirect an asteroid by removing surface material to produce a momentum exchange, maintaining precise control is not necessary. The beam spot can wander around on the surface, within limits, spallating and melting new locations, rather than being focused on one spot to operate in the vapor ablation state.

The decreasing logarithmic relationship between depth and total energy might be due to the fact that the laser beam de-focuses with distance from the focal point. The continuous-mode experiments (the longest/most energetic) produced the deepest holes, nearly penetrating the olivine sample, but still did not go deeper than 10–12 mm. This relationship only holds for the range of energies used in this experiment; longer exposure will eventually reach a maximum depth, when the laser beam de-focuses to the point where it can no longer process material. Using the spot size of 0.1 mm and beam quality

of 8 mm mrad, we can see that after 1 cm, the beam is roughly 0.8 mm, eight times wider than in focus.

The experiment setup was not designed to study any gas or vapor. Ablated vapor can block some of the incident laser irradiation, and it can occur within the first nanosecond of exposure. It must be noted that the presence of the vapor and the spattering ejecta must have blocked some of the laser beam, which could have affected the shape of the hole and the total amount of material removed.

The results showed relatively large scatter ($\sim$20%) although the measurements were relatively accurate ($<$2% error). This implies that the differences in the results are most likely due to the micro-scale material properties and/or pulse parameter settings. This is further demonstrated when considering the results obtained by multiple experiments at the same pulse parameter settings. The wide range of variability of VE and DE in olivine are most likely due to the local concentrations of forsterite and fayelite. The pyroxene and serpentine also showed relatively large variations in efficiencies, which can more readily be explained by larger-scale composition differences.

While the laser was able to process all three rocks in a similar fashion, we can only speculate how it will affect other materials. We know asteroids are not entirely homogeneous, and may contain pockets of metals, hydrocarbons, or other volatiles, which may react differently, depending on their absorption at the laser frequency.

There is also clearly a presence of re-deposited material on the surface. The build-up could be due to the shielding gas being angled slightly towards the surface, though the HSI does not show a uniform movement of all particles. Alternatives include electrostatic forces and local drag due to the expansion of the local ambient atmosphere.

5. Conclusions

The cross-disciplinary approach utilized in the present research project provided several insights into how lasers can efficiently be used to process asteroid material.

First, regardless of the material, the laser was able to produce similar melting and ejection behavior for all three samples. A 1070-nm laser is demonstrated to reliably and robustly process olivine, pyroxene, and serpentine, even at 100 W, the lowest power used in the present research project. The relatively small energy consumption and high processing efficiency therefore suggest that laser payloads are suitable for small satellites with limited power budgets.

Second, spatter produced during the first pulse is significantly smaller and faster than spatter produced later in the same experiment in both pyroxene and olivine. Serpentine did not have a rapid-outburst phase, it immediately began to melt and behaved like a mid-depth process.

Third, there is clear evidence of forces that keep more material from being ejected. These can include surface tension, wetting forces, and atmospheric pressure.

Fourth, our measurements suggest there is a trade-off with pulse length between depth and volume removal efficiencies. Short pulses make deeper holes, but longer pulses are preferred for removing the most amount of volume.

Fifth, the depth efficiency seems to be inversely related to pulse repetition rate, but volume efficiency is directly related. The continuous-mode experiments had the poorest depth efficiency.

The HSI and XMT data as well as microscope imaging of the holes are available upon request.

Acknowledgements

References

[1]   D. G. Andrews, K. Bonner, A. Butterworth, H. Calvert, B. Dagang, K. Dimond, L. Eckenroth, J. Erickson, B. Gilbertson, N. Gompertz, O. Igbinosun, T. Ip, B. Khan, S. Marquez, N. Neilson, C. Parker, E. Ransom, B. Reeve, T. Robinson, M. Rogers, P. Schuh, C. Tom, S. Wall, N. Watanabe, and C. Yoo, "Defining a successful commercial asteroid mining program," *Acta Astronautica*, vol. 108, pp. 106–118, 2015. DOI: https://doi.org/10.1016/j.actaastro.2014.10.034.

[2]   M. Gaffey and T. Mccord, "Mining outer space," *Technology Review*, vol. 79, no. 7, pp. 51–59, 1977.

[3]   B. O′Leary, "Mining the Apollo and Amor Asteroids," *Science*, vol. 197, no. 4301, pp. 363–366, 1977, ISSN: 0036-8075. DOI: https://doi.org/10.1126/science.197.4301.363-a.

[4]   C. B. Dreyer, J. Sercel, L. Gertsch, A. Lampe, T. J. Canney, and A. Abbud-Madrid, "Optical mining subscale testing," in *Earth and Space 2016*, 2016, pp. 493–506. DOI: https://doi.org/10.1061/9780784479971.047.

[5]   Pekka Janhunen, "Shielded Dumbbell L5 Settlement," *NSS Space Settlement Journal*, vol. 4, pp. 1–11, 2020. [Online]. Available: https://space.nss.org/wp-content/uploads/NSS-JOURNAL-Shielded-Dumbbell-L5-Settlement.pdf.

[6]   T. H. Prettyman, N. Yamashita, M. J. Toplis, H. Y. McSween, N. Schörghofer, S. Marchi, W. C. Feldman, J. Castillo-Rogez, O. Forni, D. J. Lawrence, E. Ammannito, B. L. Ehlmann, H. G. Sizemore, S. P. Joy, C. A. Polanskey, M. D. Rayman, C. A. Raymond, and C. T. Russell, "Extensive water ice within Ceres′ aqueously altered regolith: Evidence from nuclear spectroscopy," *Science*, vol. 355, no. 6320, pp. 55–59, Jan. 2017. DOI: 10.1126/science.aah6765.

[7]   K. Zacny, P. Chu, G. Paulsen, M. Hedlund, and B. Mellerowicz, "Asteroids: Anchoring and Sample Acquisition Approaches in Support of Science, Exploration, and In situ Resource Utilization," in *Asteroids: Prospective Energy and Material Resources*, V. Badescu, Ed. 2013, pp. 287–343. DOI: 10.1007/978-3-642-39244-3_12.

[8]   J. P. Singh and S. N. Thakur, *Laser-induced breakdown spectroscopy*. Elsevier Science, 2007. DOI: https://doi.org/10.1016/B978-0-444-51734-0.X5001-7.

[9]   T. H. Maiman, "Stimulated optical radiation in ruby," *Nature*, vol. 187, no. 4736, pp. 493–494, 1960. DOI: https://doi.org/10.1038/187493a0.

[10] I. F. Larsson, "Method and apparatus for drilling holes by means of a focused laser beam," no. USA, Patent Nr. US3410979A, 1964, 1964.

[11] M. von Allmen, "Laser drilling velocity in metals," *Journal of Applied Physics*, vol. 47, no. 12, pp. 5460–5463, Dec. 1976. DOI: https://doi.org/10.1063/1.322578.

[12] D. K. Y. Low, L. Li, and P. J. Byrd, "The effects of process parameters on spatter deposition in laser percussion drilling," *Optics Laser Technology*, vol. 32, no. 5, pp. 347–354, Jul. 2000. DOI: https://doi.org/10.1016/S0030-3992(00)00079-7.

[13] J. Pocorni, J. Powell, J. Frostevarg, and A. F. H. Kaplan, "Investigation of the piercing process in laser cutting of stainless steel," *Journal of Laser Applications*, vol. 29, no. 2, pp. 022201-1–022201-8, May 2017. DOI: https://doi.org/10.2351/1.4983260.

[14] M. Schneider, L. Berthe, R. Fabbro, M. Muller, and M. Nivard, "Gas investigation for laser drilling," *Journal of Laser Applications*, vol. 19, no. 3, pp. 165–169, Aug. 2007. DOI: `https://doi.org/10.2351/1.2567844`.

[15] C. Lehane and H. Kwok, "Enhanced drilling using a dual-pulse nd:yag laser," *Applied Physics A*, vol. 73, pp. 45–48, Jul. 2001. DOI: `https://doi.org/10.1007/s003390100819`.

[16] Z. Xu, C. B. Reed, G. Konercki, R. A. Parker, B. C. Gahan, S. Batarseh, R. M. Graves, H. Figueroa, and N. Skinner, "Specific energy for pulsed laser rock drilling," *Journal of Laser Applications*, vol. 15, no. 1, pp. 25–30, 2003. DOI: `https://doi.org/10.2351/1.1536641`.

[17] A. Riveiro, A. Mejías, R. Soto, F. Quintero, J. [Val], M. Boutinguiza, F. Lusquiños, J. Pardo, and J. Pou, "CO2 laser cutting of natural granite," *Optics & Laser Technology*, vol. 76, pp. 19–28, 2016, ISSN: 0030-3992. DOI: `https://doi.org/10.1016/j.optlastec.2015.07.018`.

[18] M. Boutinguiza, J. Pou, F. Lusquiños, F. Quintero, R. Soto, M. Pérez-Amor, K. Watkins, and W. Steen, "CO2 laser cutting of slate," *Optics and Lasers in Engineering*, vol. 37, no. 1, pp. 15–25, 2002, ISSN: 0143-8166. DOI: `https://doi.org/10.1016/S0143-8166(01)00142-7`.

[19] O. Kotova and N. Leonenko, "Physics and chemistry of minerals under laser processing," in *Materials Science and Engineering Conference Series*, ser. Materials Science and Engineering Conference Series, vol. 123, Apr. 2016, p. 012 016. DOI: `10.1088/1757-899X/123/1/012016`.

[20] N. Leonenko, E. Vanina, G. Kapustina, and E. Veselova, "Study of nonlinear effect about laser-induced processes of nanodispersed gold in mineral association," in *Material Researches and Energy Engineering*, ser. Advanced Materials Research, vol. 772, Trans Tech Publications Ltd, Nov. 2013, pp. 355–358. DOI: `10.4028/www.scientific.net/AMR.772.355`.

[21] M. Norman, P. Robinson, and D. Clark, "MAJOR- AND TRACE-ELEMENT ANALYSIS OF SULFIDE ORES BY LASER-ABLATION ICPﬀﬁﬂﬃﬄﬅﬆdMS, SOLUTION ICPﬀﬁﬂﬃﬄﬅﬆdMS, AND XRF: NEW DATA ON INTERNATIONAL REFERENCE MATERIALS," *The Canadian Mineralogist*, vol. 41, no. 2, pp. 293–305, Apr. 2003, ISSN: 0008-4476. DOI: `https://doi.org/10.2113/gscanmin.41.2.293`.

[22] R. Z. Sagdeev and A. V. Zakharov, "Brief history of the Phobos mission," *Nature*, vol. 341, no. 6243, pp. 581–585, Oct. 1989. DOI: `https://doi.org/10.1038/341581a0`.

[23] R. C. Wiens, S. Maurice, B. Barraclough, M. Saccoccio, W. C. Barkley, J. F. Bell, S. Bender, J. Bernardin, D. Blaney, J. Blank, M. Bouyé, N. Bridges, N. Bultman, P. Caïs, R. C. Clanton, B. Clark, S. Clegg, A. Cousin, D. Cremers, A. Cros, L. DeFlores, D. Delapp, R. Dingler, C. D'Uston, M. Darby Dyar, T. Elliott, D. Enemark, C. Fabre, M. Flores, O. Forni, O. Gasnault, T. Hale, C. Hays, K. Herkenhoff, E. Kan, L. Kirkland, D. Kouach, D. Landis, Y. Langevin, N. Lanza, F. LaRocca, J. Lasue, J. Latino, D. Limonadi, C. Lindensmith, C. Little, N. Mangold, G. Manhes, P. Mauchien, C. McKay, E. Miller, J. Mooney, R. V. Morris, L. Morrison, T. Nelson, H. Newsom, A. Ollila, M. Ott, L. Pares, R. Perez, F. Poitrasson, C. Provost, J. W. Reiter, T. Roberts, F. Romero, V. Sautter, S. Salazar, J. J. Simmonds, R. Stiglich, S. Storms, N. Striebig, J.-J. Thocaven, T. Trujillo, M. Ulibarri, D. Vaniman, N. Warner, R. Waterbury, R. Whitaker, J. Witt, and B. Wong-Swanson, "The ChemCam Instrument Suite on the Mars Science Laboratory (MSL) Rover: Body Unit and Combined System Tests," *Space Science Reviews*, vol. 170, no. 1-4, pp. 167–227, Sep. 2012. DOI: `https://doi.org/10.1007/s11214-012-9902-4`.

[24] P. S. Moura, B. Serpa, B. Assis, Y. Moura, V. P. Alves, K. A. Schenguer, B. L. Tumelero, A. Luz, L. G. C. Novaes, A. T. Cabral, D. V. Rotter, N. Rossini, P. M. R. Santos, T. K. Bretzke, M. de Souza, K. Morais, D. Champoski, D. Vieira, G. Spricigo, E. D. Carli, S. L. S. Taglialenha, and G. B. Hughes, "A CubeSat mission for space-environment demonstration of Remote Laser-Evaporative Molecular Absorption (R-LEMA) spectroscopy sensor system concept," in *CubeSats and NanoSats for Remote Sensing II*, T. S. Pagano and C. D. Norton, Eds., International Society for Optics and Photonics, vol. 10769, SPIE, 2018, pp. 164–173. DOI: `https://doi.org/10.1117/12.2320863`.

[25] R. P. Binzel, F. E. DeMeo, E. V. Turtelboom, S. J. Bus, A. Tokunaga, T. H. Burbine, C. Lantz, D. Polishook, B. Carry, A. Morbidelli, M. Birlan, P. Vernazza, B. J. Burt, N. Moskovitz, S. M. Slivan, C. A. Thomas, A. S. Rivkin, M. D. Hicks, T. Dunn, V. Reddy, J. A. Sanchez, M. Granvik, and T. Kohout, "Compositional distributions and evolutionary processes for the near-Earth object population: Results from the MIT-Hawaii Near-Earth Object Spectroscopic Survey (MITHNEOS)," *Icarus*, vol. 324, pp. 41–76, May 2019. DOI: `10.1016/j.icarus.2018.12.035`.

[26] V. Reddy, T. L. Dunn, C. A. Thomas, N. A. Moskovitz, and T. H. Burbine, "Mineralogy and Surface Composition of Asteroids," in *Asteroids IV*, P. Michel, F. E. DeMeo, and W. F. Bottke, Eds., 2015, pp. 43–63. DOI: `https://doi.org/10.2458/azu_uapress_9780816532131-ch003`.

[27] A. E. Rubin, "Mineralogy of meteorite groups," *Meteoritics and Planetary Science*, vol. 32, pp. 231–247, Mar. 1997. DOI: `https://doi.org/10.1111/j.1945-5100.1997.tb01262.x`.

[28] F. Deer W. A., R. A. Howie, and J. Zussman, *An Introduction to the Rock-Forming Minerals*. Mineralogical Society of Great Britain and Ireland, Jan. 2013, ISBN: 9780903056274. DOI: `https://doi.org/10.1180/DHZ`.

[29] N. L. Bowen and J. F. Schairer, "The system MgO-FeO-SiO2," *American Journal of Science*, vol. 29, no. 5, pp. 151–217, 1935. DOI: `https://doi.org/10.2475/ajs.s5-29.170.151`.

[30] G. C. C. Costa, N. S. Jacobson, and J. Fegley Bruce, "Vaporization and thermodynamics of forsterite-rich olivine and some implications for silicate atmospheres of hot rocky exoplanets,", vol. 289, pp. 42–55, Jun. 2017. DOI: `10.1016/j.icarus.2017.02.006`.

[31] H. J. Melosh, I. V. Nemchinov, and Y. I. Zetzer, "Non-nuclear strategies for deflecting comets and asteroids.," in *Hazards Due to Comets and Asteroids*, Jan. 1994, pp. 1111–1132.

[32] A. Gibbings, M. Vasile, I. Watson, J.-M. Hopkins, and D. Burns, "Experimental analysis of laser ablated plumes for asteroid deflection and exploitation," *Acta Astronautica*, vol. 90, no. 1, pp. 85–97, 2013, NEO Planetary Defense: From Threat to Action - Selected Papers from the 2011 IAA Planetary Defense Conference, ISSN: 0094-5765. DOI: `https://doi.org/10.1016/j.actaastro.2012.07.008`.

[33] J. Sloane, "Laser ablation Propulsion of Asteroids with a Sub-nanosecond Pulsed Laser," PhD thesis, University of Maryland, College Park, Jan. 2019.

[34] C. T. Rueden, J. Schindelin, M. C. Hiner, B. E. DeZonia, A. E. Walter, and et al., "ImageJ2: ImageJ for the next generation of scientific image data," *BMC Bioinformatics*, vol. 18, p. 529, 2017. DOI: `https://doi.org/10.1186/s12859-017-1934-z`.

[35] J. Schindelin, I. Arganda-Carreras, E. Frise, V. Kaynig, M. Longair, T. Pietzsch, S. Preibisch, C. Rueden, S. Saalfeld, B. Schmid, J.-Y. Tinevez, D. J. White, V. Hartenstein, K. Eliceiri, P. Tomancak, and A. Cardona, "Fiji: An open-source platform for biological-image analysis," *Nature Methods*, vol. 9, no. 7, pp. 676–682, 2012. DOI: `https://doi.org/10.1038/nmeth.2019`.
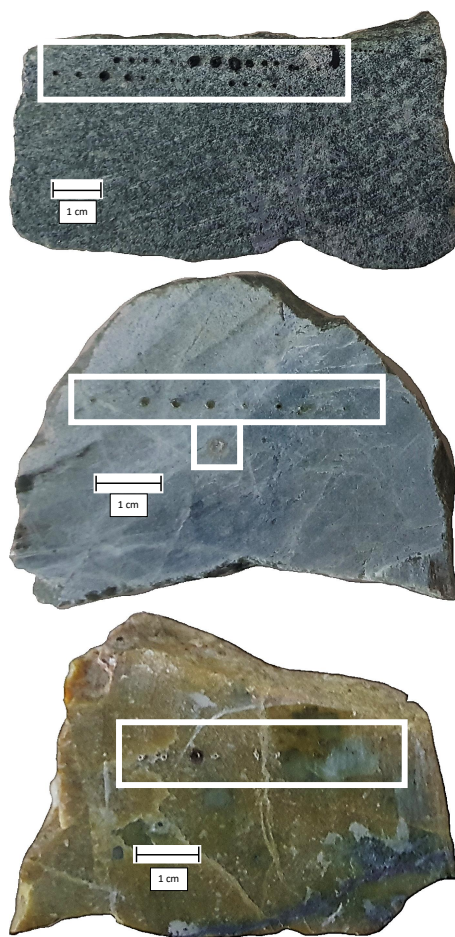
Appendix A.

Figure A.1: Images of the samples showing overall macroscopic characteristics; from top to bottom, they are: olivine, pyroxene, and serpentine. The white boxes show where the experiments were performed.
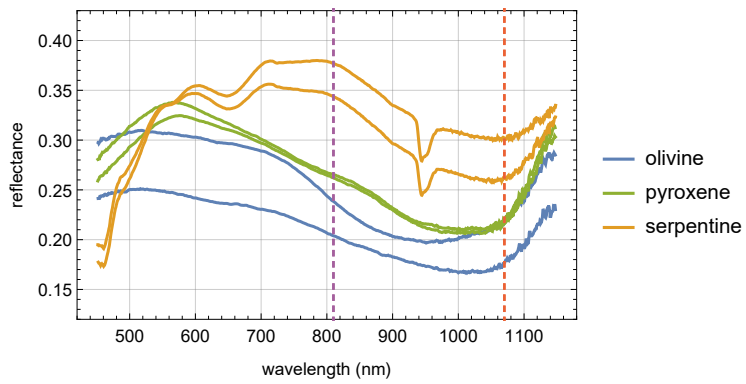
Figure A.2: Reflectance spectra of the samples. The spectra was measured in two separate spots, both presenting the typical phase of the sample, for all the three samples. The wavelength of the laser at 1070 nm is indicated with a red, dashing line in the figure, and the wavelength of the illumination for the high-speed camera at 810 nm with a violet, dashed line.
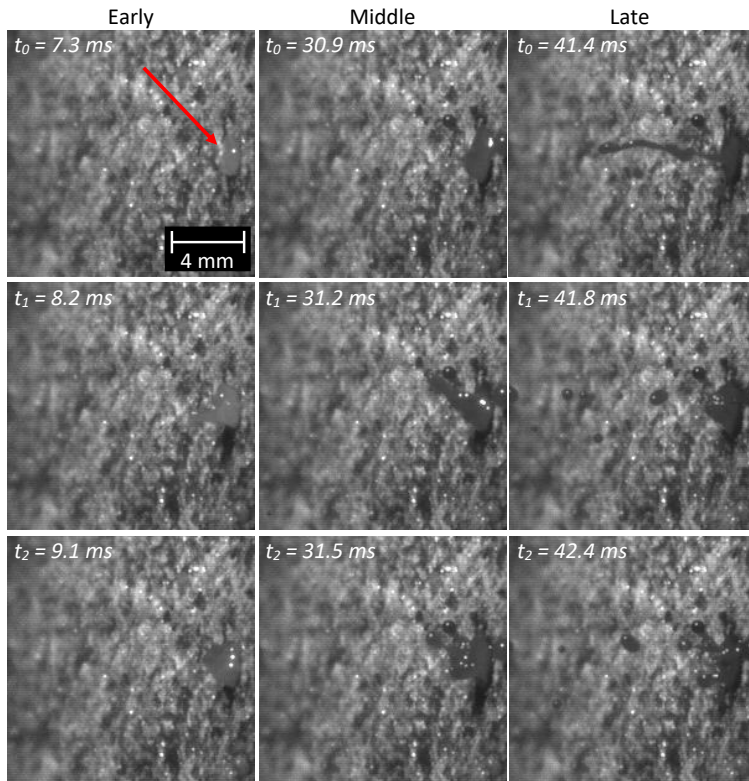
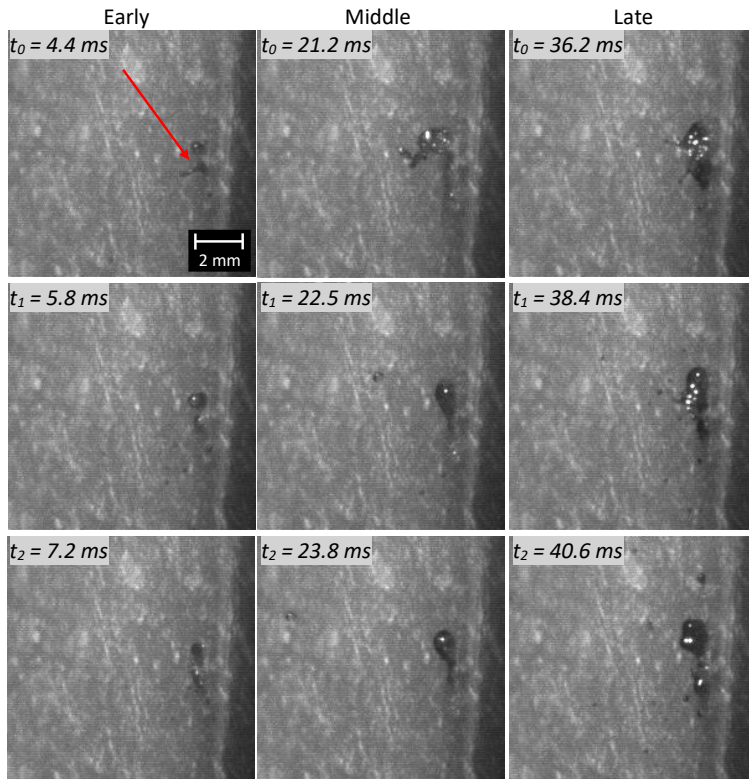Figure A.3: High-speed footage of olivine experiment over time. The power setting was 300 W, pulse length 8 ms, and pulse gap 3 ms.

Figure A.4: High-speed footage of serpentine experiment over time. The power setting was 300 W, pulse length 8 ms, and pulse gap 3 ms.
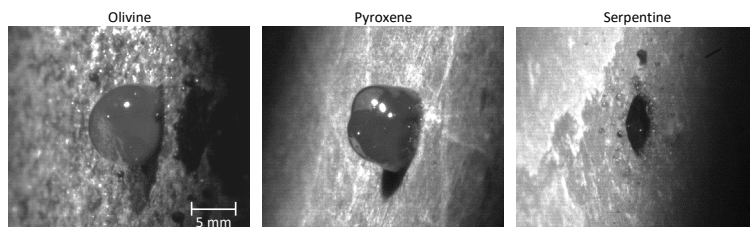
Figure A.5: Images showing the formation of translucent bubbles briefly after laser irradiation has ended.
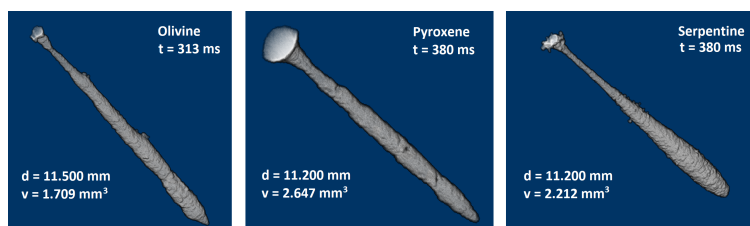

Figure A.6: XMT images of the continuous-mode experiments at 300 W. Shown are the d for depth and v for volume as well as duration of each experiment.
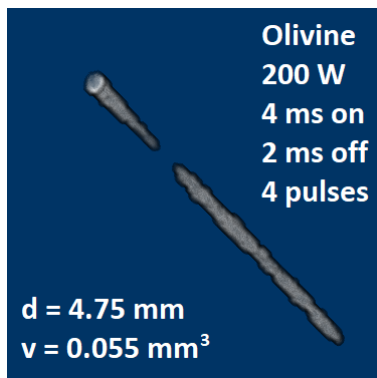

Figure A.7: XMT images of a hole in olivine exhibiting a bottle-neck. The hole corresponds to a laser power of 200 W with the irradiation being on for 4 ms and off for 2 ms.

Paper C

Laser-induced spallation of minerals common on asteroids

Authors:
Niklas Anthony, Jan Frostevarg, Heikki Suhonen, Christina Wanhainen, Mikael Granvik

Laser-induced spallation of minerals common on asteroids

Niklas Anthony[a,*], Jan Frostevarg[b], Heikki Suhonen[c], Christina Wanhainen[d], Mikael Granvik[a,c]

[a]*Asteroid Engineering Laboratory, Onboard Space Systems, Luleå University of Technology, Box 848, 98128 Kiruna, Sweden*
[b]*Department of Engineering Sciences and Mathematics, Luleå University of Technology, 97187 Luleå, Sweden*
[c]*Department of Physics, P.O. Box 64, 00014 University of Helsinki, Finland*
[d]*Division of Geosciences and Environmental Engineering, Luleå University of Technology, 97187 Luleå, Sweden*

Abstract

The ability to deflect dangerous small bodies in the Solar System or redirect profitable ones is a necessary and worthwhile challenge. One well-studied method to accomplish this is laser ablation, where solid surface material sublimates, and the escaping gas creates a momentum exchange. Alternatively, laser-induced spallation and sputtering could be a more efficient means of deflection, yet little research has studied these processes in detail. We used a 15-kW Ytterbium fiber laser on samples of olivine, pyroxene, and serpentine (minerals commonly found on asteroids) to induce spallation. We observed the process with a high-speed camera and illumination laser, and used X-ray microtomography to measure the size of the holes produced by the laser to determine material removal efficiency. We found that pyroxene will spallate at power densities between 1.5 and 6.0 kW cm^{-2}, serpentine will also spallate at 13.7 kW cm^{-2}, but olivine does not spallate at 1.5 kW cm^{-2} and higher power densities melt the sample. Laser-induced spallation of pyroxene and serpentine can be two- to three-times more energy efficient (volume removed per unit of absorbed energy) than laser-induced spattering, and over 40x more efficient than laser ablation.

Keywords: Laser Spallation, High-Speed Imaging, Asteroid Redirection, X-ray Microtomography

1. Introduction

Laser ablation is the process of using a laser to heat a small area of material beyond its sublimation temperature, which removes surface material in gas form. The first mention of using laser ablation to alter the orbits of objects in space was in 1994 [1], roughly the same time the US Congress passed its first mandate to NASA to catalogue large near-Earth asteroids (NEAs) and identify potentially hazardous ones. The same

---

*Corresponding author
Email addresses:* `niklas.anthony@ltu.se` (Niklas Anthony), `mgranvik@iki.fi` (Mikael Granvik)

process can also be used to de-spin or de-tumble an asteroid to prepare it for processing or manipulation [2]. Asteroid impacts pose a serious threat to the Earth's ecosystem. The mass-extinction event that occurred ∼65 million years ago was due to a 10–80-km-diameter asteroid impacting just off the Yucatán peninsula [3]. A more recent (and better-documented) example was the Chelyabinsk superbolide: an NEA roughly 20 m in diameter, travelling over 19 km s^{-1} with respect to the Earth, exploded in the sky near the Russian town of Chelyabinsk in early 2013 [4]. The effects of the explosion (i.e. glass breaking, knocking people and things down, etc.) injured over 1,000 people and damaged over 3,000 buildings. The famous Tunguska event was most likely caused by a 60-m-diameter object exploding a few kilometers above the forest in the Siberian wilderness [5]. It is vital that we develop technologies and systems capable of mitigating these types of threats.

The profile of a space mission to deflect a potentially hazardous object depends on a number of factors such as warning time, object size, composition, and structure. For relatively short warning times, impulsive methods such as kinetic impact, e.g., NASA's upcoming Double Asteroid Redirection Test (DART) mission, or nuclear blast would be applicable, whereas if more warning time is given, slower methods such as gravity tractor or laser ablation could be used [6]. The slower methods allow for more precise orbit control, which could also open the door for resource exploitation. A recent comparative analysis studied several methods and analyzed their effectiveness at delivering asteroids between 20 and 150 m in diameter to the Earth-Moon system (EMS) [7]. It included ion beam push, tugboat, gravity tractor, laser ablation, and mass driver. Each method has its advantages and disadvantages, such as spacecraft mass, mission duration, and robustness. Using a laser to redirect an asteroid has three advantages: 1) it can be performed without landing, 2) it does not require extra fuel, and 3) it can be used on a variety of targets.

Several challenges arise when building a laser ablation asteroid redirection model. First, all astronomical bodies are rotating or tumbling. A simple fix to account for this was mentioned in [8] where a lateral velocity requires an increase in power density to maintain an appropriate heating time per unit volume. Second, laser beams have divergence, and are thus very sensitive to focal length. While some models, like that in [9], mention the effects of this sensitivity, most assume perfect spot control. Even if the spot is perfectly maintained, the issues surrounding beam divergence will re-emerge as the hole gets deeper. Third, unless the laser is operating in the femtosecond pulse range, thermal effects will cause a melt front to appear given enough time [10].

Over 80% of the known NEAs are S-type or C-type, composed of mostly silicates and carbonaceous materials, respectively [11]. It is suggested that olivine and pyroxene make up the bulk material in these asteroids, and were thus selected for study [12]. As water is one of the most speculative space resources, serpentine was chosen to be studied as well, as it is the most common hydrated mineral found in meteorites [13]. Laboratory experiments with laser ablation have been performed in the context of asteroid redirection. Some studied the effects of a continuous-wave, 90-W laser on an olivine sample in a vacuum chamber [14, 15]. Force measurements on pyroxene as well as high-fidelity asteroid simulant powders were also performed with a 33-W average power, picosecond pulsed laser [16]. The DE-STAR system has been developed over the past six years, and have studied the effects of a phased-array laser system on basalt [17].

The fundamentals of laser cutting and drilling were outlined in 1964, just four years

after the invention of the laser [18]. These processes have been drastically improved over the decades with the addition of assist gases and new laser sources. High-Speed Imaging (HSI) has also allowed researchers to observe the processes that occur during laser irradiation, e.g. melt pool behavior [19] and spatter dynamics [20] (when molten material is ejected from the melt pool), as well as the effects of processing gases [21]. It has recently been shown that, using a 300-W laser, minerals like olivine, pyroxene, and serpentine will liquefy and sputter a significant amount of material well before a steady-state vapour "engine" forms [22]. Some research suggests that an even more efficient mechanism of material removal is spallation, where solid pieces of material break off without melting [23]. The study showed that for sandstone and slate, the power density that caused spallation (just before melting) was the most energy efficient, which is a crucial factor when considering spacecraft mass and power requirements. Here we seek to answer questions like: Will olivine, pyroxene, and/or serpentine exhibit spallation behavior? What laser parameters (i.e. power and pulse width) will produce spallation? Is the energy efficiency comparable to previous work in [22] and [23]?

2. Methodology

First, two samples each of olivine, pyroxene, and serpentine were cut into roughly 1-cm thick pieces. The source rocks were the same as the pre-characterized samples used in [22]. One sample of each mineral was pre-analyzed with X-ray microtomography (XMT), the other samples were used more experimentally to find promising laser pulse parameters, which would then be used on the pre-analyzed samples. Each experiment, both on the testing and pre-characterized samples, was recorded with a setup consisting of a high-speed camera and an illumination laser. All of the samples were then analyzed with XMT to characterize the resulting cavities.

2.1. Sample Characterization

As the samples used in this experiment were cut from the same source as in previous research, we will assume that the mineralogical and spectroscopic properties are the same as found in [22]. In summary, the petrographic analysis revealed that the pyroxene and serpentine samples show more variation than the olivine sample, meaning they have larger regions of differing compositions and clear boundaries between the regions. It also revealed that the pyroxene and serpentine had more cracks and cleavages compared to olivine. The spectroscopic analysis revealed that, at the wavelength of the laser, our serpentine sample was the most reflective (28%), followed by pyroxene (22%) and olivine (19.5%). Images of the samples were taken after the experiments, and are shown in Fig. 1.
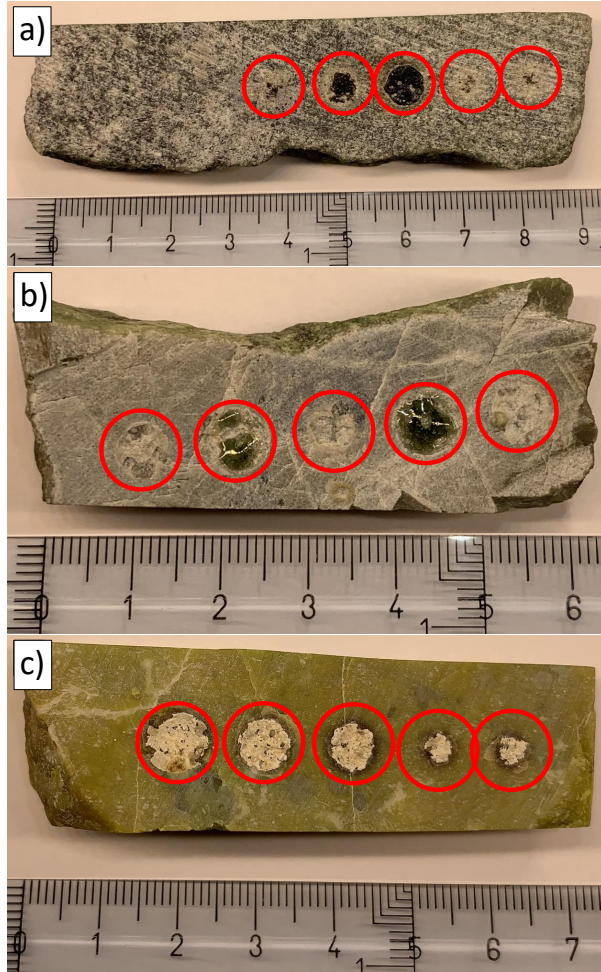
Figure 1: Images of the pre-characterized samples showing overall macroscopic characteristics; from top to bottom, they are: a) olivine, b) pyroxene, and c) serpentine. The red circles indicate the location of experiments. The units on the ruler are cm.

4

The density of olivine, pyroxene, and serpentine are 3.8 g cm^{-3}, 3.4 g cm^{-3}, and 2.6 g cm^{-3}, respectively [24].

2.2. Laser experiment and observation

The experiments were conducted with a YLR-15000-MM-WC Ytterbium fiber laser from IPG Photonics, with capabilities given in Table 1. The laser head (using mirror optics) was fixed to a crossbar and angled 15° from horizontal to prevent reflections from damaging the optics. Argon gas flowing at 20 L min^{-1} was used as a shielding gas. The target was placed on a one-dimensional platform in order to move the sample between experiments. The surfaces of the samples were placed beyond the focal plane, such that it created a 1-cm-diameter spot, allowing for power densities up to 13.7 kW cm^{-2}. The beam profile in focus was a top-hat shape, but out of focus it more resembled a Gaussian shape.

Table 1: Laser parameters.

Parameter	Value
Wavelength	1070 nm
Source power	< 15 000 W
Min. pulse length	1 ms
Core diameter	200 µm
Beam quality	10.5 mm mrad

The High-Speed Imaging (HSI) system used in these experiments was based on the setup in [19]. A high-speed camera (FASTCAM Mini UX100 type 800-M-16G) was operated at 12 500 fps at a resolution of 1024x400 to capture what physical processes occurred during laser irradiation. A 810 nm bandpass filter was used in conjunction with an illumination laser of the same wavelength (CaviLux CW) in order to filter out most of the processing light, thereby providing a clearer view of the experiment sites. The illumination laser was split into two optical heads (30 W each). The HSI camera used an exposure time of 62.5 µs per frame. An overview of the entire experiment setup is given in Fig. 2.

There were three independent variables in the experiments: laser power, pulse width, and pulse gap. We configured the laser control PC to produce the exact number of pulses required. The power varied from 1 500 W to 13 659 W, the pulse widths from 5 ms to 35 ms, and the pulse gaps from 1 to 100 ms; the exact values are given in Table 2. The maximum output power of the laser was limited due to damaged modules, so 13 659 W was the highest power setting possible.

Table 2: Parameter space used.

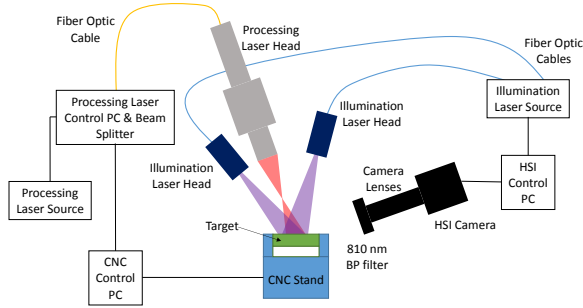| Parameter	Value
Power (kW)	$1.5, 3.0, 4.5, 5.0, 6.0$
	$6.5, 9.0, 11.7, 12.7, 13.7$
Pulse width (ms)	$5, 10, 20, 30, 35$
Pulse gap (ms)	$1, 5, 10, 20, 100$

Figure 2: Experiment setup.

The parameter selection began with the olivine test sample, as it had the most surface area to experiment on. The experiments began with the lowest power setting of 1.5 kW and a pulse width of 10 ms; the HSI footage was studied immediately after. Based on the results, the power was incrementally increased until melting just started to happen. This procedure was repeated for the other two test samples to find the power density that produced spallation before melting. Using these power densities, the pulse widths and powers were varied while maintaining the total pulse energy (e.g., halving the power required doubling the pulse length) to see if that had any effect on the results. Each sample had at least one experiment where a train of 5 pulses were sent in succession to see if more spallation would occur or if melting would dominate.

The pulse parameters were manually entered into the processing laser control PC. The CNC PC was used to toggle the shielding gas and processing laser via an ethernet connection. The recording on the HSI PC was manually activated after the CNC PC program was started. The HSI PC triggered the illumination laser and HSI camera to capture two seconds of footage. The resulting recording was analyzed, clipped, and saved to include only the part of the file where processing and cooling occurred. The manual capture method was successful in 33 out of 34 experiments.

2.3. X-ray microtomography

The XMT measurements were carried out with a GE phoenix nanotom s system. The generator settings were 100 kV and 150 µA and a 0.5 mm Cu filter was added to the beam. A total number of 1000 projections over 360 degree rotation with 3 x 500 ms exposure time were recorded to pre-characterize the samples, and 1200 projections with 1 x 500 ms exposure time were made on the post-processed samples. A voxel size of 33 µm or 40 µm was chosen for each scan. The 3D volume data was reconstructed from these data sets using datos|x reconstruction software version 2.4.0.1199 (GE phoenix).

3. Results

The results are split into two sections: the HSI observation of the processing, and the XMT measurements.

6

Olivine shows weak spallation at the powers used in the experiments. Initially, some small (micrometer-sized) pieces come off (up until 5.3 ms in Fig. 3), and soon the area at the center of the laser beam begins to melt and sputter (at 8.5 ms in Fig. 3). As the irradiation continues, the size of the melt pool increases, eventually matching the laser spot diameter of 1 cm. The size of the spatter also increases, some pieces over 1 mm in diameter. One unique feature of the olivine experiment was, what appear to be, hyperfast jets that lasted only one frame (5.3 ms in Fig. 3) before the melting began. These jets were roughly 1 mm in width, and visible 2-3 mm above the surface. Once the laser was shut off, a large, transluscent mass of bubbles formed over the irradiated area (up to 4 mm in height), possibly filled with gas from the olivine sample, and/or a combination of the shielding gas and atmosphere.
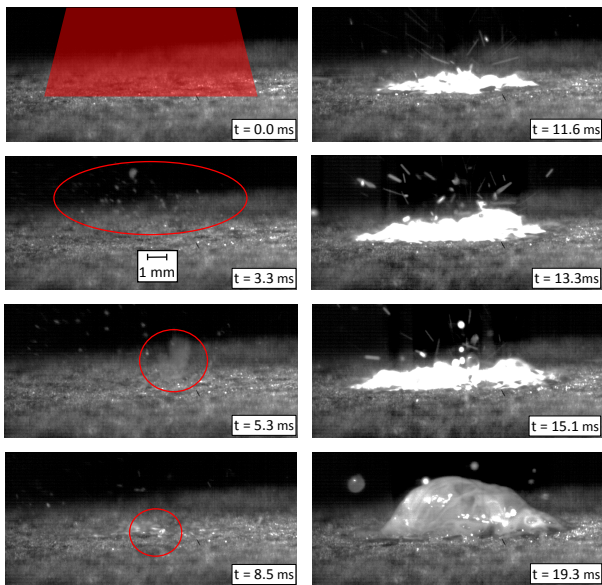

Figure 3: Frames from HSI of laser irradiation on olivine. The laser power was 5 kW and pulse length of 20 ms. Time flows from top to bottom, starting in the left column. The laser spot size is shown in the top left frame, spallation is seen at 3.3 ms, a hyperfast jet at 5.3 ms, and the sputtering processes begins at 8.5 ms. The bottom right frame shows the melt pool cooling as the laser is shut off.

Pyroxene, the next mineral to be tested, behaved notably different compared to olivine. The initial moments of the laser irradiation caused the pyroxene to become lighter (from 0.0 to 2.0 ms in Fig. 4). The discoloration continued until spallation began. The pieces ranged in size from less than 1 μm to 4–5 mm. Throughout the experiment,

areas of the pyroxene under irradiation would become lighter and then spallate. As the total energy of the experiment began to increase (i.e., more pulses were used) the pyroxene began to melt, and exhibited spattering behavior similar to that of olivine (Fig. 5). Of the five experiments, the ones with one pulse were dominated by spallation; clips from the HSI of these experiments can be seen in Supplementary Videos 1 (LINK) (Hole 1 in Table. 3), 2 (LINK) (Hole 3 in Table. 3) and 3 (LINK) (Hole 5 in Table. 3).
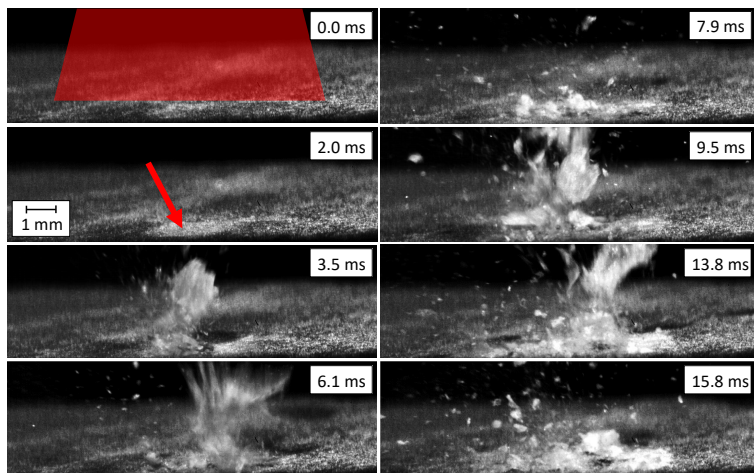

Figure 4: Frames from HSI of laser irradiation on pyroxene. The laser power was 3 kW and pulse length was 20 ms. Arrow in the 2.0 ms frame highlights the discoloration prior to spallation.
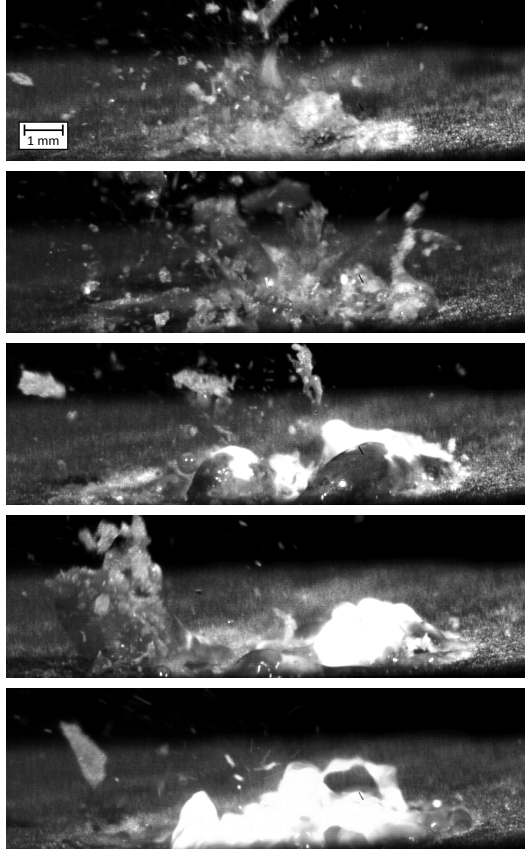
Figure 5: Frames from HSI of laser irradiation on pyroxene. Each frame is taken from the middle of each pulse in a 5-pulse experiment. The laser power was 3 kW, pulse width was 20 ms, and the pulse gaps were 100 ms.

Serpentine behaved similar to pyroxene, though it required significantly more energy to begin the process. The laser had to be turned up to the maximum power and use longer pulse lengths than those used for both olivine and pyroxene. The processing began similar to that of pyroxene, except the material darkened instead of lightened (Fig. 6). The area under the center of the laser beam began to melt and sputter sub-μm pieces until several large (1–2 mm), flat chunks came off. After the initial spallation,

the sputtering of sub-µm pieces continued and grew. As time progressed, a combination of molten and solid chunks ranging from sub-µm to 2 mm continued to break off (up to 6.6 ms in Fig. 7). A relatively large piece (4–5 mm in width) can be seen breaking off behind the spatter at 8.5 ms. As the processing area began to match the laser spot diameter (∼1 cm), the processing was dominated by what looked to be a more molten-sputtering scenario, though some spallation of millimeter-sized pieces still occurred. The melt pool behaved differently than for olivine and pyroxene. There was no one large pool that chaotically threw off material, rather a more steady stream of molten material being cast off as small pieces directly from the surface (from 8.5 to 19.5 ms in Fig. 7). A clip of the HSI where both spallation and spattering is present is given in Supplementary Video 4 (LINK) (Hole 1 in Table. 3).
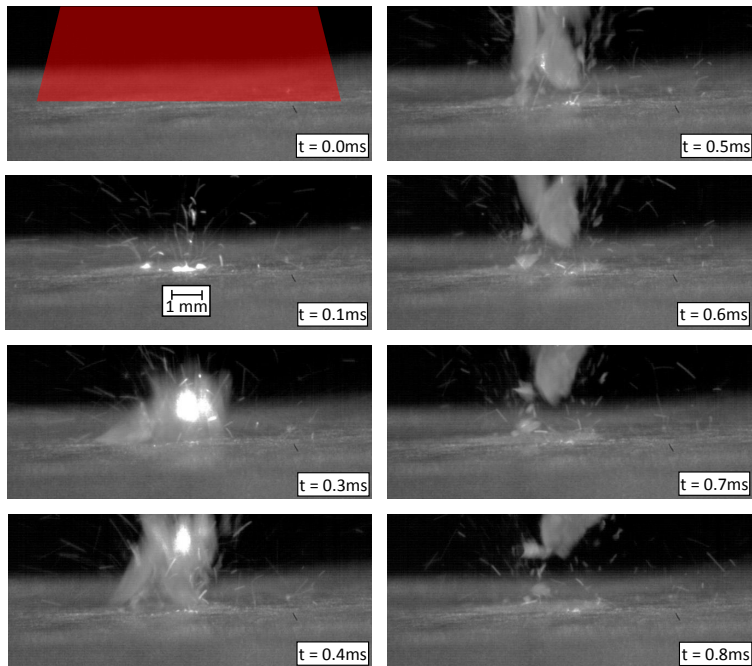

Figure 6: Frames from HSI of laser irradiation on serpentine. The power is 12.4 kW and pulse length is 20 ms. This figure captures a spallation event within the first millisecond of exposure.
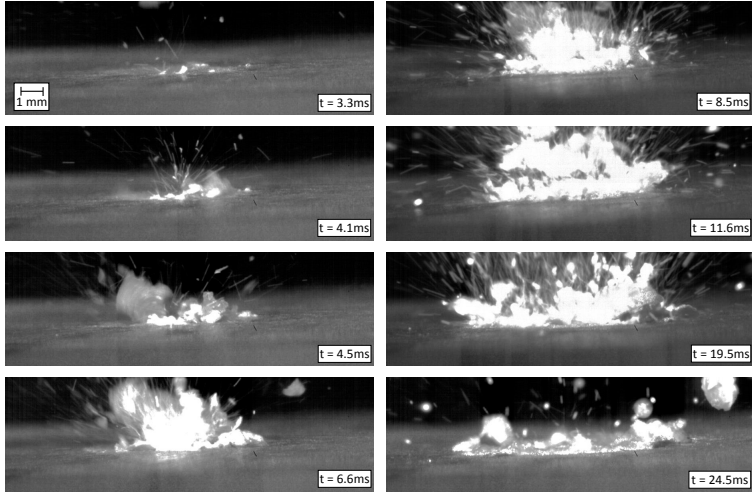
Figure 7: Frames from HSI of laser irradiation on serpentine. The power is 12.4 kW and the pulse length is 20 ms. This figure shows the spallation and sputtering of the entire pulse, including some after-effects seen at 24.5 ms. Note this is footage from the same experiment as Fig. 6.

3.2. X-ray microtomography analysis

As the holes were shallow and material began to extrude above the hole edges, calculating the volume was a challenge. Unfortunately, accurate values of volume removed could only be extracted from the pre-characterized samples. The 3D volume data was analysed using the free software Fiji (ImageJ) [25, 26] by first manually choosing a small region of interest (ROI) around each hole (see Fig. 8. First the pre-image and post-image were resampled to the same voxel size (33 μm or 40 μm) if necessary. Then the 3D images were aligned using Fijiyama plugin (version 2020-09-02) [27]. The gray scale of the pre-image was normalized so that its mean and standard deviation matched those of the post-image. Then for each ROI to be analyzed the aligned pre- and post-images were subtracted from each other to create a difference image. Prior to subtraction, the pre-images were displaced with sub-pixel accuracy along the sample surface normal to make the subtraction as accurate as possible. The best displacement was chosen such that the standard deviation of the difference image would be minimized at the surface location at the edges of the ROI (away from the hole). A threshold value was then chosen as $T = (v_{rock} - v_{air})/3$, where v_{rock} and v_{air} are the gray levels of rock material and air in the pre-image. The difference image was then segmented to into two parts: first, the hole (values below $-T$), and second, material that had re-solidified on top of the surface (values above $+T$). An outlier removal with radius of 2 pixels was run on the individual slices of the segmented data, and further a volume opening with the minimum voxel count of 100 was applied to the 3D segmented data. The volumes of the segmented com-

11

ponents were directly calculated from the data. The errors for the volume calculations were estimated as the standard deviation of the volumes when the subtraction was done with different displacements of the pre-images along the sample surface normal (range ±1 pixel).
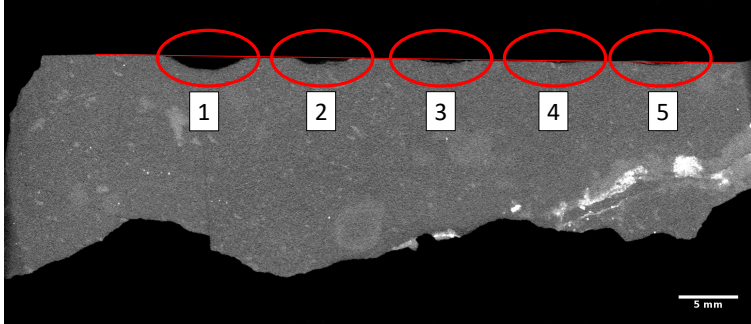

Figure 8: A cross-section image from the XMT scan of the serpentine sample post-processing. The surface is designated with a thin line, and the five experiments are circled.

A summary of the volume of material removed for each experiment is given with its measurement standard deviation in Table 3. The measured volume removed is given with a standard deviation, which was calculated by varying the surface plane height. The total energy is found by multiplying the pulse power (from the laser) by the absorptivity of the material at the laser's wavelength determined in [22]. Volume efficiency is found by dividing the volume removed by teh total energy (with unit conversion). Mass rate represents the volume removal rate, and it was calculated by dividing the volume removed by the length of the pulses and multiplying by the material density. The ranges accompanying the volume efficiency and mass rate are based on the standard deviation of the volume removed.

4. Discussion

The spot size of the laser beam was sufficiently large as to average out any microstructural differences, which led to a large variation in the results reported in [22]. The images of the holes (Fig. 1) show a consistent color among the olivine and pyroxene, though there seems to be a difference between the test and control samples of serpentine. The test sample shows the darkening feature of the initial exposure to laser irradiation, as the power levels were too low to initiate melting or spallation. The control sample has a consistently white color in all the samples, with perhaps a darkened ring on the right two sites. These rings are due to the shape of the laser profile being Gaussian (i.e. high power in the center, reducing radially.)

Due to the fact the target was placed beyond the focal point of the laser, the laser power intensity grew the further above the surface the pieces travelled, thus solid material moving upwards would show signs of melting.

Table 3: Volume removed as found by XMT analysis. Also shown are the calculated volume removal efficiencies and mass removal rate.

	Hole Nr.	Volume Removed (mm^3)	Power (W)	Pulse Length (ms)	Pulses	Total Energy (J)	Volume Efficiency ($mm^3 \cdot kJ^{-1}$)	Mass Rate ($g \cdot s^{-1}$)
Olivine	1	0.004 ± 0.007	3,000	10	1	24.2	0.2 ± 0.3	0.002 ± 0.003
	2	0.014 ± 0.009	1,500	20	1	24.2	0.6 ± 0.4	0.003 ± 0.002
	3	1.783 ± 1.003	3,000	10	5	120.8	14.8 ± 8.3	0.136 ± 0.076
	4	0.076 ± 0.050	5,000	10	1	40.3	1.9 ± 1.2	0.029 ± 0.019
	5	0.286 ± 0.442	3,000	20	1	48.3	5.9 ± 9.2	0.054 ± 0.084
Pyroxene	1	2.964 ± 1.092	6,000	10	1	46.8	63.3 ± 23.3	1.008 ± 0.415
	2	5.503 ± 0.604	6,000	10	5	234.0	23.5 ± 2.6	0.374 ± 0.046
	3	1.908 ± 0.579	3,000	20	1	46.8	40.8 ± 12.4	0.324 ± 0.110
	4	7.788 ± 0.888	3,000	20	5	234.0	33.3 ± 3.8	0.265 ± 0.034
	5	2.468 ± 0.819	1,500	35	1	41.0	60.3 ± 20.0	0.240 ± 0.089
Serpentine	1	18.845 ± 1.012	13,659	30	1	295.0	63.9 ± 3.4	1.602 ± 0.128
	2	4.926 ± 0.538	13,659	20	1	196.7	25.0 ± 2.7	0.628 ± 0.102
	3	2.031 ± 0.459	13,659	10	2	196.7	10.3 ± 2.3	0.259 ± 0.087
	4	0.254 ± 0.132	13,166	10	2	189.6	1.3 ± 0.7	0.032 ± 0.025
	5	0.870 ± 0.237	6,820	20	2	196.4	4.4 ± 1.2	0.055 ± 0.023

The spallation seen in the olivine experiments was possibly not even due to the olivine mineral, rather local concentration of other minerals like pyroxene, that do easily spallate. This can be seen in the two right-most circles in Fig. 1, as well as on the test pieces; the laser would "remove" the darker spots, leaving a lighter circle. Pyroxene was also the only material of the three tested that did not completely melt. If material can be removed without melting, the freshly-exposed and un-altered material can be compared to that on the original surface, to study the effects of space weathering.

The presence of processed material poses a challenge to the spacecraft environment. Even the earliest mention of ablation-related deflection mention that the re-deposition of gas on the solar concentrator would limit the mission to 10–30 minutes [28]. For laser systems, the gas would coat the solar panels and focusing optics, making them less efficient or breaking them completely. If the processed material is instead broken into macroscopic pieces, it changes the resulting environment around the spacecraft. Although there may still be some gas, most of the material will be relatively slow-moving particles, and thus will not accumulate on vital components.

When looking at the streaks produced by spatter in Figs. 3 and 7, we can estimate the velocity of the fastest moving particles. The streaks are roughly 1 mm long, which, divided by the camera exposure time of 62.5 µs, gives us a velocity of 16 m s^{-1}. The larger chunks move more slowly, roughly 8 m s^{-1}, which is still faster than the escape velocity of an 11.5-km-diameter spherical asteroid (assuming a density of 3 g cm^{-3}). It must be noted that these values are derived from one 2-D view, and the velocities can vary depending on their movement towards or away from the camera. The velocity derived from the streak can also vary depending on the size of the particle, though these ranges are not expected to exceed one order of magnitude.

Due to the small size of the sample pieces, they tended to heat up after some of the longer or higher-powered experiments. This could be due to low thermal conductivity compared to, say, metals. It may be beneficial to perform laser processing on the night side of an asteroid, as re-radiation of heat from the laser is more efficient.

The majority of holes (12 out of 15) had some material pushed up around the edges, or re-solidified on the surface. Only three pyroxene holes had no measurable material above the surface. The material that formed the edges is subtracted from our estimate for the volume removed to provide a more accurate estimate of the total volume that escaped the sample. The correction does not affect the results for pyroxene or serpentine much, but it does have a strong effect on experiments with olivine, because the estimate for the volume removed would otherwise often be negative. In such cases we assume that the laser irradiation sublimated or vaporized some material which became trapped in the melt pool, and reported that the experiment did not remove any material.

The highest volume processing efficiencies previously found in [22] were 25.2, 36.7, and 23.2 mm^3 kJ^{-1} for olivine, pyroxene, and serpentine, respectively, at power densities up to 900 kW cm^{-2}. The highest values found in this work were 14.8, 63.3, and 63.9 mm^3 kJ^{-1} for olivine, pyroxene, and serpentine, respectively at power densities as low as 1.4 kW cm^{-2}. For reference, the volume removal efficiencies estimated in [14] were around 1 mm^3 kJ^{-1}, and the values found in [23] were over 1,968 mm^3 kJ^{-1}. Both cases operated in the same power density region as the experiments in this paper (between 784 and 13659 W/cm2). In the first case, the experiment (on an olivine sample) was allowed to run for 10 minutes, with the explicit purpose of entering a solid-state vapour mode, which would explain the low processing efficiency. The second case was very efficient, as the targets were sandstone and shale, very brittle rocks, which spallate relatively easily; for instance, sandstone contains mostly the mineral quartz.

The HSI footage of the olivine experiments showed that besides a few microscopic flakes, the material did not spallate at any of the tested laser parameters. The material removal process was dominated by molten-sputtering. For pyroxene, the three single-pulse cases were clearly dominated by spallation. The five-pulse cases began with spallation, but quickly became dominated by sputtering after the first pulse. It is difficult to state clearly which process dominates for serpentine, as our only tool of analysis is the HSI. There are clearly large pieces that remain solid throughout their removal, especially in the first few milliseconds, but bright spatter eventually fills the field of view. Experiment #1 for serpentine has a volume removal efficiency over twice that of sputtering-driven experiments in [22], so we suggest that for that experiment, spallation was the driving process.

The highest mass removal rate found in [22] was 0.041 g s^{-1}, and the highest found in this current work was 1.602 g s^{-1}, an increase of over one and a half orders of magnitude. For reference, the estimated mass removal rate in [17] was roughly 0.016 g s^{-1}, and in [14] was roughly (0.0001 g s^{-1}). This again, has important implications for asteroid redirection. In order to maintain a gas plume, control of both the spot location and the focal plane would require extremely precise GNC equipment, perhaps two systems (one for the laser and one for the spacecraft) [2]. Our research suggests that, due to the time scale difference between spallation/spattering and ablation, these requirements can be relaxed, and the laser spot instead *should* be allowed to wander within limits, spallating and spattering new material, as opposed to creating a vapour jet.

The reported mass rate represents the material removal rate, which can not be directly

14

equated with momentum exchange, which, in turn, is relevant when considering asteroid redirection. A second path of research would need to be opened to analyze the net "thrust" generated by spallation and spatter, in addition to the thermodynamic model. A challenge there lies in the fact that we do not know the exact density of the molten material coming off of the sample, and how it changes as it cools, possibly trapping gas within it. The spallation and spatter seem to extend a full 180 degrees (also reported in [14]).

The processing performance degrades for pyroxene and serpentine when using multiple pulses. The performance degradation could be due to the material cooling back down, and the beginning segments of future pulses simply re-heat the material instead of processing it. In olivine, the multiple-pulse case was instead the most energy efficient, which could be due to the fact that it had sufficient energy to put it into the molten-spattering mode, which gives values closer to those found in previous work [22].

Serpentine contains hydroxyl (OH) groups that are located between layers of SiO_4 tetrahedra and AlO_6 octahedra. The relatively high pulse energies required to process the material could be due to the OH absorbing and dissipating energy from the hole area. Both the serpentine and pyroxene samples had characteristic cleavages, which could explain why they spallate better than olivine.

In pyroxene, two experiments can be compared: case 1 and 3, where the energies are the same, but the pulse parameters differ slightly. It appears the shorter, more powerful pulse processes the material more efficiently. On the other hand, case 5 suggests that a long, low-power pulse processes material nearly as effectively as case 1. It is possible that all three cases process material equally efficiently, as the error bars do overlap.

Building a thermodynamic model that includes spallation, spattering, and ablation will prove to be challenging. Existing laser ablation models (such as the one in [15]) include factors like specific heat, phase change enthalpies, and radiative and conductive losses. Spallation/spattering is noted, but not included in the model. One would have to determine what percentages of the total material removed is due to each process (spallation/spattering/ablation). This also does not include the energy absorbed by hydroxyl and water in hydrated minerals; a real asteroid may not consist of pure minerals, but a heterogeneous mix of minerals, metals, and volatiles.

5. Conclusions

The research presented above sought to answer the following questions: do olivine, pyroxene, and serpentine exhibit spallation behavior? If so, what power densities and pulse parameters seem to produce the most energy efficient spallation behavior? How does laser-induced spallation perform relative to laser-induced spattering or ablation? After carrying out the experiments, observing them with HSI, and measuring the hole sizes with XMT, a number of conclusions can be drawn:

1. The HSI revealed that olivine does not tend to spallate at power densities between 1.5 and 13.7 kW cm^{-2}, whereas pyroxene and serpentine will do so. It is important to have a good estimate of the surface composition of an asteroid before considering using laser-induced spallation for redirection.

2. The XMT analysis showed that processing pyroxene and serpentine at power densities between 1.5 and 13.7 kW cm^{-2} yielded volume-removal efficiencies of over

$60 \text{ mm}^3 \cdot \text{kJ}^{-1}$. This is two- to three-times more energy efficient than laser-induced spattering, and over 40 times more energy efficient than laser ablation.

3. A new laser-based asteroid redirection/detumbling model should be developed to include spallation and spattering in addition to ablation. The new energy efficiency may allow for a smaller/lighter laser, fewer solar panels, and leaner GNC system requirements.

Acknowledgements

References

[1] C. R. Phipps and M. M. Michaelis, "NEO-LISP: Deflecting near-Earth objects using high average power, repetitively pulsed lasers." Presented at the ECLIM 23: Laser Interaction With Matter, Jan. 1994.

[2] M. Vetrisano, C. Colombo, and M. Vasile, "Asteroid rotation and orbit control via laser ablation," *Advances in Space Research*, vol. 57, no. 8, pp. 1762–1782, 2016. Advances in Asteroid and Space Debris Science and Technology - Part 2.

[3] P. Schulte, L. Alegret, I. Arenillas, J. A. Arz, P. J. Barton, P. R. Bown, T. J. Bralower, G. L. Christeson, P. Claeys, C. S. Cockell, G. S. Collins, A. Deutsch, T. J. Goldin, K. Goto, J. M. Grajales-Nishimura, R. A. F. Grieve, S. P. S. Gulick, K. R. Johnson, W. Kiessling, C. Koeberl, D. A. Kring, K. G. MacLeod, T. Matsui, J. Melosh, A. Montanari, J. V. Morgan, C. R. Neal, D. J. Nichols, R. D. Norris, E. Pierazzo, G. Ravizza, M. Rebolledo-Vieyra, W. U. Reimold, E. Robin, T. Salge, R. P. Speijer, A. R. Sweet, J. Urrutia-Fucugauchi, V. Vajda, M. T. Whalen, and P. S. Willumsen, "The Chicxulub Asteroid Impact and Mass Extinction at the Cretaceous-Paleogene Boundary," *Science*, vol. 327, p. 1214, Mar. 2010.

[4] O. P. Popova, P. Jenniskens, V. Emel'yanenko, A. Kartashova, E. Biryukov, S. Khaibrakhmanov, V. Shuvalov, Y. Rybnov, A. Dudorov, V. I. Grokhovsky, D. D. Badyukov, Q.-Z. Yin, P. S. Gural, J. Albers, M. Granvik, L. G. Evers, J. Kuiper, V. Kharlamov, A. Solovyov, Y. S. Rusakov, S. Korotkiy, I. Serdyuk, A. V. Korochantsev, M. Y. Larionov, D. Glazachev, A. E. Mayer, G. Gisler, S. V. Gladkovsky, J. Wimpenny, M. E. Sanborn, A. Yamakawa, K. L. Verosub, D. J. Rowland, S. Roeske, N. W. Botto, J. M. Friedrich, M. E. Zolensky, L. Le, D. Ross, K. Ziegler, T. Nakamura, I. Ahn, J. I. Lee, Q. Zhou, X.-H. Li, Q.-L. Li, Y. Liu, G.-Q. Tang, T. Hiroi, D. Sears, I. A. Weinstein, A. S. Vokhmintsev, A. V. Ishchenko, P. Schmitt-Kopplin, N. Hertkorn, K. Nagao, M. K. Haba, M. Komatsu, and T. Mikouchi, "Chelyabinsk airburst, damage assessment, meteorite recovery, and characterization," *Science*, vol. 342, no. 6162, pp. 1069–1073, 2013.

[5] C. F. Chyba, P. J. Thomas, and K. J. Zahnle, "The 1908 Tunguska explosion: atmospheric disruption of a stony asteroid," *Nature*, vol. 361, pp. 40–44, Jan. 1993.

[6] C. Gritzner, K. Dürfeld, J. Kasper, and S. Fasoulas, "The asteroid and comet impact hazard: risk assessment and mitigation options," *Naturwissenschaften*, vol. 93, pp. 361–373, Aug. 2006.

[7] M. C. Bazzocchi and M. R. Emami, "Comparative analysis of redirection methods for asteroid resource exploitation," *Acta Astronautica*, vol. 120, pp. 1 – 19, 2016.

[8] N. Thiry and M. Vasile, "Theoretical peak performance and optical constraints for the deflection of an s-type asteroid with a continuous wave laser," *Advances in Space Research*, vol. 59, no. 5, pp. 1353–1367, 2017.

[9] R. Kahle, E. Kührt, G. Hahn, and J. Knollenberg, "Physical limits of solar collectors in deflecting earth-threatening asteroids," *Aerospace Science and Technology*, vol. 10, no. 3, pp. 256 – 263, 2006.

[10] M. Sabsabi, "Chapter 7 - femtosecond libs," in *Laser-Induced Breakdown Spectroscopy* (J. P. SINGH and S. N. THAKUR, eds.), pp. 151 – 171, Amsterdam: Elsevier, 2007.

[11] R. P. Binzel, F. E. DeMeo, E. V. Turtelboom, S. J. Bus, A. Tokunaga, T. H. Burbine, C. Lantz, D. Polishook, B. Carry, A. Morbidelli, M. Birlan, P. Vernazza, B. J. Burt, N. Moskovitz, S. M. Slivan, C. A. Thomas, A. S. Rivkin, M. D. Hicks, T. Dunn, V. Reddy, J. A. Sanchez, M. Granvik,

and T. Kohout, "Compositional distributions and evolutionary processes for the near-Earth object population: Results from the MIT-Hawaii Near-Earth Object Spectroscopic Survey (MITHNEOS)," *Icarus*, vol. 324, pp. 41–76, May 2019.

[12] V. Reddy, T. L. Dunn, C. A. Thomas, N. A. Moskovitz, and T. H. Burbine, "Mineralogy and Surface Composition of Asteroids," in *Asteroids IV* (P. Michel, F. E. DeMeo, and W. F. Bottke, eds.), pp. 43–63, 2015.

[13] A. E. Rubin, "Mineralogy of meteorite groups," *Meteoritics and Planetary Science*, vol. 32, pp. 231–247, Mar. 1997.

[14] A. Gibbings, M. Vasile, I. Watson, J.-M. Hopkins, and D. Burns, "Experimental analysis of laser ablated plumes for asteroid deflection and exploitation," *Acta Astronautica*, vol. 90, no. 1, pp. 85–97, 2013. NEO Planetary Defense: From Threat to Action - Selected Papers from the 2011 IAA Planetary Defense Conference.

[15] M. Vasile, A. Gibbings, I. Watson, and J.-M. Hopkins, "Improved laser ablation model for asteroid deflection," *Acta Astronautica*, vol. 103, pp. 382–394, 2014.

[16] J. Sloane, *Laser ablation Propulsion of Asteroids with a Sub-nanosecond Pulsed Laser*. PhD thesis, University of Maryland, College Park, Jan. 2019.

[17] P. Lubin, G. B. Hughes, J. J. Bible, J. Bublitz, J. Arriola, C. Motta, J. Suen, I. Johansson, J. Riley, N. Sarvian, D. Clayton-Warwick, J. Wu, A. Milich, M. Oleson, M. Pryor, P. Krogen, M. Kangas, and H. O'Neill, "Toward directed energy planetary defense," *Optical Engineering*, vol. 53, no. 2, pp. 1 – 19, 2014.

[18] C. M. Adams and G. A. Hardway, "Fundamentals of laser beam machining and drilling," *IEEE Transactions on Industry and General Applications*, vol. IGA-1, no. 2, pp. 90–96, 1965.

[19] J. Pocorni, J. Powell, J. Frostevarg, and A. F. H. Kaplan, "Investigation of the piercing process in laser cutting of stainless steel," *Journal of Laser Applications*, vol. 29, pp. 022201–1–022201–8, May 2017.

[20] D. K. Y. Low, L. Li, and P. J. Byrd, "The effects of process parameters on spatter deposition in laser percussion drilling," *Optics & Laser Technology*, vol. 32, pp. 347–354, July 2000.

[21] M. Schneider, L. Berthe, R. Fabbro, M. Muller, and M. Nivard, "Gas investigation for laser drilling," *Journal of Laser Applications*, vol. 19, pp. 165–169, Aug. 2007.

[22] N. Anthony, J. Frostevarg, H. Suhonen, C. Wanhainen, A. Penttilä, and M. Granvik, "Laser processing of minerals common on asteroids," *Optics & Laser Technology*, p. 106724, 2020.

[23] Z. Xu, C. B. Reed, G. Konercki, R. A. Parker, B. C. Gahan, S. Batarseh, R. M. Graves, H. Figueroa, and N. Skinner, "Specific energy for pulsed laser rock drilling," *Journal of Laser Applications*, vol. 15, no. 1, pp. 25–30, 2003.

[24] F. Deer, W. A., R. A. Howie, and J. Zussman, *An Introduction to the Rock-Forming Minerals*. Mineralogical Society of Great Britain and Ireland, 01 2013.

[25] C. T. Rueden, J. Schindelin, M. C. Hiner, B. E. DeZonia, A. E. Walter, and et al., "ImageJ2: ImageJ for the next generation of scientific image data," *BMC Bioinformatics*, vol. 18, p. 529, 2017.

[26] J. Schindelin, I. Arganda-Carreras, E. Frise, V. Kaynig, M. Longair, T. Pietzsch, S. Preibisch, C. Rueden, S. Saalfeld, B. Schmid, J.-Y. Tinevez, D. J. White, V. Hartenstein, K. Eliceiri, P. Tomancak, and A. Cardona, "Fiji: an open-source platform for biological-image analysis," *Nature Methods*, vol. 9, no. 7, pp. 676–682, 2012.

[27] R. Fernandez and C. Moisy, "Fijiyama: a registration tool for 3D multimodal time-lapse imaging," *Bioinformatics*, 09 2020. btaa846.

[28] H. J. Melosh, "Solar asteroid diversion," *Nature*, vol. 366, pp. 21–22, Nov. 1993.

17

Laboratory experiments with a laser-based attachment mechanism for spacecraft at small bodies

Authors:
Niklas Anthony, Jan Frostevarg, Heikki Suhonen, Mikael Granvik

Laboratory experiments with a laser-based attachment mechanism for spacecraft at small bodies

Niklas Anthony[a,1], Jan Frostevarg[b], Heikki Suhonen[c], Mikael Granvik[a,c]

[a]*Asteroid Engineering Lab, Onboard Space Systems, Luleå University of Technology, Box 848, 98128 Kiruna, Sweden*
[b]*Department of Engineering Sciences and Mathematics, Luleå University of Technology, E-Huset, 97754 Luleå, Sweden*
[c]*Department of Physics, P.O. Box 64, 00014 University of Helsinki, Finland*

Abstract

We present the results of two sets of experiments that investigate laser-based metal-to-rock attachment techniques. Asteroids and comets have low surface gravity which pose a challenge to landers with moving parts. Such parts can generate torques and forces which may tip the lander over or launch it into deep space. Thus, if a lander on a small body is to have moving parts, the spacecraft must be equipped with an anchoring mechanism. To this end, we sought to use a laser to melt and bind a piece of metal mimicking a part of a spacecraft to a rock mimicking the surface of a typical asteroid. In the first set of experiments, extra material was not fed in during the processing. The second set were performed using a standard wire feeder used in laser welding, which added metal to the experiment during processing. During the first experiments, we discovered that a traditional weld, where two melt pools mix and solidify to form a strong bond, was not possible—the melt pools would not mix, and when they did, the resulting weld was extremely brittle. The second set of experiments resulted in a physico-mechanical bond, where a hole was drilled with a laser, and a wire was melted and fed into the hole. These latter experiments were successful in forming bonds as strong as 115 N. Such an attachment mechanism can also be used to maneuver small boulders on asteroid surfaces, to redirect small, monolithic asteroids, or in space-debris removal.

Keywords: Spacecraft Anchoring, Laser Drilling, High-Speed Imaging, X-ray Micro-Tomography, Asteroid Mining

1. Introduction

Landing (and staying anchored) on a small body such as an asteroid or comet is a challenge due to the micro-gravity environment. The surface gravity of a 1-km-diameter asteroid (assuming a spherical shape and uniform density of $3000 \, \text{kg}/\text{m}^3$) is 0.004% of Earth's gravity. The corresponding escape velocity is only $65 \, \text{cm}/\text{s}$, meaning if a spacecraft is launched or bounces off the surface at a higher speed, it will leave the gravity well of the asteroid entirely, and drift off into deep space. The 100-kg Philae lander, part of ESA's Rosetta mission, sought to tackle this challenge with a diverse suite of landing equipment: harpoons, thrusters, and screws. The thruster and harpoon

failed to fire and the screws proved insufficient to hold the spacecraft down on their own, leading to a multiple-contact landing [1]. JAXA's Hayabusa2 mission had an alternative approach: three landers (1–10 kg in mass) were deployed from the main spacecraft, which had no landing gear at all, and were, instead, *designed* to bounce along the surface of asteroid (162173) Ryugu and these proved successful [2]. A summary of other anchoring techniques currently existing or in development is given in Zacny et al. 2013 [3].

We seek to understand the applicability of attaching metallic objects to natural materials using a laser. A potential scenario would play out as follows: a spacecraft approaches and hovers above the surface of an asteroid, lowers an anchoring unit that delivers a laser (via fiber-optic cable) and a wire feeder down to the surface, and welds the wire to a rock with the laser. The spacecraft can then be winched down with the same mechanism that lowered the anchoring unit. If the wire unintentionally breaks, more can be fed to the surface and reattached. The wire can also be intentionally cut with the laser to allow the spacecraft to move to a new location. This anchoring technique could also be used to redirect small asteroids or even space debris: rather than using the anchored wire as a winch point, the spacecraft can instead use its thrusters to pull on the object remotely (either for detumbling or for redirection). It can also be used for picking up monolithic rocks or boulders from the surface of an asteroid. This technique also has applications in space debris mitigation and removal.

Laser welding of two different materials is not a straightforward process. The differences in thermal, chemical, and physical properties lead to problems in controlling the quality of the weld joint. A review of the methods for and challenges in welding aluminum and steel are described by Wang et al. 2016 [4]. Aluminum has a melting temperature between 800 K and 1000 K, where steel's is between 1600 K and 1700 K. Under the same laser irradiation, the aluminum will melt well before the steel, creating a lop-sided melt pool, which could be a source of pores and fractures. The melting point of olivine (one of the most abundant minerals thought to exist on asteroids) is between 1700 K and 2400 K, so attempting to join aluminum or steel to olivine will be a challenge. High-speed imaging (HSI) of laser processing of olivine shows a considerable amount of vapor bubbles during and after irradiation, and microscope images confirm that the re-solidified material has visible pores [5]. Other natural materials like pyroxene and serpentine (two other minerals common on asteroids) show similar behavior, and the re-solidified material is glassy.

2. Methodology

This research spans two sets of experiments, the first set did not achieve the intended outcome, but did provide critical information in forming the second set.

The first experiment was developed under the assumption that a piece of wire or landing leg was resting on the surface of the asteroid, and the laser would sweep across it to anchor it down. To simulate this, a one-dimensional moving platform (CNC machine) was used to move the sample and the metal in tandem, keeping the processing laser and observation setup stationary. These experiments will be referred to in this paper as the moving-platform experiments (MPEs).

The second set of experiments were performed with the constraint that anchoring would occur at a single point, and wire would be fed into the spot by a dedicated feeder system. These experiments will be referred to as feeding experiments (FEs).

2.1. Methodology for moving-platform experiments

The first set of experiments were conducted with a YLS-5000 Ytterbium fiber laser from IPG Photonics, with the characteristics given in Table 1. The laser head was mounted 10° from vertical to prevent reflected processing light and ablated material from damaging the optics. Argon was pumped at $25 \, l/\min$ to prevent oxidation of the metal and mineral. The minimum spot size allowed for a maximum power density of $637 \, \mathrm{kW/cm^2}$. For an experiment, the mineral (olivine) was clamped into a vice, and a metallic (312 R stainless steel) wire or plate was laid on the surface, taped on each end.

Table 1: Laser parameters.

Parameter	Value
Wavelength	$1070 \, \mathrm{nm}$
Source power	$< 5000 \, \mathrm{W}$
Spot width	$1 \, \mathrm{mm}$
Beam quality	$8 \, \mathrm{mm\,mrad}$
Focal length	$250 \, \mathrm{mm}$

The HSI system used in this experiment is based on the one used by [6]. A high-speed camera (FASTCAM Mini UX100 type 800-M-16G) was configured to run at 10000 frames per second (fps), with a $10 \, \mu s$ shutter speed. A narrow-pass filter allowing only $810 \, \mathrm{nm}$ light through was placed in front of the lens of the camera and used in conjunction with an illumination laser of the same wavelength (CaviLux HF). This approach provided a clear view of the processing, which was captured at an angle roughly 25°above horizontal. An overview of the entire experiment setup is given in Fig. 1.
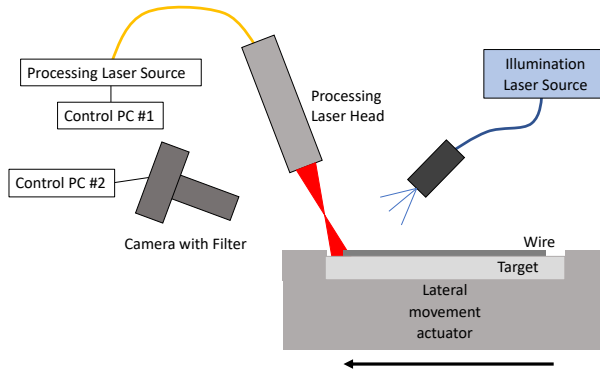

Figure 1: Experiment setup. Not to scale.

The processing laser parameters were set using the software provided by IPG Photonics and the illumination laser was manually turned on and off as needed. The HSI laptop, running Photron FASTCAM Viewer software, was manually activated to acquire

a 1.8-s video. A CNC script was configured to turn on the shielding gas and air crossjet (to protect the optics), activate the processing laser, move the sample, deactivate the laser, and then deactivate the gasses.

For a majority of the experiments, the laser power was ramped between two power levels along a fixed track length (between 3 cm and 5 cm), to see which power setting would produce the best weld seam. The laser on-time was calculated by dividing the length of a track by the movement rate of the sample (1 m/ min).

2.2. Methodology for feeding experiments

The second set of experiments were performed with a YLR-15000-MM-WC Ytterbium fiber laser from IPG Photonics, with the characteristics given in Table 2. The HSI setup was configured to be the same as the first set of experiments, but the settings were different: 4000, frame size 1280×1024, $10\,\mu s$ shutter time, total duration of 2.2 s. For longer experiments, the frame size was reduced to 1280×720 to increase the total duration of the exposure to 3.1 s. The observation angle was increased to roughly 45°from horizontal.

Table 2: Laser parameters.

Parameter	Value
Wavelength	1070 nm
Source power	< 15 000 W
Spot width	$600\,\mu m$
Beam quality	10.5 mm mrad
Focal length	250 mm

The laser head was mounted to a robotic arm at an angle 10° from vertical, again to prevent reflected processing light from damaging the optics. The spot size was set to $600\,\mu m$, allowing for power densities between up to $1760\,kW/\,cm^2$. Mison18 (18% CO_2, 82% Ar) was pumped at 25 l/ min as a shielding gas to prevent oxidation. A 1.2-mm diameter stainless steel (R 312) wire spool was loaded into a TPS4000 VMT Remote feeder, with a Fronius GMA power source and configured to feed at a rate of 2.8 m/ min, or 46.7 mm/ s. The feeder head angle was configured to be as high as possible given the experiment geometry to simulate a spacecraft lowering the wire from "above" the surface. An illustration of the setup is shown in Fig. 2.

The processing laser parameters were set on a laptop using the software provided by IPG Photonics. The laser was configured to turn on upon receiving a signal from the robot arm. The laser would be on for a short time (~ 150) to create a hole in the mineral. After the robot arm finished feeding the wire, it sent a second signal to turn off the laser. For some experiments, the power would be ramped down slowly while the wire continued to feed, or the feeding would continue for some time after the laser was turned off.

The robot arm's software also controlled the laser, gasses, and wire feeding. First, the argon gas was switched on, followed by the protective crossjet air gas. The arm would send a signal to the laser to begin processing, and after a fixed delay, would begin feeding wire into the experiment zone. After another fixed time, the arm sent a signal to the laser, which would either immediately turn off, or ramp down over a fixed time set in
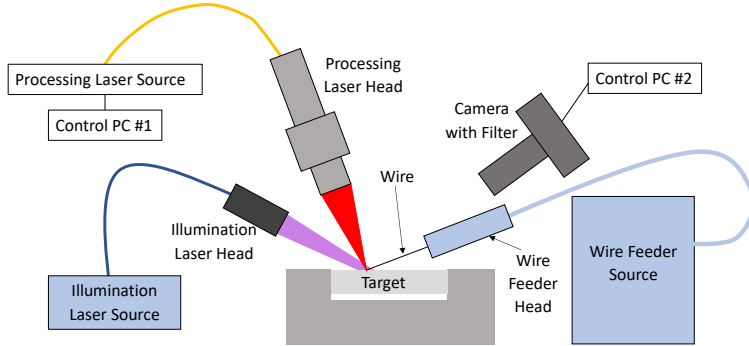
Figure 2: Experiment setup.

the laser software. After another fixed amount of time, the wire feeding would stop, and the gasses would be switched off.

The wire was then manually cut from the feeder head, and the sample moved to expose a fresh experiment site. As will be seen in the Results section, sometimes the anchored wires from previous experiments will be visible in the foreground or background of a given experiment.

2.3. Methodology for XMT analysis

The XMT measurements were carried out with a GE phoenix nanotom s system. The generator settings were $120\,\mathrm{kV}$ and $125\,\mu\mathrm{A}$, and a 1-mm Cu filter was added to the beam. A total number of 1400 projection images with a pixel size of $33\,\mu\mathrm{m}$ were recorded over a 360° rotation with an exposure time of $2 \times 250\,\mathrm{ms}$ for each image. The 3D volume data was reconstructed from these data sets using datos|x reconstruction software version 2.4.0.1199 (GE phoenix).

2.4. Methodology for anchor strength measurements

The strength of the attachment was tested using a Tinius Olsen H5KT Benchtop Tester using a 2.5-kN load cell. A custom sample holder was 3D printed using a ORIGINAL PRUSA I3 MK3S, to ensure the pull force was co-linear with the wire angle, see Fig. 3. The design includes selector pins inserted below and to the side of the sample, to align the desired pin with the direction of force.
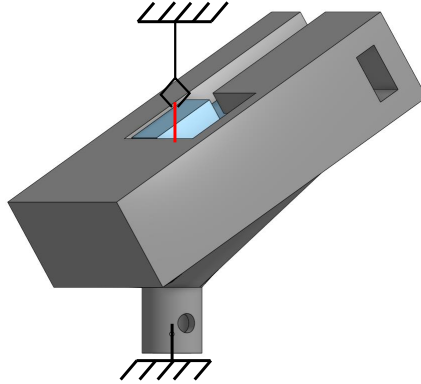
Figure 3: Rendering of sample holder.

Attaching the tester's upper (moving) arm to a wire proved difficult, but not impossible. Several attachment methods were tried, but the one successful one was to use two needle-nose pliers to bend the tip of the wire into a hook, which allowed a secure attachment point enough to perform the experiments. There was a concern that in the process of bending the wire, the anchor strength was weakened, so after the first two experiments (with the bent hook) the attachment mechanism was changed to an electrical conduit usually used to connect two loose wires.

3. Results

3.1. Moving-platform experiments

The moving-platform experiments did not provide any result that had a solid attachment. The high-speed footage from these experiments showed two phenomena: the first being a lack of wetting, and the second being a lack of mixing of melt pools. The lack of wetting can be seen in Fig. 4d. As the platform moved, the laser would melt more of the wire, causing the molten bead to increase in size. The bead would remain cohesive, no matter the size, and glide across the sample's surface.

We hypothesized that above-mentioned phenomenon could have been due to the fact that the molten metal was allowed to *move* across the surface, so the wire was replaced with a sheet of metal. This experiment geometry would simulate the welding of a landing leg of a spacecraft that already landed on the surface of an asteroid. During the experiments with the sheets no moving metal bead formed. This too, however, did not achieve the intended result, as the two melt pools would not mix. This was exemplified by two further phenomena. First, a solid barrier would form between the two melt pools (Fig. 5). Second, any time the melt pools did come in direct contact, droplets of olivine would float to the top of the steel (Fig. 6) due to the difference in densities. Olivines can have densities in the range 3.2–4.4 g/cm^3 and steels can have densities in the range 7.85–8.67 g/cm^3.
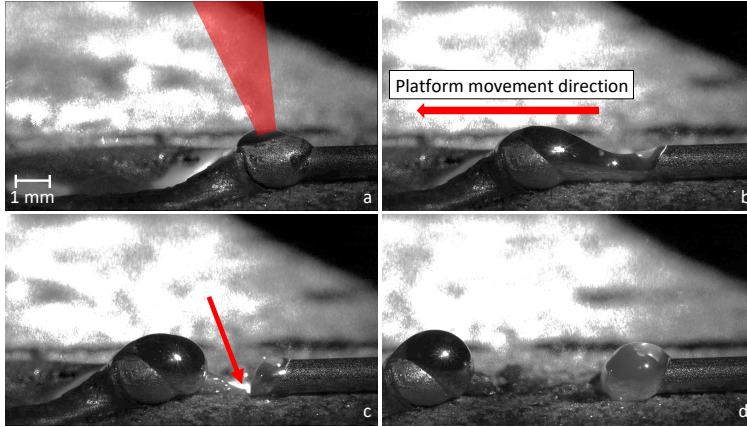
6

Figure 4: High-speed footage of an attempt to weld a stainless steel wire to olivine. Seen in frame **a** is a crater caused by the delay between turning on the laser and moving the platform. It completely melted the wire, which formed a bulb on the right side of the frame, which was taken just as the laser spot began moving from the crater. Frame **b** is 288 ms later, after the laser has passed over the bulb, and began heating the wire, which are both molten. Just before frame **c** (at 308 ms), the wire breaks as a result of the surface tension from the bulb on the left and the molten bead on the right pulling it apart. The arrow shows that the laser spot is spanning both the wire and the olivine beneath. The final frame (**d** at 528 ms) shows the molten bead following the laser spot.
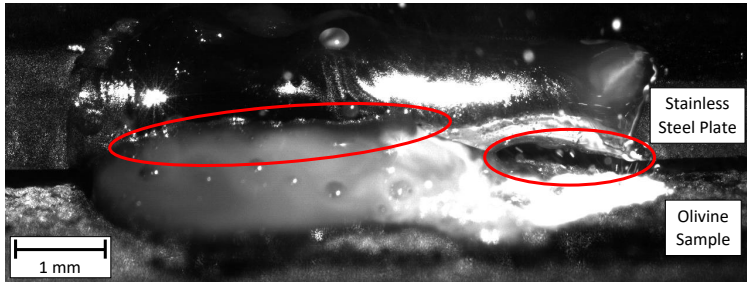

Figure 5: High-speed footage of attempt to weld a stainless steel plate to olivine. The oval to the left shows a solid barrier between the two melt pools. The oval to the right shows a gap between the melt pools, probably due to sheet deformation and melt pool dynamics.
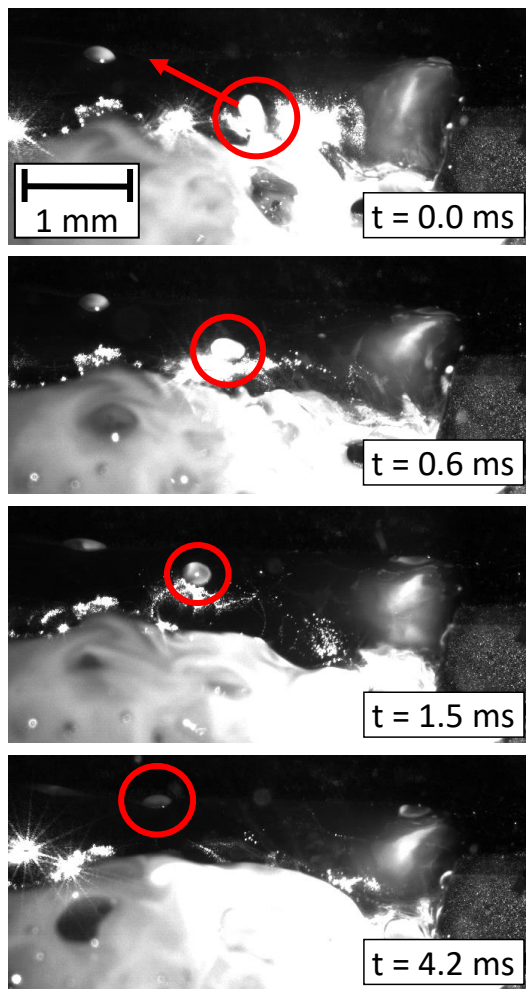
7

Figure 6: Close-up of HSI from Fig. 5 showing a small droplet of molten olivine floating on top of the molten steel.

3.2. Feeding experiments

What became clear was that it was practically impossible to create a weld in the traditional sense, that is, a mixed melt pool that re-solidifies with the same (or similar) strength as the base materials. We decided to try a mechanical approach, where a hole would be drilled, and wire would be fed into it and melted. The molten metal would fill irregular shape of the hole, and the anchor force would be generated by friction, rather than a re-solidified mass. This would not require any new equipment for the spacecraft, it would simply be used in a different manner.

We began by estimating the size of a hole based on previous research [5], and calculating how long the feed time should be to fill the hole with some excess on top. We aimed for a 10-mm-deep hole, so with a spot size of 0.6 mm, the volume was $2.82 \, \text{mm}^3$, assuming a perfect cylinder. We set the laser power to 1500 W and used a volume removal efficiency of $15 \, \text{mm}^3/\text{kJ}$. To make a hole this large, the laser would have to be on for 125 ms. To then fill the hole, the same volume of steel wire would need to be fed, in this case for 53 ms. We wanted a bit of material on top, so we elected to keep the feeder going for a total of 125 ms. We switched off the laser and wire feeder simultaneously, which had the effect of the molten metal on the sample surface to detach from the solid wire (see Fig. 7c). We note that due to delays in signal propagation, the timings were affected by a delay of roughly 10 ms, or 4% of the total time of the first experiment (250 ms).
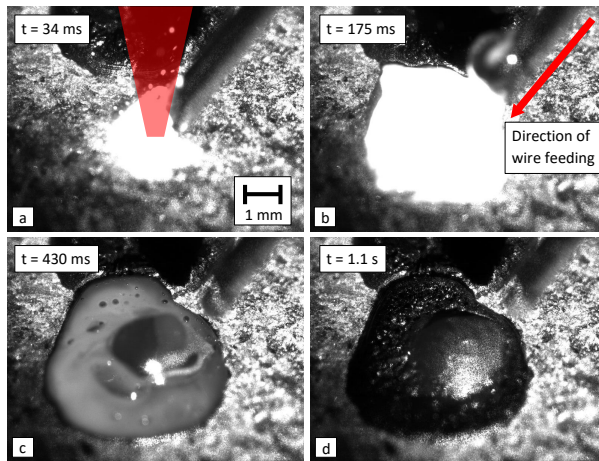

Figure 7: High-speed footage of an experiment where the wire feed was stopped simultaneously with the laser. Frame **a** shows both the wire and olivine being processed moments after the laser was turned on. Frame **b** is roughly 50 ms after the wire began to be fed. Frame **c** shows the disconnect roughly 100 ms after the laser and wire feed stop. Frame **d** shows the result after cooling. In this experiment, the laser was turned on for 125 ms followed by another 125 ms, when both the laser and the wire feeder were operating, after which both were shut off simultaneously.

9

We also expected a larger melt pool to form on the surface. For the next experiment, we increased the time that the feeder and laser were on to 500 ms, and allowed the feeder to continue feeding for an additional 500 ms after the laser was turned off. This resulted in what looks like a successful attachment (Fig. 8). An interesting phenomenon that occurred on this and subsequent experiments was an after-effect seen in Fig. 8f, where what appears to be re-solidified metal billows upwards, as if a bubble is being pushed up from below the surface.
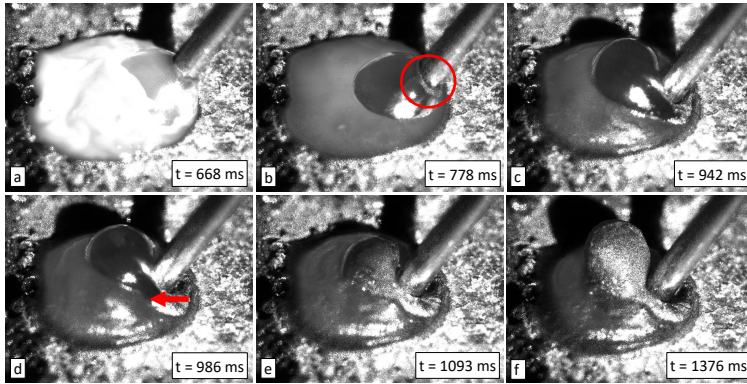

Figure 8: High-speed footage of experiment where the wire feeding was allowed to continue for an additional 500 ms after the laser was turned off. At 668 ms, frame **a**, the laser is just being turned off. The molten metal begins to solidify starting close to the relatively cold solid wire, see the circle in frame **b**. This continues to to the point that the wire physically shifts to the left before settling down (the red arrow in frame **d**)). The billowing phenomenon is seen in frame **f**).

In total, seven anchors were strong enough to be removed from the experiment platform whereas the other eight either fell off as the wire was cut from the wire feeder or from moving the sample from the stand (Fig. 9).
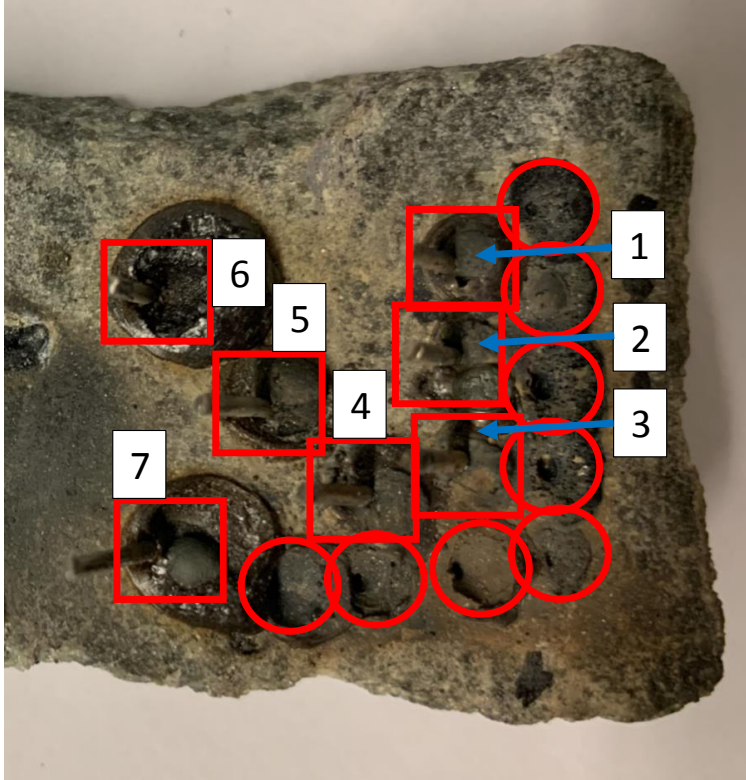
Figure 9: The olivine sample after completion of all of the anchoring experiments. Areas marked by squares are the successful anchors and have accompanying numbers for reference. The areas marked by circles are those that did not have the strength to survive being removed from the experiment platform.

3.2.1. XMT Analysis

An XMT scan revealed that varying the laser parameters does have an effect on the depth of penetration of the wire (Fig. 10). It appears that for each experiment, there is about 1–2 mm of re-solidified molten material above the surface and 1–2 mm below the surface, both forming a plug that sits at the entrance of the hole. Depths range from roughly 1 mm (#5) up to 9 mm (#6), and each one appears bent below the surface, following the shape of the hole as it was fed in. The given angle (58°) is from horizontal and represents the angle at which the wire was fed into the system for each experiment.
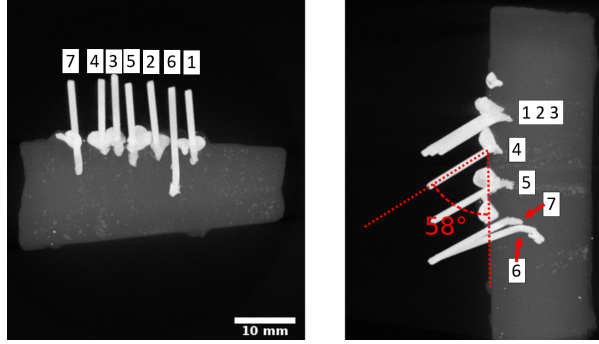
Figure 10: XMT scans of the sample after all experiments were completed. The left image is from the right side of Fig. 9 and the right image is from the bottom side of Fig. 9.

A detailed view of the holes produced by the laser shows a considerable amount of air surrounding the wires in the holes (Fig. 11). It also shows that the wire appears to be mostly intact below the surface, albeit slightly bent. There are also some bulges and bumps along the wires near the base, which suggests it was partly melted before being pushed below the surface.
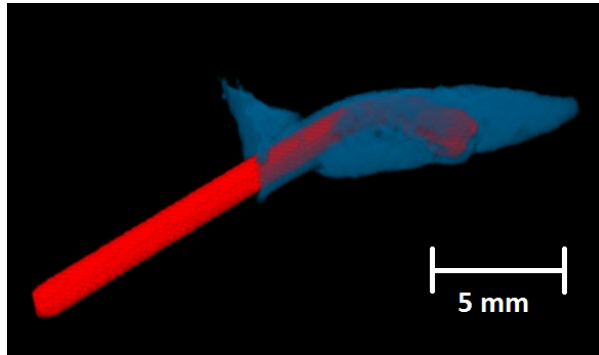

Figure 11: XMT scan of experiment #6. The red represents the wire and the blue represents the air surrounding it.

3.2.2. Anchor strength measurements

The results of the tensile testing are given in Table 3. The two methods of bending the wire tips or using an electrical conduit proved successful for all but one of the experiments:

Table 3: Results from the pullout force measurements with corresponding experiment parameters. The letters RD and F stand for "RampDown" (where the power was lowered from the power in column 2 to zero over the stated duration) and "Feed" (where the wire was fed after the laser was turned off for the stated duration).

Wire #	Power (W)	Hole Time (ms)	Feed Time (ms)	Post Feed (ms)	Pullout Force (N)
Olivine 1	1500	150	500	500 (RD+F)	85.4
Olivine 2	1500	150	500	250 (RD+F) + 250 (F)	15.0
Olivine 3	1500	150	500	500 (F)	n/a
Olivine 4	1500	250	900	500 (RD+F)	n/a
Olivine 5	1500	250	900	650 (RD+F) + 350 (RD)	83.9
Olivine 6	1500 - 4500	250	150 + 700	650 (RD+F) + 350 (RD)	115.6
Olivine 7	1500 - 3000	250	150 + 700	650 (RD+F) + 350 (RD)	113.8
Pyroxene 1	1500	250	900	250 (RD+F) + 250 (F)	7.5
Serpentine 1	1500	250	900	250 (RD+F) + 250 (F)	70.7
Steel 1	1500	250	900	250 (RD+F) + 250 (F)	>159.0

the steel plate experiment was so strong, that neither method could remain attached to the wire. The anchor strength was most likely much higher than the failed measurement result listed as lower limit. Wires #3 and #4 broke off during the attachment to the universal testing machine, and we assume their anchor strengths are $< 7.5\,\text{N}$ (the lowest value recorded of all experiments).

4. Discussions

In hindsight, the wire-based moving-platform experiments would be difficult to implement in reality at an asteroid surface due to the stiffness of the wire. The wire would have to be pre-bent and "held" against the surface to match the experiment. What the high-speed imaging did reveal was that there was a lack of wetting—the molten metal would not stick to the olivine surface. Attempts to pre-heat the surface either started melting the olivine or did not help with sticking issues. Using a number of wires bundled together (more molten metal) yielded the same result. Some experiments did bind a bit of the metal to the surface as it cooled, but the holding strength was so weak that they would fall off at the slightest touch. In reality, the surface of the asteroid will not be a smooth plane, but be ragged, which could perhaps have allowed for a better bond, but the wire would not have sat flush on the surface.

The plate-based MPEs were more promising than the initial wire MPEs, but ultimately did not yield a strong anchor either. The laser spot was illuminating both the plate and the olivine below. The metal exhibited a relatively calm melt front, while the olivine was relatively chaotic. The power level used caused the olivine to sputter a significant amount of material. The olivine melt pool had vapor bubbles and cavities mixed throughout, which are not conducive to a good weld. A solidified barrier formed between the melt pools, and remained after the metal plate came off of the sample, which suggests the lip was made of olivine, and not molten metal.

The results of the feeding experiments were sensitive to the tuning of the laser and feeder parameters. For instance, it seemed necessary to keep feeding the wire after the

laser was turned off, while the materials were still molten. The two experiments with the strongest bonds (wires #6 and #7 in olivine) had a feed time twice as long as the laser on time. We were unable to determine a meaningful mathematical relationship between the parameters and the resulting anchor strength, because the number of experiments was too small. It is clear that more experiments need to be performed in sufficient numbers to be able to determine an average strength for a given set of parameters.

The pyroxene experiment had a surprisingly low strength. This could be due to the fact that pyroxene can be more brittle than the other two materials, possibly due to its characteristic cleavages. Alternatively, the location could have been a natural weak point or the laser parameters were not optimized for the specific material.

We noted when handling the samples that one could wiggle the wires side to side, as if the wire did not fully fill the empty space below the surface and this was confirmed by the XMT scan shown in Fig. 11. In fact, most of the wire did not melt at all, and was simply *pushed* below the surface *after* the laser power decreased. We think that this is due to a process known in laser processing as bridging—if the hole diameter is relatively small, the surface tension of the melt pool will prevent the liquid from falling down into the hole. We attempted to address this in experiment #6 by increasing the power of the laser to induce a piercing process, where the laser would *force* the liquid down via vapor pressure. However, although the hold strength was the highest of the rock samples, there is still a lack of molten material deep in the hole as seen in the XMT scan.

We noticed that the amount of wire being fed into the system seemed greater than the calculated hole volume could handle. A considerable amount of molten metal is dissipated through various mechanisms. Some of it remains cohesive in the surface plug, some of it may mix with the molten olivine and sink into the many pores and cracks created during the laser processing.

The results of the work presented above can be compared to other anchoring techniques like those described by [3]. They report that the harpoon mechanism from the Philae lander would have been tightened up to 30 N, and that self-opposed drills have maximum strengths of up to 200 N for each drill, depending on the material drilled into. The self-opposing drills are limited by the fracture strength of the target material, which we can confirm as well in our experiments. The microspine gripper, developed at NASA's Jet Propulsion Laboratory, have hold strengths of up to 180 N depending on the surface roughness of their samples [7].

Our novel attachment mechanism demonstrated the strength of one 1.2-mm wire being pulled straight out of the hole. To create an even stronger anchor, one could consider drilling and inserting a wire diagonally, and pulling at an angle (similar to the self-opposed system described above.) Perhaps several anchors could be created in a small area, further increasing the total hold strength.

The "billowing" phenomenon seen in Fig. 8 and other experiments could be caused by a number of possible processes. It seems to occur after the laser has been shut off, and after most of the molten material has cooled and re-solidified. There could be vapor trapped beneath the surface, which is trying to escape. Perhaps it has to do with the differences in density of the melt pools (i.e., molten olivine becomes trapped below re-solidifying metal). Alternatively, it could be the solid wire being forced below the surface, pushing molten material or vapor upwards.

14

5. Conclusions

1. In general, we were able to demonstrate that a laser-based wire-to-stone attachment mechanism can work.
2. Due to the lack of wetting, a surface weld or "solder" was not possible under our experimental conditions.
3. The melt pools of olivine and the tested metals would not mix under our experimental conditions. In addition, molten olivine re-solidified as a glassy material, with pores and cracks, and would thus not make a strong anchor.
4. The anchors produced in the feeding experiments had a hold strength up to 115 N when pulled along the wire axis.
5. The wire-feeding technique can be used to anchor a spacecraft to the surface of a small body, pick up or move small boulders on the surfaces of small bodies, or to redirect small monolithic asteroids or space debris.

Acknowledgements

References

[1] E. Hand, "Philae probe makes bumpy touchdown on a comet," *Science*, vol. 346, no. 6212, pp. 900–901, 2014, ISSN: 0036-8075. DOI: 10.1126/science.346.6212.900. eprint: https://science.sciencemag.org/content/346/6212/900.full.pdf. [Online]. Available: https://science.sciencemag.org/content/346/6212/900.

[2] Scholten, F., Preusker, F., Elgner, S., Matz, K.-D., Jaumann, R., Biele, J., Hercik, D., Auster, H.-U., Hamm, M., Grott, M., Grimm, C., Ho, T.-M., Koncz, A., Schmitz, N., Trauthan, F., Kameda, S., Sugita, S., Honda, R., Morota, T., Tatsumi, E., Cho, Y., Yoshioka, K., Sawada, H., Yokota, Y., Sakatani, N., Hayakawa, M., Matsuoka, M., Yamada, M., Kouyama, T., Suzuki, H., Honda, C., and Ogawa, K., "The descent and bouncing path of the hayabusa2 lander mascot at asteroid (162173) ryugu," *A&A*, vol. 632, p. L3, 2019. DOI: 10.1051/0004-6361/201936757. [Online]. Available: https://doi.org/10.1051/0004-6361/201936757.

[3] K. Zacny, P. Chu, G. Paulsen, M. Hedlund, and B. Mellerowicz, "Asteroids: Anchoring and Sample Acquisition Approaches in Support of Science, Exploration, and In situ Resource Utilization," in *Asteroids: Prospective Energy and Material Resources*, V. Badescu, Ed. 2013, pp. 287–343. DOI: 10.1007/978-3-642-39244-3_12.

[4] P. Wang, X. Chen, Q. Pan, B. Madigan, and J. Long, "Laser welding dissimilar materials of aluminum to steel: An overview," *The International Journal of Advanced Manufacturing Technology*, vol. 87, no. 9, pp. 3081–3090, Dec. 2016, ISSN: 1433-3015. DOI: 10.1007/s00170-016-8725-y. [Online]. Available: https://doi.org/10.1007/s00170-016-8725-y.

[5] N. Anthony, J. Frostevarg, H. Suhonen, C. Wanhainen, A. Penttilä, and M. Granvik, "Laser processing of minerals common on asteroids," *Optics and Lasers in Engineering*,

[6] J. Pocorni, J. Powell, J. Frostevarg, and A. F. H. Kaplan, "Investigation of the piercing process in laser cutting of stainless steel," *Journal of Laser Applications*, vol. 29, no. 2, pp. 022201-1–022201-8, May 2017. DOI: https://doi.org/10.2351/1.4983260.

[7] A. Parness, M. Frost, N. Thatte, J. P. King, K. Witkoe, M. Nevarez, M. Garrett, H. Aghazarian, and B. Kennedy, "Gravity-independent rock-climbing robot and a sample acquisition tool with microspine grippers," *Journal of Field Robotics*, vol. 30, no. 6, pp. 897–915, 2013. DOI: https://doi.org/10.1002/rob.21476. eprint: https://onlinelibrary.wiley.com/doi/pdf/10.1002/rob.21476. [Online]. Available: https://onlinelibrary.wiley.com/doi/abs/10.1002/rob.21476.

Department of Computer Science, Electrical and Space Engineering
Division of Space Technology

LULEÅ
UNIVERSITY
OF TECHNOLOGY